Universidad del País Vasco Euskal Herriko Unibertsitatea

Facultad de Química-Kimika Fakultatea

Departamento de Ciencia y Tecnología de Polímeros-
Polimeroen Zientzia eta Teknologia Departamentua

Development of osteoinductive Si-based coatings to improve dental implants' performance

Memoria presentada para Optar al Grado de Doctora en Ciencias Químicas por

María Martínez Ibáñez

Bajo la dirección de las Doctoras:

Isabel Goñi Echave y Mariló Gurruchaga Torrecilla

Donostia, 2015

A mi abuelo

Al fin ha llegado el momento que parecía tan lejano, el de agradecer a todos los que me habéis acompañado y apoyado a los largo de este camino.

En primer lugar quiero agradecer a Isabel y Mariló el haber confiado en mí desde el primer momento y el haberme dado la oportunidad de trabajar con ellas. Gracias por el apoyo que siempre me habéis dado como jefas y en muchas ocasiones como segundas madres.

A mi equipo de Biomat, empezando por Marije, con quien compartí los primeros años y muy buenos momentos, aunque en alguna ocasión el *sol-gel* nos sacara de nuestras casillas. Y a mis pupilas, compañeras y sobre todo amigas Itziar y Bea, quienes aparecieron cuando más lo necesitaba, y no solo porque me han ayudado muchísimo en el trabajo, sino porque han hecho que trabajar juntas en el laboratorio sea el mejor recuerdo que me llevo de estos años.

A todo el gran equipo que empezamos a trabajar juntos en el proyecto Soldent, Julio, Miriam, Sara, Irene y la empresa Illerimplant, y quienes me han ayudado de diferentes maneras.

A toda la gente que de un modo u otro ha participado a lo largo del desarrollo de esta tesis y con quienes he aprendido el uso de nuevas técnicas, Iñaki, JI, Sofía, Miki.

Al grupo de Madrid por la manera en la que me acogieron cuando estuve trabajando allí con ellos y en general en todas las ocasiones que hemos coincidido. En especial a Julio, quien siempre ha estado dispuesto a ayudarme y quien confió en mí para abrirme las puertas hacía una nueva experiencia como fue la estancia en Estados Unidos.

I would like to thank all the people from NJCBM, starting from Dr. Kohn, who gave me the opportunity of going there to work for six months and who trusted in my ability more than myself. Thanks to Sanjeeva and the entire third floor because everyone was always willing to help me. And finally, it's hard to express my gratitude to my BioTeam for all their help. Thanks Yong for being so patient teaching me all this new biological stuff and moreover, for adopting me in your family. Amy and Tyler, it was so much fun working with you, thanks for everything and for making me feel like if I were twenty-two again. I will never forget this experience in USA.

Azken urteotan nire kexak eta negarrak jasaten egon den pertsonari. Mila esker Aitor, ez dut inoiz ahaztuko nigatik egin duzun guztia. Zuk lagundu zenidan ezkutuan neraman ausardia ateratzen atzerrian egonaldi bat egiteko, mundua ezagutzeko. Eta nahiz eta hasiera batean amesgaizto bat zirudien, momentu txarrenetan nirekin egon zinen, nire animoa igotzeko eta batez ere errealitateko zaplaztekoak eta hizketaldiak botatzeko prest.

A toda la gente con la que he coincidido a lo largo de la carrera y durante el doctorado, y con quienes he compartido tantas experiencias y buenos momentos. En especial a Ne y Lur, quienes no solo habéis sido mis compañeras, sino que con el paso de los años os habéis convertido en parte de mis mejores amigas.

Un gracias gigante para mi cuadrilla, porque tengo la suerte de tener los mejores amigos del mundo, de los cuales muchos llevan veinticinco años aguantándome, y aunque la mayoría aún no sabéis qué es lo que hago todavía en la universidad, sé que me apoyáis en todo. Angel, Diego, Erika (mi gorf), Fer, Fari (gracias por financiarme la tesis, como tú dices), Iker, Javi (contigo sigo después), Kiki, Nerea, Pot (por aguantarme más que nadie y estar conmigo de manera incondicional) y Ozio, gracias a todos, sé que nunca os vais a leer la tesis pero os imprimiré esta hoja para que conste que salís en un libro.

A Javi, quien sin entender muy bien por qué me metí en esto, siempre me ha apoyado (o por lo menos lo has intentado). Pero sobre todo gracias porque llevas aguantando la peor y la mejor versión de mí misma durante doce años y aun así nunca has dejado de cuidarme y quererme. Gracias por estar siempre a mi lado.

Y por último quiero agradecer a toda mi familia el haberme apoyado y el haber estado siempre ahí. A mis tíos, tías, primos, primas, abuelos, abuela, cuñado, cuñadas y familia pegada. No puedo ir con todos de uno en uno pero vosotros sabéis a quienes me refiero.

A mis padres, porque cada uno a su manera me ha ayudado y me ha dado fuerzas para llegar a donde estoy, y ya sea para bien o para mal, gracias a vosotros soy quien soy.

A mis hermanos porque junto con mis sobrinos sois lo mejor que tengo. A mi *bro* porque ha sido como un segundo padre y siempre me ha cuidado, aunque no

siempre para bien…Y a mi *tata*, que es mi mejor amiga y la persona que más me ha apoyado siempre, aunque en ocasiones nos matemos.

No me puedo olvidar de mi Bety, quien lleva conmigo doce años y quien sin ella saberlo ha supuesto un gran apoyo en mi vida. Nunca nadie me ha dado tanto sin esperar nada a cambio, ojalá pudiese tenerte toda la vida a mi lado.

Y por último, a las cuatro personitas que han ido dando un nuevo sentido a mi vida y me han enseñado lo que es querer de una manera tan incondicional y desmesurada, a mis sobrinos Unai, Erik, Xabi y Marc.

Ahora que ya pongo el punto y final definitivo, me doy cuenta después de haber escrito estas líneas de agradecimiento, de la suerte que tengo de contar con todos vosotros.

RESUMEN

Desde que el Profesor Brånemark introdujese el concepto de osteointegración y propusiese el titanio como la mejor opción para la producción de implantes, muchos han sido los esfuerzos e investigaciones que se han llevado a cabo para modificar la superficie de los mismos con el fin de mejorar el contacto íntimo entre el hueso y el implante, y de este modo acelerar el proceso de osteointegración, así como asegurar el éxito del tratamiento.

El uso de los implantes dentales ha sufrido un gran incremento en las últimas décadas, sin embargo siguen existiendo ciertos pacientes que pertenecen a un grupo considerado de riesgo (como por ejemplo es el caso de fumadores, diabéticos o ancianos) y que debido a su pobre capacidad de regeneración ósea no pueden ser sometidos a este tipo de tratamientos. En este contexto, el objetivo de este trabajo de tesis es por un lado acelerar el proceso de osteointegración de los implantes de titanio convencionales para reducir los periodos de carga y evitar posibles problemas que pueden aparecer durante las primeras etapas tras la intervención, y por otro favorecer la capacidad osteoinductora de los implantes para poder ser empleados en pacientes que presentan condiciones desfavorables, haciendo su uso accesible para todo tipo de personas.

Para lograr este fin, se propone el desarrollo de recubrimientos bioactivos y osteoinductores basados en el uso de precursores de silicio y obtenidos mediante la técnica sol-gel. Los recubrimientos obtenidos actuarán como soporte temporal para la formación de nuevo hueso y durante su degradación irán liberando silicio (involucrado en el proceso de formación ósea) en la interfase hueso-implante favoreciendo la osteoregeneración debido a su carácter osteoinductor.

Se seleccionaron tres precursores de silicio debido a las propiedades aportadas por cada uno de ellos al recubrimiento final: metiltrimetoxisilano (MTMOS) por aportar biocompatibilidad y estabilidad en medio acuoso, tetraetil-ortosilicato (TEOS) por aumentar el carácter inorgánico y la hidrofilia, y 3-glicidoxipropil-trimetoxisilano (GPTMS) por posibilitar la funcionalización de la superficie de los recubrimientos y la siguiente incorporación de diferentes biomoléculas covalentemente ancladas a la red.

Se diseñaron dos familias de recubrimientos partiendo de diferentes combinaciones de estos precursores, una de ellas en la que se añadieron diferentes porcentajes de TEOS a una formulación basada en MTMOS (M:T) para aumentar la hidrofilia y degradabilidad, y otra en la que se combinaron MTMOS y GPTMS (M:G) en diferentes relaciones molares para variar el grado de funcionalización de la red. Ambos sistemas fueron completamente caracterizados determinando su estructura química, el grado de entrecruzamiento de la red, la topografía, el grado de hidrofilia/hidrofobia, la cinética de la degradación hidrolítica en buffer de fosfato salino (PBS) simulando el medio fisiológico, la resistencia a la corrosión mediante medidas de electroquímica, la capacidad para liberar silicio al medio y la fuerza de adhesión al sustrato. Además, se realizó un estudio celular tras el que se eligieron los materiales que pasarían a la fase de experimentación *in vivo*, teniendo en cuenta los mejores resultados de proliferación y diferenciación osteogénica.

Los materiales seleccionados para el estudio animal en tibia de conejo de Nueva Zelanda fueron los híbridos 7M:3T y 5M:5G. De ellos, el 7M:3T fue el que presentó una mayor osteointegración en comparación al titanio, y el seleccionado como recubrimiento base para la siguiente etapa. El sistema 5M:5G, al contrario, dio lugar a la formación de una cápsula fibrosa que rodeaba a todo el implante debido a su baja velocidad de reabsorción, por lo que no fue seleccionado para los siguientes pasos de la investigación. Sin embargo, sí se tuvieron en cuenta sus propiedades, como por ejemplo la posibilidad de funcionalizar la superficie del recubrimiento, a la hora de realizar mejoras químicas en los nuevos sistemas desarrollados.

En esta segunda parte del trabajo se decidió introducir una biomolécula que favoreciese la respuesta biológica de estos recubrimientos. Por ello se añadieron diferentes cantidades de gelatina al sistema previamente seleccionado 7M:3T. Esta proteína ha sido ampliamente empleada en medicina regenerativa debido a sus propiedades de adhesión celular y completa reabsorción *in vivo*, motivos, que entre otros, hicieron de ella la candidata adecuada. También se diseñó un sistema ternario, 35M:35G:30T, con el fin de combinar las propiedades de degradabilidad aportadas por el TEOS y la posibilidad de funcionalizar la superficie mediante los grupos epóxido del GPTMS. Además, permite la unión covalente de las moléculas de gelatina a la red polisiloxánica mediante la reacción de los grupos amino y carboxilo de la misma con los anillos epoxi del precursor.

La introducción de la gelatina hizo necesario variar algunos parámetros de la ruta sintética previamente diseñada. Tras su optimización y obtención de los nuevos recubrimientos diseñados, se procedió a realizar la caracterización físico-química completa de los mismos siguiendo los pasos previamente mencionados. Los resultados obtenidos mostraron un incremento tanto en la hidrofilia como en la velocidad de degradación y liberación de silicio asociados a la incorporación de gelatina, comportamiento que era de esperar debido a la alta solubilidad en medio acuoso de esta proteína. También se pudo verificar el logro de una unión química entre la gelatina y el sistema ternario 35M:35G:30T, bajo las condiciones de síntesis diseñadas.

En esta ocasión, también se evaluó la habilidad de estos materiales para adsorber diferentes proteínas presentes en el suero fisiológico e involucradas en la posterior adhesión celular. Tras la implantación, el primer suceso que tiene lugar es la colonización de la superficie del implante por este tipo de proteínas, por lo que estos resultados pueden ayudar a predecir y justificar la siguiente etapa de adhesión celular. Dicho estudio mostró una mayor afinidad de las proteínas de adhesión para ser adsorbidas sobre los recubrimientos desarrollados en comparación al titanio, sobre todo en el caso de los recubrimientos con una superficie funcionalizada con el precursor GPTMS. Y lo que es más, la evaluación de la conformación adquirida por las proteínas mediante un estudio de aproximación, mostró una configuración más bioactiva en el caso de las que se encontraban adsorbidas sobre los recubrimientos, hecho importante sobre todo para las proteínas involucradas en la posterior adhesión celular como es la fibronectina.

A continuación, se estudió la respuesta celular de tres tipos de linajes celulares, donde se evaluaron parámetros como la citotoxicidad, adhesión, proliferación y diferenciación. A tiempos cortos, se obtuvo una mayor adhesión celular en el caso del titanio sin recubrir debido al efecto de la rugosidad; sin embargo posteriormente se observó que la velocidad de proliferación se equiparaba en todos los materiales e incluso se superaba al titanio en algunos casos. Con respecto a la cuantificación de los genes presentes en el proceso de diferenciación osteogénica de las células madre mesenquimales humanas (hMSC), se obtuvo como resultado una mayor expresión génica en el caso de las células sembradas sobre los recubrimientos, evidenciando su habilidad para promover una diferenciación temprana. Además, este estudio se llevó a cabo tanto en presencia de un medio

osteogénico, como en ausencia de un medio de inducción. En este segundo modelo experimental se comprobó como el titanio no era capaz de inducir la diferenciación, mientras que los recubrimientos seguían induciendo la conversión de las hMSC en células óseas, debido a su carácter osteoinductor asociado a la liberación de silicio.

Finalmente, se realizó una evaluación del comportamiento *in vivo* de estos últimos materiales. En esta ocasión se diseñó un nuevo método experimental para solventar los problema de estabilidad primaria obtenidos en la primera implantación. Los materiales evaluados fueron implantes comerciales de titanio sin recubrir (usado como control) y recubiertos con los sistemas 7M:3T (sin gelatina y con un 0.9% en peso de gelatina) y 35M:35G:30T (sin gelatina y con un 0.9% en peso de gelatina). Tanto el estudio cualitativo como cuantitativo de la biocompatibilidad mostraron valores levemente irritantes para todos los materiales estudiados, respuesta considerada como no agresiva y que denota la naturaleza biocompatible de los recubrimientos desarrollados.

Por otro lado, en esta ocasión el estudio de la osteointegración *in vivo*, no permitió obtener diferencias significativas entre todos los materiales estudiados, lo que se atribuyó al logro de una mayor estabilidad primaria con este nuevo diseño animal. Además, en esta segunda implantación, ninguno de los materiales desarrolló una cápsula fibrosa que envolviera el implante como sucedió en la primera implantación. Comparando los valores de los diferentes parámetros evaluados en el análisis histomorfométrico de ambas implantaciones, se comprobó que en ausencia de estabilidad primaria, los recubrimientos sol-gel, concretamente el sistema 7M:3T, era capaz de promover la formación de hueso mediante osteogénesis a distancia debido a su capacidad osteoinductora. Sin embargo, cuando se asegura una buena estabilidad primaria, tanto los materiales desarrollados como el control titanio proporcionaron una osteointegración equiparable, alcanzando niveles semejantes tras dos semanas de implantación. Estos resultados muestran una ventaja en el uso de los recubrimientos híbridos aquí diseñados en el caso de condiciones no favorables como es la ausencia de estabilidad primaria.

Para concluir, los resultados obtenidos de la caracterización físico-química muestran la obtención de recubrimientos homogéneos, transparentes, con una fuerte adhesión al sustrato y con unas propiedades de hidrofilia, degradabilidad y liberación que pueden ser controladas y diseñadas a medida en función de las

necesidades de cada caso. Además, de la evaluación tanto *in vitro* como *in vivo*, se concluyó que estos nuevos recubrimientos pueden ser una opción prometedora para su uso en implantología debido a su capacidad osteoinductora y habilidad para promover la formación de nuevo hueso en las primeras etapas tras la implantación, mejorando la capacidad del titanio en ausencia de una fijación inicial. Extrapolando este comportamiento a situaciones en las que los pacientes no presentan unas condiciones óptimas del lecho receptor y no pueden ser sometidos al tratamiento con implantes de titanio tradicionales, estos materiales podrían considerarse como una buena alternativa. Para confirmar esta aplicación, sería interesante completar el estudio con una evaluación *in vivo* usando un modelo animal osteoporótico.

Index

Chapter 1:

INTRODUCTION AND OBJECTIVES

Chapter 2:

MATERIALS AND METHODS

Chapter 3:

DESIGN OF COATINGS WITH TAILORED PROPERTIES: DEGRADABILITY AND FUCTIONALIZATION DEGREE

Chapter 4:

EFFECT OF PHYSICAL ENTRAPMENT OF DIFFERENT GELATIN AMOUNTS IN 7M:3T COATING

Chapter 5:

DESIGN OF TERNARY SYSTEM WITH FUNCTIONAL GROUPS ON THE SURFACE

Chapter 1

Introduction and objectives

Chapter 1:

INTRODUCTION AND OBJECTIVES

1.1. Introduction to Biomaterials

The field of biomaterials has been under constant evolution throughout the ages with the sole aim of prolonging human life and improving its quality. For centuries, doctors had no choice but to amputate or remove organs or tissues when they became diseased or damaged, and while the practise did indeed save lives, the patient's quality of life was severely diminished[1].

It was not until the twentieth century, due to the need of palliative treatments for illness and traumatic injuries emerged as the result of the World Wars, when the most significant developments took place in biomaterials science. Initially, there were two alternatives: Implants and Transplants, both of which have developed over time. When the damage is located in a vital organ, the most suitable and successful technique is the transplant of a healthy organ from a donor. However, if the problem is of trauma, dermal or dental origin, transplants are of limited use, hence the need to develop implants based on new materials. Moreover, the increase in life expectancy is yet another reason which has driven the unprecedented progress of biomaterials' field in recent years.

The National Institute of Health Consensus Development Conference defined a biomaterial as "any substance (other than a drug) or combination of substances, synthetic or natural in origin, which can be used for any period of time, as a whole or as a part of a system which treats, augments, or replaces any tissue, organ, or function of the body" (Boretos and Eden, 1984). While many definitions have been proposed over the years, one of the most recent definitions was proposed by Williams *et al.* in 2009. In this work he stated that "a biomaterial is a substance that has been engineered to take a form which, alone or as a part of a complex system, is used to direct, by control of interactions with components of living systems, the course of any therapeutic or diagnostic procedure, in human and veterinary system"[2]. There is a common denominator in all of them which is the undisputed special biocompatibility criterion they must meet. There are also other requirements that every biomaterial intended for use in contact with living systems needs to fulfil[3, 4]:

1. Every component of the biomaterial, as well as the ones generated as a result of its biodegradation, must be biocompatible. **Biocompatibility** refers to the acceptance of an artificial implant by the surrounding tissues and by

the body as a whole, and whose presence must not harm tissues, organs or systems.

2. The material must not release toxic materials into the living body.
3. The mechanical and physical properties of the material must be appropriate for the intended application, and they must last for the expected life of the implant.
4. The biomaterial must be sterilizable.

Some of the major advantages of using biomaterials as implants are their availability, reproducibility and biomechanical adaptation. These types of materials can be classified into four major categories: polymers, ceramics, metals and composites. Figure 1.1 shows different materials and their possible potential applications.

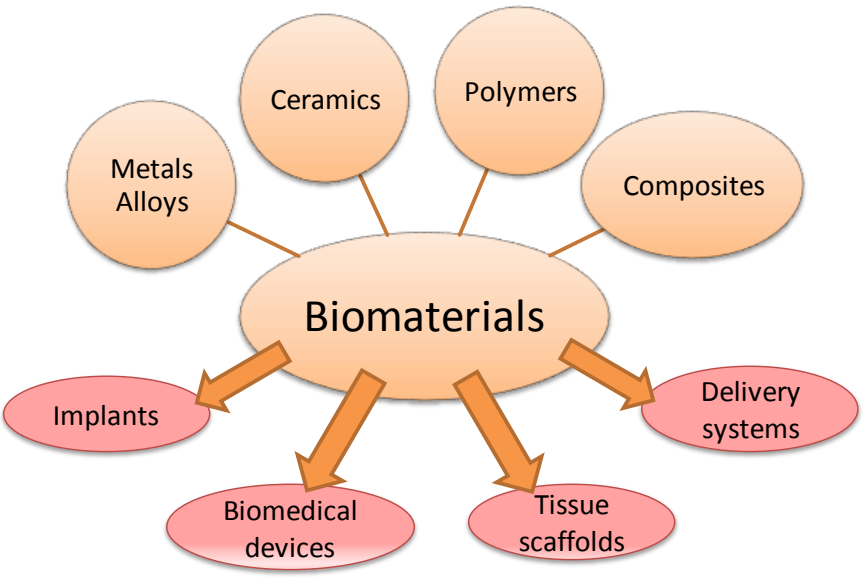

Figure 1.1. Biomaterials and their most frequent applications.

As the figure shows, biomaterials are being used in almost all areas of medicine, but particularly in orthopaedics, dentistry, aesthetic and maxillofacial reconstructive surgery, cardiovascular, ophthalmic and drug delivery systems. In the present work we are going to focus on the field of dental implants and in the development of new materials to address some of their limitations.

1.2. Dental Implantology

A dental implant is an artificial root, usually made of an inert metal or metallic alloy, which is placed on or within the osseous tissues to replace the lost tooth. In the past 20 years, the number of dental implant procedures has increased steadily worldwide. Statistics provided by the American Association of Oral and Maxillofacial Surgeons show that 69% of adults aged between 35 and 44 have lost at least one permanent tooth for different reasons; and 26% of people have lost all their permanent teeth by the age of 74[5]. Dental implants are placed in 2,000,000 people each year in the USA alone, according to the American Dental Association[6]. Nevertheless, the history of implants can be traced back to ancient civilizations like the Egyptians (2500 BC) or Mayans (600 AC).

1.2.1. Historical background

Since the immemorial, man has tried to different elements to replace teeth lost through decay, trauma or periodontal disease, both to restore the function and aesthetics. One of the main reasons for replacing teeth is obviously for mastication purposes, but good teeth are also deemed important for social status and relations.

At different times and in different cultures, teeth have been replaced in a variety of ways. In medieval times, it became fashionable for noblemen to use commoner and servant donors' teeth as dental implants. However, this practise was eventually abandoned due to continuous failure and risk of contracting contagious diseases. Thus, as even human teeth could not be used successfully as implants, the evolution of the dental techniques was put on hold.

The first intra-alveolar metallic implants were used at the beginning of nineteenth century, but without much success. However, in 1910 E. J. Greenfield established the basis of modern implantology by successfully introducing an iridium and 24 carat gold basket into an alveolus. He documented and presented innovative concepts such as the importance of the intimate union between the bone and implant substrate, the concept of the submerged implant, the healing of human tissue and the immobility of the implant (advising a period of three months without any kind of overloading)[7, 8].

In spite of these advantages, there was still a need to find the ideal metal. In 1952, Professor Brånemark started to perform some microscopic *in vitro* studies of

the bone marrow in a rabbit fibula, to investigate the anatomy and pathology of tissue injury under controlled experimental conditions. The study was carried out by introducing a commercially-pure titanium optical chamber into the rabbit bone. Once the procedure was complete, the camera could not be separated from the surrounding bone, the titanium was incorporated into the bone and the mineralized tissue was perfectly congruent with the irregularities of titanium surface. These studies indicated the possibility of establishing a firm connection between titanium and bone.

From this casual observation Professor Brånemark developed a new concept, **osseointegration**, which describes the condition and the process for having a stable loaded implant in direct contact with bone; and he established titanium as the best choice for manufacturing implants. The world of dental implantology, understood as the search for an analogous alternative for lost teeth, capable of replacing roots and living healthily with the living structures of the oral cavity, would not exist without osseointegration phenomenon[9, 10].

1.2.2. Osseointegration

Brånemark (1977), described osseointegration as "*direct structural and functional connection between ordered, living bone and the surface of a load-carrying implant*"[11]. It can be also defined as a direct interaction of bone to implant surface without the interposition of non-bone or connective tissue layer.

This definition is not clinically applicable; hence a new definition based on implant stability was proposed by Zarb & Albrektsson, "a process whereby clinically asymptotic rigid fixation of alloplastic materials is achieved and maintained in bone during functional loading"[12].

Osseointegration is not an isolated phenomenon; there are two processes by which a biomaterial can influence this response, osteoinduction and osteoconduction. **Osteoinduction** means that primitive, undifferentiated and pluripotent cells are stimulated to develop into the bone-forming cell linage, so the biomaterial by itself induces the process of osteogenesis. On the other hand, **osteoconduction** refers to bone that grows on a surface. An osteoconductive surface allows bone growth on its surface or down into pores, channels and pipes[13].

To fully understand the phenomenon of osseointegration, it is important to be familiar with the basic biology of bone, as this tissue constitutes the recipient bed of the implant.

1.2.3. Bone biology

Bone, together with cartilage, makes up the human skeletal system. Bone is a highly vascular, constantly changing (through growth, remodelling and resorption), and specialized type of mineralized connective tissue. It has three important functions:

a) Bone provides mechanical support.
b) Bone protects the viscera and surrounds bone marrow.
c) Bone serves as reservoir for calcium and other inorganic ions, participating in the calcium homeostasis in the whole body.

Bone microstructure

Bone consists of a solid mineral phase, an organic matrix of osteoid, and bone-forming and bone-resorbing cells (osteocytes, osteoblasts and osteoclasts).

Osteoblasts are uninucleate cells derived from primitive mesenchymal precursors. Osteoblasts are found along bone-forming surfaces. They synthesize the organic matrix or osteoid of the new bone, and they express alkaline phosphatase, an important enzyme in matrix mineralization. Their main functions during bone formation are: (a) they synthesize collagenous and non-collagenous proteins from the bone organic matrix, (b) they contribute to osteoid mineralization with alkaline phosphatase, (c) they mediate during the resorption process carried out by osteoclasts, by synthesising specific cytokines, (d) they synthesise growth factors[14, 15].

When the matrix is mineralized, some osteoblasts remain trapped within the matrix. These cells are called **osteocytes**. They are the most abundant cells in bone and their metabolism is extremely important for osseous vitality and maintaining the homeostasis of the organism. The osteoblasts that are not trapped in the bone by the end of the osteogenic activity assume a flattened shape and become bone lining cells.

Osteoclasts are multinucleated cells found mainly attached to the bone surface and they are in charge of the resorption process (the solubilisation of the mineral phase followed by the organic phase). These cells contain multiple enzymes such as acid phosphatases, collagenases, dehydrogenases, proteases and carbonic anhydrases, which take part in the resorption of bone, by breaking down proteins from the matrix into amino-acids and activating different growth factors. Hence, when bone is discomposed into its basic units, some substances are released into the environment which initiates its renewal[14]. Figure 1.2. illustrates this process.

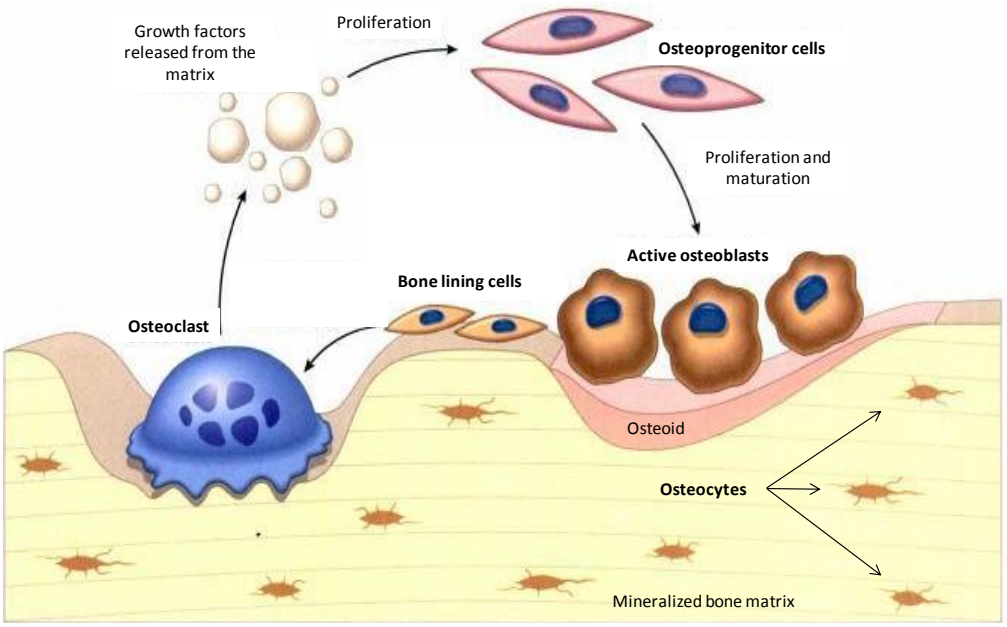

Figure 1.2. Bone formation process.

The **organic matrix** of bone, synthesized by osteoblasts, is called osteoid before it is mineralized. It is 90 to 95% type I collagen embedded within a ground of glycosaminoglycans linked to some non-collagenous proteins, principally osteocalcin and osteonectin, both of which are involved in the deposition of calcium.

The main **mineral component** that is located on the osteoid is hydroxyapatite crystal. Collagen provides the template on which the mineral is deposited, and at the same time provides the tensile strength necessary to balance the brittleness of the mineral. On the other hand, calcium and phosphate deposits show a high compression resistance.

Bone microstructure

Bone exists in two main forms, woven and lamellar. Woven bone is an immature form which is resorbed and replaced by mature bone, lamellar. This is the same sequence that also takes place in a fracture callus. Lamellar bone consists of successive layers with a highly organized infrastructure, and may be found as a solid mass (compact bone) or in an open sponge-like structure (trabecular bone). **Cortical** or **compact bone** is made of a solid and continuous mass latticed by fine longitudinal lines that host blood vessels and nerves. It is covered by a layer known as periosteum. **Cancellous** or **trabecular bone** is located under the cortical shell and consists of a three-dimensional network made of bone trabeculaes with interconnected spaces where bone marrow is located. It is covered by a layer of tissue, or endostium, which contains progenitor cells, osteoblasts and osteoclasts[10]. These structures are shown in Figure 1.3.

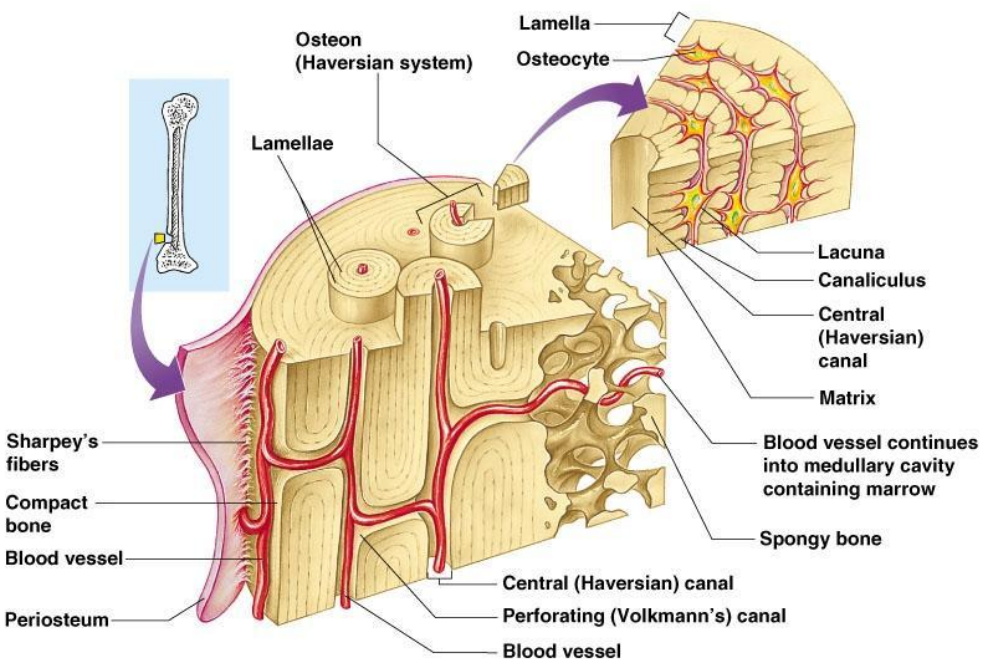

Figure 1.3. Bone structure.

Alveolar bone

Teeth are supported in the alveolar bone which consists of trabecular bone that comprises the tooth socket into which roots of tooth fit; supported by trabecular bone. The attachment between the tooth and alveolar bone is through periodontal ligament fibres.

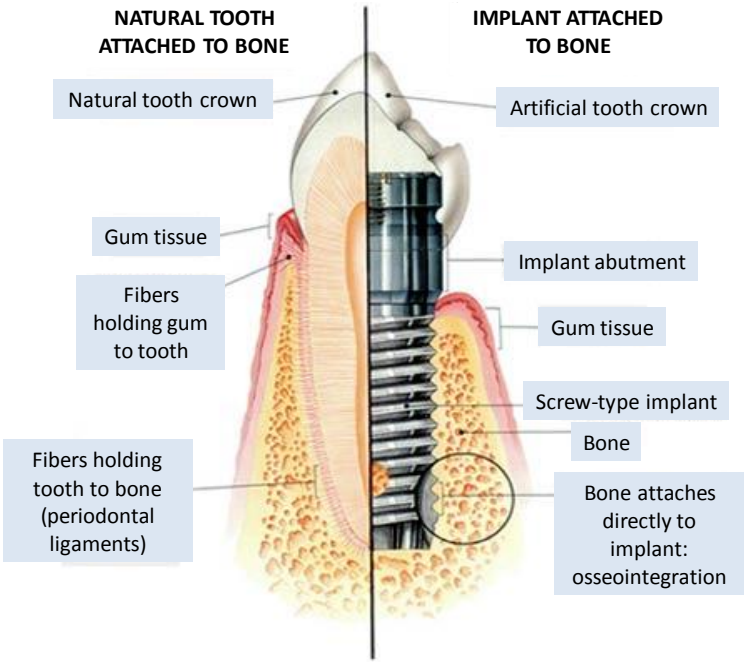

Figure 1.4. Comparison between a tooth and a dental implant fixation into the jaw bone.

Dental implants are artificial roots that will replace the lost tooth and will need to live in a healthy and natural way with surrounding tissues. To achieve the success of the implant treatment, it is essential for it to become osseointegrated. For this reason it is important to evaluate the tissue response after implantation and to study the factors which affect the osseointegration process.

1.2.4. Host response, bone healing and osseointegration process

Regardless of how careful is the preparatory technique, after the insertion of an implant, inevitably, a necrotic zone appears around any bone trauma surgically created. The amplitude of the necrotic zone around the implant will depend on

parameters related to the surgical process as well as to the created **host response**. In principle, bone can react in three different ways[11].

1. It can take place the formation of a fibrous tissue. Bone will heal permanently with the soft tissue as a response to a severe trauma. It is a non functional reaction and will lead to the loss of the implant.
2. It may happen that dead bone behaves as a *sequestrum.* If the revascularization of the necrotic area is blocked, the healing will not take place and dead bone will remain. It will be able to sustain some loads, but in spite of it may work, it is not the desired response.
3. New healing bone formation. This host answer will lead to osseointegration, where a complete replacement is achieved with ordered new bone.

Therefore, the insertion of an implant is in effect an excision-injury within bone tissue, and the process that restores the bone to its original physical and mechanical properties, **bone healing**, occurs in three distinct but overlapping stages[16, 17]:

1. Surgical procedure is followed by blood clotting and inflammatory reaction at implant surface. In this stage an hematoma develops within the fracture site during the first few hours and inflammatory cells, including neuthrophils, macrophages, monocytes and lymphocytes, and fibroblast infiltrate the site, resulting in the formation of granulation tissue, the ingrowth of vascular tissue and migration of messenchimal cells[17]. In this step also the implant surface adsorbs blood-derived proteins. This essential process has been reported to affect the subsequent cellular adhesion, proliferation and differentiation and it depends on implant surface chemistry, structure and morphology. This behaviour will be more extensively discuss in chapter 6.
2. During the repair stage, fibroblasts lay down a stroma that supports vascular ingrowth. At the same time, a collagen matrix is lay down by osteoblasts and osteoid is secreted. This is mineralized leading to the formation of a soft form of bone called callus around the repair site; and eventually, callus ossifies forming woven bone.
3. Remodeling of primary young or woven bone allows its replacement by highly mineralized lamellar and trabecular bone with improved biomechanical

properties, restoring the bone to its original shape, structure and mechanical strength.

The **osseointegration process** is summarized in Figure 1.5. Threaded bone site cannot be made perfectly congruent to implant and the bone at the interface is injured after surgical preparation **(A)**. Different regions can be found: (1) contact between fixture and bone, (2) hematoma, (3) damaged bone, (4) original undamaged bone and (5) implant. During next step **(B),** hematoma becomes transformed into new bone, callus (6) and the bone damaged during surgical procedure also heals (7). After healing period and with a controlled load, bone is in close contact with screw surface **(C)**, and border zone (8) remodels. There may occur that if the surgical trauma is too intense or if the load is applied too early, osseointegration is not achieved **(D)**, where a connective tissue layer (9) is formed in the border zone at implant[18].

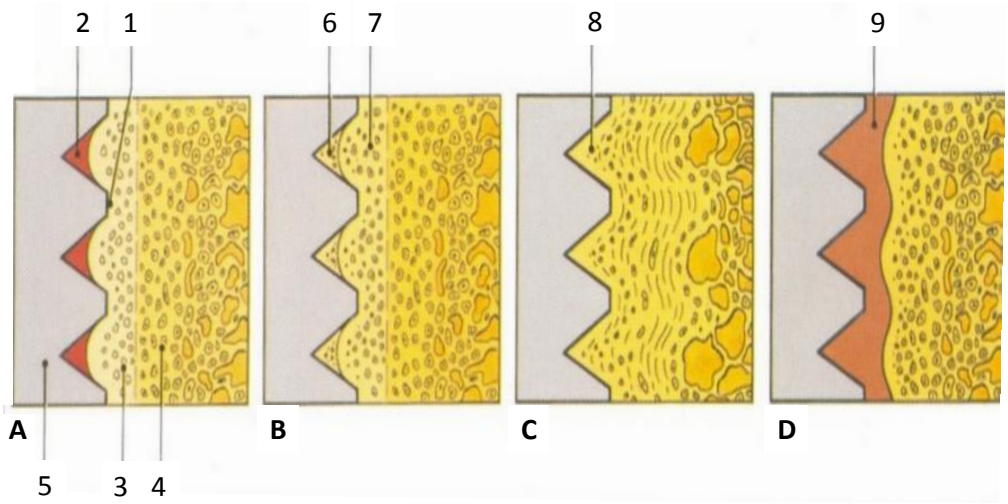

Figure 1.5. Diagrammatic representation of biology of osseointegration.

1.2.5. Prerequisites for osseointegration

The success of the implantation treatment and the achievement of osseointegration depend on different factors. The main prerequisites for osseointegration, as described by Albrektsson[19], are the implant material, its design and finish, the condition of the investing bone, a delicate surgical technique and a sufficiently long healing period before load.

1) Implant material

The implant must be manufactured from a tissue-tolerant material, inducing a tolerable reaction in host. They can be divided in bioinert or bioactive. **Bioinert** materials do not release any harmful or toxic substance, but they are biologically inactive materials. Titanium is recognized as a bioinert material. The titanium oxide film that grows spontaneously on titanium surface confers to it the excellent chemical inertness, corrosion resistance and biocompatibility. On the other hand, **bioactive** materials induce a favourable tissue reaction, either by establishing chemical bonds with tissue or promoting cellular activities involved in bone matrix formation[20].

2) Implant design

To attain osseointegration is of great importance to get an exact fit between bone and implant and a primary stability. This is more easily achieved with cylindrical threaded implants, which allow creating a maximal contact between bone and implant. Early implant movements are minimized with the screw design.

3) Implant finish (surface properties)

Protein adsorption and cell adhesion, two required processes for osteoconduction, are highly dependent on implant surface chemistry, structure and morphology and there are two main factors that play a crucial role. One of them is **roughness,** where it is widely accepted that a rough surface increases the degree of mechanical interlock and also favours the cell adhesion. A review of *in vivo* data on bone response to titanium surface topography, carried out by Albrektsson *et al.*[21], concluded that moderately rough surfaces (average roughness, S_a, between 1 and 2 μm) seem to better optimize osseointegration at the dental implant/bone interface than smoother surfaces. Another important factor to take into account is the **wettability** of the metallic implant surface, which will determine the biological cascade of events at the biomaterial/host interface. Hydrophilic surfaces, with contact angle values lower than 90°, can facilitate these initial interactions since they can interact closely with biological fluids, allowing protein adsorption onto the surface and subsequent interaction with cells[22, 23]. Figure 1.6 shows the two different interactions that may take place depending on the hydrophilicity or hydrophobicity of the surface.

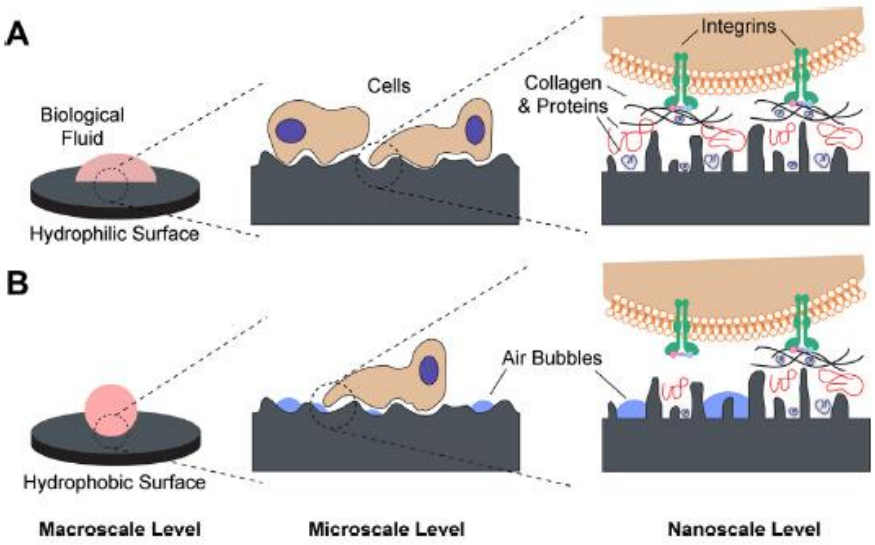

Figure 1.6. Schematic of the possible interactions with (A) hydrophilic and (B) hydrophobic surfaces at different length scales[23].

4) <u>Status of the bone</u>

The status of implant bed is decisive for proper osseointegration, where a healthy tissue is essential for the treatment success[19]. Despite the high survival and success rates of titanium dental implants, around 90-95%, there are some risk factors related to patients' diseases that may lead to the implant failure[24, 25]. These risk factors are smoking, diabetes and periodontitis; they affect healing and tissue health.

However, this success rate is related only to the placed implants, but there are many people that cannot use these types of treatment due to their poor bone regeneration ability. This is the case of the elderly or patients with osteoporosis.

5) <u>Surgical technique</u>

A delicate surgical treatment and the need of efforts to minimize any damage to the host tissue are essential to achieve the osseointegration. There are some parameters that need to be under control such as, constant cooling during surgical procedure, adequate drill geometry and speed, and careful tapping for the screw[19, 26]

6) Implant loading conditions

Osseointegration only occurs in perfectly stable situations, for what is necessary an excellent primary stability and enough time to heal without loads. It does not matter how careful the surgery is, a necrotic zone will appear immediately adjacent to the implant. Dead bone must be remodelled before implant loading is allowed. This healing time was established by Albrektsson and Brånemark to be of 3-4 months in lower jaw and 5-6 months in upper jaw[19, 26]. If an excessive load on the implant is allowed before this period of time, it can be enhanced the fibrous capsule formation and displacement at the bone–implant interface, avoiding osseointegration[16].

1.3. Titanium as biomaterial for dental implants

Titanium and its alloys have been widely used to manufacture dental implants due to their excellent mechanical properties, low specific weight, high resistance to corrosion and high biocompatibility. Commercially pure titanium (cpTi) can be classified into four grades (from 1 to 4) depending on titanium and impurity contents. These impurities are mostly oxygen, carbon and iron (Table 1.1.)[27, 28]. Most dental implants are made from 4 cpTi because of its strength in comparison with other grades, and the most common titanium alloy used is Ti6Al4V.

Table 1.1. Chemical composition of titanium and its alloys (% mass/mass).

Element	Grade 1	Grade 2	Grade 3	Grade4	Ti6Al4V
Nitrogen	0.03	0.03	0.05	0.05	0.05
Carbon	0.08	0.08	0.08	0.08	0.08
Hydrogen	0.015	0.015	0.015	0.015	0.0125
Iron	0.20	0.30	0.30	0.50	0.25
Oxygen	0.18	0.25	0.35	0.40	0.13
Aluminium	-	-	-	-	5.50-6.50
Vanadium	-	-	-	-	3.50-4.50
Titanium	Rest	Rest	Rest	Rest	Rest

1.3.1. Titanium's limitations

Even though titanium has excellent properties, there are many factors responsible for the implant failure like insufficient early osseointegration, bacterial

infection, surgical trauma, premature overloading, micro-movements, metal fatigue and inadequate quantity and quality of bone around the implant.

As mentioned above, it is well known that when titanium is exposed to air, water or any oxygen present in the atmosphere, forms spontaneously an oxide layer having 2-5 nm thickness. The inertness and excellent corrosion resistance properties are a consequence of the chemical stability and structural integrity of this titanium oxide film (TiO_2). Nevertheless, it is known that in spite of this extraordinary corrosion resistance, this oxide film will be modified as a consequence of chemical, biomechanical and cellular activity. A number of investigations have demonstrated that titanium ions can slowly diffuse into surrounding tissue and promote different side effects[29-31]. The influence of titanium and other metals' ions release on cell behaviour, mineralization and bone formation have been extensively study *in vitro*, showing that these types of ions can inhibit cell proliferation[32], ALP activity[33], extracellular mineralization and osteogenic linage differentiation[29, 34, 35].

Another limitation of titanium is that is relatively inert, so it cannot directly bind to the bone, therefore, osseointegration via the oxide layer can be a relatively long process. Nowadays, most of the investigations on titanium implants are focused on making an effort to optimize surface nature and topography, and accelerate osseointegration. Many surface modification methods have been investigated to modified titanium surface in order to fabricate implants with a higher bone-to-implant contact (BIC) ratio, enhance cell-implant interaction and promote osseointegration, faster healing and the longevity of the implant[36].

1.3.2. Titanium implant surface modification

There are three main ways to modify titanium implant surfaces: morphological, physicochemical and biochemical.

1.3.2.1. Morphological Modification on Titanium Surface

Changes in titanium surface morphology have been used to enhance osteoblast attachment, proliferation, differentiation and migration, by creating a rough surface. The best known techniques to produce macro-, micro- and nanoscale surface topographies include mechanical methods like plasma spraying, particle blasting, micromachining, grinding or polishing, and chemical methods like acid

etching, alkali etching or anodization among others. Immediately after, the most used methods are going to be described.

1) Titanium plasma-spraying

Titanium plasma-spraying method (TPS) is used to produce a rough surface. It consists in injecting titanium powders into a plasma torch at high temperature. The titanium particles are projected onto the surface of the implant where they condense and fuse together forming a film about 30 µm thick[37]. These processing results in an increase of the surface area compared to other commercially available surfaces. However, particles of titanium have been found in the bone adjacent to these implants as a consequence of dissolution, fretting or wear of the implant, and may be a source of concern due to their potentially harmful local and systemic carcinogenic effects [38, 39]. Currently, there is a consensus between professionals to use moderately rough surfaced implants rather than using plasma-sprayed implant surfaces.

2) Grit-blasting

This technique consists in projecting hard ceramic particles through a nozzle at high velocity by means of compressed air. The blasting material needs to be chemically stable, biocompatible and should not hamper the osseointegration process of the implant, it is usually performed with titania or alumina particles, and depending on their size a different surface roughness can be achieved[37]. Titanium implants blasted with titania and alumina particles with sizes from 25 µm to 75µm, have demonstrated to enhance bone formation compared with turned implants[40].

When treating the surface with alumina, these particles are difficult to remove from the implant when cleaning the surface. In some cases, these particles have been released into the surrounding tissues and have interfered in the osseointegration process. Moreover, the heterogeneity obtained in the surface with this treatment may decrease the corrosion resistance of titanium[41].

3) Acid-etching

Etching the surface with strong acids such as HCl, H_2SO_4, HNO_3 and HF is another method for roughening titanium dental implants. Acid etching removes the titanium oxide layer and produce micro-pits on the surface with sizes ranging from

0.5 to 2 µm in diameter[42, 43]. Implants manufactured with this method have shown to enhance osseointegration and long term success[44, 45]. Nevertheless, this chemical treatment might reduce the mechanical properties of titanium creating micro cracks on its surface[46].

This method is usually used in combination with others. That is the case of sandblasted and acid-etched (SLA) implants. These types of surfaces are produced by a large grit 250-500 µm blasting process followed by etching with HCl/H_2SO_4 acids. Sandblasting produce the surface roughness and acid etching leads to the microstructure[40], and both effects together promote bone integration.

4) <u>Anodization</u>

Micro-and nano- porous surfaces may be produced by anodization of titanium in strong acids (H_3PO_4, H_2SO_4, HNO_3, HF) at high current density or potential. The implant is immersed in a suitable electrolyte and becomes an anode in an electrochemical cell. When a potential is applied to the sample, an electrolytic reaction takes place at the anode, resulting in an increase of the TiO_2 layer on titanium[40]. It has been demonstrated that surfaces with an oxide thickness between 600 and 1000 nm enhance the bone anchorage of the implant in comparison with c.p. titanium implants[47]. Oxidation process changes also, the characteristics of the microstructure and the crystallinity of the titanium oxide layer. The micropores of variable diameter produced during this process, demonstrates an increment on cell attachment and proliferation[48]. It was also found that the roughness and the lower contact angle values obtained by anodization leaded to a higher removal torque of the implant in rabbit tibia, in comparison with other surface treatments mentioned above[49]. However, anodization is a complex process and there is a need of controlling various parameters such as current density, concentration of acids, composition and electrolyte temperature[37].

1.3.2.2. Physicochemical Modification of Titanium Surfaces

Physicochemical characteristics like surface-free energy, surface charge, chemical composition and surface wettability are essential parameters that influence cell behavoiur[36, 50]. These characteristics can be altered, with the aim of improving the bone-implant interface, primarily by manufacturing process or coating methods.

Calcium phosphate (CaP) coatings have been largely investigated because of their similarity to bone mineral. Metal implants have been coated with calcium phosphates mainly composed of hydroxyapatite (HA), considering that they are bioactive and osteoinductive. Bioactivity would be due to the fact that following implantation, CaP released into the periimplant region increases the saturation of body fluids and precipitates a biological apatite on the surface of the implant[51, 52]. This layer of biological apatite might contain endogenous proteins and might serve as a matrix for osteogenic cell attachment and growth[53]. As a consequence, the biological fixation of titanium implants to bone is faster with this coating than without and therefore the bone healing process around the implant is enhanced.

Different types of methods have been developed to prepare CaP coatings on dental implants. They can be divided in two groups: physical and chemical methods. The most common physical techniques include plasma spraying deposition and sputter-deposition, and chemical techniques include, among others, sol-gel coatings, electrophoretic deposition and biomimetic precipitation.

1) <u>Plasma sprayed Hydroxyapatite</u>

Plasma-spraying is a technique in which HA ceramic particles are injected into a plasma torch at high temperature and projected on the titanium surface where they condense and fuse together forming an HA film[37]. Most commercially available bioceramic coatings are processed as a 20-50 µm thick Plasma Sprayed Hydroxyapatite (PSHA) coating, and this method is usually preceded by a grit-blasting or acid etching treatment to the surface[40, 54].

The osseointegration process of dental implants with plasma-sprayed HA is faster than uncoated implants; it allows the implant to achieve direct and greater bone attachment and higher interfacial strength during the early implantation period[39]. However, this type of implant has many disadvantages, such as the porosity of the coating and residual stress at the substrate/coating interface, or the changes in the composition and crystallinity of initial CaP particles due to high temperatures of the process[55], what makes difficult to obtain a uniform coating and a uniformity of the crystallinity. Moreover this technique is not effective for coating implants with a complex shape. Plasma-sprayed HA coated implants have also been associated with clinical problems due to adhesive failures[54]. It is possible a delamination of the coating from the surface of the titanium implant and failure of the implant-coating

interface despite the fact that coating is well attached to the bone tissue leading to the failure of the implant treatment[37].

2) Sputter-deposition

To overcome PSHA's problems, sputter-deposition process was suggested, which is a useful technique for the deposition of bioceramic thin films and has the ability to provide greater control of the coating's properties and improved the adhesion between the substrate and the coating.

Sputtering is a process where atoms or molecules of a material are ejected in vacuum chamber by bombardment of high-energy ions. There are several sputter techniques and a common drawback inherent in all these methods is that the deposition rate is very low and the process itself is very slow[40]. Another disadvantage of this technique is that produces amorphous coatings of HA and, as a result, a thermal treatment with high temperatures has to be applied[52, 56].

3) Sol-gel coatings

The sol-gel method is a simple and low cost procedure to deposit thin coatings with a homogeneous chemical composition onto substrates with large dimension and complex designs. Sol-gel process has been developed to synthesize HA due to its many advantages over other coating techniques. This technique consists in preparing a homogeneous solution of a precursor in a solvent and adding an appropriate catalyst, successive reaction of hydrolysis and condensation will take place leading to the formation of a sol first and a gel latter. This gel can be applied by different coating methods on the desired substrate and finally the drying process is applied in order to obtain the rigid film. In some cases, a treatment with high temperature is required[57].

In some works it is said, that the adhesion strength between the HA and implant surface is weak, and therefore titania (TiO_2) coating needs to be placed between the HA and Ti in order to improve the bonding capability of the HA layer with respect to Ti[58]. Another drawback is the need of using high sintering temperature for HA coatings[59, 60].

4) Electrophoretic deposition

Electrophoretic deposition (EDP) of hydroxyapatite is a low-cost flexible technique that can be used to the deposit formation on conductive substrates ever for complex shape or morphology. This process essentially involves the migration of electrically charged particles under the influence of an electric field applied to a stable colloidal suspension and the subsequent deposition on the metallic substrate. Thick coating of HA can be obtained by this method controlling parameters such as deposition time and the number of depositions[61].

It is essential to get a stable suspension to achieve the desired electrophoretic level and obtain uniform layers. Owing to this, the use of additives is necessary to ensure the stability of the suspension, what could lead to problems of contamination[62]. The principle limitation of EDP is that, this process is carried out at low temperature and in this condition the deposit is in the form of a loosely held coating of particle[52, 62]. To overcome the low bonding strength between coating and substrates a heating process at elevated temperatures is necessary to sinter the HA. However this may be problematic in terms of degradation of HA coating. Other surface pretreatments, as introducing an intermediate layer[63], have been studied in order to improve the adhesion between the coating and the support.

5) Biomimetic deposition

In order to avoid the drawbacks related to HA coatings, scientists have developed a new coating method inspired by the natural formation of biomineralization. Biomimetic deposition of CaP onto surfaces of implant materials is a technique originally developed by Kokubo and co-workers[64]. This method allows the precipitation of hydroxyapatite and other CaPs onto the titanium surface from simulated body fluids (SBF) under physiological conditions of temperature and pH, on complex geometrical shapes.

The main limitation of this method is the length of the process. The classical Biomimetic CaP coating normally requires an immersion period of about 14-28 days with replenishment of SBF solution[52], making difficult its use on industrial scale. The current trend is to try to develop a new method to make this process faster and increase its practical utility[62-64]. There is also a concern about the low bonding

strength between the HA layer and implant, which is highly influenced by the substrate roughness[65].

In spite of being different methods, as shown above, to obtain an HA layer on titanium implants, plasma-spraying coating method is the only one that has been used in clinical practice, and with different failure problems[37]. For all these reasons, the clinical use of plasma-sprayed HA-coated dental implants is limited, and the latest researches are focused on the biochemical modification of the surface.

1.3.2.3. Biochemical Modification of Titanium Surface

Biochemical methods of surface modification offer an alternative or adjunct to physicochemical and morphological methods. Biochemical modification of the surface is based on the current biology and biochemistry understanding of cellular function, adhesion, differentiation and remodelling. The goal of this method is to immobilize peptides, proteins, enzymes, drugs or growth factors on the implant surface with the purpose of inducing specific cell and tissue responses, what allows controlling the tissue-implant interface by delivering these molecules directly to the interface[66-68]. The retention or delivery can be controlled depending on the immobilization method used, which can be adsorption, covalent immobilization or release from a coating.

In vitro studies with passively adsorbed extracellular matrix proteins such as fibronectin and vitronectin on titanium surface showed an increase on osteoblast adhesion, proliferation and differentiation when compared to untreated surface[69]. This physical adsorption is generally experimentally simple and often allow for the retention of biomolecular activity. However, since the passively bound molecules can be easily washed off, covalent binding was proposed[10]. This method is experimentally more delicate, but the irreversible bound molecule is much more stable under physiological conditions. Nevertheless, in some cases chemical binding can alter the conformation or orientation of the biomolecule and disturb its bioactive centre, making it less active[10].

Recent approaches have focused on using short synthetic or natural peptides that present the bioadhesive motif. The most commonly used one is arginine-glycine-aspartic acid (RGD) [70, 71] sequence which mediates bone cell attachment. The technique used to covalently attach these peptides to the surface is silanization. This

method involves coating the surface with silane molecules, which will act as a binding between the substrate and the biomolecules. In some studies using 3-aminopropyltriethoxysilane (APTES), RGD was bound to implant substrate successfully, showing a better behaviour on cell attachment, morphology, proliferation and osteocalcin mRNA expression than the bare surface[72-74]. However there are not much *in vivo* experiments about this type of treatments, and due to the weakness of the coatings, they are not expected to withstand the screw process.

Another method to immobilize biomolecules is through HA or CaP coatings. As it have been shown in previous sections, there are different techniques to obtain an HA and CaP coating. These coatings can be further functionalized with osteoinductive biomolecules like bioactive molecular cues, growth factors and drugs[68]. *In vitro* studies with nanoHA coatings functionalized with collagen[75] by sol-gel technique showed increased osteoblast activity, and covalently attached RGD to HA[76] substrate showed enhanced osteoblast adhesion and activity.

Finally, bone morphogenetic protein-2 (BMP-2) is a potent osteogenic growth factor which has been studied for bone regeneration. It has been delivered directly from the Ti surface or through a carrier scaffold, making the implant more osteoinductive and showing higher bone regeneration around the implant surface[77-79]. *In vivo* studies performed with titanium discs coated with CaP and passively adsorbed BMP-2, demonstrated ectopic bone formation[80] and sustained osteogenic activity, and also an increased volume of bone deposition[77].

Nevertheless, despite titanium surface can be modified using these biochemical modification methods, these techniques do not produce a highly controllable morphologically uniform nanoscale surface topography and chemistry. Passively bound biomolecules can be removed from the implant surface during the process of surgical implantation and in the case of covalently bound biomolecules, the release rate cannot be controlled, there may be a rapid release or a very slow delayed release[10, 66]. It is also known that HA-coated implant may fail due to poor bond strength at the HA/Ti interface, micro-cracks and improper microstructural surface architecture[37].

Due to these limitations, there is a real need on continuing the investigation on developing new titanium surfaces with controlled characteristics to enhance and accelerate the osseointegration process. Research efforts should be focused on

designing a simple, cost-effective and marketable technique to treat implant surfaces. In this context, the proposal of this work will be to develop different sol-gel coatings based on alkoxysilane precursors.

1.4. Sol-Gel Process

The sol-gel process is an inorganic polymerization considered a promising route for the fabrication of versatile materials with different applications such as optical materials, chemical sensors, ceramics, glasses, catalysts and coatings. Some of the advantages provided by this process which can be highlighted are: it allows the use of low temperatures during almost all the process, it provides materials with different structures, it is possible to apply as a coating in complex shapes, and the obtained materials are of high purity and homogeneity. These and other benefits will be discussed thoroughly later.

1.4.1. Historical Background

The sol-gel process can be reported back to 1842[81], when French chemist Ebelmen reported the synthesis of uranium oxide by heating the corresponding hydroxide. Some years later, in 1846[82], Ebelmen synthesized the first silicon alkoxide by the reaction of silicon tetrachloride ($SiCl_4$) and alcohol. He found that the compound gelled on prolonged exposure to atmosphere. However, the aging and heating process lasted almost a year to avoid cracking, which made these materials lacked of interest for almost a century[83].

It was not until 1950s, when Roy and his co-workers made the sol-gel silicate powders quite popular in the ceramics community by changing the traditional sol-gel process into the synthesis of new ceramic oxides. In 1971, the production process of so-called low-bulk density silica involving the hydrolysis of tetraethoxysilane (TEOS) in the presence of cationic surfactants was patented[84]. The next step on the evolution of these materials came in the middle 1980s, when many material scientists and chemists, represented by Schmidt and Wilkes started to synthesize organic-inorganic materials by sol-gel process. Since then, sol-gel technology has attracted a great deal of attention in many different fields.

1.4.2. Sol-Gel reaction mechanism

The sol-gel process can be described as the creation of an oxide network by progressive hydrolysis and condensation reactions of molecular precursors in liquid medium. Before going through the description of the process, some terms might be introduced. Following the definition given by Brinker and Scherer[83], a *colloid* is a suspension in which the dispersed phase is so small (1-1000 nm aprox.) that gravitational forces are negligible and interactions are dominated by short-range forces such as Van der Walls attractions and surface charges; a *sol* is a colloidal suspension of solid particles in a liquid; a *gel* is a substance that contains a continuous solid skeleton enclosing continuous liquid phase (usually the original solvent of the sol); a *xerogel* is a fully dried gel.

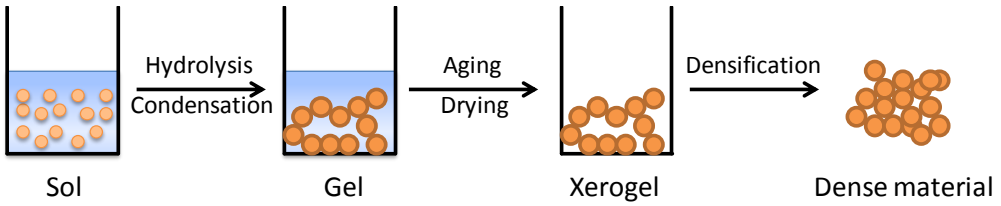

Figure 1.7. Sol-gel process.

There are essentially two ways to prepare the sol-gel materials[10, 60]. The first method involves the dispersion of colloidal particles in a liquid to form a sol, followed by the gelation to form a network in continuous liquid phase. The second method, the most widely used one, starts with a solution of monomeric metal or metalloid alkoxide precursors $M(OR)_n$ in an alcohol or other low-molecular weight organic solvent, where, M represents a network-forming element such as Si, Ti, Zr, Al, B, etc., and R is typically an alkyl group (C_xH_{2x+1}). Through hydrolysis and condensation reactions this precursor produce a polymeric gel, with an M-O-M structure network[57, 60]. The structure and morphology of resulting network depend on the relative chemical reactivity of the metal alkoxide; the sequence of reactivity is expressed as follows: $Zr(OR)_4$, $Al(OR)_3$ > $Ti(OR)_4$ > $Sn(OR)_4$ >>> $Si(OR)_4$[85]. Non-silicate metal alkoxides have much higher reactivity than silicon; they are so sensitive to moisture that, even in the absence of a catalyst, precipitation of the oxide will generally occurs as soon as water is present. Therefore, since silicon is less reactive, it allows a better control of the different parameters of the synthesis. For this and

other reasons, silicon alkoxides are still the most thoroughly studied and most widely used metal alkoxide by sol-gel process[60, 85].

1.4.3. Stages of the silicon alkoxide sol-gel process

Generally the sol-gel process occurs in five stages: (a) Hydrolysis and condensation, (b) gelation, (c) aging, (d) drying and (e) densification or sintering. However, it must be realized that in a real system, several of the steps may occur concurrently.

1) <u>Hydrolysis and condensation</u>

The monomeric silicon alkoxide is hydrolyzed in the presence of water. This first step can occur by acid catalysed or base catalysed processes. Generally, both hydrolysis and condensation reactions occur simultaneously once the hydrolysis has been initiated. Three reactions are used to describe the sol-gel process:

$$Si(OR)_4 + nH_2O \rightleftharpoons Si(OR)_{4-n}(OH)_n + nROH \qquad \text{(Eq. 1.1)}$$

$$(OR)_3SiOH + HOSi(OR')_3 \rightleftharpoons (OR)_3Si\text{-}O\text{-}Si(OR')_3 + H_2O \qquad \text{(Eq. 1.2)}$$

$$(OR)_3SiOR + HOSi(OR')_3 \rightleftharpoons (OR)_3Si\text{-}O\text{-}Si(OR')_3 + ROH \qquad \text{(Eq. 1.3)}$$

The hydrolysis reaction (Eq. 1.1) replaces alkoxide groups (OR) by hydroxyl groups (OH). Condensation reaction can be water condensation (Eq. 1.2, oxolation), where water is produced as by-product, or alcohol condensation (Eq. 1.3, alcoxolation), where the alcohol ROH is the by-product. Condensation reaction involves the siloxane bonds formation (Si-O-Si). Because water and alkoxysilanes are immiscible a mutual solvent such as alcohol is usually used as a homogenizing[10, 83].

2) <u>Gelation</u>

Gelation occurs when links are formed between silica sol particles, produced by hydrolysis and condensation, to such an extent that a giant spanning cluster reaches across the containing vessel, that is, a three-dimensional network or the gel is formed. At this point, the mixture has a high viscosity, but there are still many isolated sol particles entrapped and entangled in the spanning cluster. There is not

endothermic or exothermic process, nor any chemical change at the gel point, just the sudden viscosity increment. Following gelation, further cross-linking and chemical inclusion of the isolated sol particles into the spanning cluster continues, leading to an increase in the elasticity of the sample. The control of gelation is important in applications requiring processing of fluid (e.g. spin- or dip-coating) [86].

3) Ageing

The term aging is applied to the process of change in structure and properties after gelation. During aging, polycondensation in silica gels continues because of the large number of labile hydroxyl groups. This can continue for months for samples at room temperature, the rate of the reaction depends on temperature, initial precursor mixture composition and pH of the solution. The net effect of these processes is a stiffening and shrinkage of the sample. Ageing usually improves the properties of the material[86].

4) Drying

This step involves the loss of water, alcohol and other volatile components, first as syneresis (expulsion of the liquid as the gel shrinks), and then as evaporation of liquid from within the pore structure. It is very important to carefully control this process since it has associated a development of capillary stress which may lead to cracking[86].

5) Densification

Although there are many applications of silica gels prepared at or near room temperature (in applications which involve entrapping functional organic or biological molecules), heat treatment is necessary for the production of dense glasses and ceramics from gels. This thermal treatment leads to the collapse of the open structure of the gel and it is also known as sintering. There are three stages in this last process. At low temperatures (T<200°C) weight loss occurs as water or alcohol is desorbed, but little shrinkage takes place. At intermediate temperatures (from 150-200°C to 500-700°C), samples show weight loss and shrinkage. Three processes occur in this range: loss of organics (leads to weight loss and little shrinkage), further condensation (produces both weight loss and shrinkage) and structural relaxation (gives shrinkage without weight loss). The spaces occupied by organic species become pores with similar size. At temperatures above the one of

the second region (T>500-700°C) there is a sharp increase in shrinkage with little or no weight loss; a decrease of the surface area takes place[86].

The overall reaction of the sol-gel process is summarized in Eq. 1.4.

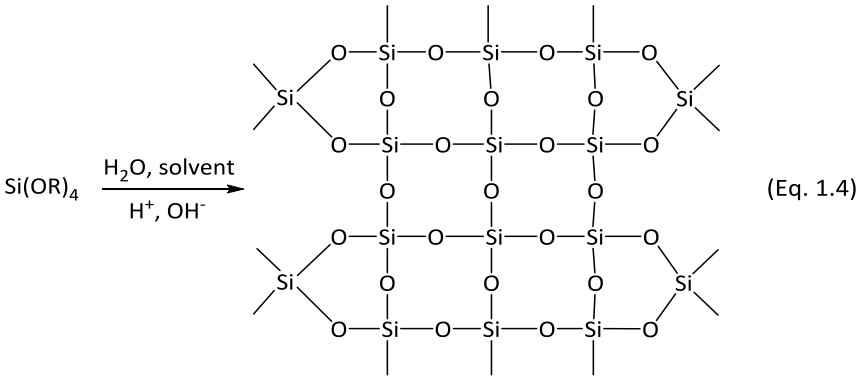

(Eq. 1.4)

1.4.4. Influence of parameters in sol-gel process

There are numerous parameters involved in the sol-gel process with an important influence on the properties of the synthesized material. Such properties as transparency, porosity, pore size distribution or surface functionality, can be controlled by controlling the conditions during the different stages of the process. This allows to one can tune the characteristics of the resulting material. Next are presented the most relevant parameters to control.

1) <u>pH/ Catalyst</u>

As mentioned previously, alkoxysilanes are less reactive than other alkoxide metals; therefore there is the need of using a catalyst to start the hydrolysis and condensation reactions. Both reactions typically proceed with either an acid or base as catalyst. The effect of catalyst may be judge by comparing the rate of reaction at different pH values, what also will lead to the formation of materials with different final properties[85, 87, 88].

For acid catalysed reactions, the first step of the hydrolysis is the fastest, and the product of this first step also undergoes the fastest condensation. It means that once the $(RO)_3Si(OH)$ species is formed, it will be more favoured the condensation reaction of this silanol group than the hydrolysis of a new alkoxy group. Hence, acid

catalyst promotes the development of linear or polymer-like molecules in the initial stage, followed by further hydrolysis and cross-condensation reactions. On the other hand, in base catalysed conditions a negatively charged intermediate state is formed, which becomes more stable as more hydroxyl groups replace the alkoxy groups. Thus successive hydrolysis steps take place rapidly forming fully hydrolysed species that undergoes the fastest condensation reactions. Therefore this environment tends to produce highly cross-linked large sol particles which eventually link to form gel with large pore between the interconnected particles[86]. Figure 1.8 shows the different network structures obtained by both pH conditions.

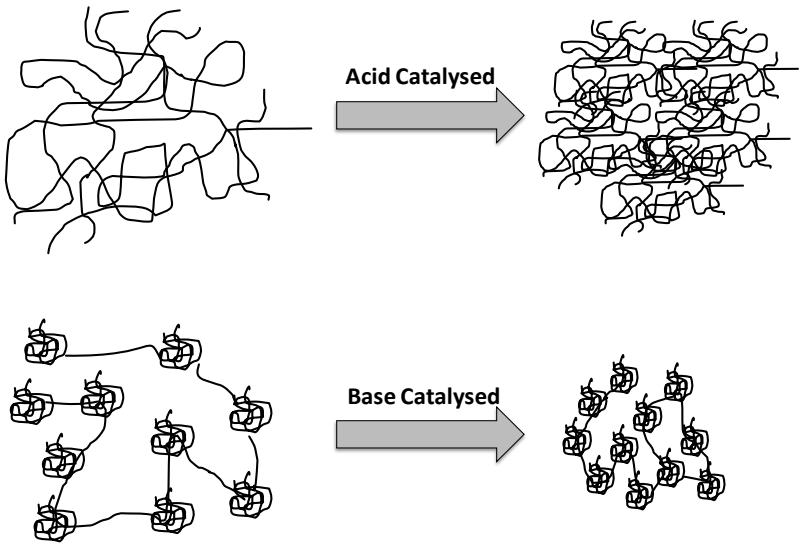

Figure 1.8. Obtained network structure depending on the catalyst conditions.

According to this is clear that sol-gel process is strongly pH dependent, where acid conditions lead to dense microporous (pore size < 2 nm) networks and in alkaline condition mesoporous (2 nm < pore size < 50 nm) gels are obtained[89]. Thus, properties like film thickness, shrinkage, porosity and optical density depend on the type of catalyst used in the preparation of the precursor solution[87].

2) <u>The precursor</u>

There are two general requirements for sol-gel precursors: (1) they have to be soluble in the reaction media; (2) they have to be reactive enough to participate at the gel formation[90].

Hydrolysis reaction of the silicon alkoxide is very sensitive to steric hindrance. Larger alkoxy groups lead to more steric hindrance and on un-reacted or not completely reacted monomers which remain in the system. Hence, branching and increasing of the chain length of the precursor substituent decreases hydrolysis rate[86]. The reactivity of silicon precursor owing to the alkoxy length will be as follows: $Si(OCH_3)_4$ > $Si(OC_2H_5)_4$ > $Si(O^nC_3H_7)_4$ > $Si(O^iC_3H_7)_4$ > $Si(O^nC_4H_9)_4$ > $Si(OC_6H_{13})_4$[90].

Another condition of the precursor that will influence the sol-gel process, as well as final material's properties, is the possibility of using hybrid molecules where an organic chain has been introduced. These organically modified silicate (ORMOSIL) precursors are hybrid molecules containing one or more non-hydrolysable substituent linked to the silicon atom. Schmidt and co-workers were one of the first groups working with these organic/inorganic hybrid materials and they termed ORMOSILs in the early 1980's[91]. The structure of these kind of molecules is $R'_nSi(OR)_{4-n}$, where (OR) are the alkoxy groups and R' the non hydrolysable substituent. R' group is a carbon chain that may contain a functional group and which is linked to the silicon network by a covalent, strong and non hydrolysable Si-C bond. The mechanism of the sol-gel process is the same as in the case of tetra-alkoxy silanes; with the only difference of the presence of the R' group in the formed material, as shown in Eq. 1.5. However, it will have a dramatic effect on the obtained material after condensation of the hydrolyzed monomers[86].

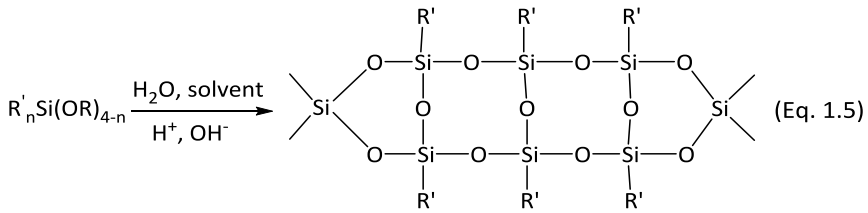

The introduction of a non-hydrolysable substituent will lower the connectivity of the network by leaving "dead ends". The presence of these "dead ends" will affect the chemical composition of the pore surface, that is, the porosity will depend both on size and rigidity of the organic chain[86]. Furthermore, apart from porosity, other chemical properties of the silicate matrix such as hydrophobicity, flexibility, reactivity and stability, can be readily tailored through the choice of R'[91].

3) Hydrophobic effect and co-solvents

In addition to the above mentioned steric effect of the substituent, the hydrophobic or hydrophilic character of the precursor must also be taken into account. In general, most of the silicon alkoxide precursors are immiscible in water due to the hydrophobic nature of alkoxy groups. For that reason, as mentioned before, it is necessary to add a co-solvent in order to achieve miscibility to facilitate hydrolysis. The most commonly used solvents are alcohols[86, 90].

4) Effect of Water: Alkoxide ratio (R)

As seen from Eq. 1.1, 1.2 and 1.3, the quantity of water in the sol-gel solution strongly influences the hydrolysis and condensation kinetics, and this leads to the formation of materials with different properties[92-94]. The time of gelation and pore size are influenced by the molar ratio of water:alkoxide. Under low R-value a matrix with a more open structure is produced due to incomplete hydrolysis and consequently less cross-linking in the sol-gel[90]. In the case of tetraalkoxy silanes, as is the case of TEOS, a stoichiometric ratio for complete hydrolysis is 4. However, less water than this can be used since the condensation reaction leads to production of water (Eq. 1.2). Nevertheless, if the amount of water becomes very small, the hydrolysis rate slows down, but if very large amounts are used the alkoxide is diluted and gel time increases[86].

5) Aging temperature and Drying effect

These parameters may have influence in some aspects like homogeneity, purity and porosity of the formed material. Because of hydrolysis and condensation reactions are not completed after gelation process, a heat treatment is required. An increase in temperature will accelerate aging step and also will determine the properties of the network[86]. Increasing thermal treatment leads to increase in the porosity[90].

Drying process involves the loss of volatile components, what leads to gel shrinkage and, as a consequence, to high stress in the structure. This may create additional random porosity, deformation and breaking. This stress can be reduced by the introduction of non-hydrolyzing organic groups (ORMOSILS), which allow structural relaxation during the drying stage and decrease the risk of cracking[90].

1.4.5. Advantages of sol-gel process

From a chemical and materials perspective, sol-gel derived materials have many advantages[86, 90, 95]:

- The temperature required for all stages apart from densification are low. This allows the incorporation of different molecules and avoids the thermal degradation of both the material itself and the possible entrapped species. The added reagents can be incorporated in a stable host matrix by simply adding them to the sol before the gelation (Figure 1.9.A).
- It provides high purity homogeneous materials.
- Material in various configurations (films, fibers, monoliths, powders) can be prepared (Figure 1.9.B). It is also possible to obtain homogeneous coatings in substrates with large and curved shapes.
- Materials are chemically, photochemically and electrochemically stable. They are also transparent, which is a plus for optical characterization.

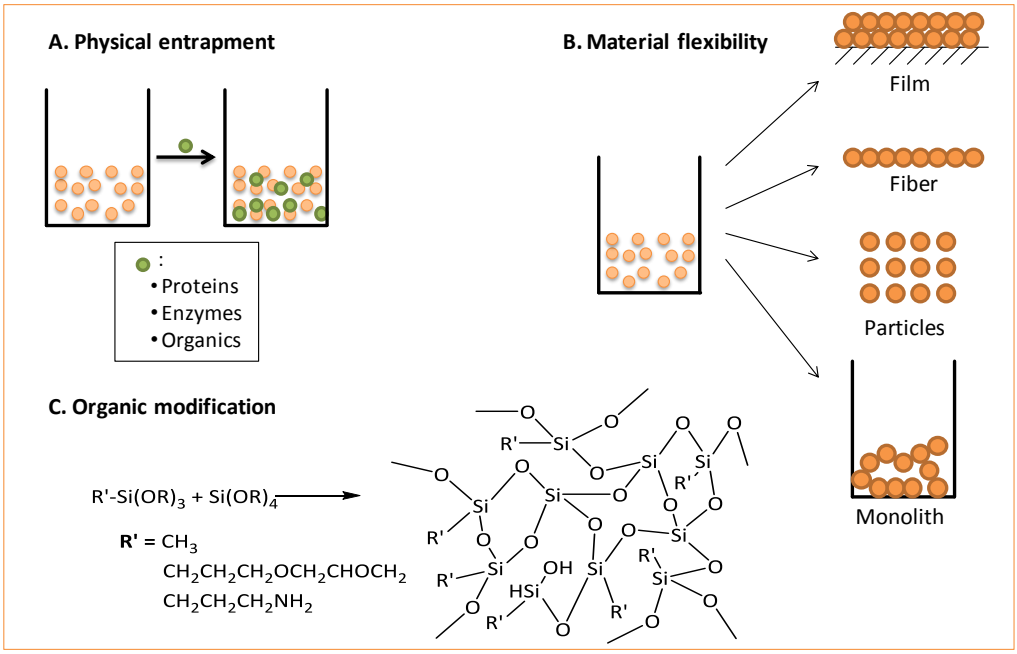

Figure 1.9. Schematic representation of sol-gel coatings' versatility.

The blending of inorganic precursors (TEOS and tetramethyl orthosilicate (TMOS)) with organoalkoxysilanes (ORMOSIL) leads to materials with added

properties compared to the ones prepared alone (Figure 1.9.C). So relative to the pure inorganic sol-gel materials, ORMOSILs posses the next advantages:

- Flexibility of the silica film is improved, enabling the preparation of thick, crack-free films.
- Possibility of covalently attach specific functional groups to the siloxane network by the use of organofunctional alkoxysilane precursors. This may be used for the subsequent anchor of different biomolecules.
- Higher concentration of incorporated reagents can be achieved, compared to physical entrapment.

In spite of its numerous advantages, there are also some disadvantages as for example the high cost of some precursors, long-process duration and difficulties in the chemistry process with respect to properties control and reproducibility. For that reason, it needs to be emphasised the need of optimising sol-gel process to exploit their advantages to the maximum in applications where they can provide properties not attainable by other methods.

1.5. Silica sol-gel coatings on metals for corrosion resistance

Metals like stainless steel, Co-based alloys, titanium and titanium alloys are widely used in the production of biomedical implants due to their excellent mechanical properties and biocompatibility. However, there are some surface originated problems associated with the metallic implants: corrosion and wear in biological environments resulting in ions release[30, 31, 96, 97]. Most implanted metallic materials have a tendency to lose electrons in solution and as a result they show a high potential to corrode in the biological environments, which usually cause inflammation and loosing of the implant[98].

A generic way to protect metals from corrosion is to apply protective films or coatings, which also allows the designing of the desired properties of the substrate by the chemical modification of the coating, such as mechanical strength, optical appearance, bioactivity, etc. Most of the effective corrosion protection systems for metals contain chromates. Hexavalent chromium-containing compounds are one type of inhibitor which exhibit far better corrosion resistance than any other inhibitor[99, 100]. Nevertheless, in spite of good corrosion protection, the leachability and superior oxidation properties of chromates make them environmentally

unfriendly. Since the hexavalent chromium was recognized as a known carcinogenic and toxic compound by United State Environmental Protection Agency (US-EPA)[101], there is a restriction on its use. Furthermore, this agency together with Registration, Evaluation, Authorization and Restriction of Chemicals (REACH) in Europe, have forced coating formulators to adopt alternate development methodologies using environmentally friendly benign chemicals[102].

Since last decade sol-gel derived thin films have attracted high interest owing to their enhanced corrosion resistance along with number of useful coating properties and no or very low health hazards compared to conventional systems. Hence, sol-gel process is considered one of the most promising ways to obtain environmentally friendly materials to protect metal substrates, also known as green coatings[100, 101].

1.5.1. Type of protective sol-gel coatings

There can be found two types of sol-gel coatings: inorganic sol-gel coatings and organic-inorganic hybrid coatings. The inorganic component confers enhanced mechanical properties while the organic component leads to increased flexibility and allows the possibility for functionalization and tailoring properties of the final material, as well as the used of this coatings as intermediate layer to enhance the compatibility between metal surface and the subsequent coating[100].

1) <u>Inorganic sol-gel coatings</u>

As it has been commented before, historically the first type of sol-gel treatments were inorganic oxide sol-gel derived films. SiO_2 can improve the oxidation and acidic corrosion resistance of metals under different temperatures due to its high heat resistance and chemical resistance[84]. The most commonly used alkoxysilanes precursors are TMOS and TEOS. Studies based on SiO_2 coatings obtained on stainless steel using TEOS as precursor demonstrated an improvement in anti-corrosion performance of this metal, as well as, the possibility to produce thin, homogeneous and free of crack coatings[103]. Another use of these materials, allows enhancing both corrosion resistance property and the bioactivity. SiO_2-CaO-P_2O_5 coatings were studied obtaining a combined effect of good adherence with higher corrosion resistance acting as a diffusion barrier and could be used as potential material for implantation purposes[104].

2) Organic-inorganic hybrid sol-gel coatings

From the section above, it can be concluded that inorganic coatings can provide good protection on metal substrates. However, there are still some other drawbacks such as[84]:

- Obtained films are brittle.
- It is difficult to obtain thick coatings (> 1 μm) without cracking.
- High temperatures (400-800°C) are required to achieve good properties.

To overcome these limitations, much work has been done to introduce organic components into the inorganic sol-gel. All the advantages of these hybrid materials were commented on section 1.4.5. Organically modified sol-gel coatings can be classified into two groups based on the type of organoalkoxysilane organic part (R'):

1. Non-functional organoalkoxysilanes: methyl groups are the most commonly used organic group for hybrids with no functionalization[105-107].
2. Organofunctional alkoxysilanes: the commonly used organofunctional precursors are epoxy[106, 108, 109], acrylic[110], amino[111], vinyl-functional organosilane[112, 113].

The simplest hybrid coating is the methyl modified silica; the most used precursors are methyl trimethoxysilane (MTMOS) and methyl triethoxysilane (MTEOS). These types of coating show better protection against corrosion than inorganic sol-gel coatings[114-116]. It was also found that when increasing the carbon number of the organic chain, the corrosion resistance increases[117].

Some of the used organofunctional groups allow the sol-gel films to chemically interact with organic molecules, what means that they are opened to further reactions. This can be of great interest for the design of multilayer coatings or for its use as intermediate adhesive layer for corrosion resistance coatings[100, 101]. For example, epoxy groups contained in the sol-gel coating can react with amine groups of a topcoat or vice versa. The amino groups are very capable to react with epoxy polymer coatings and provide an excellent binding[118]. However, it was found that amino containing coatings were water sensible and could not provide an adequate barrier against water after curing at room temperature[118].

Epoxy-based sol-gel films have gained much attention due to the higher crosslink density and better mechanical properties due to the additional cross-linking of the epoxy group. This is the case of the silicon precursor: 3-glicidoxypropyl trimethoxysilane (GPTMS). The epoxy ring can be opened due to the interaction with water according to the following equation[109, 119]:

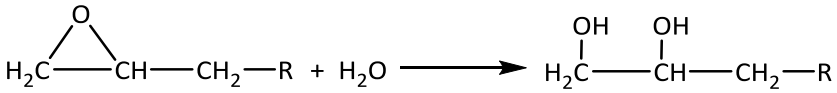

(Eq. 1.6)

A decrease of the pH and an increase of the water content in the system tend to accelerate the ring-opening process[119]. In this way, surface properties can be controlled for the subsequent reaction of these epoxy groups (converted into hydroxyl groups) with amino groups. Apart of the application as protective coatings, it can be thought on the use of the functionalization to covalently immobilize biomolecules, such as peptides or proteins, on the surface of the implant. This can be done through the reaction between the epoxies of the organoalkoxysilane and the amino groups of the proteins. The mechanism would be as follows[119]:

(Eq 1.7)

To summarize, the inorganic components contribute to the increase of scratch resistance, durability and adhesion to the metal substrate, while the organic component increases density, flexibility and functional compatibility with other molecules. These properties, among others, make them a potential material for biomedical application.

1.5.2. Bonding between metal substrate and siloxane network

When the sol is applied on the metal substrate, the silanol groups of hydrolyzed silane are in contact with the hydroxyl groups (Me-OH) on the metal surface. Therefore, the silanol groups can interact not only among themselves (intra-condensation), but also with the hydroxyl groups on metal substrates (inter-condensation)[101]. First of all, this interaction will be through temporary weak hydrogen bonding. Upon drying and curing process, condensation reaction occurs

and the formation of strong covalent metallo-siloxane bonds takes place[101, 120], according to:

$$\text{Si-OH}_{\text{(Solution)}} + \text{M-OH}_{\text{(Surface)}} \rightleftharpoons \text{Si-O-M}_{\text{(Interface)}} + H_2O \qquad \text{(Eq. 1.8)}$$

According to many authors, there is a general accepted bonding mechanism of silanes to metal surfaces[84, 100, 120-122], which is represented in Figure 1.10.

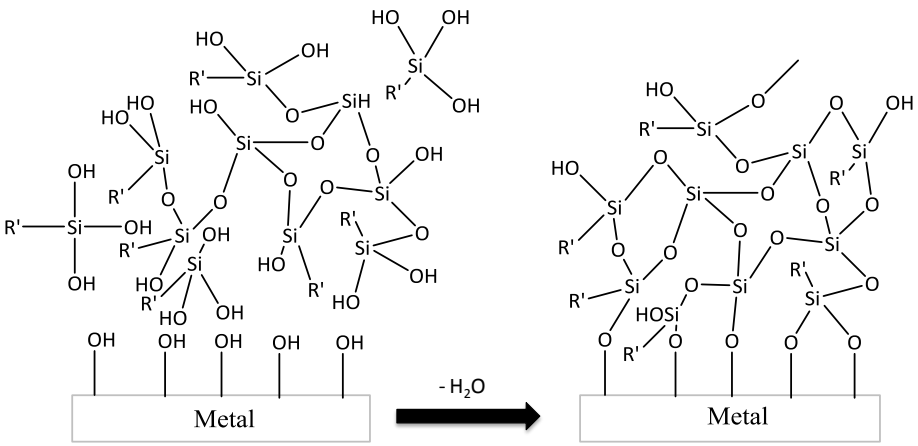

Figure 1.10. Covalent bonding between sol-gel coating and metal substrate.

Me-O-Si covalent bond is assumed to be responsible of the excellent adhesion between sol-gel coatings and metal surfaces. This behaviour is of great interest, since one of the most serious drawbacks of coated implants *in vivo* is the delamination of the coating due to a poor adhesion strength, which may lead to the failure of dental implant treatment.

1.5.3. Sol-Gel derived coating techniques

One of the most technologically important aspects of sol-gel processing is that prior to gelation, the fluid sol or solution is ideal for preparing films on different surfaces[83]. After starting the hydrolysis and condensation reactions and once the sol is obtained, it can be applied on the surface of a metallic substrate by different methods, where the two main techniques are dip-coating and spin-coating. Finally, the gel will be formed and the heat treatment will lead to the film densification (Figure 1.11).

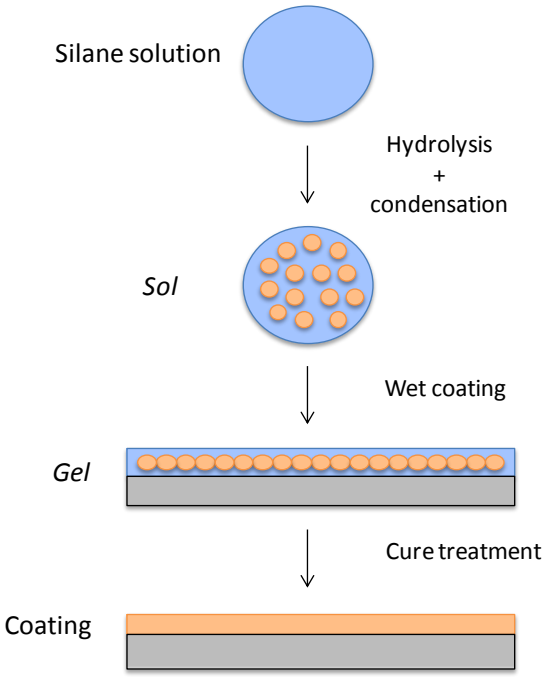

Figure 1.11. Scheme of the process to obtain sol-gel coatings.

1) Dip-Coating

Dip-coating can be described as a process where the substrate to be coated is progressively immersed into a solution (sol) and then is extracted with a well-defined withdrawal speed (Figure 1.12)[57, 83].

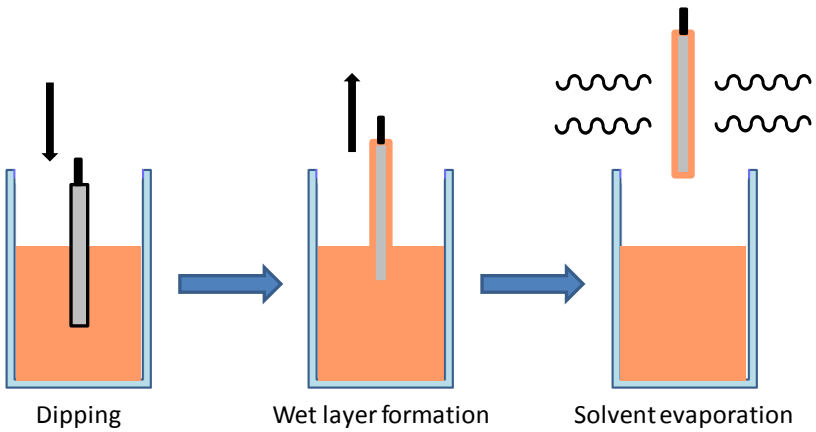

Figure 1.12. Scheme of dip-coating process.

Solvent evaporation leads to a gelation process and the formation of a transparent homogenous film is produced. This film has to be densified by thermal treatment and the temperature will depend on the composition. The coating thickness depends on the coating solution properties such as density, viscosity and surface tension, as well as withdrawal speed[123].

2) Spin-Coating

In spin-coating process the substrate spins around an axis perpendicular to the coating area at high speed in order to spread the fluid by centrifugal force (Figure 1.13). The spin coating process is carried out in different stages: deposition, spin-up, spin-off and gelation by solvent evaporation. An excess of liquid is dispensed on the surface at the first stage. During the spin-up, the liquid flows radially outward, and in the spin-off stage, excess liquid flows to the perimeter and leaves as droplets. In the last stage, evaporation takes place and a thin, homogeneous film is formed[83].

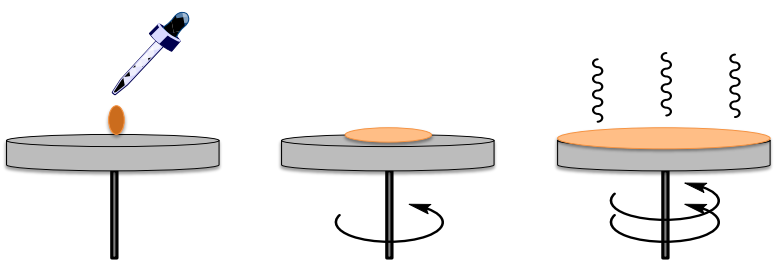

Figure 1.13. Scheme of spin-coating process.

As in the case of dip coating, film thickness will depend on various parameters like the viscosity of the sol, drying rate, surface tension and the parameters chosen for the spin process (spin speed and temperature)[123]. Higher spin speed and longer times lead to the formation of thinner films. The thickness of the film is generally smaller than that by dip-coating with the same solutions. An additional drying step is necessary for the densification of the coating.

1.6. Sol-gel coatings for biomedical applications

As it was said in section 1.3.1, titanium and its alloys are the most used metals for implant manufacturing due mainly to their excellent mechanical

properties, biocompatibility and corrosion resistance. However, some ions can be leached in the implant/bone interface producing an undesirable response. Furthermore, titanium does not possess the capacity to establish the formation of tight chemical bond with bone tissue[37].

Sol-gel derived materials have proved to be good biomaterials to obtain coatings on metallic surfaces and enhance the bioactivity of the surface. The low processing temperature of sol-gel technology combined with the intrinsic biocompatibility and environmental friendliness makes it an ideal candidate for the fabrication of bioactive materials[124]. A bioactive material is defined as a material that elicits a specific response at the interface of the material, which results in the formation of a bond between the tissue and the material[125].

This section will be focused on the advantage of the use of silica-based bioactive coating, owing to silicon which has a beneficial role in bone formation *in vivo*[126], and the potential applications of these biomaterials due to the low temperature processing that allows to incorporate various biomolecules during the formation of the gel[124].

1.6.1. Bioactive silica-based sol-gel coatings

Coatings for metal implants in bone applications should not only provide a protective layer but should also take an active part in the bone reconstruction process. This property, termed bioactivity, involves the formation of a HA layer on the surface that will promote a strong bond between the living tissue and the implants[127].

At this point, the most commonly used material was HA. Its mechanical strength is fairly poor and therefore, for many purposes, bulk materials cannot be used as implants. In order to obtain bioactive materials with high mechanical strength, metal implants are coated with a thin layer of HA using plasma spray technique. However, as said previously in section 1.3.2.2, there are some important drawbacks as the lack of exact stoichiometry and the occurrence of glassy phases in the ceramic layer (some of them do not show bioactive behaviour or dissolve in biological environment[124]), and the weak bonding strength between the HA layer and implant, what may lead to delamination. For that reason, sol-gel was chosen as method to obtain bioactive HA coatings. Dip coating of substrates using viscous

precursors' solutions and subsequent drying and sintering is a method of choice for the formation of thin fully dense HA coatings[126].

Balamurugan *et al*[128] prepared these types of films onto prefinished low carbon 316L stainless steel using alkoxide based sol-gel technique. Their experimental results revealed that the crystallinity, microstructure corrosion resistance and morphology of the coatings prove the formation of HA coating appropriate for biomedical applications.

Gan and Pillar, synthesized and characterized thin sol-gel CaP films on porous surface Ti6Al4V implants[129], and they evaluated the *in vivo* behaviour by placing them in distal femoral rabbit condyle sites. The study showed that films significantly enhance the rate of bone ingrowths compare to Ti6Al4V implant without coating[130].

Titanium (grade 2) discs' surface was modified with HA films by a sol-gel method by Kim et al[131]. They studied the influence of the crystallinity of the HA layer on cell response obtaining that human osteoblast-like (HOS) cells attached to higher degree on the HA films with higher crystallinity, what also improved ALP and osteocalcin OC expression. However, the time to obtain these gels was too long and the response compared to Ti without treatment in some cell studies was not significant enough.

In spite of good results obtained by different groups there is a general concern about the use of HA as coating due to the poor bond strength and insufficient chemical stability. For that reason various silicate coatings have been proposed for the improvement of different properties such as bioactivity, bone bonding and adhesive bonding ability to the substrate. The surface dissolution and the breakdown of silica network form silanol groups (Si-OH) that repolymerize to form a hydrated, high surface-area and silica-rich layer. This surface enhances the migration of Ca^{2+} and PO_4^{3-} groups to the surface forming an amorphous layer, which is further crystallized in a hydroxycarbonate apatite (HCAp) layer[126].

Yoshida *et al.*[132, 133], prepared silica sol-gel coatings on titanium-based implants by sol-gel dipping process with excellent surface properties. The formed films, using TEOS as silicon precursor, resulted in high bond strength to the metal

substrate and extremely small amounts of metallic ion release, proving that they may be useful as materials for dental implantology.

Vitreous coatings of SiO_2-CaO system were prepared on Ti6Al4V substrates by the sol-gel method by Izquierdo-Barba *et al.*[134, 135], using TEOS as silicon precursor. Their reactivity in simulated body fluid SBF and osteoblast cell culture was assessed. They found that textural parameters of the coatings (porosity and roughness) and thickness of the films obtained increased when the concentration of the precursor solutions was raised, and consequently cell functions (attachment, spreading, proliferation and differentiation) were enhanced. They concluded that the behaviour of these coatings makes them potential candidates for clinical applications.

Nanoporous silica films prepared by sol-gel processing coupled with evaporation-induced self assembly (EISA) technique were prepared on titanium surface for the first time by Gomez-Vega *et al.*[136, 137]. These coatings exhibited the ability to form apatite when soaked in SBF, and this was attributed to the nanoporous structure and to the presence of abundant silanol groups. However they did not report the effect on the osteogenic behaviour of bone-forming cells. Inzunza *et al.*[138] showed later, the ability of these coatings, especially the ones doped with calcium and phosphate, to promote the osteogenic differentiation of human bone marrow mesenchymal stem cells.

Another way to obtain bioactive coatings was described by Ääritalo *et al.*[139], where sol-gel derived TiO_2-SiO_2 mixed oxide coatings consisting of 10-100% SiO_2 were prepared on titanium substrates, by carefully controlling the process parameters to obtain silicon-releasing coatings. Silicon release was observed to be dependent on the SiO_2 amount added to the gel, and calcium phosphate was able to nucleate on the coatings. However, they suggested that the apatite layer formed on TiO_2 does not ensure the direct interaction coating-tissue, for that reason they proposed to add SiO_2 as osteoinductive material. In further cell studies, they observed prolonged osteoblast activity on the coatings as a function of increased amount of released silicon[140].

Next step on the finding of a suitable surface for enhancing osseointegration would combine the properties of these inorganic bioactive coatings with the

advantages of the incorporation of an organic component, such as controlling the flexibility, hydrophobicity, stability or the functionalization of the network.

1.6.2. Bioactive organically modified silicates

The low process temperature of inorganic materials using the versatile sol-gel techniques allows producing inorganic/organic hybrid materials with improved and tunable properties. The molecular interaction and bonding between two phases will determine the final properties of the material. There can be two type of hybrids: Class I, where bonding is through weak forces (Van de Waals, hydrogen or ionic bonding between inorganic and organic component), and the Class II where phases are bound by strong covalent bonds (use of organosilanes)[141].

The simplest organoalkoxysilane is methyltrimethoxysilane (MTMOS), where a methyl group is introduced by covalent bonding in the final network. Beganskiene *et al.*[142], prepared and characterized modified sol-gel derived silica coatings in which amino and methyl groups were introduced onto the colloidal silica by using (3-aminopropyl) triethoxysilane (APTES) and MTMOS respectively. They found that methyl-modified coating was the best substrate for cell proliferation.

Ballarre *et al.*[143] found a beneficial behaviour when coating stainless steel with a TEOS-MTEOS-SiO_2 system. Sol-gel coatings enabled the isolation of potentially toxic ions coming from the alloy to the surrounding environment and by the incorporation of glass ceramic the formation and growth of hydroxyapatite layer was promoted.

Another way to overcome the weakness of silica inorganic materials is the incorporation of a natural polymer as is the case of chitosan. Jun *et al.*[144], hybridized a silica xerogel, TMOS, with chitosan for use it as coating on commercially pure titanium (cpTI) discs. They conclude that due to silicon ion in the xerogel, coatings were able to promote a rapid apatite formation. As the silica content in the hybrid was increased cell adhesion and ALP activity were enhanced.

Catauro *et al.*[145], synthesized class I organic/inorganic materials by sol-gel method from a solution containing TEOS and different percentages of (ε-caprolactone) (PCL). The entrapment of PCL, improved the coating elasticity achieving crack-free coatings. However, the main contribution to the biocompatibility was provided by the inorganic component.

For most medical applications, both components of the network should be cross-linked in order to improve its mechanical properties and control its biodegradability. This may be achieved by the use of an organofunctional alkoxysilanes. The use of these types of materials in literature is limited to applications such as scaffolds or membranes.

Ren *et al.*[146, 147] prepared biodegradable gelatin-siloxane hybrid scaffolds by covalently crosslinking gelatin with GPTMS. The epoxy end group of GPTMS molecule reacted with one of the amino acid residues of gelatin chain (Eq. 1.7), and the rate of biodegradation of hybrids was controlled by the GPTMS content. These hybrids showed bioactivity due to the existence of silanol groups derived from GPTMS and the incorporation of Ca^{+}.

Tsuru *et al.*[148] prepared gelatin-GPTMS-TEOS hybrid scaffolds. Silicon release was controlled by GPTMS-TEOS rate. They found these hybrids as useful materials to prepare scaffolds that stimulate cell differentiation and tissue regeneration.

Shiroshaki *et al.*[149] made an extensive work on materials based on GPTMS-chitosan. In one of their first works, they compared the *in vitro* behaviour of three hybrid membranes: chitosan, chitosan-GPTMS and chitosan-GPTMS-Ca. They found that the addition of Ca(II) improved the wettability, but also reduced the release of Si(IV) which seemed to have higher impact on cell proliferation. Later, they compared the performance of hybrids with different amounts of GPTMS finding that attachment, proliferation and function of osteoblastic like cells were greatly improved in the hybrids as compared to chitosan[150]. That is, the Si-OH and Si-O-Si groups derived from GPTMS favoured cell behaviour.

In subsequent studies, this group, introduced TEOS in order to increase the silicon release, and its effect on proliferation and differentiation of MG63 osteoblastic cells was assessed. MG63 cells were much proliferated in chitosan-GPTMS hybrid membranes than on chitosan-GPTM-TEOS, whereas on the ALP activity inverse effects were observed[151]. Therefore, they concluded that Si(IV) release decreased cell proliferation rate, while it promoted cell differentiation.

This review shows the potential use of organic-inorganic coatings for metal implants due to the possibility of tailoring properties of the produced material and the incorporation of different molecules in the network.

1.6.3. Silicon effect

It has been mentioned in prior sections the importance of having Si-OH groups on the surface of the coating for enhancing bioactivity and osteocompatibility, as well as the beneficial effect of silicon release. This behaviour is going to be explained in more detail in this section.

It has been proposed by many authors that hydrated silica plays an important role in forming a biologically active apatite layer on the surfaces of bioactive glasses and glass-ceramics in the body, and all of them agree on the important role of silanol groups in the surface acting as nucleation points for HA[152]. The sequence of interfacial reactions between bone and bioactive glasses is shown in Figure 1.14, proposed by Hench *et al.*[153]

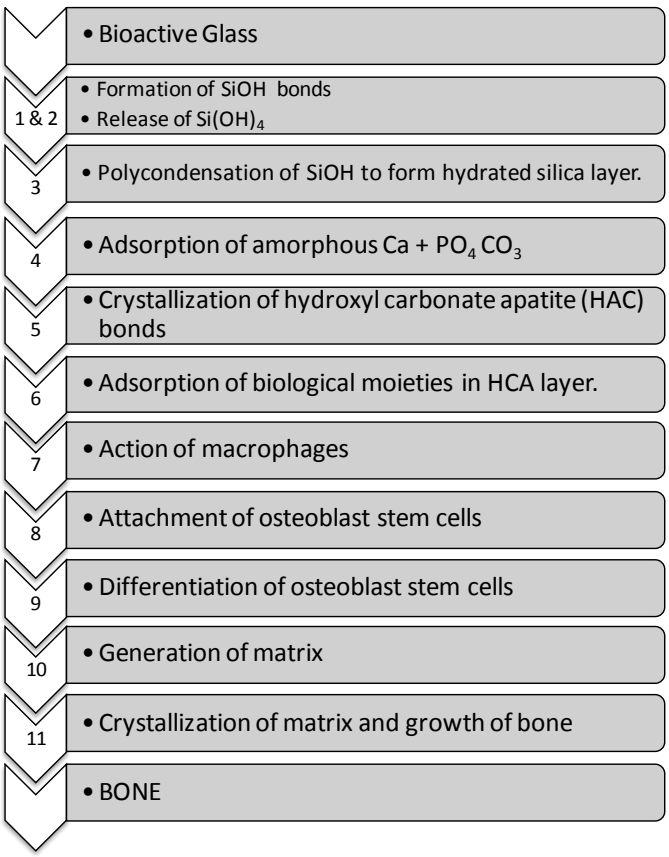

Figure 1.14. Scheme of HA formation on biomaterial surface.

Kokubo *et al.*[154-156] have extensively studied the ability of apatite forming of different bioactive glasses. Furthermore, they showed that pure silica hydrogel, obtained by the sol-gel process of TEOS, induced the formation of bone-like apatite on its surface when soaked in SBF with ion concentration nearly equal to those in human blood plasma.

The potential mechanism of apatite formation on the surface is presented in Figure 1.15. Water molecules in the SBF react with the Si-O-Si bond to form Si-OH groups. These Si-OH groups induced apatite nucleation by first combining with the calcium ions from the solution to form an amorphous calcium silicate on the surface, and then creating a cluster of amorphous carbonate apatite by assembling further phosphate, carbonate and calcium ions. With soaking time, the amorphous carbonate apatite will grow into crystalline carbonate apatite[157, 158].

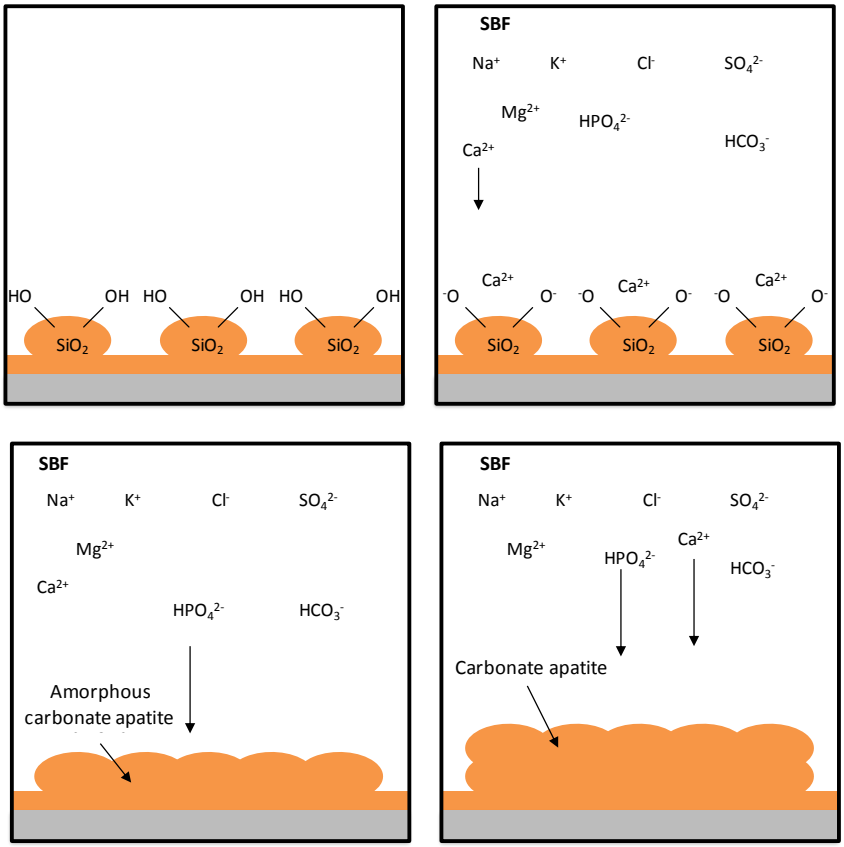

Figure 1.15. HA formation mechanism mediated by silanol groups on the surface.

Moreover, silica based sol-gel materials are resorbable, and their dissolution via hydrolysis reaction is presented in (Eq. 1.9)[159]. These dissolution products are non-toxic at low concentrations and have been found to be stimulatory to bone-forming cells[160].

$$SiO_2\,(s) \quad + \quad 2H_2O \longrightarrow Si(OH)_4\,(aq) \qquad \text{(Eq 1.9)}$$

Silicon is an essential trace element existing in many organisms, and the lack of it may lead to bone diseases and joint diseases. The role of Si in bone mineralization has been largely investigated. In early 1970s, Carly *et al.* reported that silicon deficiency in chicks and rats led to abnormally shaped bones and defective cartilaginous tissue, both of which were restored upon the addition of soluble silica to their diet. Si could promote bone mineralization. Related studies also found that Si is able to increase extracellular matrix of connective tissue, thus it has been suggested that Si may be involved in the synthesis and stabilization of the collagen matrix. The exact nature of the association between Si and collagen is not clear, although a number of possible mechanism have been suggested[161, 162].

Reffit *et al.*[163], found that physiological concentrations of orthosilicic acid, $Si(OH)_4$, stimulated collagen type I synthesis in human osteoblastic-like cells and promote osteoblastic differentiation. They suggested that Si may act as a cofactor for enzymes involved in collagen synthesis, including prolyl hydroxylases. A critical step in collagen type I synthesis and its secretion into the extracellular space is the hydroxylation of the proline residues of the collagen chains, a reaction catalyzed by propyl hydroxylase (P4H). It was reported that optimal activity of this enzyme appears to depend on the presence of adequate concentrations of Si.

Qiu *et al.*[162] studied silica-doped hydroxyapatite and its promotive effect on bone mineralization. The mechanism proposed, as well as Reffit, was based on enhancing the bioactivity of P4H enzyme by Si. On rough endoplasmatic reticulum (RER), P4H hydroxylate proline of precollagen (peptide chains) into hydroxyproline (a characteristic amino acid of collagen) to form procollagen. In this hydroxylation, Fe^{2+} is an important cofactor. However, the binding site of Fe^{2+} could be competitively bond by Al^{3+}, inhibiting enzyme activity. When the SiO_4^{4-} dissolved from surface, enters in cell and reaches RER, is able to react with Al^{3+} to form aluminosilicate and,

in that way, relieves the inhibitory effect on P4H activity. Figure 1.16 shows this mechanism.

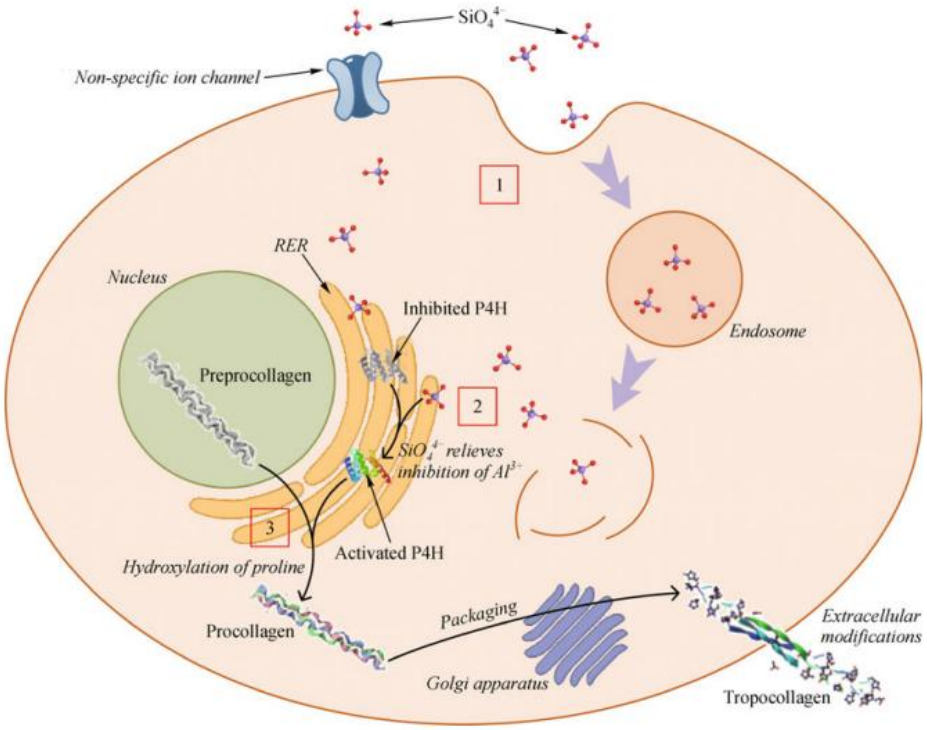

Figure 1.16. Schematic diagram of probable PH4 pathways that Si promotes biosynthesis of collagen[162].

More recently, Jugdaosingh *et al.*[164] hypothesized that Si may play a crucial role in forming cross-links between procollagen chains during collagen synthesis and between collagen units in the extracellular matrix.

1.6.4. Sol-gel coatings as release systems

The sol-gel derived materials provide excellent matrices for entrapping a variety of biologically important molecules. The organics introduced in, do not need to be a component of the network, the sol-gel can work as a carrier for the control release of different biomolecules.

Since 1990, when Braun *et al.* described the properties of entrapping enzymes in TEOS-derived sol-gel matrices, the use of these materials rapidly extended to other fields such as antibodies, proteins, growth factors, drugs or biocides[89]. The addition of these molecules can be done before or after the sol is formed, and with the drying process, the entrapment will be achieved. The possibility of tailoring characteristics of the network such as thickness, hydrophobicity or pore size by controlling parameters of the synthesis (selection or silica precursor, catalyst, solvents, temperature or condensation and drying) makes these materials of interest for the design of drug delivery systems.

Controlled release materials are designed to deliver controlled amounts of therapeutic agents to specific target sites over extended duration of time. It is usually desirable to release an initial large concentration of drugs post-operatively, followed by a steady long-term release. This could be the case of anti-inflammatory drugs or bactericidal molecules. Moreover, the local delivery eliminates the risks of side effect associated with oral or parenteral therapies, and also improves the efficacy of the treatment by achieving higher concentration at the desired site[165].

Bacterial infection due to an implanted medical device is a potential serious complication that may lead to premature implant removal, which is costly, traumatic to the patient and might be lethal[124]. Despite the effort for using preventive procedures such as sterilization, meticulous surgical procedures and following proper infection control guidelines, invasion of bacteria can be found at almost 90% of implantation site immediately after surgery.

The entrapment of an antimicrobial agent in the sol-gel matrix is an interesting possibility to avoid post-operatory infections. Radin *et al.*[166] prepared TEOS-based thin sol-gel coatings on a Ti-alloy substrate which contained Vancomycin, a potent antibiotic used in treating osteomyelitis. They studied the effect of processing parameters on matrix degradation and vancomycin release, finding a close correlation between release and degradation rates. The bactericidal properties suggested great potential to prevent and treat bone infections in clinical settings.

Silver is another extensively used bactericidal agent. Several studies have shown that silver or silver ions have a broad-spectrum antibacterial activity and that sol-gel coating process is an effective procedure to develop antimicrobial coatings to

release these particules[167, 168]. Jeon *et al.* prepared silver-doped TEOS-derived silica films by the sol-gel process showing an antibacterial effect.

These works are just some examples of the potential use of silica-based sol-gel coatings as matrixes for the entrapment of biomolecules to promote bone formation and avoid infections after implantation.

1.7. Objectives

After all the previously presented, it is clear the need of finding new systems that promote and accelerate the osseointegration process of dental implants in the first stages after the implantation in order to ensure the success of the treatment and enhance the post-operatory recovering of patients. There is also the need of finding systems that induce bone formation thinking about patients with poor bone regeneration ability; that is the case of old people, smokers or chronic ill people (osteoporotic patients).

As it has been reported, dental implantology market is being globally expanding and the research in this field is being carried out by many groups. However, in spite of the numerous techniques proposed for titanium surface modification and improvement, due to different limitations there is still a real need of continuing the search in order to obtain and design a simple, cost-effective and marketable technique to treat implant surfaces.

In this context, the main aim of this work is the development of coatings obtained by the silica sol-gel process, which must be able to promote bone formation in order to overcome the limitations mentioned above, and also could be used as matrix for the entrapment of different biomolecules for enhancing the cell adhesion properties of the coating and the general behaviour of it. The advantages that these materials can offer are:

- Sol-gel method provides strong adhesion between coating and titanium substrate. This will avoid delamination problems associated to other surface modification methods, as well as an initial protective barrier against the release of undesirable particles to the surrounding environment.
- Siloxane network will be resorbable *in vivo*. The degradation rate may be tailored by the used of different organoalkoxysilane precursors and controlling different parameters of the synthesis.

- During the hydrolytic degradation, silicon will be released, which is believed to induce bone formation.
- This method will allow the incorporation of biologically active molecules as part of the network.

To get these objectives, work was structured in the next way:

1) Selection of the appropriate alkoxysilane precursors with different organic chains and functionalization in order to control matrix characteristics, and establish and optimize synthesis parameters to obtain homogenous, uniform and crack-free coatings.

2) Synthesis and characterization of two different binary coatings were both of them will have in common the use of MTMOS as basis material. On one hand, different amounts of TEOS will be added to the matrix to increase the inorganic character and the hydrophilicity of the network, and to control the degradation rate and silicon release. On the other hand, functionality will incorporated to the MTMOS sol-gel coating by adding GPTMS in various molar rates. The steps in this stage will be:

    - Development of coatings and complete morphological and chemical characterization, study of the degradability and silicon release rate *in vitro*, and evaluation of the corrosion protection ability.
    - Study of the cellular viability, proliferation and differentiation.
    - Selection of one coating from each group for study the biocompatibility and osseointegration *in vivo*.

3) Development of a new family of hybrid coatings using the chosen matrixes in the previous step and adding different amounts of a bioactive molecule. Gelatine will be incorporated due to its cell adhesion properties and biocompatibility, degradability *in vivo* and because it is obtained from collagen, which is main constituent of all extracellular matrix of all tissues, but is more practical from a material processing point of view.

    - Synthesize and characterize coatings with different amounts of gelatin. In one type, gelatin will be physically entrapped, while in the other type it will be covalently linked to the siloxane network through the epoxy groups of GPTMS.

- Evaluate the ability of these coatings to adsorb different proteins presented in blood serum, which plays a crucial role in subsequent cell attachment.
- Study cell viability, proliferation and differentiation by different methods and different cell lines.
- Selection of the best materials for the *in vivo* study.

Thus, in the present work all the process involved in the development and design of new materials will be covered; starting from the selection and evaluation of the basic materials, followed by the design of more complex hybrid materials to fulfill the desired properties, and their complete characterization, and arriving to final *in vivo* evaluation. The work methodology is presented in Figure 1.17.

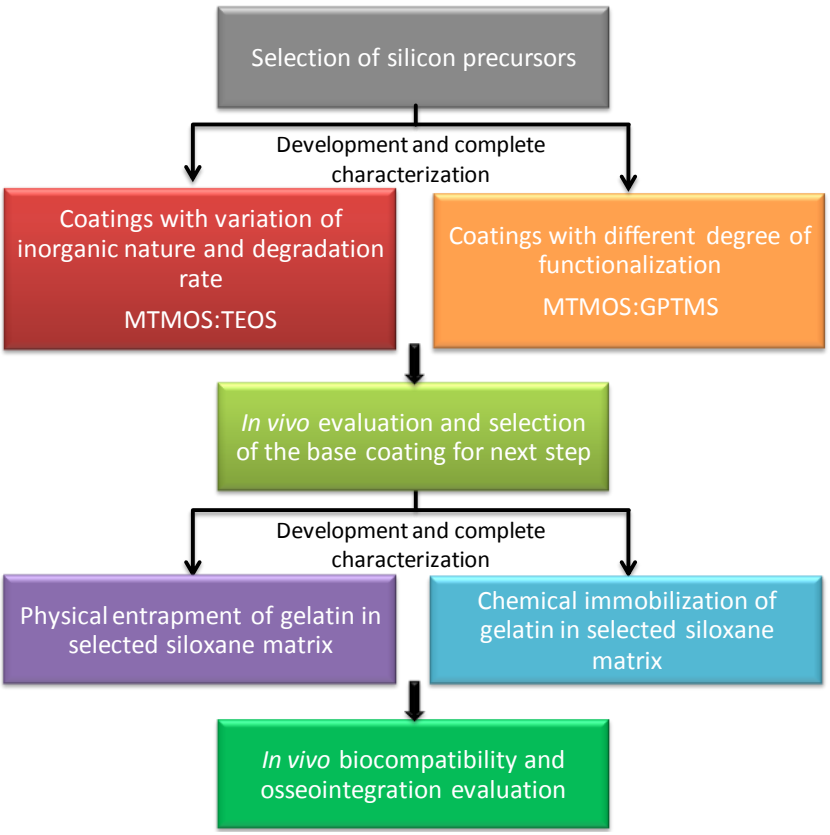

Figure 1.17. Schematic representation of used methodology to achieved the different objectives of the planning of this thesis.

References

1. Sastre R, San Román J, de Aza S. *Biomateriales.* Faenza Editrice Ibérica, 2004.

2. Williams DF. On the nature of biomaterials. *Biomaterials.* 2009; **30:** 5897-909.

3. Park J, Lakes RS. *Biomaterials: An Introduction.* Springer Science & Business Media, 2007.

4. Shi D. *Biomaterials and Tissue Engineering.* Springer, 2004.

5. Gaviria L, Salcido JP, Guda T et al. Current trends in dental implants. *Journal of the Korean Association of Oral and Maxillofacial Surgeons.* 2014; **40:** 50-60.

6. Ratner BD, Hoffman AS, Schoen FJ et al. Introduction - biomaterials science: An evolving, multidisciplinary endeavor. In: Lemons,Buddy D.RatnerAllan S.HoffmanFrederick J.SchoenJack E. ed. Biomaterials Science (Third Edition). Academic Press, 2013; xxv-xxxix.

7. Peñarrocha Diago M. *Implantología Oral.* Barcelona: Ars medica, 2001.

8. Abraham C. A brief historical perspective on dental implants, their surface coatings and treatments. . *The Open Dentistry Journal.* 2014; **8:** 50-55.

9. de Anitua Aldecoa E. *Manual Quirúrgico :Implantología Oral.* Team Work Media España, 2013.

10. Brunette DM. *Titanium in Medicine :Material Science, Surface Science, Engineering, Biological Responses, and Medical Applications.* Springer, 2001.

11. Brånemark P, Zarb G, Albrektsson T. *Prótesis Tejido-Integradas: La Oseointegración En La Odontología Clínica.* Barcelona: Quintessence, 1999.

12. Albrektsson T, Zarb GA. Current interpretations of the osseointegrated response: Clinical significance. *Int J Prosthodont.* 1993; **6:** 95-105.

13. Albrektsson T, Johansson C. Osteoinduction, osteoconduction and osseointegration. *European Spine Journal.* 2001; **10:** S96-S101.

14. Robbins SL, Kumar V, Cotran RS. *Pathologic Basis of Disease.* W. B. Saunders, 1984.

15. Hernández-Gil IF, Gracia MAA, del Canto Pingarrón M et al. Bases fisiológicas de la regeneración ósea I. histología y fisiología del tejido óseo. *Medicina Oral.* 2006; **11:** E47-51.

16. Sela JJ, Bab IA. *Principles of Bone Regeneration.* Springer Science & Business Media, 2012.

17. Williams D. *Essential Biomaterials Science.* Cambridge: Cambridge University Press, 2014.

18. Branemark P. Osseointegration and its experimental background. *J Prosthet Dent.* 1983; **50:** 399-410.

19. Albrektsson T, Brånemark P, Hansson H et al. Osseointegrated titanium implants: Requirements for ensuring a long-lasting, direct bone-to-implant anchorage in man. *Acta Orthopaedica.* 1981; **52:** 155-70.

20. Schenk RK, Buser D. Osseointegration: A reality. *Periodontol 2000.* 1998; **17:** 22-35.

21. Wennerberg A, Albrektsson T. Effects of titanium surface topography on bone integration: A systematic review. *Clin Oral Implants Res.* 2009; **20:** 172-84.

22. Rupp F, Gittens RA, Scheideler L et al. A review on the wettability of dental implant surfaces I: Theoretical and experimental aspects. *Acta Biomaterialia.* 2014; **10:** 2894-906.

23. Gittens RA, Scheideler L, Rupp F et al. A review on the wettability of dental implant surfaces II: Biological and clinical aspects. *Acta Biomaterialia.* 2014; **10:** 2907-18.

24. Klokkevold PR, Han TJ. How do smoking, diabetes, and periodontitis affect outcomes of implant treatment? *Int J Oral Maxillofac Implants.* 2007; **22 Suppl:** 173-202.

25. Koldsland OC, Scheie AA, Aass AM. Prevalence of implant loss and the influence of associated factors. *J Periodontol.* 2009; **80:** 1069-75.

26. Adell R, Lekholm U, Rockler B et al. A 15-year study of osseointegrated implants in the treatment of the edentulous jaw. *Int J Oral Surg.* 1981; **10:** 387-416.

27. Arango S, Peláez-Vargas A, García C. Coating and surface treatments on orthodontic metallic materials. *Coatings.* 2012; **3:** 1-15.

28. ASTM F67-13, standard specification for unalloyed titanium, for surgical implant applications (UNS R50250, UNS R50400, UNS R50550, UNS R50700), ASTM international, west conshohocken, PA, 2013, www.astm.org.

29. Liao H, Wurtz T, Li J. Influence of titanium ion on mineral formation and properties of osteoid nodules in rat calvaria cultures. *J Biomed Mater Res.* 1999; **47:** 220-7.

30. Matusiewicz H. Potential release of in vivo trace metals from metallic medical implants in the human body: From ions to nanoparticles – A systematic analytical review. *Acta Biomaterialia.* 2014; **10:** 2379-403.

31. Wachi T, Shuto T, Shinohara Y et al. Release of titanium ions from an implant surface and their effect on cytokine production related to alveolar bone resorption. *Toxicology.* 2015; **327:** 1-9.

32. Puleo DA, Huh WW. Acute toxicity of metal ions in cultures of osteogenic cells derived from bone marrow stromal cells. *Journal of Applied Biomaterials.* 1995; **6:** 109-16.

33. Thompson G, Puleo D. Ti-6Al-4V ion solution inhibition of osteogenic cell phenotype as a function of differentiation timecourse in vitro. *Biomaterials.* 1996; **17:** 1949-54.

34. Sun ZL, Wataha JC, Hanks CT. Effects of metal ions on osteoblast-like cell metabolism and differentiation. 1997; .

35. Mine Y, Makihira S, Nikawa H et al. Impact of titanium ions on osteoblast-, osteoclast-and gingival epithelial-like cells. *Journal of Prosthodontic Research.* 2010; **54:** 1-6.

36. Subramani K, Ahmed W. *Emerging Nanotechnologies in Dentistry: Processes, Materials and Applications.* William Andrew, 2011.

37. Le Guéhennec L, Soueidan A, Layrolle P et al. Surface treatments of titanium dental implants for rapid osseointegration. *Dental Materials.* 2007; **23:** 844-54.

38. Browne M, Gregson P. Effect of mechanical surface pretreatment on metal ion release. *Biomaterials.* 2000; **21:** 385-92.

39. Ong JL, Carnes DL, Bessho K. Evaluation of titanium plasma-sprayed and plasma-sprayed hydroxyapatite implants in vivo. *Biomaterials.* 2004; **25:** 4601-6.

40. Anil S, Anand PS, Alghamdi H et al. Dental implant surface enhancement and osseointegration. In: Ilser Turkyilmaz ed. *Implant Dentistry - A Rapidly Evolving Practice*. InTech, 2011; .

41. Aparicio C, Gil FJ, Fonseca C et al. Corrosion behaviour of commercially pure titanium shot blasted with different materials and sizes of shot particles for dental implant applications. *Biomaterials.* 2003; **24:** 263-73.

42. Massaro C, Rotolo P, De Riccardis F et al. Comparative investigation of the surface properties of commercial titanium dental implants. part I: Chemical composition. *J Mater Sci Mater Med.* 2002; **13:** 535-48.

43. Zinger O, Anselme K, Denzer A et al. Time-dependent morphology and adhesion of osteoblastic cells on titanium model surfaces featuring scale-resolved topography. *Biomaterials.* 2004; **25:** 2695-711.

44. Wong M, Eulenberger J, Schenk R et al. Effect of surface topology on the osseointegration of implant materials in trabecular bone. *J Biomed Mater Res.* 1995; **29:** 1567-75.

45. Cho S, Park K. The removal torque of titanium screw inserted in rabbit tibia treated by dual acid etching. *Biomaterials.* 2003; **24:** 3611-7.

46. Yokoyama K, Ichikawa T, Murakami H et al. Fracture mechanisms of retrieved titanium screw thread in dental implant. *Biomaterials.* 2002; **23:** 2459-65.

47. Sul Y, Johansson CB, Röser K et al. Qualitative and quantitative observations of bone tissue reactions to anodised implants. *Biomaterials.* 2002; **23:** 1809-17.

48. Gupta A, Dhanraj M, Sivagami G. Status of surface treatment in endosseous implant: A literary overview. *Indian J Dent Res.* 2010; **21:** 433-8.

49. Elias CN, Oshida Y, Lima JHC et al. Relationship between surface properties (roughness, wettability and morphology) of titanium and dental implant removal torque. *Journal of the Mechanical Behaviour of Biomedical Materials.* 2008; **1:** 234-42.

50. Ponsonnet L, Reybier K, Jaffrezic N et al. Relationship between surface properties (roughness, wettability) of titanium and titanium alloys and cell behaviour. *Materials Science and Engineering: C.* 2003; **23:** 551-60.

51. Daculsi G, Laboux O, Malard O et al. Current state of the art of biphasic calcium phosphate bioceramics. *J Mater Sci Mater Med.* 2003; **14:** 195-200.

52. Ballo AM, Omar O, Xia W et al. Dental implant surfaces – physicochemical properties, biological performance, and trends. In: Turkyilmaz I ed. Implant Dentistry - A Rapidly Evolving Practice. InTech, 2011; .

53. Davies JE. Understanding peri-implant endosseous healing. *J Dent Educ.* 2003; **67:** 932-49.

54. Coelho PG, Granjeiro JM, Romanos GE et al. Basic research methods and current trends of dental implant surfaces. *Journal of Biomedical Materials Research Part B: Applied Biomaterials.* 2009; **88:** 579-96.

55. Radin S, Ducheyne P. Plasma spraying induced changes of calcium phosphate ceramic characteristics and the effect onin vitro stability. *J Mater Sci Mater Med.* 1992; **3:** 33-42.

56. Yoshinari M, Hayakawa T, Wolke G et al. Influence of rapid heating with infrared radiation on RF magnetron-sputtered calcium phosphate coatings. 1997; .

57. Attia SM, Wang J, Wu G et al. Review on sol-gel derived coatings: Process, techniques and optical applicat. *J. Mater. Sci. Technol.* 2002; **18:** 211-217.

58. Xu W, Hu W, Li M et al. Sol–gel derived hydroxyapatite/titania biocoatings on titanium substrate. *Mater Lett.* 2006; **60:** 1575-8.

59. Roop Kumar R, Wang M. Functionally graded bioactive coatings of hydroxyapatite/titanium oxide composite system. *Mater Lett.* 2002; **55:** 133-7.

60. Wang D, Chen C, Liu X et al. Effects of sol–gel processing parameters on the phases and microstructures of HA films. *Colloids and Surfaces B: Biointerfaces.* 2007; **57:** 237-42.

61. Wang C, Ma J, Cheng W et al. Thick hydroxyapatite coatings by electrophoretic deposition. *Mater Lett.* 2002; **57:** 99-105.

62. Xiao XF, Liu RF. Effect of suspension stability on electrophoretic deposition of hydroxyapatite coatings. *Mater Lett.* 2006; **60:** 2627-32.

63. Stoch A, Brożek A, Kmita G et al. Electrophoretic coating of hydroxyapatite on titanium implants. *J Mol Struct.* 2001; **596:** 191-200.

64. Kokubo T, Kushitani H, Sakka S et al. Solutions able to reproduce in vivo surface-structure changes in bioactive glass-ceramic A-W3. *J Biomed Mater Res.* 1990; **24:** 721-34.

65. Chen X, Li Y, Hodgson PD et al. Microstructures and bond strengths of the calcium phosphate coatings formed on titanium from different simulated body fluids. *Materials Science and Engineering: C.* 2009; **29:** 165-71.

66. Puleo D, Nanci A. Understanding and controlling the bone–implant interface. *Biomaterials.* 1999; **20:** 2311-21.

67. Morra M. Biochemical modification of titanium surfaces: Peptides and ECM proteins. *Eur Cell Mater.* 2006; **12:** .

68. de Jonge LT, Leeuwenburgh SC, Wolke JG et al. Organic–inorganic surface modifications for titanium implant surfaces. *Pharm Res.* 2008; **25:** 2357-69.

69. Ku Y, Chung C, Jang J. The effect of the surface modification of titanium using a recombinant fragment of fibronectin and vitronectin on cell behaviour. *Biomaterials.* 2005; **26:** 5153-7.

70. Dettin M, Conconi MT, Gambaretto R et al. Effect of synthetic peptides on osteoblast adhesion. *Biomaterials.* 2005; **26:** 4507-15.

71. Chen W, Ko C. Roughened titanium surfaces with silane and further RGD peptide modification in vitro. *Materials Science and Engineering: C.* 2013; **33:** 2713-22.

72. Zreiqat H, Akin FA, Howlett C et al. Differentiation of human bone-derived cells grown on GRGDSP-peptide bound titanium surfaces. *Journal of Biomedical Materials Research Part A.* 2003; **64:** 105-13.

73. Secchi AG, Grigoriou V, Shapiro IM et al. RGDS peptides immobilized on titanium alloy stimulate bone cell attachment, differentiation and confer resistance to apoptosis. *Journal of Biomedical Materials Research Part A.* 2007; **83:** 577-84.

74. Kämmerer P, Heller M, Brieger J et al. Immobilisation of linear and cyclic RGD-peptides on titanium surfaces and their impact on endothelial cell adhesion and proliferation. *Eur Cell Mater.* 2011; **21:** 364-72.

75. Zhu X, Eibl O, Scheideler L et al. Characterization of nano hydroxyapatite/collagen surfaces and cellular behaviours. *Journal of Biomedical Materials Research Part A.* 2006; **79:** 114-27.

76. Durrieu M, Pallu S, Guillemot F et al. Grafting RGD containing peptides onto hydroxyapatite to promote osteoblastic cells adhesion. *J Mater Sci Mater Med.* 2004; **15:** 779-86.

77. Liu Y, Enggist L, Kuffer AF et al. The influence of BMP-2 and its mode of delivery on the osteoconductivity of implant surfaces during the early phase of osseointegration. *Biomaterials.* 2007; **28:** 2677-86.

78. Lan J, Wang ZF, Shi B et al. The influence of recombinant human BMP-2 on bone–implant osseointegration: Biomechanical testing and histomorphometric analysis. *Int J Oral Maxillofac Surg.* 2007; **36:** 345-9.

79. Hunziker EB, Enggist L, Küffer A et al. Osseointegration: The slow delivery of BMP-2 enhances osteoinductivity. *Bone.* 2012; **51:** 98-106.

80. Liu Y, de Groot K, Hunziker EB. BMP-2 liberated from biomimetic implant coatings induces and sustains direct ossification in an ectopic rat model. *Bone.* 2005; **36:** 745-57.

81. Ebelmen. Ueber einige verbindungen des urans. *Justus Liebigs Ann Chem.* 1842; **43:** 286-318.

82. Ebelmen. Untersuchungen über die verbindungen der borsäure und kieselsäure mit aether. *Justus Liebigs Ann Chem.* 1846; **57:** 319-55.

83. Brinker CJ, Scherer GW. *Sol-Gel Science: The Physics and Chemistry of Sol-Gel Processing.* Boston: Academic press, 1990.

84. Wang D, Bierwagen GP. Sol–gel coatings on metals for corrosion protection. *Progress in Organic Coatings.* 2009; **64:** 327-38.

85. Wen J, Wilkes GL. Organic/inorganic hybrid network materials by the sol-gel approach. *Chemistry of Materials.* 1996; **8:** 1667-81.

86. Wright JD, Sommerdijk NA. *Sol-Gel Materials: Chemistry and Applications.* CRC press, 2001.

87. Fardad M. Catalysts and the structure of SiO2 sol-gel films. *J Mater Sci.* 2000; **35:** 1835-41.

88. Silva RF, Vasconcelos WL. Influence of processing variables on the pore structure of silica gels obtained with tetraethylorthosilicate. *Materials Research.* 1999; **2:** 197-200.

89. Avnir D, Coradin T, Lev O et al. Recent bio-applications of sol–gel materials. *Journal of Materials Chemistry.* 2006; **16:** 1013-30.

90. Milea CA, Bogatu C, Duta A. The influence of parameters in silica sol-gel process. *Bulletin of the Transilvania University of Braşov.* 2011; **4:** 59-66.

91. Collinson MM. Analytical applications of organically modified silicates. *Microchimica Acta.* 1998; **129:** 149-65.

92. Musgo J, Echeverría JC, Estella J et al. Ammonia-catalyzed silica xerogels: Simultaneous effects of pH, synthesis temperature, and ethanol:TEOS and

water:TEOS molar ratios on textural and structural properties. *Microporous and Mesoporous Materials.* 2009; **118:** 280-7.

93. Karasiński P. Influence of technological parameters on the properties of sol-gel silica films. *Opt.Appl.* 2005; **35:** 117-28.

94. Qureshi HF, Nijmeijer A, Winnubst L. Influence of sol–gel process parameters on the micro-structure and performance of hybrid silica membranes. *J Membr Sci.* 2013; **446:** 19-25.

95. Collinson MM. Recent trends in analytical applications of organically modified silicate materials. *TrAC Trends in Analytical Chemistry.* 2002; **21:** 31-9.

96. Okazaki Y, Gotoh E. Comparison of metal release from various metallic biomaterials in vitro. *Biomaterials.* 2005; **26:** 11-21.

97. Cortada M, Giner L, Costa S et al. Metallic ion release in artificial saliva of titanium oral implants coupled with different metal superstructures. *Biomed Mater Eng.* 1997; **7:** 213-20.

98. Wang G, Zreiqat H. Functional coatings or films for hard-tissue applications. *Materials.* 2010; **3:** 3994-4050.

99. Zhao J, Xia L, Sehgal A et al. Effects of chromate and chromate conversion coatings on corrosion of aluminum alloy 2024-T3. *Surface and Coatings Technology.* 2001; **140:** 51-7.

100. Zheludkevich M, Salvado IM, Ferreira M. Sol–gel coatings for corrosion protection of metals. *Journal of Materials Chemistry.* 2005; **15:** 5099-111.

101. Balgude D, Sabnis A. Sol-gel derived hybrid coatings as an environment friendly surface treatment for corrosion protection of meals and their alloys. *Journal of Sol-Gel Science and Technology.* 2012; **64:** 124-134.

102. Tiwari A, Hihara LH. Chapter 10 - sol-gel route for the development of smart green conversion coatings for corrosion protection of metal alloys. In: Tiwari A, Rawlins J, Hihara LH eds. Intelligent Coatings for Corrosion Control. Boston: Butterworth-Heinemann, 2015; 363-407.

103. Vasconcelos DCL, Carvalho JAN, Mantel M et al. Corrosion resistance of stainless steel coated with sol–gel silica. *J Non Cryst Solids.* 2000; **273:** 135-9.

104. Galliano P, De Damborenea JJ, Pascual MJ et al. Sol-gel coatings on 316L steel for clinical applications. *J Sol Gel Sci Technol.* 1998; **13:** 723-7.

105. Amato LE, López DA, Galliano PG et al. Electrochemical characterization of sol–gel hybrid coatings in cobalt-based alloys for orthopaedic implants. *Mater Lett.* 2005; **59:** 2026-31.

106. Conde A, Durán A, de Damborenea JJ. Polymeric sol–gel coatings as protective layers of aluminium alloys. *Progress in Organic Coatings.* 2003; **46:** 288-96.

107. Gallardo J, Galliano P, Duran A. Bioactive and protective sol-gel coatings on metals for orthopaedic prostheses. *J Sol Gel Sci Technol.* 2001; **21:** 65-74.

108. Voevodin NN, Kurdziel JW, Mantz R. Corrosion protection for aerospace aluminum alloys by modified self-assembled NAnophase particle (MSNAP) sol–gel. *Surface and Coatings Technology.* 2006; **201:** 1080-4.

109. Metroke TL, Kachurina O, Knobbe ET. Spectroscopic and corrosion resistance characterization of amine and super acid-cured hybrid organic–inorganic thin films on 2024-T3 aluminum alloy. *Progress in Organic Coatings.* 2002; **44:** 185-99.

110. Smarsly B, Garnweitner G, Assink R et al. Preparation and characterization of mesostructured polymer-functionalized sol–gel-derived thin films. *Progress in Organic Coatings.* 2003; **47:** 393-400.

111. Ni H, Simonsick Jr. WJ, Skaja AD et al. Polyurea/polysiloxane ceramer coatings. *Progress in Organic Coatings.* 2000; **38:** 97-110.

112. Liu Y, Sun D, You H et al. Corrosion resistance properties of organic–inorganic hybrid coatings on 2024 aluminum alloy. *Appl Surf Sci.* 2005; **246:** 82-9.

113. Hernández-Escolano M, Juan-Díaz MJ, Martínez-Ibáñez M et al. The design and characterisation of sol–gel coatings for the controlled-release of active molecules. *Journal of Sol-Gel Science and Technology.* 2012; **64:** 442-451.

114. Gallardo J, Durán A, de Damborenea JJ. Electrochemical and in vitro behaviour of sol–gel coated 316L stainless steel. *Corros Sci.* 2004; **46:** 795-806.

115. Pepe A, Galliano P, Ceré S et al. Hybrid silica sol–gel coatings on austempered ductile iron (ADI). *Mater Lett.* 2005; **59:** 2219-22.

116. Juan-Díaz MJ, Martínez-Ibáñez M, Hernández-Escolano M et al. Study of the degradation of hybrid sol–gel coatings in aqueous medium. *Progress in Organic Coatings.* 2014; **77:** 1799-806.

117. Metroke TL, Gandhi JS, Apblett A. Corrosion resistance properties of ormosil coatings on 2024-T3 aluminum alloy. *Progress in Organic Coatings.* 2004; **50:** 231-46.

118. Joshua Du Y, Damron M, Tang G et al. Inorganic/organic hybrid coatings for aircraft aluminum alloy substrates. *Progress in Organic Coatings.* 2001; **41:** 226-32.

119. Metroke TL, Kachurina O, Knobbe ET. Spectroscopic and corrosion resistance characterization of amine and super acid-cured hybrid organic–inorganic thin films on 2024-T3 aluminum alloy. *Progress in Organic Coatings.* 2002; **44:** 185-99.

120. Palanivel V, Zhu D, van Ooij WJ. Nanoparticle-filled silane films as chromate replacements for aluminum alloys. *Progress in Organic Coatings.* 2003; **47:** 384-92.

121. Zhu D, van Ooij WJ. Corrosion protection of AA 2024-T3 by bis-[3-(triethoxysilyl)propyl]tetrasulfide in sodium chloride solution.: Part 2: Mechanism for corrosion protection. *Corros Sci.* 2003; **45:** 2177-97.

122. Zhu D, van Ooij WJ. Corrosion protection of metals by water-based silane mixtures of bis-[trimethoxysilylpropyl]amine and vinyltriacetoxysilane. *Progress in Organic Coatings.* 2004; **49:** 42-53.

123. Muresan LM. Chapter 17 - corrosion protective coatings for ti and ti alloys used for biomedical implants. In: Tiwari A, Rawlins J, Hihara LH eds. Intelligent Coatings for Corrosion Control. Boston: Butterworth-Heinemann, 2015; 585-602.

124. Gupta R, Kumar A. Bioactive materials for biomedical applications using sol–gel technology. *Biomedical Materials.* 2008; **3:** 034005.

125. Cao W, Hench LL. Bioactive materials. *Ceram Int.* 1996; **22:** 493-507.

126. Chatzistavrou X, Kontonasaki E, Paraskevopoulos KM et al. 7 - sol-gel derived bioactive glass ceramics for dental applications. In: Vallittu P ed. Non-Metallic Biomaterials for Tooth Repair and Replacement. Woodhead Publishing, 2013; 194-231.

127. Hench L, Polak J, Xynos I et al. Bioactive materials to control cell cycle. *Material Research Innovations.* 2000; **3:** 313-23.

128. Balamurugan A, Balossier G, Kannan S et al. Elaboration of sol–gel derived apatite films on surgical grade stainless steel for biomedical applications. *Mater Lett.* 2006; **60:** 2288-93.

129. Gan L, Pilliar R. Calcium phosphate sol–gel-derived thin films on porous-surfaced implants for enhanced osteoconductivity. part I: Synthesis and characterization. *Biomaterials.* 2004; **25:** 5303-12.

130. Gan L, Wang J, Tache A et al. Calcium phosphate sol–gel-derived thin films on porous-surfaced implants for enhanced osteoconductivity. part II: Short-term in vivo studies. *Biomaterials.* 2004; **25:** 5313-21.

131. Kim H, Kim H, Salih V et al. Sol-gel-modified titanium with hydroxyapatite thin films and effect on osteoblast-like cell responses. *Journal of Biomedical Materials Research Part A.* 2005; **74:** 294-305.

132. Yoshida K, Kamada K, Sato K et al. Thin sol-gel-derived silica coatings on dental pure titanium casting. *J Biomed Mater Res.* 1999; **48:** 778-85.

133. Yoshida K, Tanagawa M, Kamada K et al. Silica coatings formed on noble dental casting alloy by the sol-gel dipping process. *J Biomed Mater Res.* 1999; **46:** 221-7.

134. Izquierdo-Barba I, Vallet-Regi M, Rojo J et al. The role of precursor concentration on the characteristics of SiO2-CaO films. *J Sol Gel Sci Technol.* 2003; **26:** 1179-82.

135. Izquierdo-Barba I, Conde F, Olmo N et al. Vitreous SiO 2–CaO coatings on Ti6Al4V alloys: Reactivity in simulated body fluid versus osteoblast cell culture. *Acta Biomaterialia.* 2006; **2:** 445-55.

136. Gomez-Vega J, Hozumi A, Saiz E et al. Bioactive glass–mesoporous silica coatings on Ti6Al4V through enameling and triblock-copolymer-templated sol-gel processing. *J Biomed Mater Res.* 2001; **56:** 382-9.

137. Gomez-Vega J, Hozumi A, Sugimura H et al. Ordered mesoporous silica coatings that induce apatite formation in vitro. *Adv Mater.* 2001; **13:** 822-5.

138. Inzunza D, Covarrubias C, Marttens AV et al. Synthesis of nanostructured porous silica coatings on titanium and their cell adhesive and osteogenic differentiation properties. *J.Biomed.Mater.Res.A.* 2013; **102:** 37-48.

139. Ääritalo V, Areva S, Jokinen M et al. Sol-gel-derived TiO2–SiO2 implant coatings for direct tissue attachment. part I: Design, preparation and characterization. *J Mater Sci Mater Med.* 2007; **18:** 1863-73.

140. Areva S, Ääritalo V, Tuusa S et al. Sol-gel-derived TiO2–SiO2 implant coatings for direct tissue attachment. part II: Evaluation of cell response. *J Mater Sci Mater Med.* 2007; **18:** 1633-42.

141. Poologasundarampillai G, Ionescu C, Tsigkou O et al. Synthesis of bioactive class II poly (γ-glutamic acid)/silica hybrids for bone regeneration. *Journal of Materials Chemistry.* 2010; **20:** 8952-61.

142. Beganskiene A, Raudonis R, Jokhadar SZ et al. Modified sol-gel coatings for biotechnological applications. In: *Journal of Physics: Conference Series, 2007.* p. 012050. IOP Publishing, .

143. Ballarre J, Manjubala I, Schreiner WH et al. Improving the osteointegration and bone–implant interface by incorporation of bioactive particles in sol–gel coatings of stainless steel implants. *Acta Biomaterialia.* 2010; **6:** 1601-9.

144. Jun S, Lee E, Yook S et al. A bioactive coating of a silica xerogel/chitosan hybrid on titanium by a room temperature sol–gel process. *Acta Biomaterialia.* 2010; **6:** 302-7.

145. Catauro M, Bollino F, Papale F. Surface modifications of titanium implants by coating with bioactive and biocompatible poly (ε-caprolactone)/SiO 2 hybrids synthesized via sol–gel. *Arabian Journal of Chemistry.* 2015; .

146. Ren L, Tsuru K, Hayakawa S et al. Sol–gel preparation and in vitro deposition of apatite on porous gelatin–siloxane hybrids. *J Non Cryst Solids.* 2001; **285:** 116-22.

147. Ren L, Tsuru K, Hayakawa S et al. Novel approach to fabricate porous gelatin–siloxane hybrids for bone tissue engineering. *Biomaterials.* 2002; **23:** 4765-73.

148. Tsuru K, Robertson Z, Annaz B et al. Sol-gel synthesis and in vitro cell compatibility analysis of silicate-containing biodegradable hybrid gels. *Key Eng Mat.* 2008; **361:** 447-50.

149. Shirosaki Y, Tsuru K, Hayakawa S et al. In vitro cytocompatibility of MG63 cells on chitosan-organosiloxane hybrid membranes. *Biomaterials.* 2005; **26:** 485-93.

150. Shirosaki Y, Tsuru K, Hayakawa S et al. Physical, chemical and in vitro biological profile of chitosan hybrid membrane as a function of organosiloxane concentration. *Acta Biomaterialia.* 2009; **5:** 346-55.

151. Shirosaki Y, Tsuru K, Hayakawa S et al. Effects of si (IV) released from chitosan-silicate hybrids on proliferation and differentiation of MG63 osteoblast cells. *Bioceram Dev Appl.* 2011; **1:** 1-4.

152. Pereira MM, Hench LL. Mechanisms of hydroxyapatite formation on porous gel-silica substrates. *J Sol Gel Sci Technol.* 1996; **7:** 59-68.

153. Hench LL. Chronology of bioactive glass development and clinical applications. *New Journal of Glass and Ceramics.* 2013; **3:** 67-73.

154. Li P, Ohtsuki C, Kokubo T et al. Process of formation of bone-like apatite layer on silica gel. *J Mater Sci Mater Med.* 1993; **4:** 127-31.

155. Kokubo T. Apatite formation on surfaces of ceramics, metals and polymers in body environment. *Acta Materialia.* 1998; **46:** 2519-27.

156. Li P, Ohtsuki C, Kokubo T et al. Apatite formation induced by silica gel in a simulated body fluid. *J Am Ceram Soc.* 1992; **75:** 2094-7.

157. Kokubo T, Kim H, Kawashita M. Novel bioactive materials with different mechanical properties. *Biomaterials.* 2003; **24:** 2161-75.

158. Yan S, Yin J, Cui L et al. Apatite-forming ability of bioactive poly(l-lactic acid)/grafted silica nanocomposites in simulated body fluid. *Colloids and Surfaces B: Biointerfaces.* 2011; **86:** 218-24.

159. Saravanapavan P, Jones JR, Pryce RS et al. Bioactivity of gel–glass powders in the CaO-SiO2 system: A comparison with ternary (CaO-P2P5-SiO2) and quaternary glasses (SiO2-CaO-P2O5-Na2O). *Journal of Biomedical Materials Research Part A.* 2003; **66:** 110-9.

160. Reiner T, Kababya S, Gotman I. Protein incorporation within ti scaffold for bone ingrowth using sol-gel SiO2 as a slow release carrier. *J Mater Sci Mater Med.* 2008; **19:** 583-9.

161. Jugdaohsingh R. Silicon and bone health. *J Nutr Health Aging.* 2007; **11:** 99-110.

162. Qiu Z, Noh I, Zhang S. Silicate-doped hydroxyapatite and its promotive effect on bone mineralization. *Frontiers of Materials Science.* 2013; **7:** 40-50.

163. Reffitt D, Ogston N, Jugdaohsingh R et al. Orthosilicic acid stimulates collagen type 1 synthesis and osteoblastic differentiation in human osteoblast-like cells in vitro. *Bone.* 2003; **32:** 127-35.

164. Jugdaohsingh R, Pedro LD, Watson A et al. Silicon and boron differ in their localization and loading in bone. *Bone Reports.* 2015; **1:** 9-15.

165. Radin S, Ducheyne P. Nanostructural control of implantable xerogels for the controlled release of biomolecules. In: Anonymous Learning from Nature how to Design New Implantable Biomaterialsis: From Biomineralization Fundamentals to Biomimetic Materials and Processing Routes. Springer, 2005; 59-74.

166. Radin S, Ducheyne P. Controlled release of vancomycin from thin sol–gel films on titanium alloy fracture plate material. *Biomaterials.* 2007; **28:** 1721-9.

167. Jeon H, Yi S, Oh S. Preparation and antibacterial effects of Ag–SiO2 thin films by sol–gel method. *Biomaterials.* 2003; **24:** 4921-8.

168. Baheiraei N, Moztarzadeh F, Hedayati M. Preparation and antibacterial activity of ag/SiO2 thin film on glazed ceramic tiles by sol–gel method. *Ceram Int.* 2012; **38:** 2921-5.

Chapter 2

Materials and methods

Chapter 2:

MATERIALS AND METHODS

2.1. Introduction

As said before, the main goal of this work is the development of a coating which increases the osseointegration ability of titanium dental implants. With this aim sol-gel method was selected due to its several advantages commented in section 1.4.5. Different alkoxysilane precursors with the general structure of $R'_nSiOR_{(4-n)}$ were chosen. R' is the organic chain which will remain in the final material and will provide specific properties to it, and OR is the alkoxy group which through the hydrolysis and condensation reactions of sol-gel process will lead to the formation of the polysiloxane network. The obtained sol will be applied in diverse substrates, depending on the test for which it is intended.

2.2 Materials

Different coatings were developed starting from one single silicon precursor or the combination of some of them in order to create a network with tailored properties. The selected alkoxysilane precursors were methyltrimethoxysilane (MTMOS), 3-glicydoxypropyltrimethoxysilane (GPTMS) and tetraethyl orthosilicate (TEOS), purchased from Sigma-Aldrich and employed without further purification. Their structure is presented in Figure 2.1.

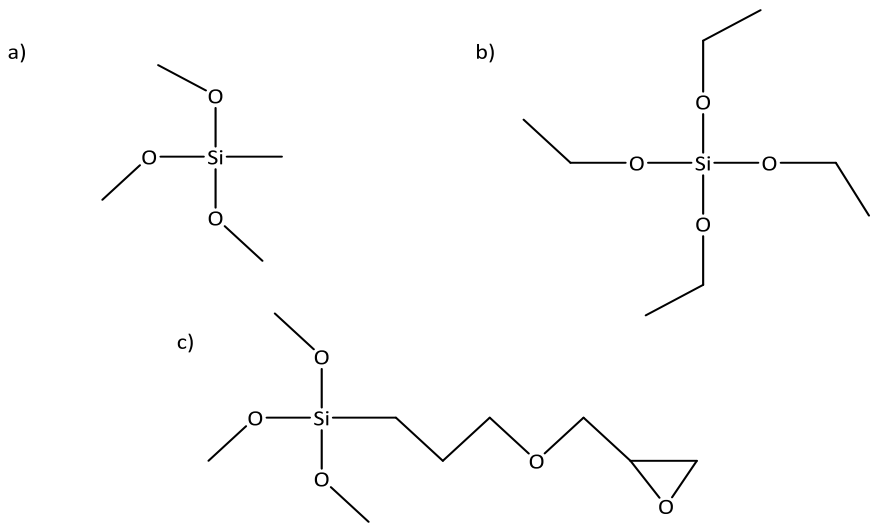

Figure 2.1. Chemical structures of alkoxysilane precursors (a) MTMOS, (b) TEOS and (c) GPTMS.

The selected protein was gelatin (from porcine skin), which was also purchased from Sigma-Aldrich and used without further purification. A basic unit of gelatin molecule is shown in Figure 2.2.

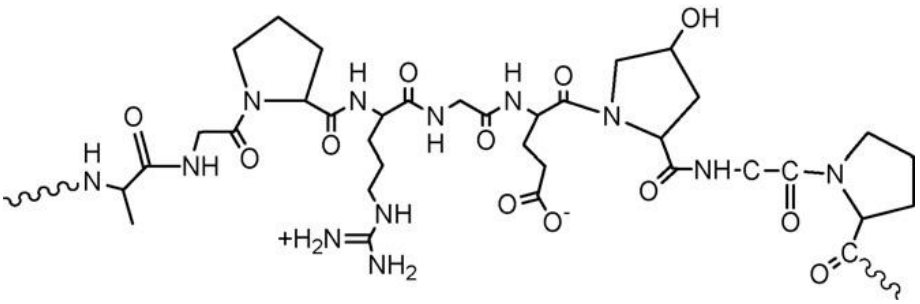

Figure 2.2. A basic unit of gelatin molecule.

All the developed systems will have the same basic precursor in common, MTMOS. In a previous study of this group, different precursors were evaluated finding the properties of MTMOS the most suitable for the aim of the work due to its integrity, ability to obtain homogeneous films, adhesion to the substrate, corrosion resistance and biocompatibility. The incorporation of TEOS will increase the inorganic nature of the coating, increasing the cross-linking degree, as well as the silicon release ability. The objective of adding GPTMS is to functionalize the surface of the coating introducing epoxy groups; this will allow a further molecular chemical immobilization.

As mentioned above, different substrates were used depending on the assay (Figure 2.3). Free films were also prepared in some cases. The used substrates were:

- Stainless steel sheets type AISI 316, provided by Ramon Navarrete, S.L. (Spain).
- Microscope slides ground edges (76 mm x 26 mm x 1 mm, LineaLAB).
- Glass Coverslips (Ø= 18 mm, Afora).
- Titanium discs cpTi grade IV, provided by Illerimplant S.L. (Ø= 12 and 10 mm) (Spain).
- Teflon molds to obtain free films (Ø= 5 cm, 2 mm depth).

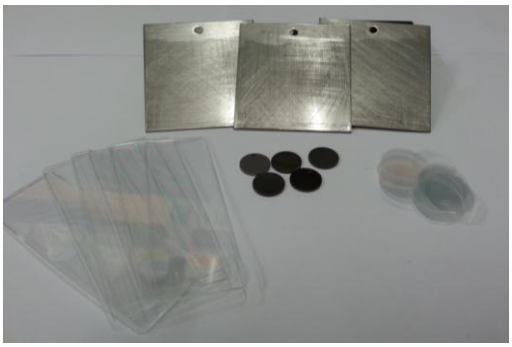

Figure 2.3. Different types of substrates.

2.3. Synthesis and obtaining of coatings

After various studies to optimize the different synthesis parameters, the catalyst type, the water:alkoxysilane rate, the aging time and the drying and curing temperature and time were established, in order to get a homogeneous crack free coating with the desired properties. The overall process is shown in Figure 2.4.

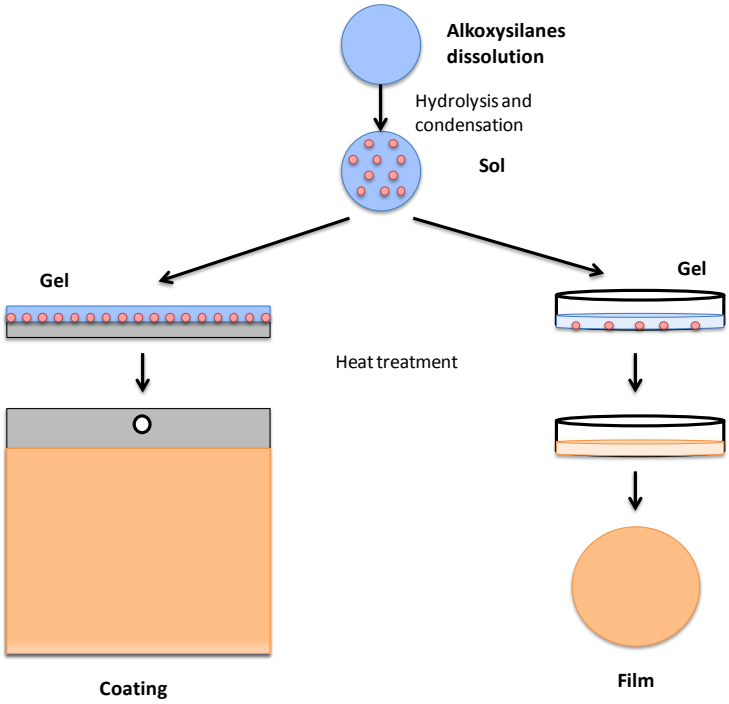

Figure 2.4. Scheme of sol-gel process to obtain coatings and free films.

2.3.1. Hydrolysis, condensation and ageing

The starting solution is a mix of the different silicon precursors with an organic solvent. The selected solvent was isopropanol (Sigma-Aldrich) because all the reagents are miscible with it, it is also miscible with water and it has a low boiling point what allows to use low temperatures in the drying step. The rate alcohol:precursor was 1:1 in volume. This solution was stirred with a magnetic stir plate. The added water is in a stoichiometric proportion to the alkoxy groups that are present in the solution. In the case of TEOS this proportion was 4, R=4, and for MTMOS and GPTMS, this factor was 3. Since the reactivity of silicon precursors is low, the added water was acidified by the hydrochloric acid HCl, to obtain pH=1. Once the catalyst was added, the hydrolysis and condensation reactions started. The reaction was kept under stirring for 1 hour to ensure the homogeneity of the sol, and after this period of time, it was set at room temperature for another hour before its deposition on the different substrates.

2.3.2. Coating application, drying and curing process

After preparing the reaction and once the sol was obtained, it was applied on different substrates in order to obtain the coating or the free film.

a) <u>Outfitting of substrate surface</u>

First of all, every substrate needs to be cleaned. Depending on substrate type different protocols were carried out.

An ultrasonic cleaning process was applied to microscope slides. First, they were sonicated in an ultrasonic bath Sonoplus HD 3200 in a solution HNO_3 (25%, w/w) for 15 minutes with a power of 30 W. Afterwards, they were cleaned and sonicated in distilled water three times to ensure all the impurity was gone. Finally, they were dried in an oven at 100 °C and kept in the desiccator until their use.

Glass cover-slips were cleaned in the same way as microscope slide. However before coating them with the sol, there was the need of activating their surface. With that purpose, a plasma argon treatment was applied to the surfaces in order to increase their wettability. This process was carried out in a plasma chamber where argon flow was 200 scm for 300 s under a pressure of 50 Pa and a power of 300 W. Cover-slips were coated just after the activation treatment.

Stainless steel sheets were rough down with a sandpaper of 1000p to avoid the heterogeneities and impurities from the surface that they may have due to the manufacturing process. Later, they were cleaned several times with water and finally with acetone to remove possible mechanical oil and humidity. Finally they were kept in a clean and dry place until their use.

Titanium discs were provided by Illerimplant S.L. free of impurities and sterilized by gamma radiation. They had a heterogeneous topography as a result of a sandblasted-acid etching surface pre-treatment. They were received in an individual packing and kept in that way until they were coated.

b) Coating techniques

Depending on the assay and the substrate, different coating methods were used. These techniques were flow-coating, dip-coating and drop-coating.

Stainless steel sheets and microscope slides were coated by flow-coating. In this technique, the sol was poured over the substrate as shown in Figure 2.5. The coating thickness depends on the angle of inclination of the substrate, the liquid viscosity and the solvent evaporation rate. In this case, they were coated with an inclination angle of 45° and this process was repeated three times to ensure the homogeneity of the coated surface.

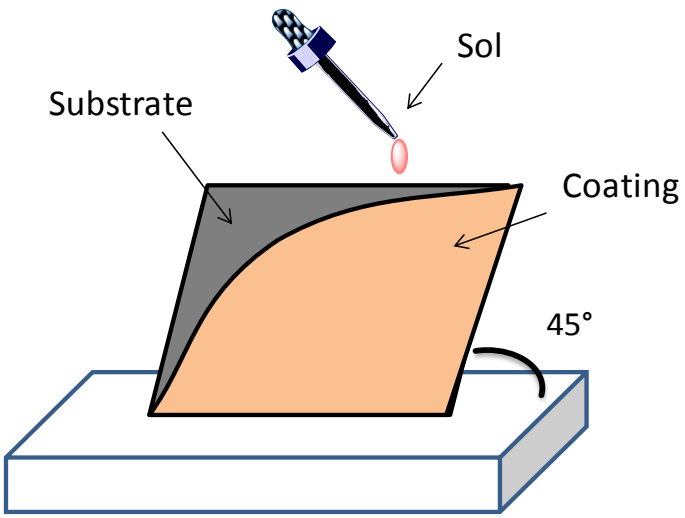

Figure 2.5. Scheme of the flow-coating process.

As it was said in the first chapter, the dip-coating technique can be described as a process where the substrate is immersed in a liquid and then withdrawn at a well defined withdrawal speed and after a previously established immersion time (Figure 2.6). A KSV Instrument dip-coater was used, model KSVD. Stainless steel and titanium discs were coated by this method. These substrates were introduced in the sol at an immersion speed of 100 cm/min, they were kept into the solution for 1 min and then remove at a withdrawal speed of 100 cm/min.

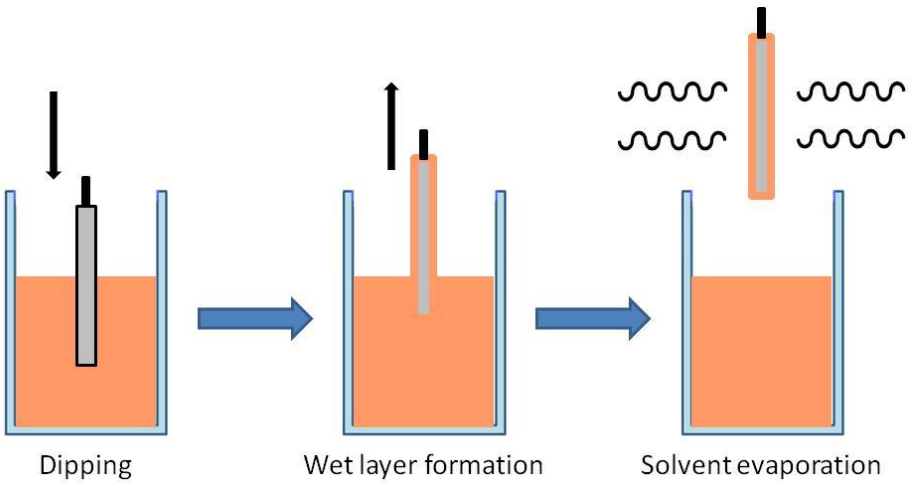

Figure 2.6. Stages of the dip-coating process.

Glass cover slips were coated by drop-casting method. 10 µL of the sol were placed on the substrate and the droplet was spontaneously spread out covering the entire surface. The scheme of the process is presented in Figure 2.7.

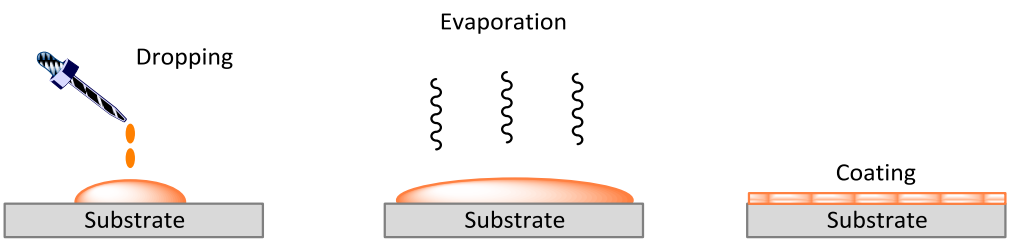

Figure 2.7. Scheme of the drop-casting process.

Finally, films were obtained using teflon moulds with a diameter of 5 cm and a depth of 2 mm. 3 mL of the sol were placed in each mould to obtain thin films.

c) Heat treatment

Immediately after coating the different substrates, they were subjected to a heat treatment in order to accelerate condensation reactions, obtaining a close network, and also to remove the isopropanol, water and other volatiles. Different temperatures and curing times were applied to the coatings to study their final structure by different methods. Final heat treatments were established depending on the alkoxysilane precursors that were involved in the network formation.

2.4. Coatings characterization

2.4.1. Chemical characterization

Chemical characterization was carried out by Nuclear Magnetic Resonance and Infrared Spectrometry.

a) 29-Silicon Nuclear Magnetic Resonance (^{29}Si-NMR) Spectrometry

In this study ^{29}Si-NMR was used with two different purposes. Firstly, it allows studying the different stages and species formed during the sol-gel process in liquid state, the obtained structure after the curing process, and the achieved cross-linking degree of the network.

^{29}Si-NMR in liquid state was used to follow the evolution of hydrolysis and condensation reactions of the sol-gel process. The spectra were measured, at 79.47 MHz, with a FT-NMR Bruker 400 Avance spectrometer and a spectral window of 180 ppm. A pulse sequence of 10 ms with a CPMG (Car-Purcell-Meiboom-Gill) filter, an acquisition time of 2 s and a number of scans of 384 were used.

The reaction mixture was prepared in a NMR tube and spectra were recorded before and after adding the catalyst, monitoring the reaction for two hours, and recording spectra each hour to study the evolution of different species. Chromium acetylacetonate, Cr(acac)3, (Aldrich) was added to each sample with a final concentration of $2.5 \cdot 10^{-3}$ M. The role of Cr(acac)3 was that of a spin relaxation agent for the NMR spectrometry, what allowed to obtain the silicon atom spectrum in a shorter period of time[1]. The external lock solvent was d-MeOH (Aldrich). Spectra were proton broad band decoupled, recorded at room temperature and they were

electronically referenced with respect to an external tetramethylsilane (TMS) at 0 ppm.

The final structure of the network obtained after the heat treatment was studied by solid state ^{29}Si-NMR spectroscopy with a Bruker 400 Avance III WB PLUS spectrometer 9.40T equipped with a CP-MAS (Cross Polarization Magic Angle Spinning) probe. By using CP-MAS technique, ^{29}Si NMR spectra in reasonable times (minutes to hours) and with a highly useful level of resolution can be obtained. The powder samples were placed in a rotor of 4 mm. ^{29}Si CP-MAS measurements were done at 10 KHz using a 90° pulse protons of 3.5 µs, 2.0 ms of contact time and 5 ms of recycle time. The spectra were collected using a 4mm CP-MAS probe at 79.5 MHz, a time domain of 2 K and a spectral width of 30 KHz.

The annotation system described by Lippmaa and coworkers[2, 3] was used. The criterion used was as follow: each Si atom is designated T or Q depending on the oxygen atoms to which are connected. In this way, MTMOS and GPTMS have a Si atom bound to three alkoxy groups, so T will be used to describe them. On the other hand, TEOS will be Q specie since it has four alkoxy groups bound to the Si atom. Furthermore, these symbols go with a numeric subscript, which refers to the amount of oxygen atoms that have condensed and bound to another silicon atom. In Figure 2.8 the scheme of all the possible structures that may appear in the cross-linking process are presented.

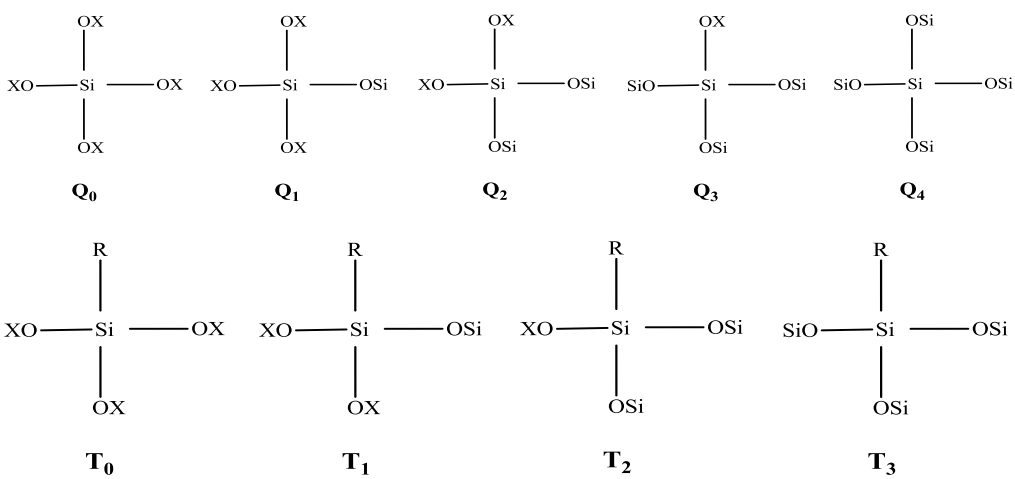

Figure 2.8. Silicon structures that can coexist during the sol-gel process designated by the criteria of Lippmaa *et al*.

b) 13-Carbon Nuclear Magnetic Resonance (^{13}C-NMR) Spectrometry

This method was used to determine the stability of the epoxy group under the sol-gel reaction conditions, that is, to clarify the opening or not of this functional group of GPTMS. This study was performed in solid state.

Solid state ^{13}C-NMR spectra were recorded by using a Bruker 400 AVANCE III WB spectrometer 9.40T (^{1}H= 400MHz) under Magic Angle Spinning (MAS). ^{13}C CP-MAS measurements were done at 10 KHz using a 90° pulse protons of 3.5 µs, 1.5 ms of contact time and 5 ms of recycle time. The spectra were collected using a 4 mm CP-MAS probe at 100.6 MHz, a time domain of 2 K and a spectral width of 30 KHz.

c) Fourier-transform Infrared Spectroscopy (FTIR)

The structure of the obtained materials was examined by Fourier-transform infrared (FTIR) spectroscopy. Spectra were recorded on the attenuated reflectance (ATR) mode with a Nicolet 6700 FTIR spectrometer, in the wavelength range between 4000 and 600 cm^{-1}. For this study free films were used.

d) X-ray Photoelectron Spectroscopy (XPS)

The chemical composition of the surfaces was assessed with an X-ray photoelectron spectrometer (K-Alpha XPS Instrument, Thermo Scientific). Survey spectra were recorded with a pass energy of 200 eV, a scan size of 400 µm, a binding energy range from -10 to 1350 eV, and 5 scans per point. Resulting spectra were analyzed by the use of the Advantage Data Spectrum Processing Software, and the resulting peaks areas were used to calculate the elemental compositions.

2.4.2. Morphological characterization

a) Cross-cut test

The adhesion of the coating to the substrate was determined by the cross cut test under the ISO rule 2409. For this assay, coated stainless steel sheets were used.

Sheets were placed in a firm and plane base and two cuts, perpendicular to each other, were made using the cross-cut tool. The first cut was made through the film to the substrate in one steady motion, using just enough pressure to reach the

substrate. The second cut was made at 90° and centered on the original cuts to create a grid pattern in the film. Any detached flakes or ribbons from the film were brushed several times back and forth along each of the diagonal lines of the lattice pattern, and the cut area was examined. Subsequently, tape was placed over the grid and rubbed firmly to ensure a good contact. After waiting for 30 s the tape was removed quickly with an angle of 180°. Finally, cut area was studied using an optical microscope Leica M165C with increases of x1.25 and x2.00 and coating's adhesion was classified according to the scale shown in Figure 2.9.

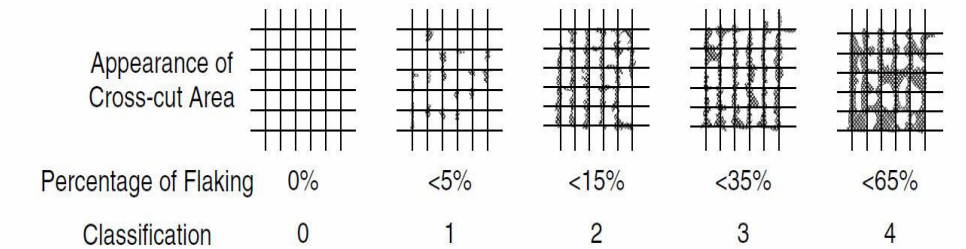

Figure 2.9. Classification according to ISO 2409.

b) <u>Atomic Force</u>

Atomic force microscopy images of the sol-gel coated titanium discs were obtained using a Nanoscope III Multimode AFM Controler (Bruker). Measurements were carried out in tapping mode with etched silicon TESP-V2 tips; the force constant of the tip was around 42 N/m and the resonance frequency was 320 Hz. A frequency of 1 Hz and an angle of 0° were used to perform the assays and collect the images.

2.4.3. Determination of hydrophobicity/hydrophilicity

The surface wettability of a biomaterial is an important parameter that in combination with other surface characteristics will determine the biological cascade of events at the biomaterial/tissue interface. It influences protein adhesion on implant surface and subsequent cell recruitment[4, 5]. This will also determine the water adsorption capacity of coatings which will have influence in the hydrolytic degradation of them.

The wettability of coatings was determined by the measurement of the contact angle of deionised water onto coated stainless steel sheet surfaces using an

automatic contact goniometer DATAPHYSICS OCA 20. Tests were carried out at room temperature and a sessile drop of 10 µL was used. Three sheets for each type of coating were used and 10 replicates for sheet.

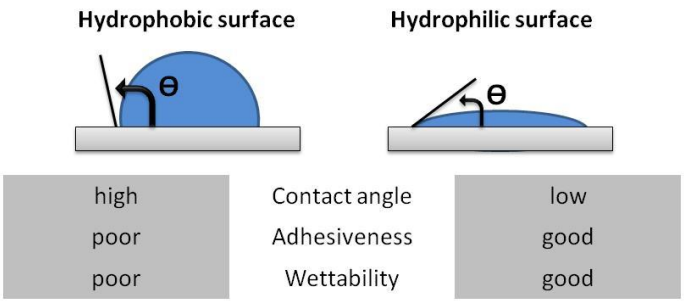

Figure 2.10. Scheme of the contact angle measurement between a liquid and a coated sheet.

The contact angle can be ranged from 0 to 180°, indicating that the wetting liquid is being drawn towards the surface (spreading of the drop) or is being repelled by the surface (beading of the drop). Water contact angles lower than 90° designate surfaces as hydrophilic, while surfaces with contact angles above 90° are considered to be hydrophobic.

2.4.4. Hydrolytic degradation test

The developed sol-gel coatings are resorbable *in vivo*. In an aqueous media they will suffer an hydrolytic degradation[6, 7] and, as said before, during their degradation they will release osteoinductive particles. The design of different siloxane matrixes will lead to the formation of coatings with different profiles of degradation and release.

The hydrolysis degradation test was performed by soaking the coatings in phosphate buffer saline (PBS) (Aldrich), keeping them at 37°C in an incubator for 8 weeks. The degradation kinetic was evaluated by weight loss of coatings before and after soaking in PBS for different periods of time. After soaking, samples were dried in a vacuum oven at 37°C for 24 hours before weighting them, to reach a constant weight. Each data point is an average of three individual measurements. Weight loss was calculated as shown in Eq. 2.1, where W_b and W_a are weights before and after being soaked respectively.

$$\text{Weight loss } (\%) = \frac{\text{Wb}-\text{Wa}}{\text{Wb}} \cdot 100 \qquad \text{(Eq. 2.1)}$$

2.4.5. Silicon release test

Siloxane coating will release Si to implant surrounding area which will have a positive effect[8, 9]. As it was discussed in the introduction chapter of this work, Reffit *et al*[10]., among other authors, found that orthosilicic acid promotes bone formation by stimulating procollagen synthesis in human osteoblastic-like cells, leading to osteoblastic differentiation.

For the quantification of the Si release the technique used was inductively coupled plasma mass spectrometry (ICP-MS), with the equipment Agilent 7700 Series IPC-MS. This technique is employed for analyzing inorganic elements with an excellent sensitivity and determining elemental concentrations at the part-per-trillion (ppt) level. The aqueous sample is converted to aerosol via a nebulizer and transported to the inductively coupled argon plasma which is a high temperature zone (8000-10000°C) and works as an ionization source. There the sample is desolvated, atomized and ionized. The resulting sample ions are then transferred to the mass spectrometer, where are separated based on their mass/charge ratio by a quadrupole mass analyzer and measured by an electron multiplier detection system. Each elemental isotope appears at a different mass with a peak intensity directly proportional to the initial concentration of that isotope in the sample.

This study was performed in the same conditions as the hydrolytic degradation test. Samples were immersed in 50 mL of PBS prepared with ultrapure water, and kept for 8 weeks. Aliquots of 50 µL were removed for each time point, and this was done in triplicate for each type of coating. All samples were acidified before analysis to ensure stability. Furthermore, an acid digestion was performed to ensure that all released species were in their atomic form before introducing them in the equipment; for that, HNO_3 (0.5 %, v/v) and HCl (0.1%, v/v) acid solutions were used. The cumulative Si release value was obtained by the use of a standard curve obtained by different concentration dilutions of a Si standard (Alfa Aesar).

2.4.6. Electrochemical Impedance Spectroscopy (EIS)

To complete the hydrolytic degradation study, electrochemical impedance spectroscopy (EIS) technique was used. EIS can generate data related to the quality

of the coating on a metal substrate. It is a very sensitive detector of the condition of coated metal, so the EIS response can indicate changes in the coating long before any visible damage occurs. It does not give absolute measurements, so an EIS spectrum only gives information when it is compared to another EIS spectrum. This is a very severe test, which aim is not to reproduce the physiological environment, but rather emphasizes it for a quick assessment that characterizes the behaviour of these coatings in an aqueous environment. Since the coatings used for this study are no designed to give a long term barrier against corrosion and are biodegradable, the aim of using this method is the correlation of EIS data with data obtained from degradation study by other methods mentioned before[11, 12].

The electrochemical impedance (Z) is a measure of a circuit's tendency to resist the flow of an alternating electrical current (AC). In this test the response of the electrochemical system to a disturbance caused by an AC voltage of varying frequency is analyzed and the obtained response is the system impedance, in this case coating's impedance. The impedance is a vector described by the modulus or magnitude of the impedance $|Z|$ and the rotation of the vector which is the phase angle Θ. Z has two components, where Z' is the real part and Z'' is the imaginary part of the impedance. These parameters are plotted on what is known as Nyquist and Bode plot.

The Nyquist plot (Figure 2.11) represents the variations of impedance with frequency, but the frequency is not explicitly shown, it must be obtained from the raw data point. It is a plot of the imaginary part of the impedance, Z'', versus the real part, Z'. This has properties that allow seeing whether a system is stable or unstable.

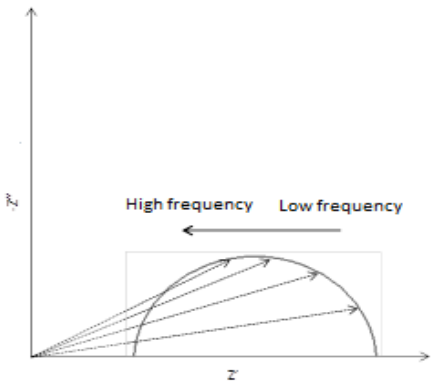

Figure 2.11. Nyquist plot.

A Bode diagram consists of two graphs: one is a plot of the logarithm of the magnitude of impedance (|Z|) and the other is a plot of the phase angle (θ), and both are plotted against the frequency (Figure 2.12). It is exactly the same information as in Nyquist plot just plotted in a different format.

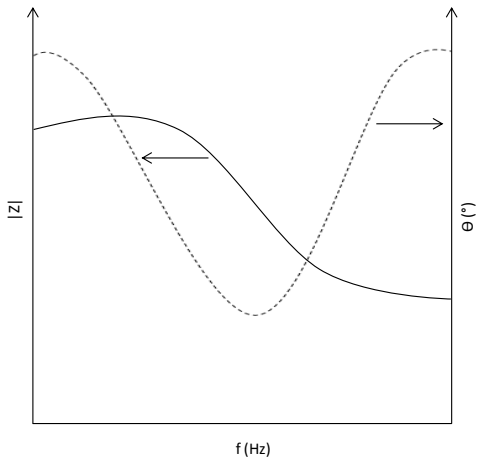

Figure 2.12. Bode diagram.

Electrochemical systems such as coated surfaces or corroding metals often behave like simple electronic circuits. Thus, an electrochemical system can be represented as the combination of various electrical components so that the overall assembly is representative of the physical and chemical processes occurring in the system under study. Therefore, equivalent circuit models can be used to model the various phenomena going on at the interface.

The Randles circuit (Figure 2.13.) is one of the simplest and most common electrochemical cell model, where a capacitor and two resistors are combined. This electrical circuit can be used to represent a coating or a corroding metal, although the values and meanings of the components are different. When this equivalent circuit model is applied to a coating immersed in an electrolyte, R_1 represents the resistance of the electrolyte solution (R_e) between the reference electrode tip and the surface of the coating. The resistor R_2 is associated with the resistance of the coating. It is a property of the material of the coating and varies with thickness and composition. The capacitor, C, represents the coating and can be characterized by the thickness and dielectric constant of the coating material[11].

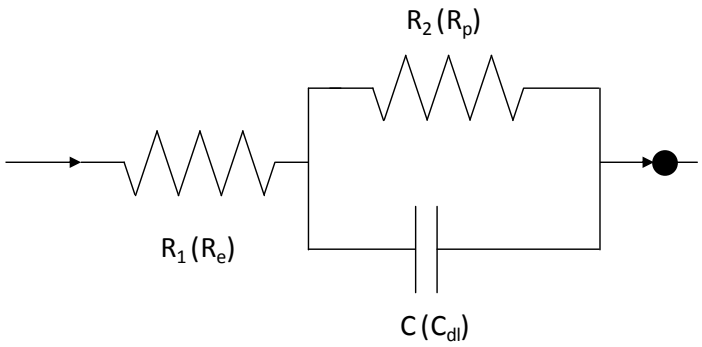

Figure 2.13. The Randles cell equivalent circuit.

The same equivalent circuit can also be applied to a bare metal in an electrolyte solution. R_1 is again associated with the electrolyte resistance (R_e). However, here the capacitor, C, is associated with the double layer capacitance (C_{dl}) of the metal/electrolyte interface and the resistance R_2 is the polarization resistance (R_p).

The frequency dependence of the impedance of the simple Randles cell is displayed in the Nyquist and Bode plots presented in Figure 2.14.

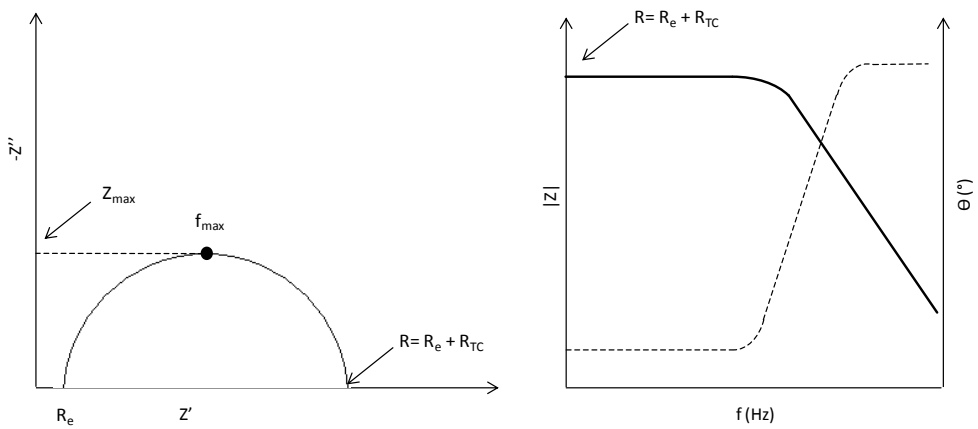

Figure 2.14. Nyquist plot (left) and Bode plot (right) for the Randles cell.

The selection of a suitable equivalent circuit that suits to the reaction mechanism occurring in the system is essential, since the information of resistance

and capacitance is obtained from these diagrams, providing also information about integrity and degradation of the coating.

Electrochemical impedance spectroscopy tests were carried out on coated samples deposited on a metallic substrate exposed to NaCl (3.5%, w/w) in deionised water up to 24 h. A three electrode electrochemical cell was obtained by sticking a glass cylinder onto the sample sheet and filling it with the test solution. The exposed surface area was 16.6 cm^2. A carbon sheet acted as the counter-electrode and an Ag/AgCl electrode was used as the reference electrode. The AC impedance data was obtained at the free corrosion potential using an IM6/6eX Zahner-elektrik potentiostat and a frequency response analyser. The impedance tests were performed over a frequency range of 100 KHz down to 10 mHz using a sinusoidal voltage of 10 mV as the amplitude inside a Faraday cage. This was in order to minimize external interferences on the system. Figure 2.15 shows the electrolytic cell used for the test.

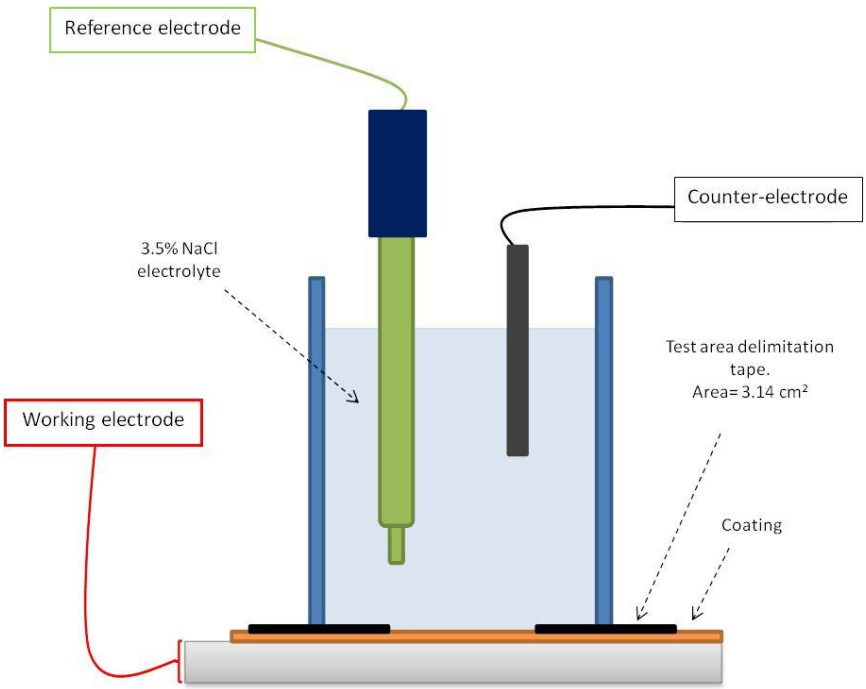

Figure 2.15. Set-up of a three electrode electrochemical cell for impedance measurement.

References

1. Jitianu A, Britchi A, Deleanu C et al. Comparative study of the sol–gel processes starting with different substituted si-alkoxides. *J Non Cryst Solids.* 2003; **319:** 263-79.

2. Lippmaa E, Mägi M, Samoson A et al. Structural studies of silicates by solid-state high-resolution silicon-29 NMR. *J Am Chem Soc.* 1980; **102:** 4889-93.

3. Magi M, Lippmaa E, Samoson A et al. Solid-state high-resolution silicon-29 chemical shifts in silicates. *J Phys Chem.* 1984; **88:** 1518-22.

4. Rupp F, Gittens RA, Scheideler L et al. A review on the wettability of dental implant surfaces I: Theoretical and experimental aspects. *Acta Biomaterialia.* 2014; **10:** 2894-906.

5. Gittens RA, Scheideler L, Rupp F et al. A review on the wettability of dental implant surfaces II: Biological and clinical aspects. *Acta Biomaterialia.* 2014; **10:** 2907-18.

6. Reiner T, Kababya S, Gotman I. Protein incorporation within ti scaffold for bone ingrowth using sol-gel SiO2 as a slow release carrier. *J Mater Sci Mater Med.* 2008; **19:** 583-9.

7. Xynos I, Hukkanen M, Batten J et al. Bioglass® 45S5 stimulates osteoblast turnover and enhances bone formation in vitro: Implications and applications for bone tissue engineering. *Calcif Tissue Int.* 2000; **67:** 321-9.

8. Ääritalo V, Areva S, Jokinen M et al. Sol-gel-derived TiO2–SiO2 implant coatings for direct tissue attachment. part I: Design, preparation and characterization. *J Mater Sci Mater Med.* 2007; **18:** 1863-73.

9. Areva S, Ääritalo V, Tuusa S et al. Sol-gel-derived TiO2–SiO2 implant coatings for direct tissue attachment. part II: Evaluation of cell response. *J Mater Sci Mater Med.* 2007; **18:** 1633-42.

10. Reffitt D, Ogston N, Jugdaohsingh R et al. Orthosilicic acid stimulates collagen type 1 synthesis and osteoblastic differentiation in human osteoblast-like cells in vitro. *Bone.* 2003; **32:** 127-35.

11. Loveday D, Peterson P, Rodgers B. Evaluation of organic coatings with electrochemical impedance spectroscopy. part 1: Fundamentals of electrochemical impedance spectroscopy. *JCT Coatings Tech.* 2004; **8:** 46-52.

12. Loveday D, Peterson P, Rodgers B. Evaluation of organic coatings with electrochemical impedance spectroscopy. part 2: Application of EIS to coatings. *JCT CoatingsTech.* 2004; 88-93.

Chapter 3

Design of coatings with tailored properties: degradability and functionalization degree

Chapter 3:

DESIGN OF COATINGS WITH TAILORED PROPERTIES: DEGRADABILITY AND FUCTIONALIZATION DEGREE

3.1. Introduction

In a previous study of our research group[1], different alkoxy silane precursors were studied and evaluated as possible candidates for the development of coatings with biomedical applications. Such precursors were MTMOS, triethoxyvinylsilane (VTES), GPTMS and TEOS. From the results obtained in the chemical, morphological and biological characterization of these materials, it was concluded that the coating containing MTMOS offered the best properties for the purpose of this study. However, this material still had some limitations that need to be addressed, so different binary systems were designed in this part of the work with this aim in mind.

These materials were developed as temporary substrates for tissue growth, where silicon released during their degradation would positively impact the degree, quality and progression of bone healing[2, 3]. For this purpose it was important to synthesize coatings with a controllable rate of degradation. MTMOS presented a slow degradation kinetic and consequently the amount of silicon released was poor; so there was a need to improve their reabsorption and release rates in order to accelerate the osseointegration process. One way to achieve this objective is to increase the hydrophilicity of the coating and thus enhance its water uptake ability.

With this aim, new materials were designed by adding TEOS in order to achieve varying degrees of hydrophilicity. The literature shows how the addition of this precursor augments the hydrophilicity of the coating[4] and accelerates the degradation kinetic[5, 6] and silicon release[7] of the silica network, giving rise to enhanced osteogenesis. The results obtained in the characterization of the MTMOS:TEOS hybrids with different molar ratios are presented in this chapter.

Additionally, coatings based on only MTMOS do not allow different biomolecules to be covalently anchored in further steps of this research project, property that could be used for the immobilization of cue factors that promote cell adhesion. Therefore, another binary system was developed. GPTMS was chosen in the formulation of the hybrids because its epoxy ring enables the surface to be functionalized. This compound has been used by many authors as a coupling agent between the silica phase and different natural polymers such as gelatin[8] and chitosan[9]. Thus, MTMOS:GPTMS hybrids were synthesized. The process is described in the section below.

MTMOS:TEOS and MTMOS:GPTMS, both hybrids with different molar ratios were used. Morphological, chemical and biological evaluation was performed in order to design a material with optimum adhesion to the substrate, degradation rate and *in vitro* behaviour.

A chemical characterization of the coatings was carried out by nuclear magnetic resonance of the silicon atom (^{29}Si-NMR) in the liquid and solid state, and by infrared spectroscopy (FT-IR). The sol-gel reaction process was followed by liquid ^{29}Si-NMR and from the results of this study, appropriate synthesis conditions were established. The network obtained after the curing treatment was studied by solid state ^{29}Si-NMR and was examined to see whether the heat treatment applied produced a more cross-linked network and if so, to assess the degree of this cross-linking. FT-IR helped to determine the formation of this siloxane network and more importantly, the hybrid nature of the end product.

Given the end use of these materials, it is necessary to establish their behaviour in aqueous media. Therefore, different trials were performed to determine their hydrophobic/hydrophilic character, hydrolytic degradation rate, the silicon release over time and ability to act as a corrosion protection barrier.

To assess the suitability of the coatings for biomedical applications, the cellular proliferation of mesenchymal stem cells (MSC) onto developed materials was evaluated as well as their ability to differentiate into osteoblasts and mineralize.

Finally, from each type of hybrids, the ones which behaved best in aqueous media and in contact with cells were selected for the *in vivo* study with New Zealand rabbits as animal model.

3.2. Synthesis of MTMOS:TEOS and MTMOS:GPTMS material series

As mentioned previously, two different types of hybrids were synthesized by adding different amounts of TEOS and GPTMS to MTMOS. The synthesis performed is described in section 2.3.

For the MTMOS:TEOS series, different molar ratios ranging from 0 % TEOS to 100 % were studied. In all cases, transparent and homogeneous sols were obtained. However, once they were applied onto different surfaces and subjected to heat treatment, it was not possible to obtain continuous and homogeneous coatings. The

addition of more than 30 % TEOS resulted in a brittle coating with insufficient physical integrity and substrate adhesion. For this reason, molar ratios of 9:1, 8:2 and 7:3 MTMOS:TEOS were selected. Table 1 summarizes the relation between all the reagents to synthesize the sol, where constant alcohol:precursor volumetric relation of 1:1, and stoichiometric molar ratio between catalyst and hydrolysable groups in the precursor were kept.

Table 3.1. The reagent ratios for obtaining MTMOS:TEOS sols.

	MTMOS:TEOS		
molar ratio	9:1	8:2	7:3
alcohol:precursor (v/v)	1:1	1:1	1:1
catalyst pH=1:precursor	Stoich.	Stoich.	Stoich.

The same reaction conditions were used to synthesize the MTMOS:GPTMS hybrids (Table 3.2). The selected molar ratios were 8M:2G, 5M:5G and 2M:8G. Homogeneous and transparent sols were obtained in all cases and they all became increasingly more viscous as the amount of GPTMS precursor was raised.

Table 3.2. The regent ratios for obtaining MTMOS:GPTMS sols.

	MTMOS:GPTMS		
molar ratio	8:2	5:5	2:8
alcohol:precursor (v/v)	1:1	1:1	1:1
catalyst pH=1:precursor	Stoich.	Stoich.	Stoich.

After obtaining the sol, all the materials were applied on different substrates as outlined in section 2.3.2.

3.3. Chemical characterization

As a preliminary part of this work, the evolution of hydrolysis and the condensation reactions were studied by ^{29}Si-NMR in the liquid state, which allowed different parameters, such as the reaction time, to be established. This was set at two hours, since no changes in the signals in the recorded spectrum were detected after this period of time. Afterwards, a heat treatment was applied to promote the condensation reactions and obtain a highly cross-linked network. The characterization of the end product was carried out by ^{29}Si-NMR in the solid state. A

FT-IR study was also done, to confirm the siloxane network formation as well as the hybrid nature of the film.

3.3.1. 29-Silicon Nuclear Magnetic Resonance (^{29}Si-NMR)

^{29}Si-NMR study was performed on MTMOS:TEOS and MTMOS:GPTMS under synthesis conditions of pH 1, water: precursor stoichiometric molar ratio and 2 hours reaction time. They were studied by first recording the spectrum of the precursors in isopropanol. Next, the catalyst was added and a spectrum of time zero (t=0h) was obtained. The degree of the reaction and the species that developed were studied by recording one spectrum every hour (t=1h and t=2h). Figure 3.1 and figure 3.2, show the spectra obtained for the 7M:3T and 5M:5G formulations. The behaviour recorded for the other hybrids was similar, no significant differences were detected.

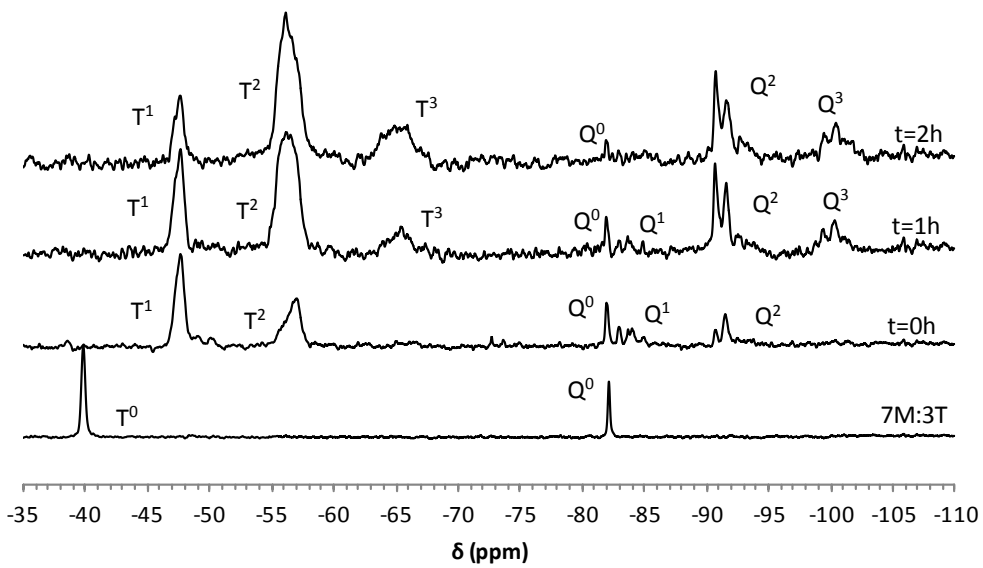

Figure 3.1. ^{29}Si-NMR liquid state spectra of 7M:3T.

The spectrum of the mixture of the MTMOS and TEOS precursors in isopropanol before the addition of the catalyst shows two peaks: one at -40 ppm and another at -82 ppm, which correspond to the MTMOS and TEOS respectively. In the spectrum at t=0h, signals indicating hydrolysis and condensation started to appear as soon as the catalyst was added. The reaction in the case of MTMOS was faster according to the appearance of condensed species, T^1 and T^2, and the disappearance of the precursor signals. A reduction in the precursor signal was

observed in the TEOS, as well as the formation of some condensed species, Q^1 and Q^2. Small signals at -38 ppm and -74 ppm were related to MTMOS(OH) and TEOS(OH) completely hydrolyzed species respectively.

After one hour of reaction the intensity of the T^1 and T^2 species increased, and a new signal of a more condensed T^3 species appeared. In the case of TEOS, the signal of hydrolyzed species disappeared, the intensity of Q^2 increased and a Q^3 species was formed. After two hours of reaction, the spectrum did not reflect a significant evolution of species compared with the spectrum recorded at t=1h, which is why the curing process was started after this period of time. The chemical shifts[10] for all the species involved in the formation of the MTOS:TEOS network, are presented in table 3.3.

Table 3.3. Chemical shift values (δ) for the different species formed during the sol-gel process for the MTMOS:TEOS hybrid, obtained by ^{29}Si-NMR.

MTMOS:TEOS	δ(ppm)								
	T^0	T^1	T^2	T^3	Q^0	Q^1	Q^2	Q^3	Q^4
MTMOS	-40	-47	-57	-65	-	-	-	-	-
TEOS	-	-	-	-	-82	-84	-91	-100	-

The presence of the T^1, T^2, T^3, Q^2 and Q^3 species, confirms that both the methoxy groups of MTMOS and the ethoxy groups of TEOS were hydrolyzed leading to the formation of silanol groups (Si-OH), which condense to form the siloxane network (Si-O-Si). Based on these results, it can be concluded that the sol-gel process takes place in 9M:1T, 8M:2T and 7M:3T hybrids. Nonetheless, it was necessary to apply the heat treatment due to the non-existent or weak intensity of the most condensed species.

The spectra recorded for the 5M:5G hybrid (Figure 3.2) were similar to that of 7M:3T. The spectrum of the precursor mixture showed two signals: one at -40 ppm for MTMOS and another at -42 ppm for GPTMS. Once the catalyst was added, more condensed species started to form and their intensity increased throughout the reaction time. In Table 3.4 the chemical shifts[10, 11] for all the species are presented in detail.

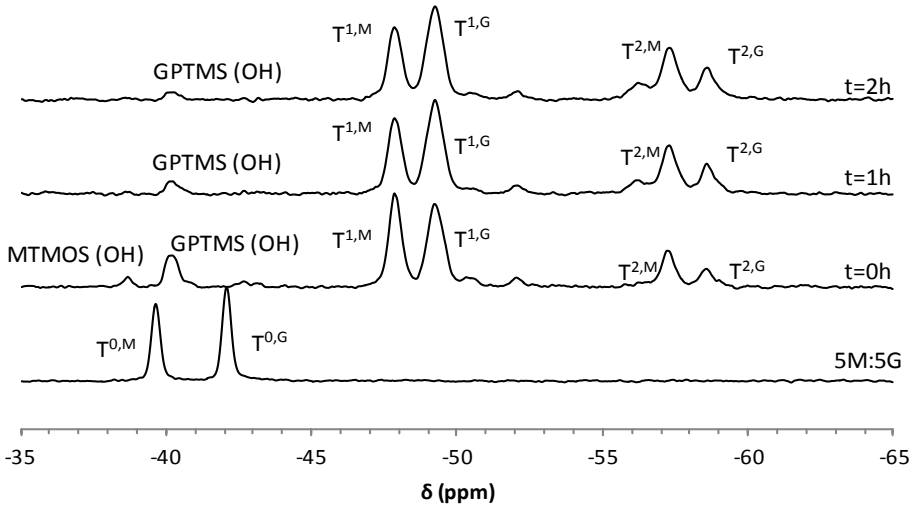

Figure 3.2. ^{29}Si-NMR liquid state spectra of 5M:5G.

The main difference between MTMOS:GPTMS to MTMOS:TEOS hybrids, is their reaction speeds. After two hours of reaction, in the spectra for the 5M:5G material, there are no peaks for the T^3 species of MTMOS precursor and the intensity of T^2 signal (split in two) is lower than the one for T^1. This behaviour was attributed to the presence of the GPTMS precursor, which seemed to interfere with the hydrolysis and condensation reaction rate of the MTMOS precursor. The presence of the glycidyl propyl group of GPTMS has a steric effect, inhibiting condensation and lowering the reaction speed of the overall process. However, despite the slowing down of the process, the synthesis parameters were not changed since it was still possible to appreciate the evolution of the reaction over time and the emergence of condensed species.

Table 3.4. Chemical shift values (δ) for the different species formed during the sol-gel process for the MTMOS:GPTMS hybrid, obtained by ^{29}Si-NMR.

MTMOS:GPTMS	δ (ppm)			
	OH	T^0	T^1	T^2
MTMOS	-39	-40	-47	-57
GPTMS	-40	-42	-49	-58

As stated before, it was necessary to apply heat treatment in order to obtain a highly cross-linked network. To study the structure of obtained materials after this

treatment, ^{29}Si-NMR spectroscopy was used. Different heat treatments were applied and the obtained spectra were analyzed determining the structure of the end product, thus establishing the necessary parameters for optimal heat treatment. The selected thermal treatments for the MTMOS:TEOS matrixes are presented in table 3.5 and for the MTMOS:GPTMS matrixes in table 3.6.

Table 3.5. Thermal treatment applied to MTMOS:TEOS hybrid coatings.

Coating	9M:1T	8M:2T	7M:3T
Temperature (°C)	80	80	80
Time (min)	120	120	120

In the case of the MTMOS:GPTMS hybrids, a temperature ramp was applied from 100 °C to 140 °C at a rate of 3 °C/min, and they were then kept at this temperature for 120 minutes. This was found to be the best way to obtain a homogeneous, uniform and highly cross-linked polysiloxane network.

Table 3.6. Thermal treatment applied to MTMOS:GPTMS hybrid coatings.

Coating	8M:2G	5M:5G	2M:8G
Temperature (°C)	140	140	140
Time (min)	120	120	120

In all cases, the materials were obtained as free films and were ground before being analyzed by ^{29}Si-NMR in the solid state. Figure 3.3 shows the spectrum obtained for the 7M:3T hybrid after being subjected to the heat treatment as an example.

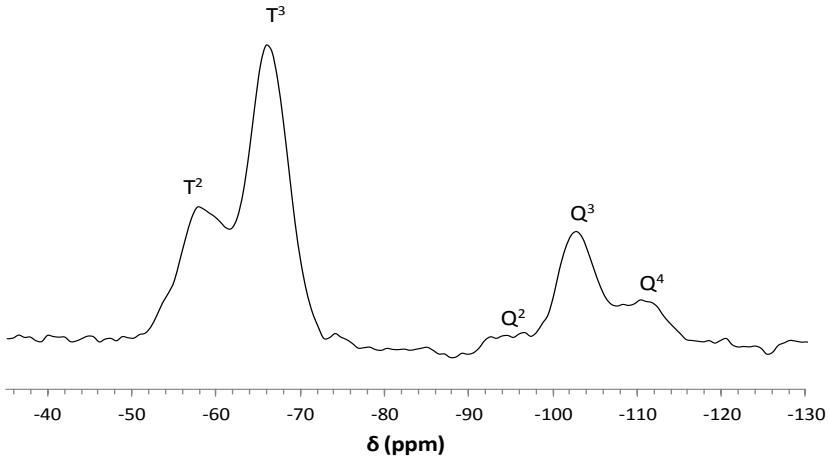

Figure 3.3. ^{29}Si-NMR spectrum for 7M:3T after the curing process.

The spectrum of the 7M:3T hybrid showed signals associated with the T^2 and T^3 species of the MTMOS precursor, and the Q^2, Q^3 and Q^4 species of TEOS. Their chemical shifts are presented in table 3.7.

Table 3.7. Chemical shift values (δ) obtained by ^{29}Si-NMR for MTMOS:TEOS hybrids and the ratio of peak areas.

7M:3T	δ (ppm)					Ratio of peak areas
	T^2	T^3	Q^2	Q^3	Q^4	$T^2/T^3/Q^2/Q^3/Q^4$
MTMOS	-56	-66				20/43/3/22/12
TEOS			-94	-102	-110	

In the spectra obtained by ^{29}Si-NMR in the liquid state after two hours of reaction (Figure 3.1), the species with the least condensation or with signals attributed to the unreacted precursor were obtained; T^1, T^2 and T^3 in the case of MTMOS and Q^0, Q^2 and Q^3 for TEOS. However, here there are no signals for species T^1, Q^0 and Q^1 due to the heat treatment. Moreover, the intensity of the most cross-linked species has increased, proving the efficacy of the selected heat treatment. This behaviour was also observed for the 9M:1T and 8M:2T hybrids.

In figure 3.4, the spectrum for the 5M:5G composition after being subjected to the curing process is shown as an example.

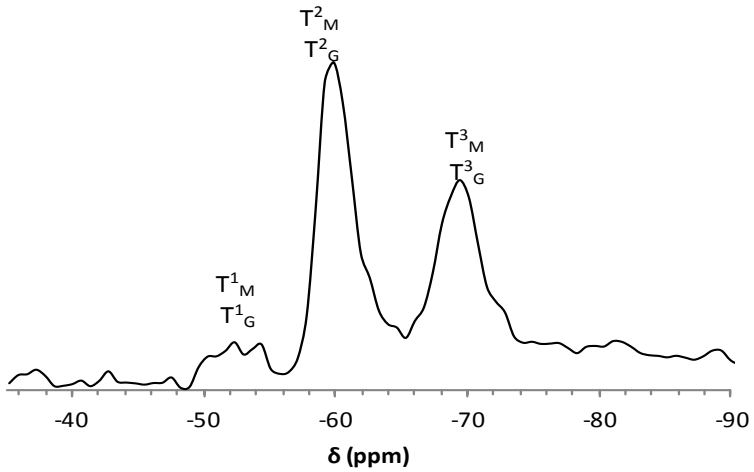

Figure 3.4. ^{29}Si-NMR spectrum for 5M:5G after the curing process

The spectrum above shows signals for Si atoms with a chemical environment type T^1, T^2 and T^3. In this case, unlike MTMOS:TEOS, the signals for both precursors, MTMOS and GPTMS, are overlapped, so it is impossible to identify the contribution of each precursor to the mixture. The chemical shifts for each species and their peak area correlation for 5M:5G coating are summarized in Table 3.8.

Table 3.8. Chemical shift values (δ) obtained by ^{29}Si-NMR for MTMOS:GPTMS hybrids and the ratio of peak areas.

MTMOS:GPTMS	δ (ppm)			Ratio of peak areas
	T^1	T^2	T^3	$T^1/T^2/T^3$
5M:5G	-52	-60	-70	0/48/52

In the liquid state ^{29}Si-NMR spectrum for 5M:5G after two hours of reaction, the most abundant species for both precursors were T^1 (Figure 3.2), but as a consequence of the heat treatment, this signal decreased significantly leading to the predominance of T^2 and T^3 types. Spectra for 8M:2G and 2M:8G are not presented because the same behaviour was observed and no further information was obtained. So by using this technique, the efficacy of the applied treatment was confirmed.

Nevertheless, it is obvious that a completely closed network was not obtained. The only way to obtain such a network would be by employing more

severe thermal treatments. However, this would lead to the formation of a brittle material whit lower substrate adhesion (which led us to select this particular curing process). In addition, designing materials with residual silanol groups is of particular interest, since they have been proven to have a beneficial effect on hydroxyapatite nucleation during the bone forming process[12]. It also needs to be considered, the possibility of adding bioactive components or biomolecules in the network, which could be damaged by the use of high temperatures.

3.3.2. Infrared Spectroscopy (FT-IR)

The chemical characterization of synthesized coatings after thermal treatment was completed by infrared spectroscopy. The chemical composition of both types of hybrids, MTMOS:TEOS and MTMOS:GPTMS, was studied dependant on their TEOS or GPTMS percentage. With this purpose, infrared spectra of free films from each material were recorded, using the attenuated total reflection (ATR) technique in the range 4000-500 cm^{-1}.

In Figure 3.5, the spectrum obtained for the 7M:3T hybrid is shown as an example. Regarding the TEOS %, the study performed by FT-IR for MTMOS:TEOS series of materials did not reveal significant differences among them, as it was expected.

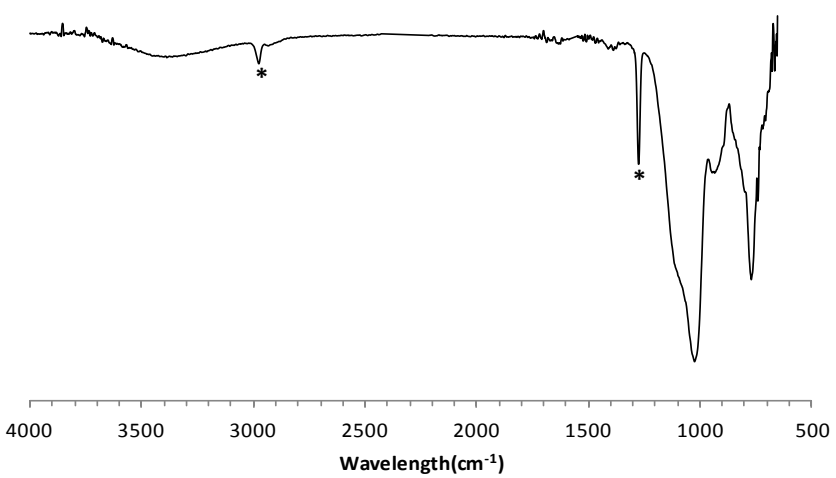

Figure 3.5. IR spectrum for 7M:3T coating.

All the MTMOS:TEOS hybrids show the characteristic vibration bands related to the siloxane bonds, Si-O-Si[13-15] at 1115 cm^{-1} and 1005 cm^{-1} (ν_{as} Si-O-Si), 950 cm^{-1} (ν Si-O-(H)) and 780 cm^{-1} (δ Si-O-Si). In addition, the vibration corresponding to the methyl groups bonded to the silicon atoms were identified (*): ν CH_3 at 2975 cm^{-1}, δ_S CH_3 at 1280 cm^{-1} (C-H methyl rock band), and ν_{as} C-Si at 770 cm^{-1}. The presence of these bands confirms the formation of a polysiloxane network with an organic-inorganic nature.

In Figure 3.6 the spectra for MTMOS:GPTMS hybrid types are shown. In this case, due to the differences in the bands' intensity depending on the GPTMS content, all the compositions are presented.

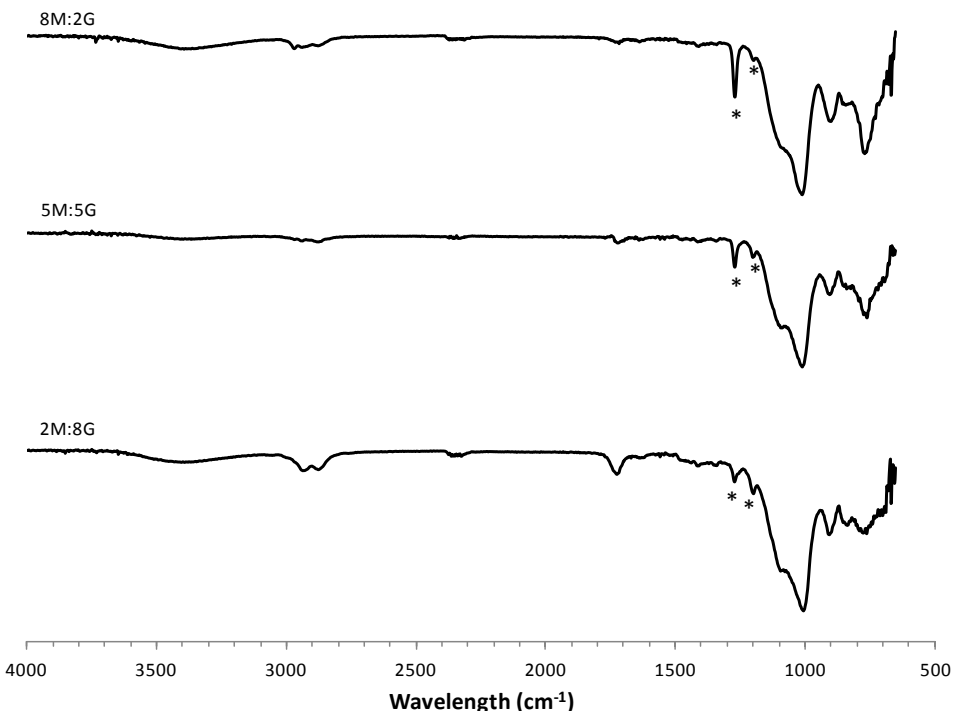

Figure 3.6. IR spectrum for MTMOS:GPTMS coatings.

All the materials show the characteristic vibrations of Si-O-Si, where the most intense band is the one split in two peaks at 1100 cm^{-1} and 1010 cm^{-1}. Bands assigned to the organic part are also presented. The vibration band of the methyl group of the MTMOS precursor appears at 1280 cm^{-1}, and the epoxy group of the

GPTMS absorbs near 1200, 900 and 800 cm^{-1} due to asymmetric and symmetric stretching of C-O-C (ring breathing). However, the bands at 900 and 800 cm^{-1} are often obscured by the silanol bands which also appear around this area[16]. Bands at 1280 and 1200 cm^{-1} (*), corresponding to the MTMOS and GPTMS respectively, change their intensity depending on the composition. From 8M:2G to 2M:8G, the intensity of the band at 1200 cm^{-1} increases due to the increase in GPTMS amount. FT-IR study confirms the formation of a material mainly based in a polysiloxane network organically modified, and suggests that surfaces with different functionalization degrees can be designed varying the composition of the hybrid. Table 3.9 summarizes the band assignment of the most relevant vibration for each precursor.

Table 3.9. Assignment of the vibration bands in IR spectra of different precursors.

Precursor	Wavelength (cm^{-1})	Assignment
MTMOS	2975	$-CH_3$
	1275	$-CH_3$
	1115, 1005	Si-O-Si
TEOS	1170, 1060	Si-O-Si
GPTMS	2950, 2860	$-CH_2-$
	1200	Epoxi ring
	1110, 1020	Si-O-Si
	900, 800	Epoxi ring

The chemical characterization for both types of hybrids confirms that the selected synthesis and thermal treatment parameters are appropriate to obtain highly cross-linked networks with an adjustable organic character.

3.4. Morphological characterization

For all the formulations (MTMOS:TEOS and MTMOS:GPTMS with different molar ratios), homogeneous and crack free coatings were obtained. Phase separation was not observed in any case. Furthermore, once applied on the metallic substrates, all of them were transparent and had a glossy finish. Figure 3.7 shows the appearance of two coated stainless steel sheets.

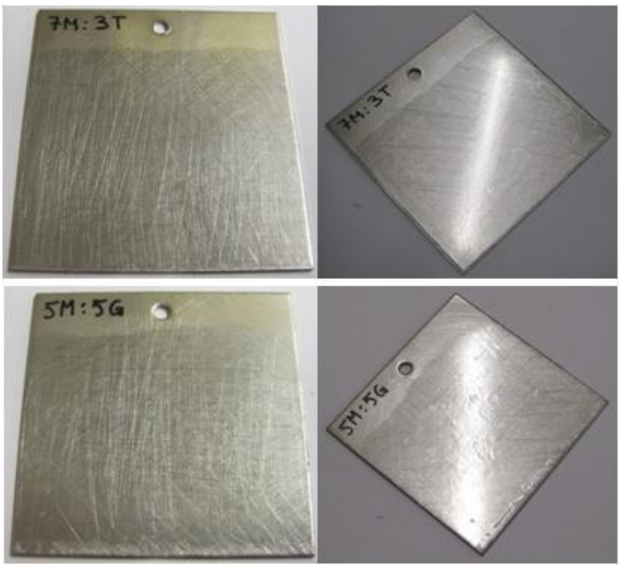

Figure 3.7. Stainless steel sheets coated with 7M:3T (above) and 5M:5G (below) hybrids.

Cross-cut adhesion test was performed to evaluate the adhesion achieved between the coating and the substrate, obtaining materials with high adhesion strength in all the cases.

It could be appreciated how with the introduction of TEOS the brittleness of the film increased. In the other hand, the addition of GPTMS to the formulation, led to the formation of a more flexible material, probably due to the incorporation of a longer organic chain into the structure.

3.5. Determination of hydrophilicity/hydrophobicity

As it was explained before, one of the purposes of designing MTMOS:TEOS hybrids, was to obtain hydrophilic surfaces by the introduction of different amounts of the TEOS precursor. In this way, degradation speed and, in consequence, the silicon release will be increased, what will become in a higher osteoinductive capacity.

Contact angle measurements were carried out with water in order to determine the ability of the different surfaces to interact with an aqueous media. This measurement is of great interest since the hydrophilic/hydrophobic nature of the material will determine its interaction with biological fluids. It is widely accepted

that surfaces with contact angle values below 90° can closely interact with biological fluids, allowing the protein adsorption and the subsequent interaction with cells[17, 18]. So, depending on the obtained values for the developed materials, it could be predicted their *in vitro* and *in vivo* behaviour.

Contact angle values for 9M:1T, 8M:2T and 7M:3T are presented in table 3.10, where they are also compared with the values of pure precursors. The value of TEOS was obtained from literature since it was not possible to get a continuous and uniform coating under our process conditions.

Table 3.10. Contact angle values for the MTMOS:TEOS series.

Coating	MTMOS	9M:1T	8M:2T	7M:3T	TEOS[4]
Contact angle (°)	75,9±1,6	73,2±2,3	69,0±0,9	70,0±0,8	57,9

The coating synthesized with MTMOS presented a contact angle value of 76°. This value was decreased by the incorporation of TEOS, proving its effect on increasing the hydrophilicity of the film. For 8M:2T and 7M:3T, values were around 70°, which is described in literature as optimum value for cell adhesion[4].

In the case of the MTMOS:GPTMS hybrids, the GPTMS precursor was introduced to the formulation to obtain a functionalized surface. By contact angle measurements, the effect of these epoxy groups on surface's hydrophilic/hydrophobic character was tested. The obtained values are compiled in table 3.11.

Table 3.11. Contact angle values for the MTMOS:GPTMS series.

Coating	MTMOS	8M:2G	5M:5G	2M:8G	GPTMS
Contact angle (°)	74,7±2,4	76,6±0,6	66,9±2,0	68,4±2,1	64,8±2,0

As in the previous case, the coating based in MTMOS presented the highest contact angle values. The effect of GPTMS addition was more clear for 5M:5G and 2M:8G hybrids. A higher content in glycidyl propyl groups increased the polarity of the surface, making the interaction with fluids easier and, in consequence, improving the wettability (more hydrophilic). The values obtained for these coatings, in the same way as happened for the MTMOS:TEOS series, are in the range considered to be optimum for cells interaction in literature.

3.6. Hydrolytic degradation test

As said before, these coatings will work as temporary substrate for tissue growth, and they will be gradually reabsorbed while releasing silicon to the surrounding environment of the implant. This property is the responsible of the osteoinductive ability of these types of materials.

In order to simulate the final application of the coatings, PBS was used as aqueous media mimicking the biological fluid. Glass cover-slips coated with the different hybrids were immersed in PBS for different periods of time until 8 weeks. Mass loss results were expressed in percentage with respect to the weight before immersion. Results for MTMOS, 9M:1T, 8M:2T and 7M:3T are plotted in Figure 3.8.

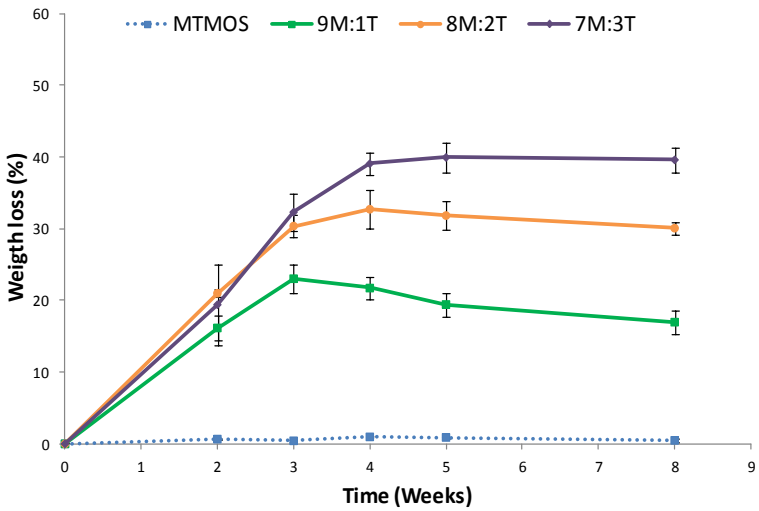

Figure 3.8. Mass loss due to the hydrolytic degradation of MTMOS, 9M:1T, 8M:2T and 7M:3T coatings.

Coating based on pure MTMOS, showed a mass loss of 1% after 8 weeks of immersion in PBS. This behaviour can be attributed to different facts. Firstly, in a previous study of this group, it was found how the network obtained by MTMOS had a higher cross-linking degree than the one obtained by TEOS and other types of precursors[19]. This was studied by ^{29}Si-NMR in solid state after the heat treatment. The most predominant species in the MTMOS were T^3, what means a completely condensed network. However, in the case of the TEOS, the most intense signal was

for Q^3, giving as a result more residual silanol groups as well as a more open network. Owing to this explanation, it was expected that the incorporation of TEOS led to a more open network, making easier the entrance of water and, in consequence, the dissolution of the Si-O-Si bonds.

Another effect that needs to be taken into account is the hydrophilic/hydrophobic nature of each material. In the section above this property was studied for all the hybrids, finding that the addition of TEOS to the formulation gave a higher wettability. This will also facilitate the interaction with PBS and will favour the degradation.

Focusing on the obtained results, the effect of the incorporation of TEOS to the hybrid is evident, making the film more soluble. The highest values of losses appeared during the first weeks, after this period of time, the degradation kinetic was slowed down.

In Figure 3.9 the results obtained on the gravimetric degradation test for MTMOS:GPTMS hybrids are presented. The study was performed in the same conditions as for MTMOS:TEOS material series.

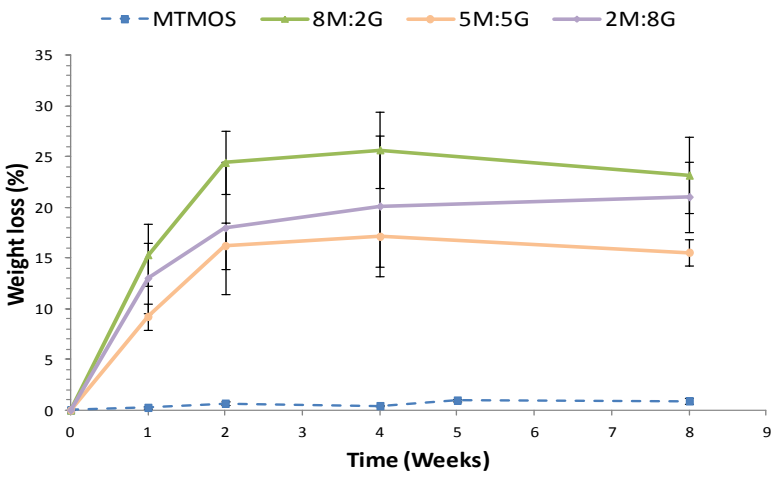

Figure 3.9. Mass loss due to the hydrolytic degradation of MTMOS, 8M:2G, 5M:5G and 2M:8G coatings.

The obtained results show that the highest hydrolytic stability of all the materials was for MTMOS coating, and how the incorporation of GPTMS had the

same effect in the three types of hybrids increasing the degradability. This was due to the denser network and the less hydrophilic nature of the MTMOS compared with GPTMS. This precursor increases the wettability of the coating and it also decreases the cross-linking degree. It was found by ^{29}Si-NMR, how in the network obtained by pure GPTMS there were less condensed species than in pure MTMOS. These two facts together can explain the behaviour obtained in MTMOS:GPTMS hybrids.

After 8 weeks of immersion, all the materials showed an intermediate mass loss between the values for MTMOS (1%) and GPTMS (32%). However, due to the technical limitation, it is not easy to establish a clear tendency on the degradation rate with the increase in the GPTMS amount. The values obtained are very close to each other, and taking into account the deviations, there are not significant differences among 8M:2G, 5M:5G and 2M:8G. Comparing them to MTMOS:TEOS hybrids, lower values were obtained due to the brittleness of the first type of coatings where delamination occurs and bigger pieces of material are lost.

From these results it can be concluded that the degradability of the film is highly dependent on the hydrophilicity and the packaging of the siloxane network. In consequence, it is important to highlight the possibility of designing materials with different dissolution rates and controlled properties.

3.7. Silicon release test

After the study of the degradation rate of coatings in aqueous media and finding that both, the incorporation of TEOS and GPTMS had the same effect on the MTMOS matrix, making it more soluble, next step was to assess their role in the silicon release.

As it was said in the introduction of this chapter, the addition of TEOS will favour the silicon release, which is known to be osteoinductive and in this way will promote the differentiation of hMSC into bone forming cells[5]. Shirosaki *et al.* demonstrated by a study with GTPMS-TEOS-Chitosan hybrids, that the increase of TEOS improved osteocompatibility and ALP activity, while the addition of GPTMS improved the proliferation ability of cells on its surface[7].

Assays were performed in the same conditions as for the degradation study. The obtained results for the cumulative silicon released over immersion time are presented in Figures 3.10 and 3.11.

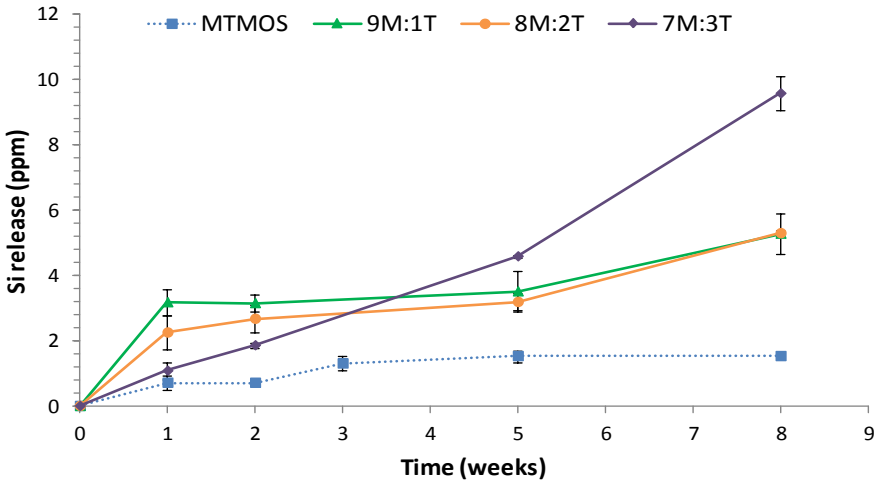

Figure 3.10. Cumulative Si release from MTMOS:TEOS hybrids up to 8 weeks in PBS.

Likewise it happened with the mass loss test, TEOS has the same effect making the matrix more soluble and, in consequence, improving the silicon delivery rate. All the coatings showed the same behaviour, giving a progressive Si release over time and obtaining the highest value for the 7M:3T material, in which the delivery ability is more than fivefold higher than for MTMOS.

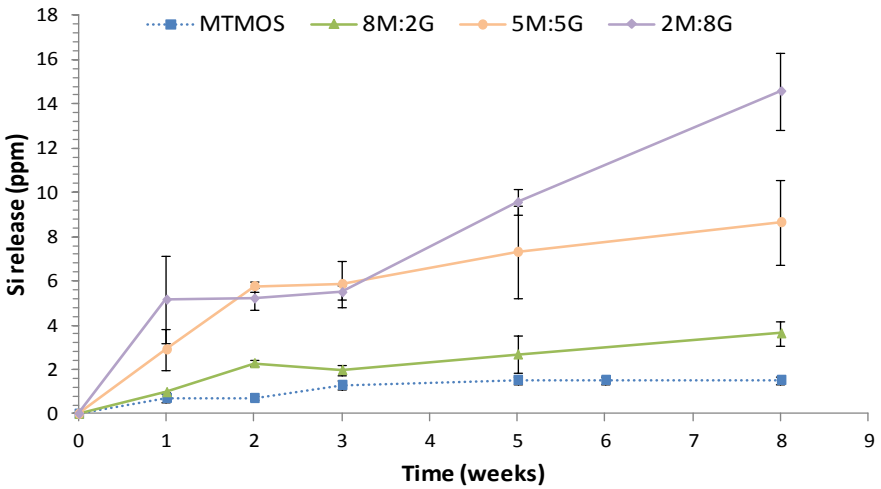

Figure 3.11. Cumulative Si release from MTMOS, 8M:2G, 5M:5G and 2M:8G hybrids up to 8 weeks in PBS.

Results for the MTMOS:GPTMS hybrids show an increase in Si release when adding GPTMS to the formulation and obtaining the highest values for 5M:5G, 8 ppm, and 2M:8G, 14 ppm, after 8 weeks of immersion in PBS. Such behaviour can be explained, as in the case of the hydrolytic degradation test, with the differences in the network packing and hydrophobic/hydrophilic nature of each material, where the introduction of GPTMS gives more open networks and increases the wettability.

By this study it is clear the effect of TEOS and GPTMS improving the interaction with biological fluids and making the matrix more soluble. It is also evident the possibility of regulating the amount of Si released and its rate by controlling precursors' molar rate.

3.8. Electrochemical Impedance Spectroscopy (EIS)

The EIS test is usually used to test coatings' ability to protect the metallic substrate against corrosion. In the case of biomaterials, this protection avoids the release of metallic ions into the surrounding tissues, which have been prove to have negative effect on regeneration process[20, 21] and may lead to the clinical failure of the treatment.

However, in this case, since these materials were designed to be resorbable, these measurements will be used as a complementary method for the study of the degradation mechanism of the different coatings, where information about porosity and water uptake can be obtained.

For this study, stainless steel sheets coated by dip coating were used and they were placed in the electrochemical chamber which was fit out as it was shown in figure 2.14. Impedance measurements were performed at different time points while the coating was in contact with the electrolyte: 0, 4, 8 and 24 hours. By the analysis, using the Z-view software, of the obtained Nyquist and Bode diagrams and the selection of the appropriate equivalent circuit model, different parameters related to the coating behaviour in aqueous media were obtained.

The pore resistance, R_{po}, is a measure of the porosity and the deterioration of the coating. It determines the ionic resistance through the pores of the coating and is inversely proportional to the extent and number of defects in the coating. The evolution of R_{po} during the exposure time with the electrolyte, gives information about the coating capacity to avoid the formation of pores across the film due to its

degradation. High and constant values are attributed to coatings which do not degrade during electrolyte exposure and the most common behaviour is to decrease with time.

Figure 3.12 shows pore resistance parameters obtained from the response of the MTMOS:TEOS coating series.

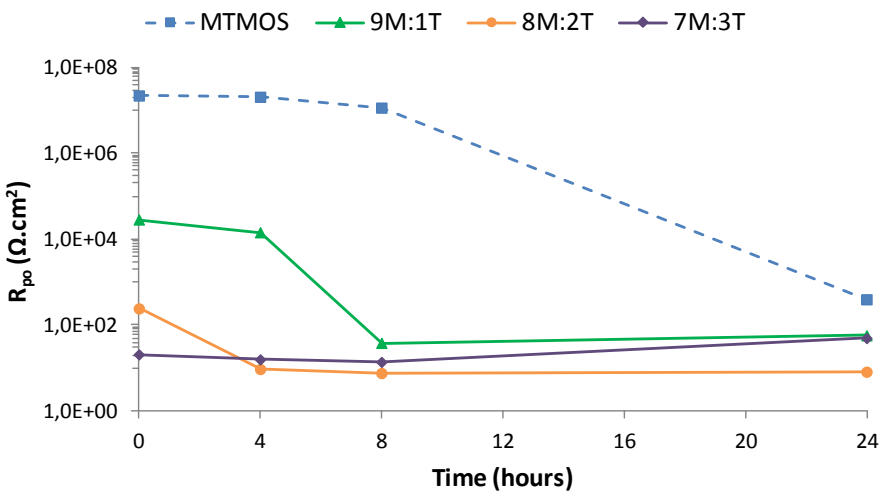

Figure 3.12. Evolution of the pore resistance versus contact time with the electrolyte, of the MTMOS, 9M:1T, 8M:2T and 7M:3T coatings.

The MTMOS coating shows an initial R_{po} value of $2x10^7$ Ω·cm^2, and this value remains almost constant until 8 h of contact with the electrolyte, where there is a drastic decrease to a value of 390 Ω·cm^2 at 24 h of contact. The coating 9M:1T presents an initial value of 28000 Ω·cm^2 and a final value of 570 Ω·cm^2. For 8M:2T and 9M:1T the initial pore resistance values are much more lower, 241 and 20 Ω·cm^2 respectively and, in this cases, the pore evolution is not so pronounced.

It can be seen that as TEOS is added to the MTMOS coating, the R_{po} value decreases significantly, especially for 8M:2T and 7M:3T. The 9M:1T coating shows an initial value of R_{po} three magnitudes smaller than the one for MTMOS, while 8M:2T is five magnitudes lower and 7M:3T six. So the addition of more than a 10% of TEOS makes the coating very permeable to the water flow.

The results obtained for pore resistance of MTMOS:GPTMS hybrid types are presented in figure 3.13. These results show a GPTMS content dependent behaviour, the higher the amount of this precursor in the formulation, the lower the R_{po} value.

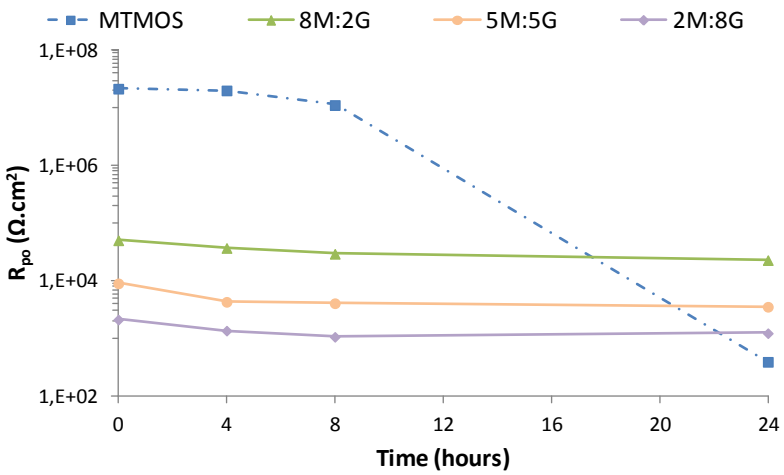

Figure 3.13. Evolution of the pore resistance versus contact time with the electrolyte, of the MTMOS, 8M:2G, 5M:5G and 2M:8G coatings.

All the hybrids show lower R_{po} values than the MTMOS coatings. The 8M:2G coating presents an initial R_{po} value of $5x10^4$ Ω·cm^2 and it decreases until $2x10^4$ Ω·cm^2 after 24 h in contact with the electrolyte. The values for 5M:5G and 2M:8G are $9x10^3$ and $2x10^3$ Ω·cm^2 respectively at time 0 h, and they maintain almost constant for the 24 h of assay.

Comparing the obtained values for both types of hybrids, it can be appreciated that TEOS presents more effect decreasing pore resistivity than GPTMS. This is in good agreement with the obtained values for hydrolytic degradation test, where there were higher mass losses for MTMOS:TEOS hybrids than for MTMOS:GPTMS. Such behaviour is not so clear in the case of Si release study, because using ICP just ionic species can be detected, and during hydrolytic degradation and EIS study the effect of bigger particles it is being also detected (delamination).

Figures 3.14 collects the results obtained for the coating capacitance in the MTMOS:TEOS hybrids; parameter related to the ability of the coating to absorb water.

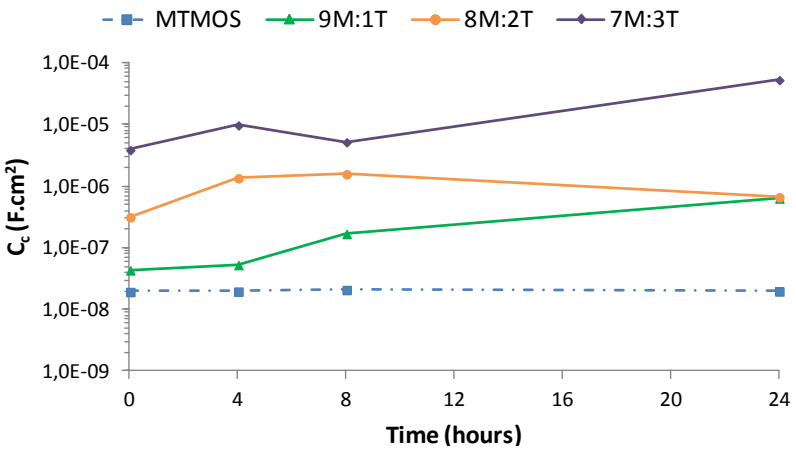

Figure 3.14. Evolution of the coating capacitance versus contact time with the electrolyte, of the MTMOS, 9M:1T, 8M:2T and 7M:3T coatings.

The MTMOS coating shows a constant value of $2x10^{-8}$ F·cm^2, while the rest of the MTMOS:TEOS formulations show upper values and a trend to increase with the addition of more TEOS. The 9M:1T coating shows an initial capacitance of $4x10^{-8}$ F·cm^2 and a final value of $6x10^{-8}$ F·cm^2, 8M:2T coating's capacitance value evolved from $3x10^{-7}$ F·cm^2 to $6x10^{-7}$ F·cm^2, and 7M:3T ranks from $4x10^{-6}$ F·cm^2 to $5x10^{-5}$ F·cm^2. In all the cases, the final C_c values are bigger than the initial ones showing that exposure to the electrolyte with time causes the increase of water content in the coatings, and it is also increased with TEOS content.

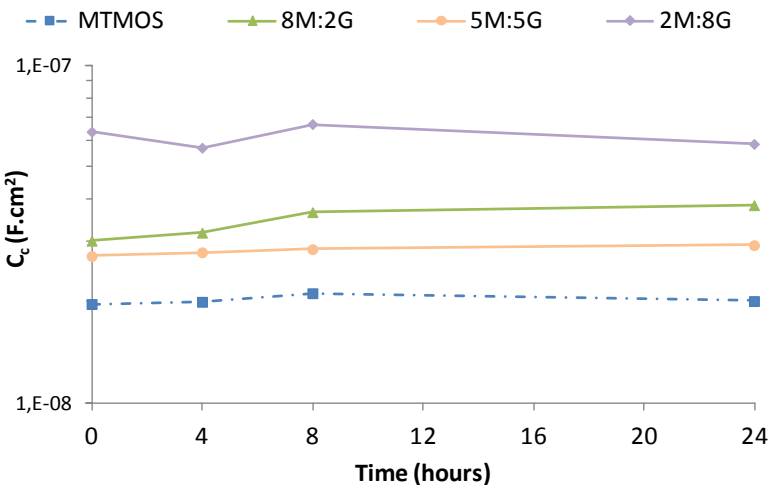

Figure 3.15. Evolution of the coating capacitance versus contact time with the electrolyte, of the MTMOS, 8M:2G, 5M:5G and 2M:8G coatings.

In the case of MTMOS:GPTMS hybrids, Figure 3.15, it can be seen how the incorporation of GPTMS to the coating increases its capacitance, or what is the same, its water uptake ability.

The results obtained for coating capacitances are, as the ones for pore resistance, in agreement with those obtained by hydrolytic degradation, Figures 3.8 and 3.9, where the incorporation of TEOS or GPTMS increases the coating degradability. So, from all these studies, it is concluded that the addition of these precursors to MTMOS materials increases the permeability of the coating and causes more channels. Consequently, it is easier for the water to penetrate into the coating increasing its content in them, and making the hydrolysis degradation more accessible.

3.9. *In vitro* test

As explained before, the aim of these materials is to promote bone formation by enhancing the osteoinduction process. Osseointegration starts with the differentiation of mesenchymal stem cell (hMSC) into osteoprogenitor cells. Next, these cells will develop into osteoblasts, which produce calcium-rich deposits as consequence of the mineralization, it means the osseointegration.

In a previous study, it was obtained that none of the selected precursors were cytotoxic, and also the ability of MTMOS improving titanium's behaviour regarding human osteoblasts' proliferation was proved[22]. In this way, adhesion and proliferation of hMSC and their differentiation and mineralization ability was studied onto the different developed materials, in order to test the effect of TEOS and GPTMS incorporation.

3.9.1. Experimental methods

For this study, glass cover-slips were coated by drop-casting method with all the different hybrids.

a) <u>Sterilization and preparation of samples</u>

For *in vitro* studies, all materials need to be sterilized prior to culture. With this aim, materials were placed on a sterile surface and both faces were exposed to UV radiation for 30 minutes.

Additionally, for the right conditioning of the materials, they were immersed in the culture media (in accordance with the cell type) during 16 hours before the culture was conducted. After this period of time, the media was removed and cells were spread.

b) Proliferation study of human Mesenchymal Stem Cells (hMSC)

The aim of this study is to assess the ability of proliferation of hMSC on developed coatings. The hMSC used were obtained from human adipose tissue by the company Histocell S.L.

hMSC cells were incubated (47.000 cells/ well) at 37 °C on materials using 1.5 mL culture media DMEM-Glutamax (Gibco) for 1, 7 and 14 days. Mitochondrial activity was quantified using the MTT Kit (Roche). Before the addition of the MTT solution, materials were transferred to a new culture plate to analyze only the proliferation of cells adhered to the coating and not the ones on the bottom of the well. After the pre-established culture time, the reagent was added with a final concentration of 0.5 mg/mL, cells were kept for 24 hours, 100 µL of "solubilisation" solution were added and it was kept overnight. Subsequently, the supernatant was analyzed with a spectrophotometer using a multiplate reader (Multiskan Ascent) measuring at a wavelength (λ) of 550 nm. The significance of the results was determined statistically, coatings' values were compared against reference material to examine whether there were significant differences between them.

To perform this test, glass substrates coated with the different sol-gel hybrids by drop-casting were used. Each material was tested in triplicate, and at the same time, each replicate was tested three times to determine the absorbance.

c) Differentiation and mineralization of hMSC

The aim of this study is the *in vitro* evaluation of the osteogenic capacity of hMSC cells adhered to the developed coatings. This osteogenic capacity was analyzed by the quantification of calcium deposits formed by the hMSC differentiated to bone cells in osteogenic inductive media.

To perform this study, the hMSC cells (7600 cells/well) on different materials were incubated at 37 °C for 7 days, using as culture media 1.5 mL of DMEM-Glutamax (Gibco) with 10% SBF. After this period of time, the differentiation was

induced by culturing cells in osteogenic media StemPro Osteoblast Differentiation media (Gibco) for 14 days, renewing the media with a fresh one every 72-96 hours. Finally, at 7 and 14 days time point, the formed extracellular calcium was quantified by red alizarine test (Sigma-Aldrich). Before adding this reagent, materials were transferred to a new culture plate to analyze only the differentiated cells adhered to the surface of the coating. After, they were washed with PBS, fixed with 10% formaldehyde and washed again with PBS. The staining with 2% Red Alizarine at pH 4.1-4.3 was performed in darkness for 15 minutes. Subsequently, they were cleaned with mili-Q water. The extraction of this reagent was done with cetylpyridinium chloride for 3 hours at room temperature under stirring. These extracts were analyzed with a spectrophotometer using a multiplate reader (Multiskan Ascent) at a wavelength of 550 nm. The significance of the results was determined statistically, coatings' values were compared against reference material to examine whether there were significant differences between them or not.

To perform this test, glass substrates coated with the different sol-gel hybrids by drop-casting were used. Each material was tested in triplicate, and each replicate was measured three times to determine the absorbance.

3.9.2. Biological assessment's results

Cell adhesion and proliferation were measured by analyzing mitochondrial activity using a colorimetric cell proliferation test kit (MTT) at different culture times. With this method only alive and stuck onto the surface cells' activity is measured. Figures 3.16 and 3.17 collect the obtained results for proliferation.

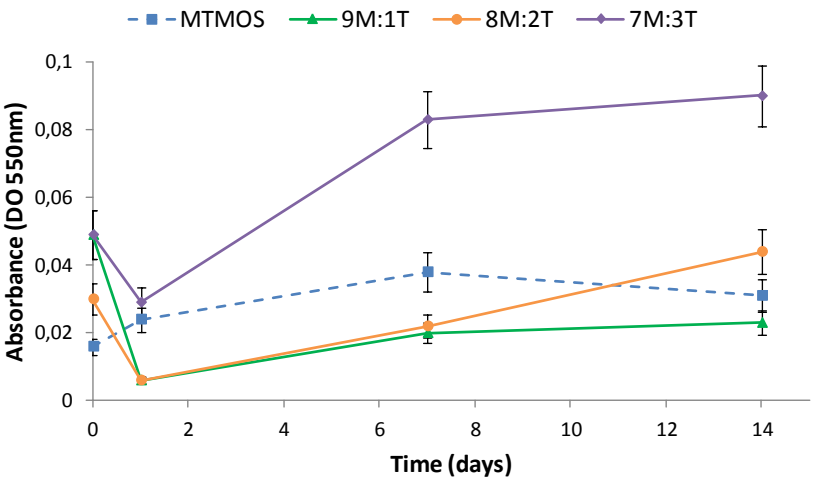

Figure 3.16. hMSCs' proliferation seeded onto the MTMOS:TEOS hybrids.

As seen in Figure 3.16, 9M:1T and 8M:2T coatings do not improve the proliferation in comparison to pure MTMOS film. After 14 days of culture they show a similar value of absorbance. However, the addition of a 30% of TEOS, 7M:3T hybrid, improves the proliferation significantly with respect to MTMOS. It has the highest adhesion value at day 0 and, in spite of a slight decrease at day 1, it shows an upward trend until the end of the assay.

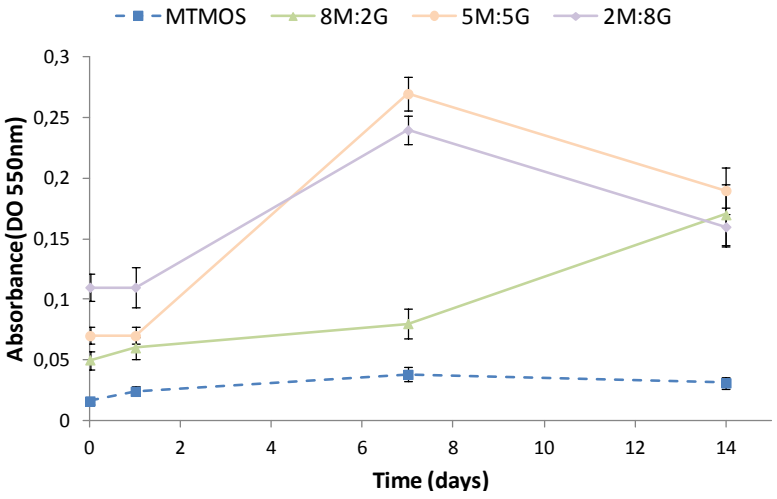

Figure 3.17. hMSCs' proliferation seeded onto the MTMOS:GPTMS hybrids.

In the case of the MTMOS:GPTMS hybrids (Figure 3.17), the incorporation of GPTMS is translated into an improvement of adhesion and proliferation for all the studied time points regarding MTMOS. The most noticeable increase in cell number is in 5M:5G and 2M:8G hybrids from day 1 to day 7 of culture, afterward they decrease reaching a value 6 folds higher than the one in MTMOS after 14 days. Such behaviour can be attributed to different factors. On the one hand, it is widely accepted that a hydrophilic surface favours cell adhesion and proliferation[18], and as it was found it section 5.5, the incorporation of GPTMS decreased the contact angle value. On the other hand, the cell adhesion is conditioned by the previous step of blood protein adsorption. This process is highly dependent on the wettability and the chemistry of the surface (functional groups on the surface)[23]. So the improvement achieved by the incorporation of GPTMS could be due to the influence of its epoxy group on cell adhesion.

After testing the adhesion and proliferation ability, it was important to determine if this pluripotent and undifferentiated cells were able to develop into bone forming cells and produce mineralized extracellular matrix. To analyze this property, the calcium-rich deposits formed by cells in an osteogenic culture medium were measured using Alizarin Red staining.

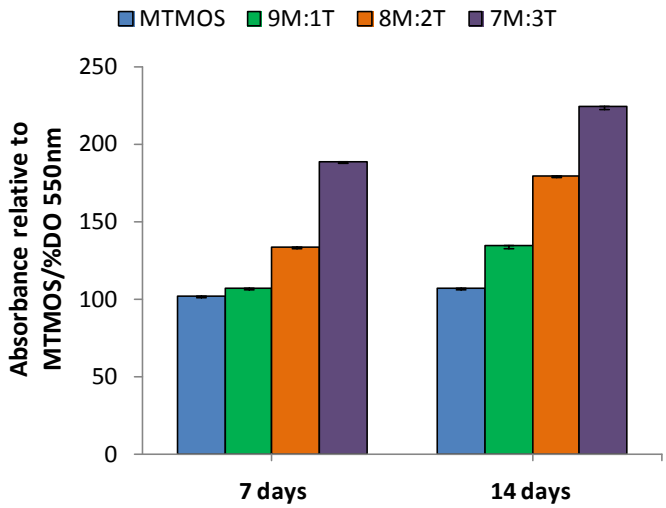

Figure 3.18. Quantification of mineralization by analyzing calcium-rich deposits on the MTMOS:TEOS coatings (values normalized to MTMOS calcium value).

In Figure 3.18 are presented the results obtained from the quantification of the calcium sediments formed by the differentiation of hMSC on different MTMOS:TEOS coatings. Values are normalized against those obtained for MTMOS. Results show how on 9M:1T, 8M:2T and 7M:3T calcium deposits values exceed the value of mineralization for MTMOS. After 7 days of induction, the recorded results show a relative absorbance regarding MTMOS of 104 %, 131 % and 184 %, for 9M:1T, 8M:2T and 7M:3T respectively. After 14 days all the materials are over the value of the control, MTMOS, in the case of 7M:3T it is doubled.

This increase can be due to the higher amount of Si released when TEOS is incorporated to the formulation. As said before and as it was proved by other researchers[7], Si has a beneficial effect inducing the osteogenic differentiation, what, in this case, was translated in a higher formation of calcium deposits.

The differentiation induction ability of the MTMOS:GPTMS coatings was performed in the same conditions explained above. The results are plotted in Figure 3.19. They show how cells seeded onto 8M:2G, 5M:5G and 2M:8G materials, produce large amount of calcium deposits, and the fast increase of these values from day 7 to day 14 of culture in osteogenic media. At day 7, the coating with a 50 % of GPTMS is the one that reach the highest value. However after 14 days, 8M:2G equalizes it and 2M:8G overcomes it. In all the cases the MTMOS:GPTMS coatings produce a mineralization a 500 % higher than pure MTMOS coating.

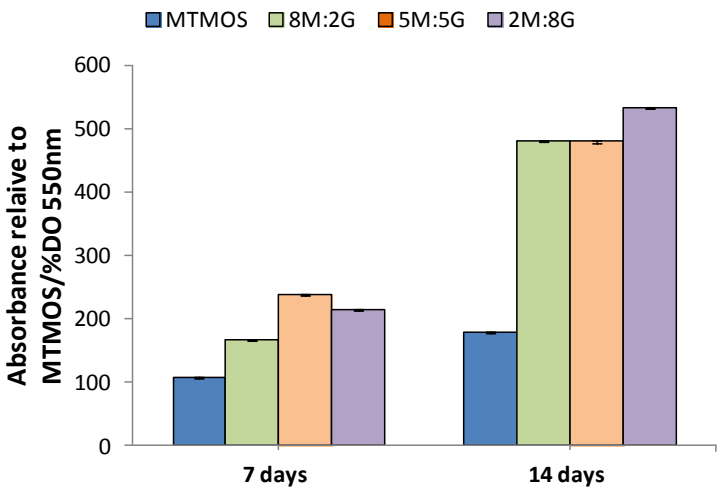

Figure 3.19. Quantification of mineralization by analyzing calcium-rich deposits on the MTMOS:GPTMS coatings (values normalized to MTMOS calcium value).

This behaviour is attributed to the higher Si release when adding GPTMS. The incorporation of this precursor leads to the formation of a network with a higher porosity (Figure 3.13), making easier the dissolution of the Si-O-Si bonds and, in consequence, the release of Si promoting bone formation.

3.10 Selection of suitable matrix for *in vivo* study

Taking into account all the obtained results for the MTMOS:TEOS and MTMOS:GPTMS series, it was concluded that they fulfil the desired properties to work as coatings for titanium implants: coatings with a high cross-linked network which are resorbable and release osteoinductive particles, and also present a suitable surface for cell adhesion and growth.

In this way, the chosen material from the MTMOS:TEOS series was 7M:3T since it was the one which gave the best value of mineralization rate. In the case of MTMOS:GPTMS hybrid type, all of the series show a similar behaviour, but 5M:5G seem to induce faster the hMSC activity at day 7 of culture, both for proliferation and differentiation. Therefore, 5M:5G was selected.

3.11. *In vivo* biocompatibility and osseointegration ability of coatings

In vivo study of biomaterials is an essential step when testing devices that are going to be implanted in humans. In spite of the *in vitro* studies giving important information about cell and material interaction, they cannot replace the *in vivo* study.

As stated in chapter 1, any implantation process can be considered as a source of irritation or of stimulus to the surrounding tissue. The inflammation will be the first reaction, and under normal conditions, this will be followed by a repair process and eventually the scarring. As a consequence of the implantation, the bone becomes inflamed, and regardless of how careful is the surgical technique used, a necrotic area around the created bone trauma will appear. The extent of the necrotic area will depend on the frictional heat generated during the surgical process and also in the vascularisation degree of the area, which may vary considerably even in different regions of the same bone[24].

Therefore, it is important to study the reaction of living tissue when an external material is placed into it. To perform this study two parameters were

evaluated: biocompatibility and osseointegration ability. We are going to focus on the most relevant results which led us to the selection of one of the materials as base coating for next steps of this work.

a) Experimental design

In order to assess the histological response of selected coatings, dental implants were surgically placed in the tibial metaphysis of rabbits *(Oryctolagus cuniculus)* from New Zealand. The experimental study met the ethical and legal conditions laid in R.D. 223/1988 of March 14th and the Order of October 13rd, 1988, about the protection of animals used for experimental experimentation and other scientific purposes. This part of the work was performed in Laboratory Animal Facility at Murcia University.

The dental implants used for this study were provided by Ilerimplant S.L., GMI Frontier internal connection hexagonal implants were selected (Figure 3.20). They are machined in CP grade IV titanium with a 3.75 mm of diameter and a length of 8 mm. To promote the adhesion and growth of bone cells, the outer surface of the implants are subjected to ADS® treatment (Advanced Double-Grip Surface) which combines a white corundum micro-bubble treatment and acid etching, for a non-smooth and heterogeneous roughness.

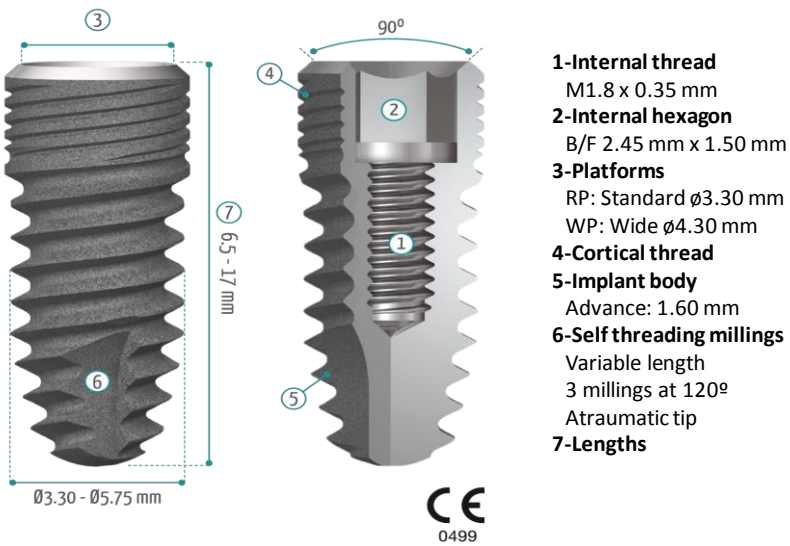

Figure 3.20. Internal connection GMI Frontier Implant.

Implants were coated by dip-coating with 7M:3T and 5M:5G hybrids. In each leg of the rabbit one coated implant and an uncoated one, as a control, were placed. After the corresponding periods of implantation (1, 2, 4 and 8 weeks) animals were euthanized and samples were subjected to the corresponding treatment for their posterior analysis.

b) Biocompatibility assessment

The biocompatibility of a material can be defined as the biological acceptance of it once is placed in the organism. This can be examined by looking at different parameters. In this case, tissue response was studied after implantation in order to determine the biocompatibility of coatings. To asses this response, such parameters as the bone marrow state, foreign body reaction giant cells presence and the fibrous capsule evolution, were evaluated.

- **Giant cells presence**

Implantation triggers a cascade of inflammatory and repair responses called foreign body reaction. Here, the appearance of giant cells and the formation of a fibrous capsule lead to the isolation of the implant as a consequence of the damages produced on the surrounding tissues. These cells are arranged around the device introduced into the body in order to protect the organism from it.

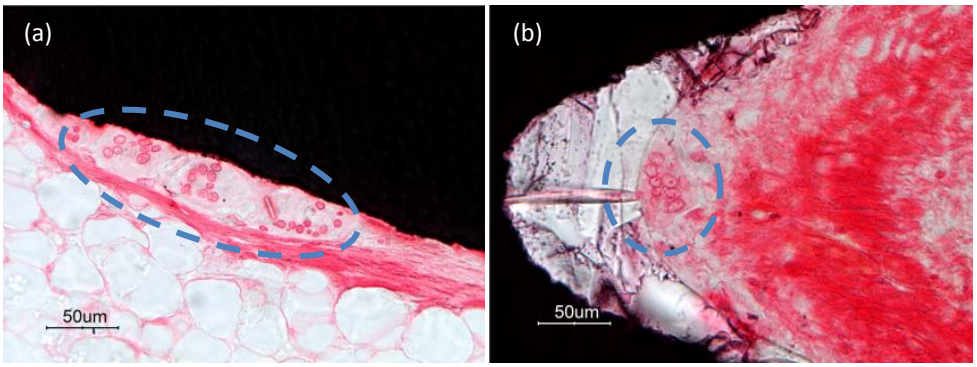

Figure 3.21. Foreign-body giant cells around (a) Titanium control and (b) 7M:3T coating.

Thus, the presence of foreign-body giant cells was studied, but only a few were found after 1 and 2 weeks of implantation for control and 7M:3T (Figure 3.21), they were not found in the case of 5M:5G. However, their amount in both cases did

not exceed the physiological response reaction to the presence of the implant; it was the normal behaviour against this type of stimulus

- **Bone marrow state**

Bone marrow is a spongy tissue located inside some bones. It is composed of hematopoietic stem cells, adipose cells and reticular cells. In this study the status of cellular load and the morphology of adipose cells were evaluated. In a healthy bone marrow, cellular load is predominant and adipose cells present a round morphology. As a consequence of the surgery, bone marrow is subjected to a damage what may lead to a traumatic bone marrow, where the cellular load is decreased and adipose cell are increased in number and loss their shape.

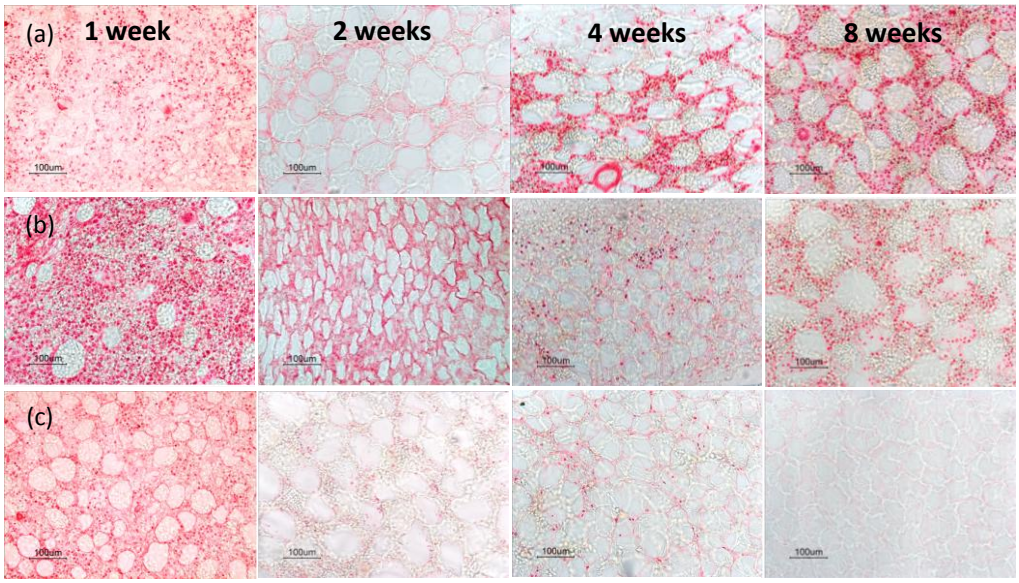

Figure 3.22. Bone marrow state for the studied different implantation times for (a) titanium control, (b) 7M:3T and (c) 5M:5G.

A good initial state of the bone marrow for uncoated titanium and 7M:3T coating was observed after 1 week of implantation, which got worse after 2 weeks, losing cell load and their architecture. Nevertheless, it was almost completely recovered after 8 weeks. In the case of 5M:5G we started from a traumatized bone that failed to recover after 8 weeks, obtaining a totally aplastic marrow.

- **Fibrous tissue layer development**

Following implantation, a fibrous layer is formed around the implant which is constituted by fibroblast layers and collagen fibres. An appropriate healing response implies the resorption of this capsule to allow the formation of bone. In this way, the evolution of the fibrous tissue layer will determine the success of the osseointegration.

It was obtained that the presence and evolution of the fibrous capsule was different according to their location along the implant. Its behaviour can be divided in two types: in contact with cortical bone or with trabecular bone.

Figure 3.23 shows the presence of a fibrous capsule between the cortical bone and the implant. This behaviour was observed for all the studied materials, what led us to think that the selected implantation model was not able to provide the necessary primary stability. Coating could also be observed even after 8 weeks of implantation, proving the impossibility of being reabsorb in cortical bone.

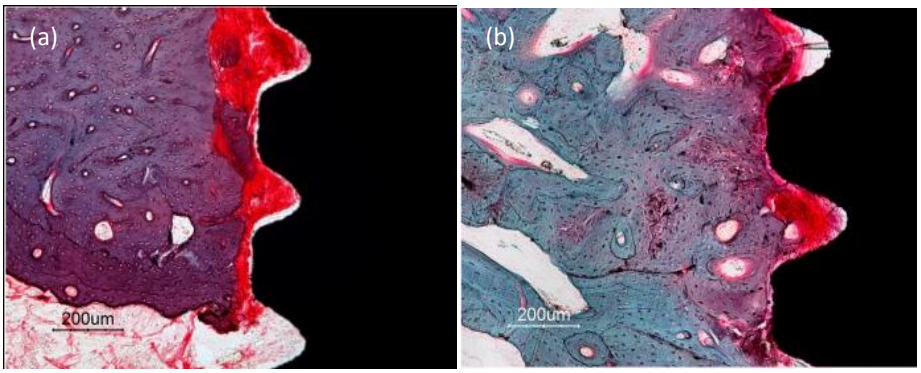

Figure 3.23. State of the fibrous tissue layer in the cortical bone for (a) titanium at week 4 and (b) 7M:3T at week 8.

Finally, when studying the behaviour of the fibrous capsule in contact with trabecular bone, a direct contact between new formed spongy bone and the implant without any intervening connective tissue layer was observed for uncoated titanium and 7M:3T coating (Figure 3.24). In the case of the 7M:3T coating the complete degradation of the film can be observed.

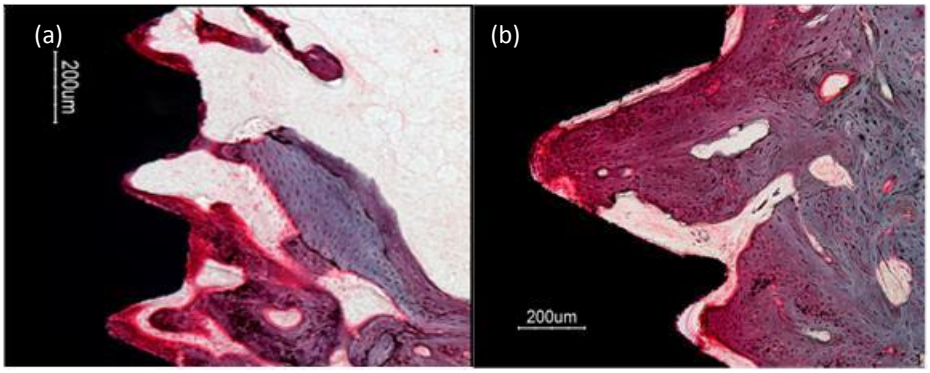

Figure 3.24. State of the fibrous tissue layer in the spongy bone after 8 weeks of implantation for (a) titanium and (b) 7M:3T.

For 5M:5G coating, fibrous capsule appeared during all the studied periods all around the implants. After 4 weeks, the presence of a dense fibrous capsule can be observed in Figure 3.25. After 8 weeks, there are some areas where the fibrous layer between the formed new bone (purple colour) and the coating (transparent) appears. This was due to the poor in vivo reabsorption ability of this coating, which after 8 weeks of implantation remained unmodified.

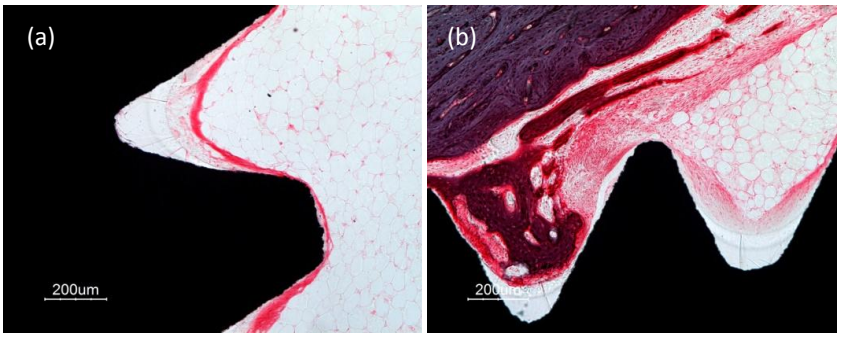

Figure 3.25. State of the fibrous capsule in the 5M:5G coating after (a) 4 and (b) 8 weeks of implantation.

c) Study of the osseointegration

Brånemark described the osseointegration as the direct structural and functional connection between ordered living bone and the surface of a load-carrying implant[24]. To assess the osseointegration ability of developed coatings, both the cortical and spongy bone reactions were studied. The studied parameters were:

regeneration of cortical bone by the osseointegration of implants' head, and osteoblastic activity and spicules formation to determine the osseointegration of trabecular bone.

- **Osseointegration in cortical bone**

As said before, due to the lack of primary stability almost all the samples showed a fibrous layer between the implant and the bone, what did not allow the integration of the implant in cortical bone. Albrektsson[25] stated some prerequisites to achieve the osseointegration and this was one of them.

In the case of titanium control and 7M:3T it was observed a small number of integrated cortical bones. For 5M:5G, no implant was able to lead to the osseointegration.

- **Osseointegration in trabecular bone**

In Figure 3.26 the osseointegration process for uncoated titanium implants is shown. Image (a) corresponds to the implantation period of 2 weeks, where little osteoblastic activity and not many spicules are observed. After 4 weeks (b), osteoblastic activity increased, reaching a high degree of osseointegration after 8 weeks.

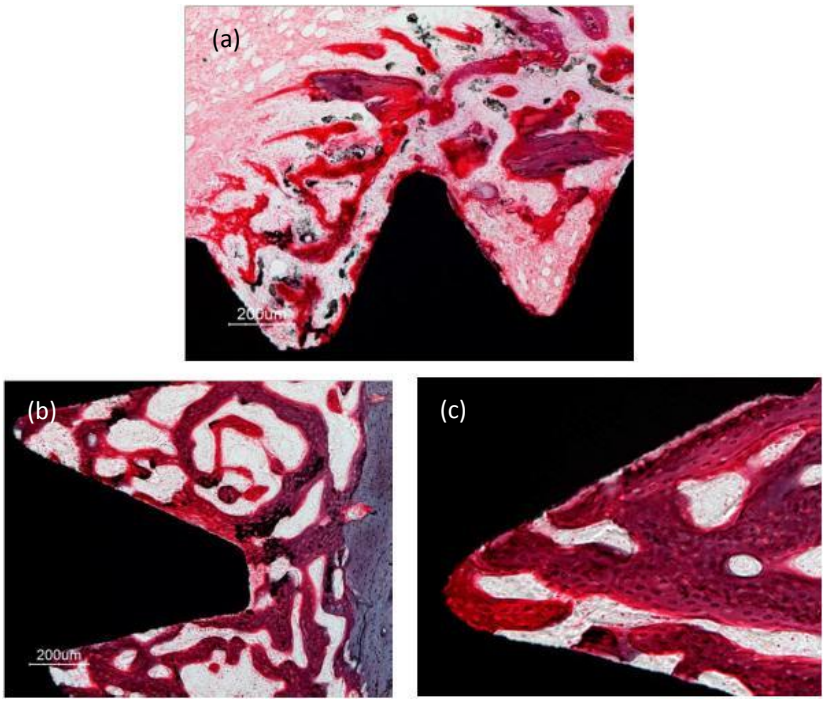

Figure 3.26. Osseointegration process for titanium control for (a) 1 week, (b) 4 weeks and (c) 8 weeks.

For the 7M:3T coating, osseointegration in trabecular bone was also observed. The osteoblastic activity at short periods of implantation was higher than for control (Figure 3.27. (a)), reaching at the end of the study, the formation of good mature trabeculae. It can also be seen the complete resorption of the coating after 8 weeks (b, c), where the release of silicon has induced the formation of new trabecular bone in its place.

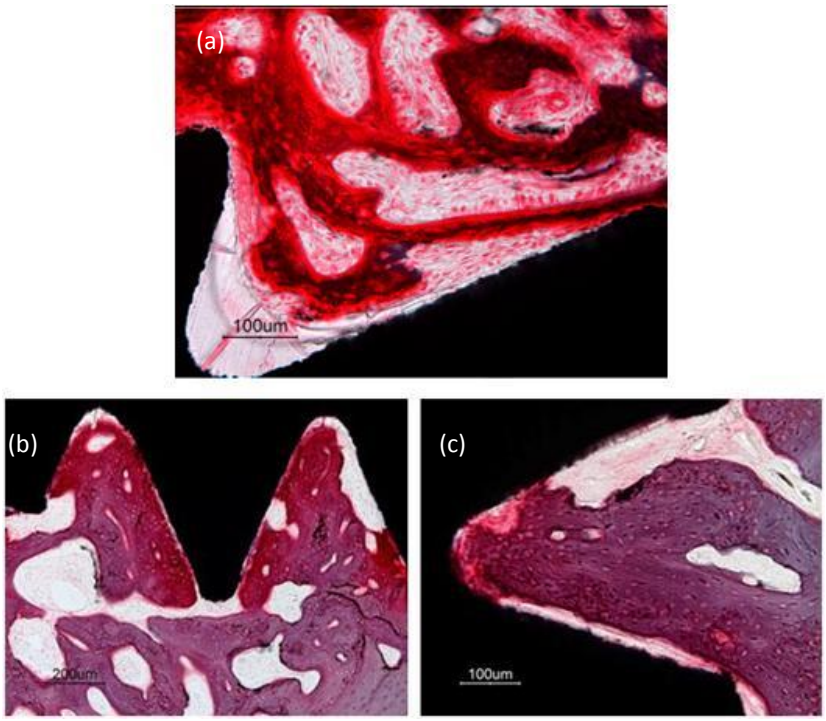

Figure 3.27. Osseointegration process for 7M:3T coating for (a) 1 week, (b) 4 weeks and (c) 8 weeks.

The 5M:5G coating showed a completely different behaviour as shown in Figure 3.28. Osteoblastic activity for all the studied periods of implantation was very poor and the obtained spicules were thin and with a few interconnection and a chaotic formation. Furthermore, the coating was not degraded after 8 weeks.

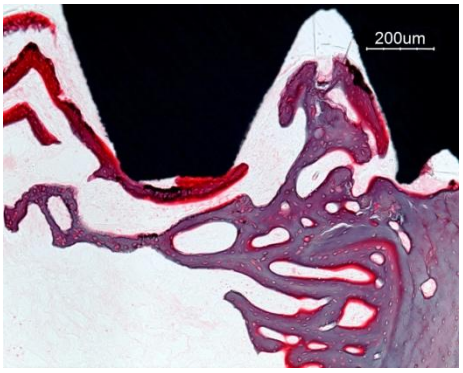

Figure 3.28. Osseointegration process for 5M:5G coating after 8 weeks of implantation.

To conclude, Figure 3.29 shows the image of the panoramic view of the uncoated implant (a) and the 7M:3T coating(b) after 2 weeks of implantation. For short periods of time, 7M:3T coating showed a higher ability of osseointegration. The material was able to promote the osteoblastic activity by distance osteogenesis from the endosteum. This was attributed to its degradation and Si release ability, which promoted bone formation.

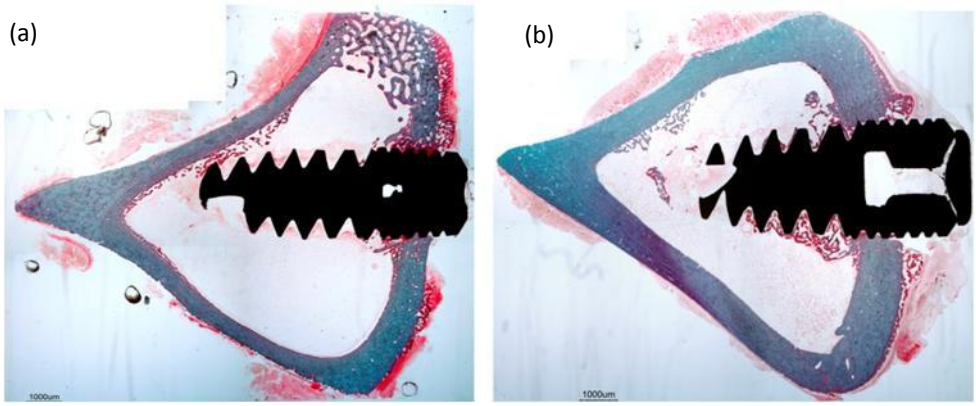

Figure 3.29. Osseointegration ability after 2 weeks of implantation for (a) uncoated titanium and (b)7M:3T.

3.12. Selection of the matrix for next steps

As it have been seen in the *in vivo* study, in the absence of primary stability, the 7M:3T coating is able to promote the osteoinduction due to the effect of Si release, while the osteoconduction of titanium is altered due to the absence of this stability. After 8 weeks, both control and 7M:3T showed a good quality of osseointegration. However it was found how during the first periods after the implantation, this process was favoured in the cases where the coating was there.

This behaviour, combined with its hydrophilicity, adhesion strength to the substrate and silicon release ability, makes 7M:3T the ideal material for the next steps of this study, where two type of matrixes will be designed. First one based on the incorporation of different amounts of gelatin, a protein which has gained interest in regenerative medicine due to favourable properties. And the second type of hybrid will be based in the design of a ternary system with the incorporation of GPTMS in order to add functionalization to the siloxane network

References

1. Hernández Escolano M. Desarrollo de recubrimientos híbridos osteoinductores para implantes dentales. 2012.

2. Hing KA, Revell PA, Smith N et al. Effect of silicon level on rate, quality and progression of bone healing within silicate-substituted porous hydroxyapatite scaffolds. *Biomaterials.* 2006; **27:** 5014-26.

3. Kim E, Bu S, Sung M et al. Effects of silicon on osteoblast activity and bone mineralization of MC3T3-E1 cells. *Biol Trace Elem Res.* 2013; **152:** 105-12.

4. Zolkov C, Avnir D, Armon R. Tissue-derived cell growth on hybrid sol–gel films. *J.Mater.Chem.* 2004; **14:** 2200-5.

5. Tsuru K, Robertson Z, Annaz B et al. Sol-gel synthesis and in vitro cell compatibility analysis of silicate-containing biodegradable hybrid gels. *Key Eng Mat.* 2008; **361:** 447-50.

6. Hernández-Escolano M, Juan-Díaz MJ, Martínez-Ibáñez M et al. The design and characterisation of sol–gel coatings for the controlled-release of active molecules. *Journal of Sol-Gel Science and Technology.* 2012; **64:** 442-451.

7. Shirosaki Y, Tsuru K, Hayakawa S et al. Effects of si (IV) released from chitosan-silicate hybrids on proliferation and differentiation of MG63 osteoblast cells. *Bioceram Dev Appl.* 2011; **1:** 1-4.

8. Mahony O, Yue S, Turdean-Ionescu C et al. Silica–gelatin hybrids for tissue regeneration: Inter-relationships between the process variables. *J Sol Gel Sci Technol.* 2014; **69:** 288-98.

9. Connell LS, Romer F, Suárez M et al. Chemical characterisation and fabrication of chitosan–silica hybrid scaffolds with 3-glycidoxypropyl trimethoxysilane. *Journal of Materials Chemistry B.* 2014; **2:** 668-80.

10. Jitianu A, Britchi A, Deleanu C et al. Comparative study of the sol–gel processes starting with different substituted si-alkoxides. *J Non Cryst Solids.* 2003; **319:** 263-79.

11. Daniels M, Francis L. Silane adsorption behaviour, microstructure, and properties of glycidoxypropyltrimethoxysilane-modified colloidal silica coatings. *J Colloid Interface Sci.* 1998; **205:** 191-200.

12. Tsuru K, Ohtsuki C, Osaka A et al. Bioactivity of sol–gel derived organically modified silicates: Part I: In vitro examination. *J Mater Sci Mater Med.* 1997; **8:** 157-61.

13. Zaharescu M, Jitianu A, Braileanu A et al. Thermal stability of SiO2-based inorganic-organic hybrid materials. *Journal of Thermal Analysis and Calorimetry.* 1999; **56:** 191-8.

14. Zaharescu M, Jitianu A, Braileanu A et al. Ageing effect on the SiO2-based inorganic-organic hybrid materials. *Journal of Thermal Analysis and Calorimetry.* 2001; **64:** 689-96.

15. Zaharescu M, Jitianu A, Brăileanu A et al. Composition and thermal stability of SiO2-based hybrid materials TEOS-MTEOS system. *Journal of Thermal Analysis and Calorimetry.* 2003; **71:** 421-8.

16. Bertelsen CM, Boerio FJ. Linking mechanical properties of silanes to their chemical structure: An analytical study of γ-GPS solutions and films. *Progress in Organic Coatings.* 2001; **41:** 239-46.

17. Rupp F, Gittens RA, Scheideler L et al. A review on the wettability of dental implant surfaces I: Theoretical and experimental aspects. *Acta Biomaterialia.* 2014; **10:** 2894-906.

18. Gittens RA, Scheideler L, Rupp F et al. A review on the wettability of dental implant surfaces II: Biological and clinical aspects. *Acta Biomaterialia.* 2014; **10:** 2907-18.

19. Juan-Díaz MJ, Martínez-Ibáñez M, Hernández-Escolano M et al. Study of the degradation of hybrid sol–gel coatings in aqueous medium. *Progress in Organic Coatings.* 2014; **77:** 1799-806.

20. Puleo DA, Huh WW. Acute toxicity of metal ions in cultures of osteogenic cells derived from bone marrow stromal cells. *Journal of Applied Biomaterials.* 1995; **6:** 109-16.

21. Thompson G, Puleo D. Ti-6Al-4V ion solution inhibition of osteogenic cell phenotype as a function of differentiation timecourse in vitro. *Biomaterials.* 1996; **17:** 1949-54.

22. Juan-Díaz MJ. Desarrollo de recubrimientos hibridos bioactivos para implantes dentales. 2013; .

23. Arima Y, Iwata H. Effect of wettability and surface functional groups on protein adsorption and cell adhesion using well-defined mixed self-assembled monolayers. *Biomaterials.* 2007; **28:** 3074-82.

24. Brånemark P, Zarb G, Albrektsson T. *Prótesis Tejido-Integradas: La Oseointegración En La Odontología Clínica.* Barcelona: Quintessence, 1999.

25. Albrektsson T, Brånemark P, Hansson H et al. Osseointegrated titanium implants: Requirements for ensuring a long-lasting, direct bone-to-implant anchorage in man. *Acta Orthopaedica.* 1981; **52:** 155-70.

Chapter 4

Effect of physical entrapment of different gelatin amounts in 7M:3T coating

Chapter 4:

EFFECT OF PHYSICAL ENTRAPMENT OF DIFFERENT GELATIN AMOUNTS IN 7M:3T COATING

4.1. Introduction

From the study presented in chapter 3, it was concluded that 7M:3T coating was the one that provided the most desirable *in vivo* behaviour. However, in spite of enhancing biocompatibility, increasing osteoblastic activation and promoting osteogenesis in short periods of time after implantation (1 and 2 weeks), there were not almost differences when comparing the osseointegration degree achieved after 8 weeks compared with pure titanium. In this context, we decided to continue searching for an improvement of developed materials.

This research proposes the development of new coatings through the sol-gel process with the idea of combining synthetic and natural polymers, such as proteins.

Many research groups focus their work on the design of materials to mimic the native extracellular matrix (ECM) in order to regulate cellular behaviour. Native ECM is mainly composed of collagen, so this protein has been widely used in pharmaceutical and medical fields. In spite of many advantages, these types of materials usually suffer from poor physicochemical properties[1], which limit their application and, due to their low solubility, they also present some drawbacks from a material processing point of view[2].

For that reason, gelatin was the selected protein for this study. Gelatin is a natural biopolymer derived from partial hydrolysis of collagen, keeping many attributes from it for its use as biomaterial for tissue engineering, but improving the solubility and processing ability. Among all the benefits that the use of gelatin presents, low cost, good biocompatibility, biodegradability, nontoxicity, water solubility and capacity to facilitate cell adhesion, migration and proliferation[3, 4], can be highlighted. Gelatin contains many functional motifs such as arginine-glycine-aspartic acid (RGD) sequence, which can modulate cell specific adhesion via RGD-integrin conjugation[5, 6]. Its ability to improve cell proliferation has been also attributed to the presence of polar functional carboxyl (COOH) and amino (NH_2) groups at the surface. They act as traps for cells and also may intervene as nucleation sites for HA[7].

Focussing on the most recent works, the incorporation of gelatin is mostly related to its biodegradability and bioadhesive properties. Mahony *et al*.[2] designed silica-gelatin scaffolds with diverse applications in both hard and soft tissue due to

their tailorable properties. Lim *et al.*[4] incorporated gelatin to a modified polyvinyl alcohol (PVA) hydrogel obtaining that this incorporation did not alter the physical and mechanical properties of the base polymer, but did significantly improve the cellular interactions. It was also found by Shi *et al.*[6], the effect of gelatin increasing the wettability and cell growth and proliferation, when grafting this protein to their polycarbonate urethane (PCU) scaffolds. Moreover, Vlierberghe *et al.*[8] successfully immobilized gelatin on titanium surface by silanization reaction, to work as an implant coating. However when evaluating the *in vitro* behaviour, they did not find coated implants to be more cell interactive than the uncoated Ti6Al4V[9].

Therefore, we decided to design novel siloxane-gelatin coatings with the aim of incorporating the minimal amount of gelatin for the required cellular functions, without perturbing too much the physical and mechanical properties of the 7M:3T matrix. The abundant residual active groups, amino and carboxyl groups, presented along gelatin chains, make possible the interaction with the siloxane matrix thought hydrogen bonding and electrostatic interactions with silanol groups[10, 11].

In this case, nuclear magnetic resonance of silicon atom (^{29}Si-NMR) in liquid state was used to study the sol-gel reaction degree and to evaluate the influence of incorporating different amounts of gelatin (wt%) in siloxane network formation. The chemical characterization of obtained coatings was completed by the use of solid state ^{29}Si-NMR, FT-IR and XPS measurements to confirm the effective incorporation of the protein. Finally the possibility of regulating wettability and dissolution properties of the film by the gelatin amount was assessed by contact angle measurements, hydrolytic degradation test and released silicon quantification.

4.2. Synthesis of 7M:3T-Gelatin hybrids

To prepare the sol of 7M:3T with gelatin, there was the need of changing some aspects of the synthesis process described in chapter 2. In this case, the used solvent was a mixture of isopropanol and water, since gelatin is not soluble in alcohols and some precursors were immiscible with water, as was the case of TEOS. After testing different isopropanol:water rates, 1:1 (v/v) showed to fulfil all the requirements for the synthesis and allowed to obtain homogeneous and transparent sols.

The synthesis starts with the precursors solution with the molar ratio established in chapter 3, 7M:3T, to which gelatin dissolved in the catalyst (0.1M HCl solution) is added drop by drop under stirring. The stirring was continued for two hours at 37 °C. The aim of increasing the temperature was to favor the solubility of gelatin and the formation of a homogeneous sol.

The concentration of gelatin in the silica sol was varied as 0, 0.2, 0.9 and 2 wt%. If the concentration was increased above 2 wt% a white precipitate was obtained indicating saturated concentration of gelatin, under the present experimental conditions. Table 4.1 collects all the used reagents and their rate.

Table 4.1. Relation between all the reagents to obtain the 7M:3T-Gelatin sols.

Coating nomenclature	7M:3T	7M:3T-0.2%	7M:3T-0.9%	7M:3T-2.0%
gelatin amount (wt%)	0	0.2	0.9	2.0
solvent:precursor (v/v)	1:1	1:1*	1:1*	1:1*
catalyst pH=1:precursor	Stoich.	Stoich.	Stoich.	Stoich.

*solvent = isopropanol:water (1:1, v:v)

Finally, different substrates were coated with the synthesised sols and the heat treatment was applied. This consists in an isotherm at 80 °C for 2 h. This temperature was selected because it allowed obtaining homogeneous coatings and the solvent evaporation, but it was low enough to ensure the stability of the incorporated biomolecule.

4.3. Chemical characterization

As it has been done in the previous chapter, the evolution of successive hydrolysis and condensation reactions of the sol-gel process was followed by liquid ^{29}Si-NMR, recording one spectrum hourly. The films obtained after the heat treatment were studied by solid ^{29}Si-NMR, FT-IR and XPS in order to test the effect of the introduction of gelatin in the siloxane network formation.

4.3.1. 29-Silicon Nuclear Magnetic Resonance (^{29}Si-NMR)

The study of all 7M:3T-Gelatin hybrids started recording the spectrum corresponding to the precursors in solvent. Next, the gelatin dissolved in the catalyst was added and a new spectrum was recorded, denominated time zero (t= 0h). From

this moment, the reaction was monitored for the two hours that last the process. Figure 4.1 shows the spectra obtained for 7M:3T-0.9% as an example.

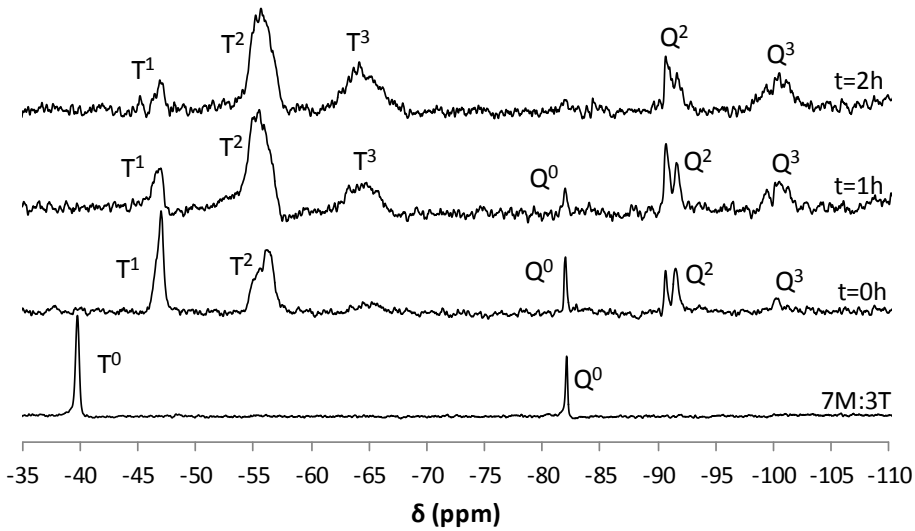

Figure 4.1. ^{29}Si-NMR liquid state spectra of 7M:3T-0.9%.

The spectrum corresponding to the precursors' solution shows two signals, one at -40 ppm and another one at -82 ppm, belonging to MTMOS and TEOS respectively. Afterwards, the catalyst with gelatin was added and the spectrum corresponding to this exact moment was recorded. It can be seen how as soon as the catalyst was added, the reaction started to take place rapidly, obtaining signals for condensed species. As it can be seen in next spectra, the intensity of these signals evolved proving the development of a more cross-linked network over reaction time and it also suggests that gelatin does not interfere in hydrolysis process.

To assess the effect of gelatin incorporation to the hybrid during the network formation, in Figure 4.2 the spectra recorded for all the 7M:3T-Gelatin sols after two hours of reaction are compared. It can be seen that there are no significant differences among all of them. The intensity of the entire signals attributed to each Si atom species are quite similar in all the spectra. As expected, the connectivity of the network remains intact, since gelatin is trapped by electrostatic and hydrogen bonding interactions. This could have an effect in the porosity of the film due to the immobilization of such a big molecule, what might be tested by the dissolution

properties. Owing to these results, it can be concluded that gelatin does not interfere in siloxane network formation during initial hydrolysis/condensation process.

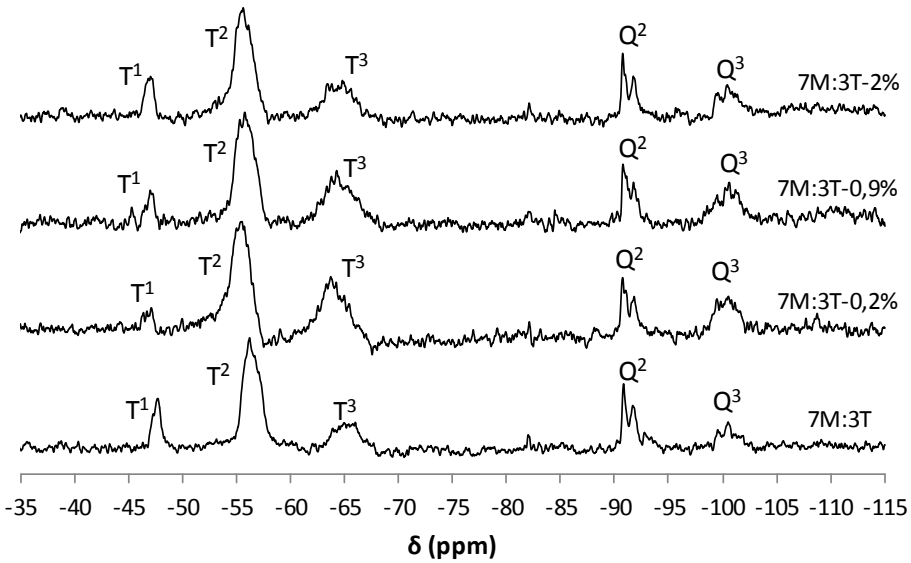

Figure 4.2. ^{29}Si-NMR liquid state spectra of 7M:3T-Gelatin hybrids after 2 h of reaction.

As said before, it was necessary to apply a heat treatment in order to obtain a highly cross-linked network and promote the solvent release. To study the structure of obtained materials after this treatment, ^{29}Si-NMR spectroscopy was used. In all the cases, materials were obtained as free films and they were grinded before being analyzed by ^{29}Si-NMR in solid state. Figure 4.3, shows, the comparison of the spectra for all 7M:3T-Gelatin hybrids.

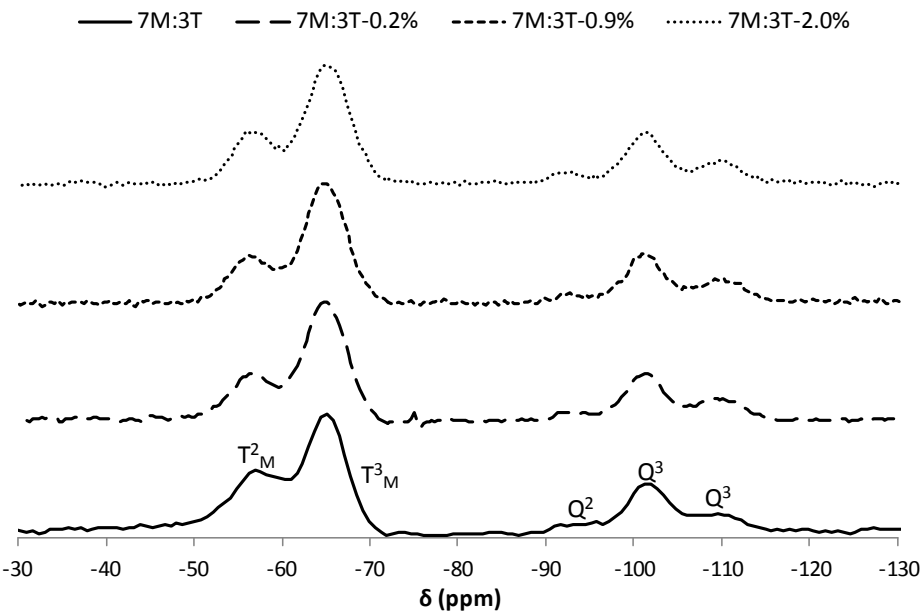

Figure 4.3. ^{29}Si-NMR spectra of obtained 7M:3T-Gelatin films after heat treatment.

All the spectra show the same signals and it is clear the effectiveness of the selected heat treatment allowing to obtain a closer network. Peaks T^2 and T^3 associated to MTMOS precursor, and Q^2, Q^3 and Q^4 to TEOS can be observed. In the same way as happened in liquid ^{29}Si-NMR study, the intensity of the signals is apparently the same in all species. Peak fitting of every spectrum was done, allowing the quantification of each silicon species present in hybrids. Furthermore, the degree of condensation (D_C), or connectivity, was determined from the previously calculated percentage values of Q and T species using the following equation[12, 13]:

$$D_C = \frac{4Q^4+3Q^3+2Q^2+Q^1}{4} + \frac{3T^3+2T^2+T^1}{3} \qquad \text{(Eq. 4.1.)}$$

Where Q^n represents the abundance, as percentage, of each Q species and T^n is the abundance of T species.

From the qualitative analysis of obtained spectra, it was concluded that in spite of the gelatin introduction, all hybrids had very similar inorganic structure. The quantification of this data, Table 4.2, showed only very slight variation in the relative abundance of Q and T species, which can be attributed to fitting process deviations.

By summation of Q and T species according to Eq. 4.1, the degree of condensation was obtained revealing that silica network connectivity was almost unmodified.

Table 4.2. Percentage abundance of silicon species present in 7M:3T-Gelatin hybrids and network connectivity.

Coating	T^2	T^3	Q^2	Q^3	Q^4	D_C
7M:3T	20	43	3	22	12	86.3
7M:3T-0.2%	22	46	2	21	9	86.4
7M:3T-0.9%	22	48	2	20	8	86.6
7M:3T-2.0%	21	43	3	22	11	86.0

4.3.2. Infrared Spectroscopy (FT-IR)

First of all, the structure of the used commercial gelatin was studied, in order to determine its more relevant vibration signals and try to find them latter in the hybrid compound. Protein's spectrum is presented in Figure 4.4, which was recorded in same conditions as for the films described in Chapter 3.

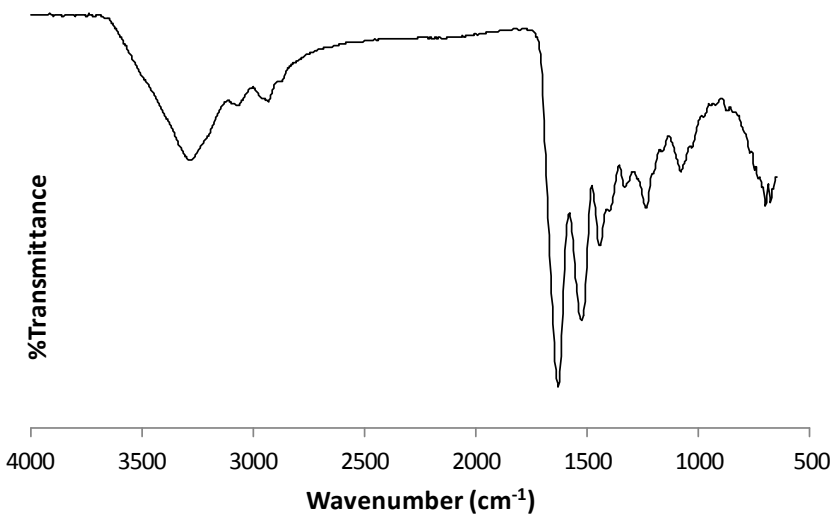

Figure 4.4. FT-IR spectra of gelatin.

FTIR spectra of pure gelatin is characterized by a width band at 3400 cm^{-1} corresponding to NH stretching vibrations, some small bands around 2900 cm^{-1} attributed to CH stretching vibrations and two sharp bans at 1640 and 1520 cm^{-1} due

to the amide I (C=O stretching) and amide II (N-H in plane bend) bands respectively[11, 14].

After thermal treatment synthesized coatings were also characterized by FT-IR, in order to determine the organic-inorganic nature of the coating and the possible effect of gelatin incorporation on hybrid structure. Figure 4.5 shows the comparison of two spectra, 7M:3T and 7M:3t-2%, to determine the differences produced in characteristic signal of the 7M:3T hybrid.

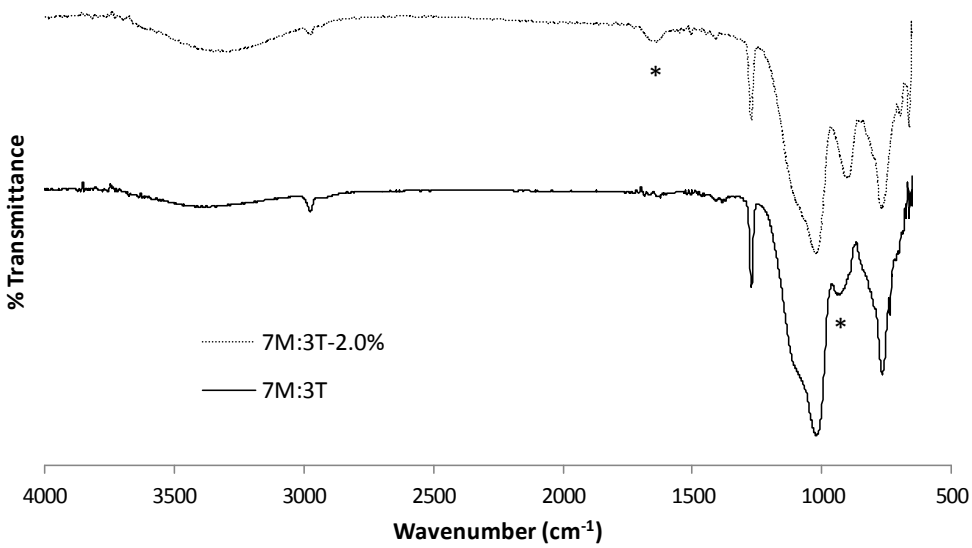

Figure 4.5. FT-IR spectra of 7M:3T and 7M:3T-2.0%.

First, the characteristic vibration bands of siloxane network and methyl groups of MTMOS precursor described in chapter 3 can be seen in both cases, large split band at 1100 cm^{-1} and a sharp smaller one at 1270 cm^{-1} respectively. After comparing the effect of gelatin introduction, two main differences can be appreciated. The first one lies on the fact that the band at 940 cm^{-1} corresponding to silanol (Si-O-(H)) stretching vibration[15], is shifted to lower values of wave number. This can be due to the hydrogen bonding between silanol groups of the siloxane phase and the carboxyl and amino groups of the gelatin. The second difference is based on the appearance of a new small band in the case of 7M:3T-2% hybrid at 1640 cm^{-1} belonging to Amide I vibration and confirming the presence of the gelatin. However, due to the weak intensity of this band, the small amount of gelatin

introduced into the formulation and the large size of siloxane bond vibration bands, it is difficult to confirm the presence of the protein by this method.

4.3.3. X-ray Photoelectron Spectroscopy (XPS)

Chemical characterization was completed with XPS measurements, where the chemical composition of the surface of coatings was studied. In Figure 4.6, the atomic averages obtained for 7M:3T and 7M:3T-0.9%, are shown as an example.

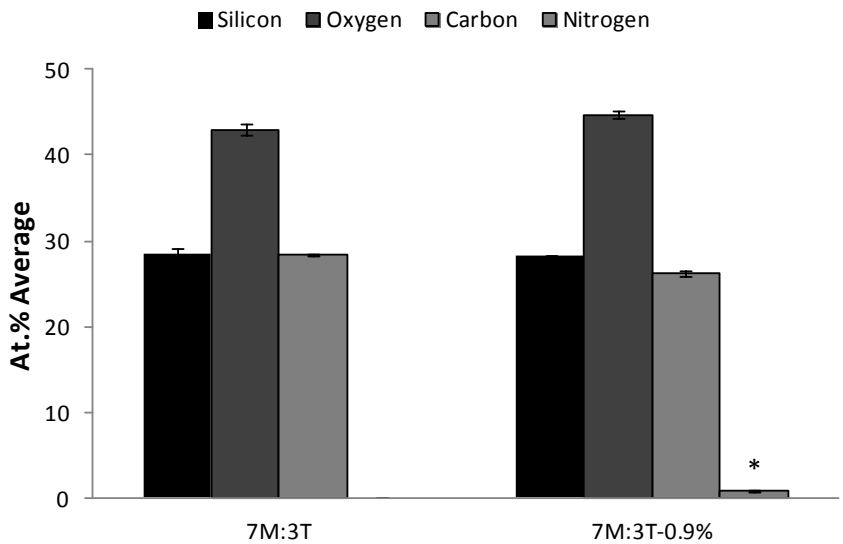

Figure 4.6. XPS elemental composition of 7M:3T and 7M:3T-0.9% coatings.

As expected, great differences were not obtained among all the different coatings. The main one was the appearance of a small signal due to nitrogen in coatings with gelatin. This helped confirming the effective incorporation of the biomolecule in the siloxane network and the surface modification. In spite of being a minor band, related to a 0.6 % atomic average, it was enough to confirm the presence of gelatin since it was not found in any of the 7M:3T hybrids.

4.4. Morphological characterization

Obtained films were homogeneous, transparent and crack free. Different microscopic methods were used to study their morphological properties, as well as their adhesion strength to the substrate.

4.4.1. Cross-cut adhesion test

In order to test the adhesion strength obtained for these hybrids, cross-cut adhesion test was performed, in the same way as it was done for MTMOS:TEOS hybrids in the prior chapter. The results were evaluated visually (Figure 4.7.(a)) and by optical microscopy (Figure 4.7.(b)).

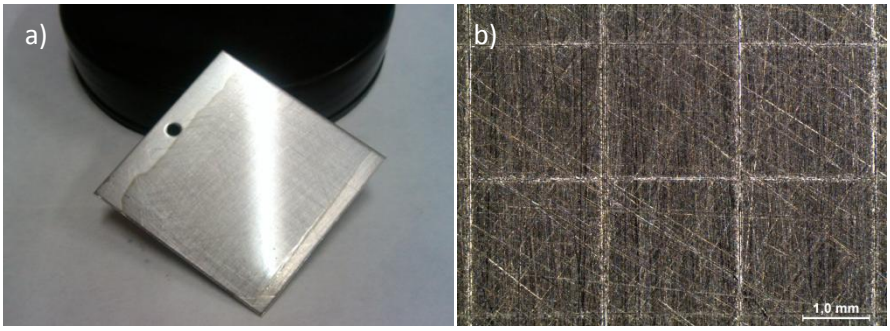

Figure 4.7. 7M:3T-0.9% coating's appearance by (a) a first sight and (b) optical microscope after cross-cut test.

In the picture on the left, the glossy finish and uniformity of the coating can be seen. On the right, there is a picture obtained by optical microscopy after the cross-cut adhesion test, where all the materials show an excellent adhesion due to the no detachment of any of the squares during the assay. However, it cannot be clearly appreciated in this figure due to the abrasive treatment of the substrate.

4.4.2. Atomic Force Microscopy (AFM)

After confirming the good surface properties of developed coatings and enough adhesion strength, next step was to evaluate their homogeneity and differences on roughness related to hybrid composition by phase images and height images respectively, obtained by AFM.

For this study smooth titanium discs were used, which were dip-coated with the different formulations. Results showed how the incorporation of gelatin meant a slight decrease on coating roughness; Table 4.3 collects roughness average values (R_a).

Table 4.3. Roughness values for 7M:3T-Gelatin hybrids.

	7M:3T	7M:3T-0.9%	7M:3T-2.0%
R_a (nm)	0.50 ± 0.20	0.48 ± 0.10	0.42 ± 0.09

These values show that obtained coatings are completely smooth; they do not present any topography by themselves, what could be interesting for the cases where it is necessary to reproduce as much as possible substrates' topography.

Figure 4.8 shows two AFM images obtained for 7M:3T and 7M:3T-0.9% coatings. In both cases the same texture and also the homogeneity of the synthesized materials can be appreciated.

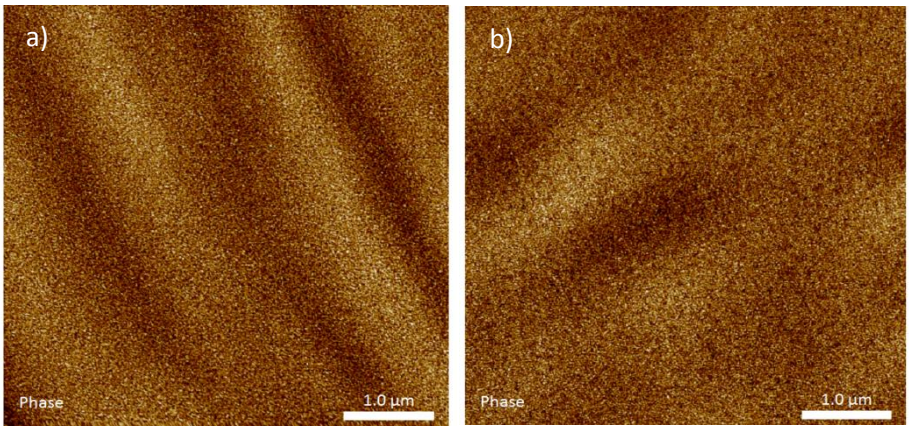

Figure 4.8. Phase AFM images for (a) 7M:3T and (b) 7M:3T-0.9% coatings.

In spite of the fact that AFM has ended up being a good method to prove the homogeneity and smooth finish of developed coatings, it was not possible to determine the roughness of the same materials when they were applied on rough Ti discs. We tried to study by the same method, how the roughness of Ti discs (produced by a commercial surface treatment) changes as a consequence of coating them with the 7M:3T-Gelatin hybrids. However, the precipitous topography of these types of discs made impossible the use of the AFM.

Further studies related to the topography and the effect of coated commercial implants on the biological response will be shown in chapter 7, mainly focusing on the effect of roughness on cell adhesion and proliferation.

4.5. Determination of hydrophobicity/hydrophilicity

In the same way done in section 3.5, the hydrophobic/hydrophilic nature of new synthesized hybrids was determined by water contact angle measurements. The aim was to test the effect of gelatin in this property since, as explained before, it is an important feature which will condition the biological cascade of interactions with serum proteins and cells after implantation[16]. Results are presented in Table 4.4.

Table 4.4. . Contact angle values for 7M:3T-Gelatin series.

Coating	7M:3T	7M:3T-0.2%	7M:3T-0.9%	7M:3T-2.0%
Contact angle (°)	70.0 ± 0.8	60.9 ± 2.5	58.2 ± 3.1	52.6 ± 1.8

Results show how the water contact angle value of modified coatings decreases successively compared to the blank 7M:3T hybrid (70.0° ± 0.8°), what indicates that more hydrophilic surfaces were achieved by immobilizing gelatin. The introduction of a small amount of gelatin, such as 2 wt%, was enough to decrease this value from 70.0° to 52.6°, which may have also effect on resorption behaviour of the coating, as it will be studied later.

4.6. Hydrolytic degradation test

In the *in vivo* study showed in the previous chapter, it was found that 7M:3T coating was completely reabsorbed after 8 weeks of implantation, what allowed the osseointegration of the implant. Owing to the relevance of this property, in this case, the effect of the incorporation of a water soluble protein (gelatin) in the siloxane matrix on the hydrolytic degradation kinetic was tested.

Glass substrates coated with different formulations were immersed in PBS at 37 °C for 8 weeks and their mass loss was determined at previously established time points. Results obtained from this gravimetric study are plotted in Figure 4.9.

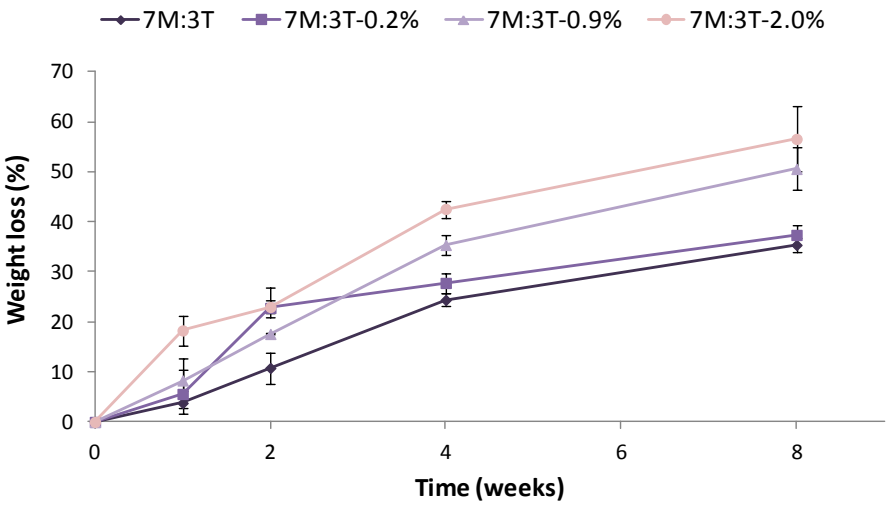

Figure 4.9. Mass loss due to hydrolytic degradation of 7M:3T-Gelatin coatings.

In all the cases a progressive degradation over immersion time is observed. As expected the mass loss increases with the incorporation of gelatin, all the hybrids show the same trend. Gelatin is a natural polymer able to dissolve in aqueous media within a few minutes, for that reason, its incorporation improves the resorption properties of the coatings. This is also in good agreement with the results obtained with the goniometer, where the wettability was significantly increased in the case of 7M:3T-Gelatin films compared to blank 7M:3T.

Furthermore, the physical entrapment of gelatin into the siloxane network may result in an increase of the pore size, making easier the entrance of water and in consequence the dissolution. Smitha *et al.*[11] found how the incorporation of a 2 wt% of gelatin in silica matrix produced a mesoporous structure, increasing the pore size due to the immobilization of a polymeric molecule with such a big size as gelatin.

In addition, the connectivity of the silica phase studied in section 4.3, did not reveal significant differences among all 7M:3T-Gelatin hybrids. Therefore, the observed different behaviour with the gelatin introduction can be attributed to the physical rearrangement of gelatin chains in siloxane network[13], and also to its high wettability.

4.7. Silicon release test

Apart from the gravimetric study, another performed test to evaluate the dissolution properties of the hybrids consists on monitoring the release of Si over time. This assay has a double aim. Firstly, support the results obtained in the previous section regarding the effect of gelatin introduction in matrix properties, and secondly, as mentioned at different parts of this thesis, make a quantitative study of the Si released since it will influence the osteogenic ability of the developed materials[17].

Assay was performed in the way described in chapter 2 and under the same conditions of the hydrolytic degradation test. In Figure 4.10 Si release values measured by ICP for the 7M:3T, 7M:3T-0.2%, 7M:3T-0.9% and 7M:3T-2.0% coatings are plotted.

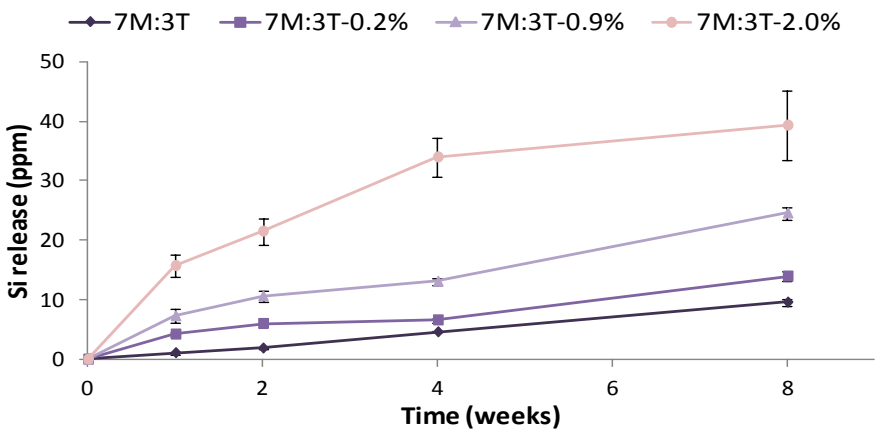

Figure 4.10. Release profiles of Si in PBS measured by ICP.

The Si release profiles show similar trends to mass loss profiles. When increasing the gelatin percentage in the hybrid, the cumulative Si released to the media increases. In this way, after 8 weeks of immersion time, 7M:3T releases around 10 ppm, value that is quadrupled when incorporating 2 wt% gelatin to the coating, reaching about 40 ppm Si.

As it was explained before, this fact is attributed to the high increase in wettability when incorporating gelatin, its water uptake ability and the possible

effect of immobilizing a molecule of such size in the global porosity of the siloxane network.

4.8. Electrochemical Impedance Spectroscopy (EIS)

Electrochemical impedance spectroscopy measurements were performed as a complementary method for the study of the degradation kinetics of the different coatings. This study will give information about the possible mechanism of degradation, related to the porosity of studied materials. In Figure 4.11 the results obtained for the evolution of the pore resistance are plotted.

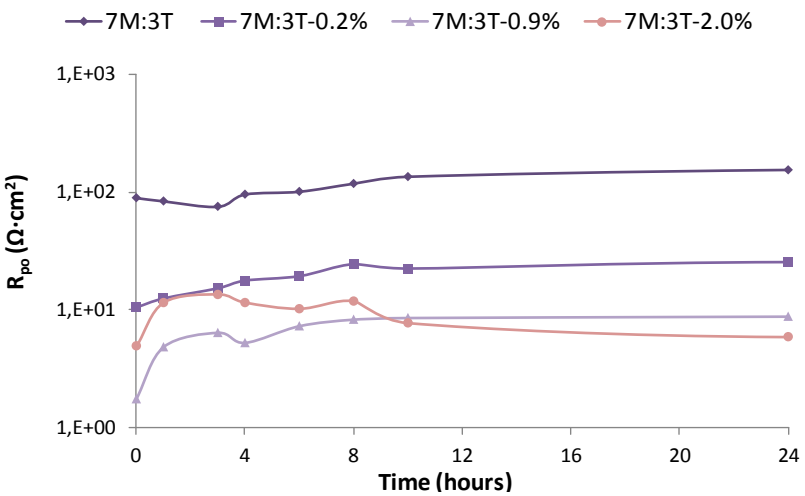

Figure 4.11. Evolution of the pore resistance versus contact time with electrolyte of the coatings 7M:3T, 7M:3T-0.2%, 7M:3T-0.9% and 7M:3T-2.0%.

It can be clearly seen in Figure 4.11 that coatings with gelatin have lower R_{po} values than those observed for 7M:3T coating, and this pore resistance decreases with the increase in gelatin content. Coatings with gelatin showed higher hydrophilicity (contact angle measurements), offering no resistance to the flow of water through the pores. Furthermore, there is no covalent coupling between the siloxane network and the biomolecule, so it will be easily release in contact with aqueous media favouring the pore formation along the network.

Therefore, these results are in good agreement with the previous obtained ones for hydrolytic degradation test and cumulative silicon release quantification.

4.9. Conclusions

From the results obtained for this type of hybrids, different conclusions can be taken. Firstly, from the chemical and morphological characterization, the successful obtaining of transparent, homogeneous and uniform coatings where gelatin is effectively immobilized can be confirmed. Furthermore, the contact angle and dissolution study proved the possibility of designing materials where key properties, like dissolution rate and Si release amount, can be controlled and tailored by varying the gelatin percentage, without altering the material chemistry (Figure 4.3).

Finally, in chapter 7, it will be studied if this noticeable increase of dissolution profiles with the gelatin incorporation leads to a better matrix mineralization due to a higher Si content, or in contrast, if it results in a worsening of proliferation due to a too rapid degradation.

References

1. Hu Y, Liu L, Gu Z et al. Modification of collagen with a natural derived cross-linker, alginate dialdehyde. *Carbohydr Polym.* 2014; **102:** 324-32.

2. Mahony O, Tsigkou O, Ionescu C et al. Silica-Gelatin hybrids with tailorable degradation and mechanical properties for tissue regeneration. *Advanced Functional Materials.* 2010; **20:** 3835-45.

3. Thein-Han WW, Saikhun J, Pholpramoo C et al. Chitosan–gelatin scaffolds for tissue engineering: Physico-chemical properties and biological response of buffalo embryonic stem cells and transfectant of GFP–buffalo embryonic stem cells. *Acta Biomaterialia.* 2009; **5:** 3453-66.

4. Lim KS, Alves MH, Poole-Warren LA et al. Covalent incorporation of non-chemically modified gelatin into degradable PVA-tyramine hydrogels. *Biomaterials.* 2013; **34:** 7097-105.

5. Huang Y, Onyeri S, Siewe M et al. In vitro characterization of chitosan–gelatin scaffolds for tissue engineering. *Biomaterials.* 2005; **26:** 7616-27.

6. Shi C, Yuan W, Khan M et al. Hydrophilic PCU scaffolds prepared by grafting PEGMA and immobilizing gelatin to enhance cell adhesion and proliferation. *Materials Science and Engineering: C.* 2015; **50:** 201-9.

7. Brasack I, Böttcher H, Hempel U. Biocompatibility of modified silica-protein composite layers. *J Sol Gel Sci Technol.* 2000; **19:** 479-82.

8. Van Vlierberghe S, Vanderleyden E, Boterberg V et al. Gelatin functionalization of biomaterial surfaces: Strategies for immobilization and visualization. *Polymers.* 2011; **3:** 114-30.

9. Vanderleyden E, Van Bael S, Chai YC et al. Gelatin functionalised porous titanium alloy implants for orthopaedic applications. *Materials Science and Engineering: C.* 2014; **42:** 396-404.

10. Coradin T, Bah S, Livage J. Gelatine/silicate interactions: From nanoparticles to composite gels. *Colloids and Surfaces B: Biointerfaces.* 2004; **35:** 53-8.

11. Smitha S, Mukundan P, Pillai PK et al. Silica–gelatin bio-hybrid and transparent nano-coatings through sol–gel technique. *Mater Chem Phys.* 2007; **103:** 318-22.

12. Connell LS, Romer F, Suárez M et al. Chemical characterisation and fabrication of chitosan–silica hybrid scaffolds with 3-glycidoxypropyl trimethoxysilane. *Journal of Materials Chemistry B.* 2014; **2:** 668-80.

13. Mahony O, Yue S, Turdean-Ionescu C et al. Silica–gelatin hybrids for tissue regeneration: Inter-relationships between the process variables. *J Sol Gel Sci Technol.* 2014; **69:** 288-98.

14. Lei B, Shin K, Noh D et al. Nanofibrous gelatin–silica hybrid scaffolds mimicking the native extracellular matrix (ECM) using thermally induced phase separation. *Journal of Materials Chemistry.* 2012; **22:** 14133-40.

15. Zaharescu M, Jitianu A, Braileanu A et al. Ageing effect on the SiO2-based inorganic-organic hybrid materials. *Journal of Thermal Analysis and Calorimetry.* 2001; **64:** 689-96.

16. Gittens RA, Scheideler L, Rupp F et al. A review on the wettability of dental implant surfaces II: Biological and clinical aspects. *Acta Biomaterialia.* 2014; **10:** 2907-18.

17. Shirosaki Y, Tsuru K, Hayakawa S et al. Effects of si (IV) released from chitosan-silicate hybrids on proliferation and differentiation of MG63 osteoblast cells. *Bioceram Dev Appl.* 2011; **1:** 1-4.

Chapter 5

Design of a ternary system with functional groups on the surface

Chapter 5:

DESIGN OF TERNARY SYSTEM WITH FUNCTIONAL GROUPS ON THE SURFACE

5.1. Introduction

After the study done in chapter 3 with MTMOS:GPTMS hybrid series, where the amount of functional groups was varied by the addition of GPTMS, 5M:5G was chosen as the coating with the best properties. However, the *in vivo* study of this material did not give so promising results as expected, due to the absence of resorption of the coating after 8 weeks of implantation and, in consequence, the formation of a fibrous capsule around the implant.

Owing to this results, 7M:3T was selected as base coating for next steps of the study. Nevertheless, the introduction of an epoxy group through the use of GPTMS precursor opens a wide range of possibilities. For that reason it was decided to design a ternary system MTMOS:GPTMS:TEOS, where the molar rate between MTMOS and GPTMS was kept 1:1, and the amount of TEOS in the hybrid was a 30 %, in the same way as the 7M:3T hybrid. The aim of adding different amounts of gelatin is to tailor the degradability and Si release properties of the coating, as well as because of its cell adhesive properties explained in the previous chapter.

As mentioned above, there are different reasons to make us decide to design a coating with functional groups in its surface. First of all, it is likely that this epoxy groups may have a favourable effect in tissue response. In spite of the mechanism is not completely understood, it is widely documented that biomaterial surface properties can affect protein adsorption, subsequent cell recruitment and tissue responses[1-5]. Among all this properties, the type and the density of surface charge, balance between hydrophobicity/hydrophilicity, topography, chemical structure and functional groups can be highlighted.

The surface functional groups can influence cell growth, likely due to the fact that surface chemical functionality affects adsorbed proteins and subsequent protein:cell interactions[6]. Keselowsky *et al.*[1] investigated the effects of surface chemistry on fibronectin (Fn) adsorption and conformation onto self-assembled monolayer (SAM) surfaces with four different terminal functional groups: $-CH_3$ -OH, -COOH, and $-NH_2$. Their results indicated differences in accessibility to binding domains in Fn, integrin binding, and cell adhesion as function of underlying surface chemistry following the trend OH > COOH = NH_2 > CH_3. These findings were consistent with other works where it was found a preferential cell growth on functional polar groups rather than on CH_3[7]. In spite of further discussion about

surface properties' effect on protein adsorption will be done in chapter 6, this review makes clear the incentive to design a material with the epoxy functional group.

Another important benefit provided by the use of GPTMS, is the possibility of covalently bonding different biomolecules on the surface, gelatin in this case. This precursor has been used in many works, mainly related to scaffolds, to obtain a tough composite material that degrades as one material due to the strong covalent links between the inorganic and organic chains[8-10]. These links are the result of the reaction between epoxy groups of GPTMS and the residual nucleophilic groups like amino or carboxylic of gelatin[11-13]. In this chapter the achievement or not of them under the used synthesis conditions will be studied. Furthermore, GPTMS will work as a compatibilizer agent between the silica and gelatin phases.

The proposed study plan was the same as in chapter 4, starting with the chemical and morphological characterization of the new developed material, followed by the study of the resorption properties of the coating using a gravimetric study and Si released quantification. These results will be compared to the ones obtained in the previous chapter.

5.2. Synthesis of 35M:35G:30T-Gelatin hybrids

As told before, based on the binary hybrids previously studied, it was decided to keep the molar rate 1:1 between MTMOS and GPTMS precursors and a 30% of TEOS in relation to them. In this way the molar rate among all the precursors was 35:35:30 (MTMOS:GPTMS:TEOS). The concentration of gelatin in the silica sol was 0, 0.2, 0.9 and 2.0 wt%, the same percentages chosen for 7M:3T hybrids. Table 5.1 collects all the reagents and their rate.

Table 5.1. Relation between all the reagents to obtain 35M:35G:30T-Gelatin sols.

Coating nomenclature	35M:35G:30T	35M:35G:30T-0.2%	35M:35G:30T-0.9%	35M:35G:30T-2.0%
gelatin amount (wt%)	0	0.2	0.9	2.0
solvent:precursor (v/v)	1:1	1:1*	1:1*	1:1*
catalyst:precursor	Stoich.	Stoich.	Stoich.	Stoich.

*solvent = isopropanol:water (1:1, v:v)

Due to the possibility of covalently linking gelatin to the siloxane network through the epoxy group of GPTMS, the synthesis protocol was slightly changed (Figure 5.1).

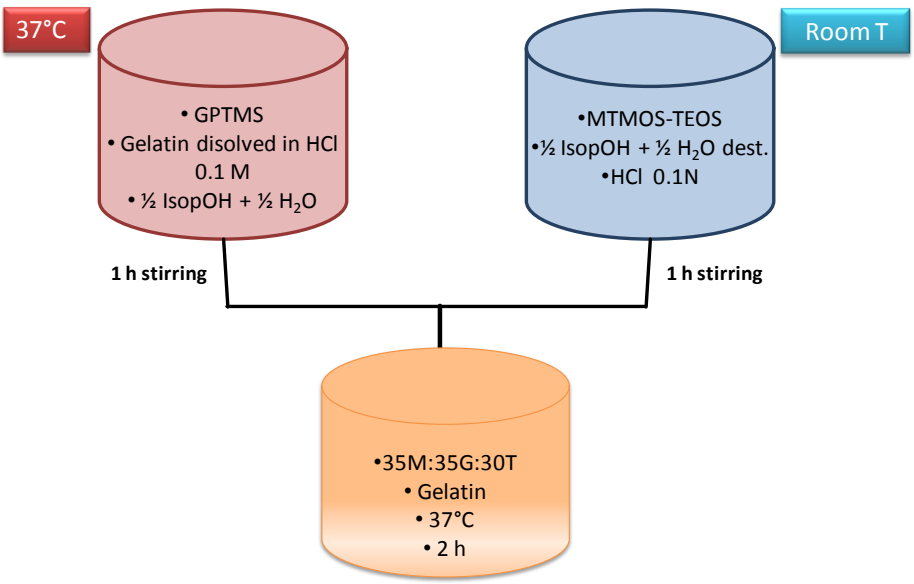

Figure 5.1. Scheme showing the reaction steps involved in the synthesis of 35M:35G:30T-Gelatin hybrids.

Initially, GPTMS reacted with gelatin using IsopOH/H_2O as solvent and dilute hydrochloric acid (0.1 M) as catalyst. It was hypothesized that the epoxy ring was opened and it reacted with amino[14] (Eq. 5.1) and/or carboxylic acid groups[10] of gelatin (Eq. 5.2).

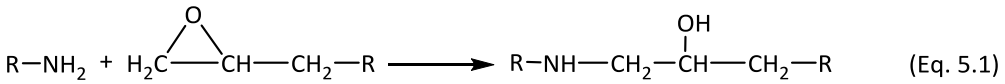

(Eq. 5.1)

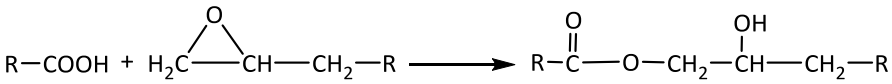

(Eq. 5.2)

Simultaneously, MTMOS and TEOS were hydrolyzed separately in the same conditions of solvent and catalyst. After one hour of reaction, both solutions were

mixed and it was kept for another two hours under stirring for allowing the formation of more Si-O-Si bonds among all the precursors and assure the homogeneity of the sol.

Once the sol was obtained, different substrates were coated and the heat treatment was applied. A thermal treatment of 80 °C for 2 hours was demonstrated to be appropriate to obtain a dense, solid and defect free coating and allow the evaporation of the solvent.

5.3. Chemical characterization

Firstly, the evolution of network formation with the new protocol by liquid ^{29}Si-NMR was studied. Obtained solid films were characterized by solid state ^{29}Si-NMR, FT-IR, XPS and in this case it was also used ^{13}C-NMR to confirm the link between GPTMS and gelatin.

5.3.1. 29-Silicon Nuclear Magnetic Resonance (^{29}Si-NMR)

The study of the sol-gel synthesis started with the spectrum of the precursors in solvent and continued recording one spectrum hourly after the addition of the catalyst. In the case of 35M:35G:30T the synthesis protocol was the one established in chapter 3, and the obtained spectra are presented in Figure 5.2.

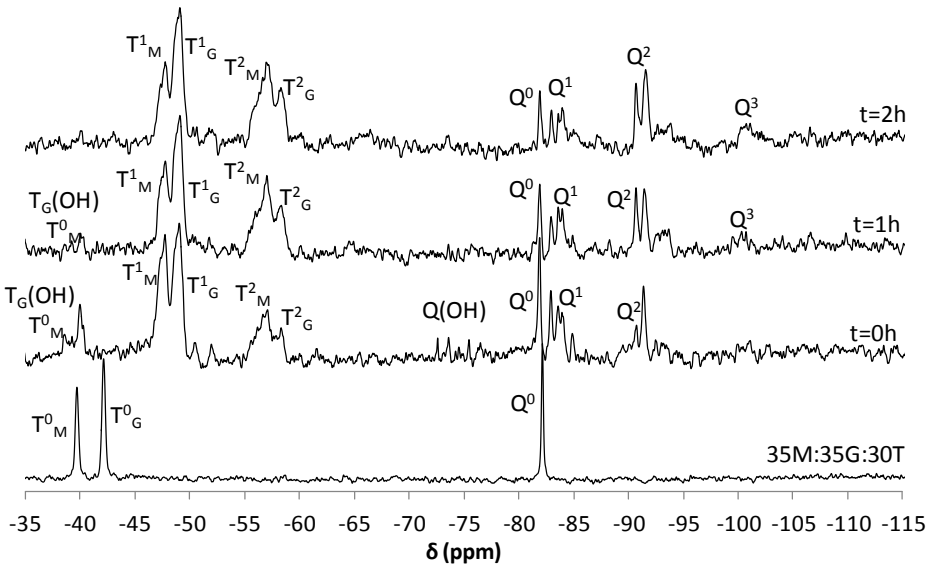

Figure 5.2. ^{29}Si-NMR liquid state spectra of the 35M:35G:30T hybrid.

In the first spectrum, three peaks appear at -40, -42 and -82 ppm corresponding to MTMOS, GPTMS and TEOS respectively. As soon as the catalyst was added, signals belonging to condensed species started to be detected due to the reaction speed. However, the velocity was slowed down after 2 hours.

In Figure 5.3, the study of the 35M:35G:30T-0.9% hybrid is shown. The spectra on the top correspond to the two reactions that take simultaneously place, (a) GPTMS with the appropriate amount of gelatin and (b) MTMOS and TEOS. As it can be seen, GPTMS condenses slower than the other precursors. This behaviour was found in all the hybrids and it was more noticeable with the increase of gelatin percentage. After mixing both solutions the evolution of the reaction was slower than in the case of the hybrid without the protein incorporation. For that reason it was kept under stirring at 37 °C for two hours to ensure the homogeneity and, after that, the cure treatment was applied.

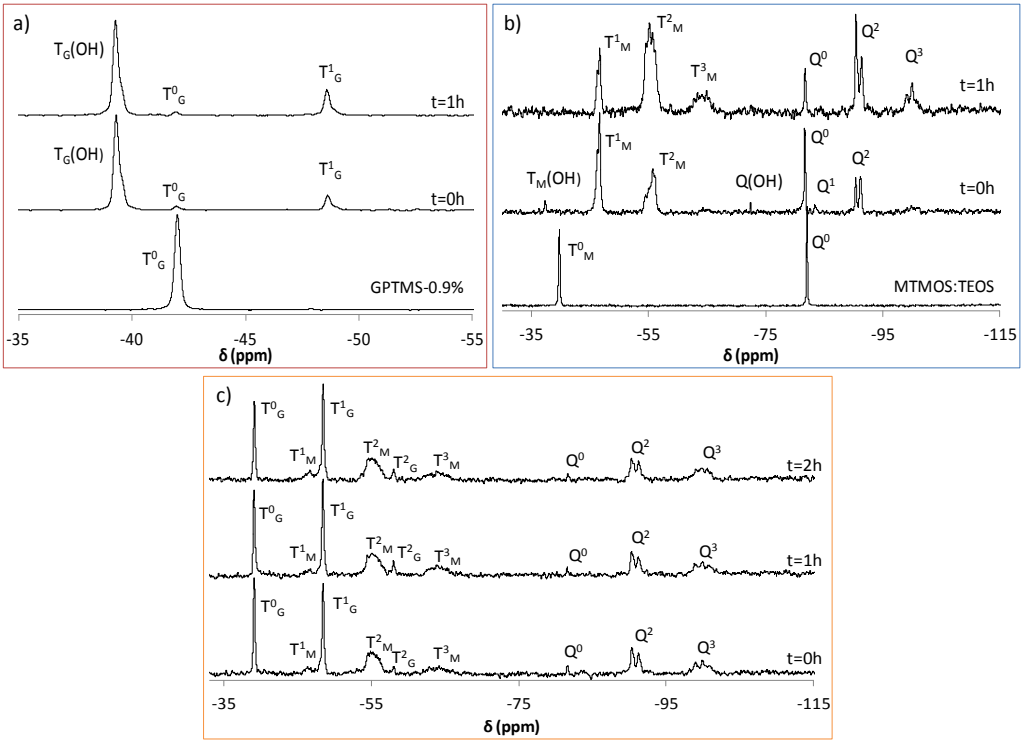

Figure 5.3. ^{29}Si-NMR liquid state spectra of new protocol for 35M:35G:30T-0.9% hybrid: (a) reaction between GPTMS and gelatin, (b) pre-hydrolysis of MTMOS and TEOS and (c) mixture of both solutions.

In order to test the effect of gelatin in siloxane network formation, all the spectra recorded at the end of the reaction time for each type of hybrid are compared in Figure 5.4.

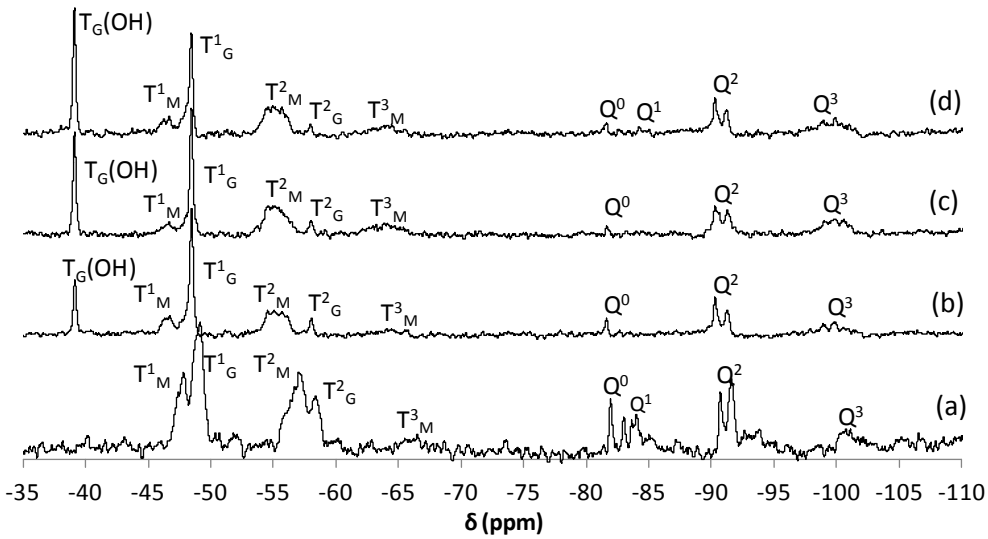

Figure 5.4. ^{29}Si-NMR liquid state spectra of the 35M:35G:30T hybrid with (a) 0 %, (b) 0.2 %, 0.9 % and (d) 2.0 % of gelatin, before heat treatment.

The intensity of the signal corresponding to GPTMS hydrolyzed species is the most evident difference among all the spectra. In the case of the hybrid without gelatin, all the GPTMS molecules have already condensed due to the absence of the band at -39 ppm. However, in the case of hybrids with gelatin, more molecules remained completely hydrolyzed (uncross-linked) at the end of the synthesis, and this behaviour was more emphasized with the increase of gelatin amount.

Such results were attributed to the possibility of the gelatin being bond to GPTMS. The added HCl is catalyzing both reactions, the hydrolysis/condensation reactions of the sol-gel process and also the gelatin linkage to the epoxy group. The fact of grafting such a big molecule as gelatin to the siloxane network interferes in condensation process of silanol groups, as it can be concluded from the obtained results. With the use of other complementary techniques, which will be shown later, this assumption will be confirmed.

Solid state ^{29}Si-NMR spectroscopy was used to study the final cross-linking degree achieved by the curing treatment. Figure 5.5 shows the recorded spectra for all type of hybrids.

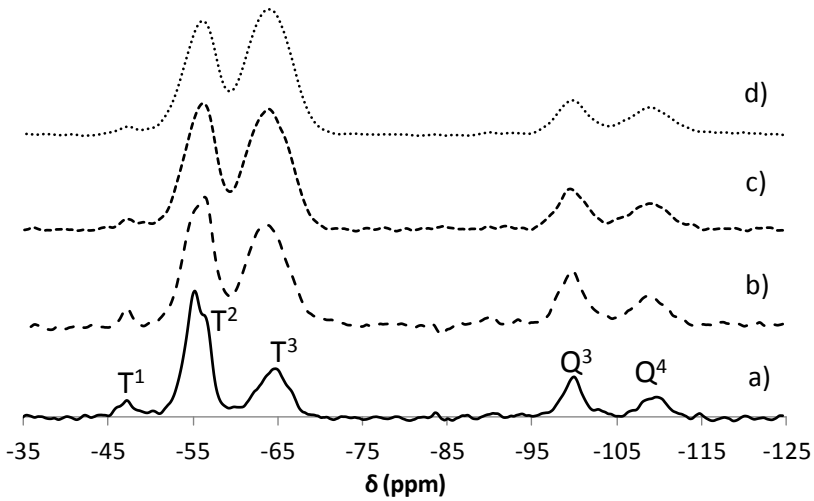

Figure 5.5. ^{29}Si-NMR spectra of 35M:35G:30T-Gelatin films after heat treatments: (a) 35M:35G:30T, (b) 35M:35G:30T-0.2%, (c) 35M:35G:30T-0.9% and (d) 35M:35G:30T-2.0% .

In the case of solid state spectra, it cannot be distinguished between signals of MTMOS and GPTMS due to their overlapping. For that reason we will only differentiate between T species for both MTMOS and GPTMS and Q for TEOS.

The most significant difference is the evolution of T species. In the case of the hybrid without gelatin, T^2 is the most abundant, and with the addition of gelatin the intensity of more condensed species, T^3, started to increase gradually until the case of 35M:35G:30T-2.0% where T^3 is the sharpest signal. This trend was not observed for Q^3 and Q^4, where no significant changes were appreciated.

In Figure 5.4 it was found how after the sol-gel process hybrids with gelatin remained with more unreacted silanol groups and that behaviour was more obvious with the increase of gelatin amount. Owing to the obtained results after the heat treatment, it can be hypothesized that these silanol groups undergo a faster condensation due to the effect of the temperature during curing process. In this way the cross-linking in hybrids with gelatin compared to 35M:35G:30T is promoted.

Table 5.2 shows the relative abundance of each Si species for the four types of coatings, as well as the condensation degree achieved calculated by using Eq. 4.1.

Table 5.2. Percentage abundance of silicon species present in 35M:35G:30T-Gelatin hybrids and network connectivity.

Coating	T^1	T^2	T^3	Q^3	Q^4	D_C
35M:35G:30T	5	49	24	16	6	76.3
35M:35G:30T-0.2%	3	34	38	17	8	82.4
35M:35G:30T -0.9%	2	35	42	11	10	84.2
35M:35G:30T -2.0%	1	33	45	10	11	85.8

These results prove quantitatively what it could be observed in Figure 5.5 in a qualitative way. The relative amount of T^1 and T^2 decrease at the same time that T^3 increases due to the addition of more gelatin into the hybrid. As a result, the connectivity factor (D_c) is also increased from 35M:35G:30T to 35M:35G:30T-2.0%. In all the cases, for these type of hybrids, obtained values are slightly lower than the ones obtained for 7M:3T-Gelatin films (Table 5.2).

5.3.2. 13-Carbon Nuclear Magnetic Resonance (^{13}C-NMR)

Solid state ^{13}C-NMR was used to confirm the previously hypothesized reaction between the epoxy group of GPTMS and the nucleophilic groups of gelatin.

First of all, in Figure 5.6, the spectrum obtained for 35M:35G:30T with the peak assignment[15, 16] is presented. The GPTMS molecule posses six C atoms, labeled 1-6, which are attributed to six resonance peaks at approximately 10 ppm (1), 25 ppm (2), 45 ppm (6), 51 ppm (5), 71 ppm (4) and 75 ppm(3). The small signal at 62 ppm (*) proves the transformation of a small amount of epoxy ring to a diol group. Apart of GPTMS's Cs, there is also a peak at -5 ppm which corresponds to the non-hydrolysable methyl group of MTMOS. From here, it can be deduced that all the methoxy and ethoxy groups of the three precursors were successfully hydrolyzed with the new protocol, due to the absence of resonance peaks corresponding to them. That is the reason why it is not possible to identify TEOS by this technique, because after the sol-gel reaction there are no Cs in its structure.

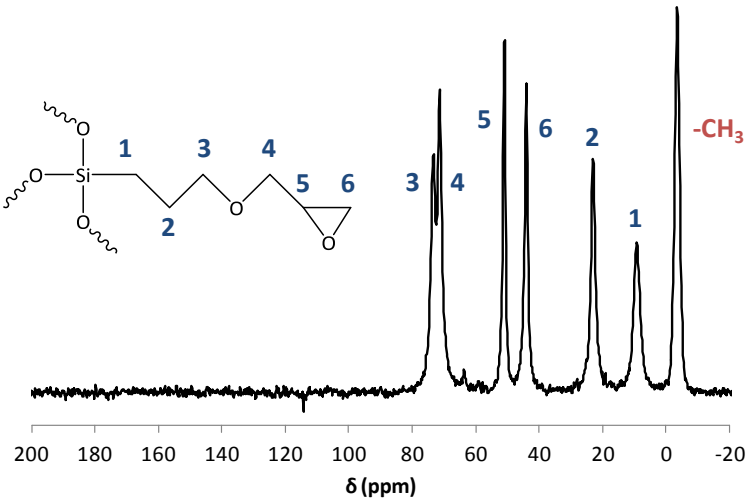

Figure5.6. ^{13}C-NMR spectra of 35M:35G:30T.

In Figure 5.7 the recorded spectra for 35M:35G:30T and 35M:35G:30T-2.0% are compared, considering not necessary to show the spectra for hybrids with different amounts of gelatin since they followed the same trend.

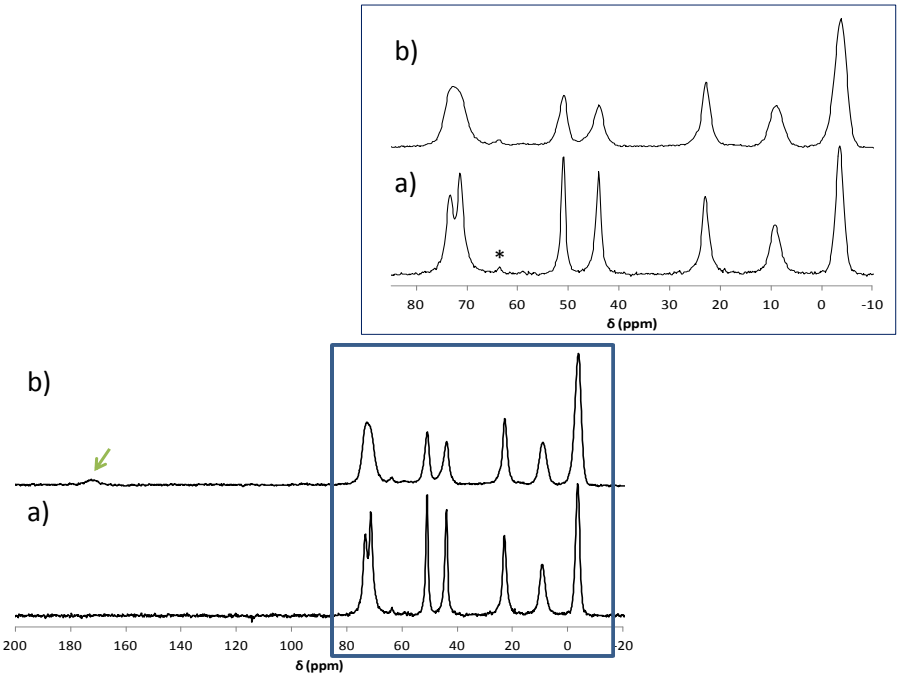

Figure 5.7. ^{13}C-NMR spectra of (a) 35M:35G:30T and (d) 35M:35G:30T-2.0%.

Focussing on the area of low chemical shifts (enlarged area) same signals can be appreciated in both materials. However, in the case of the hybrid without gelatin, peaks from the epoxy ring Cs (5 and 6) are sharp and strong, indicating that many of the epoxy ring are intact, while in the coating with 2 %wt of gelatin peaks are much broader. Such differences are attributed to the epoxy ring opening and subsequent reaction with the amino group[17, 18], Eq. 5.1. It is also clear that the relative intensities from Cs 5 and 6 greatly reduced, what demonstrates that many of these epoxy groups have been opened.

Moreover, looking to the area of high chemical shifts, in the 35M:35G:30T-2.0% hybrid's spectrum, an small signal appears at 175 ppm (green arrow). It indicates the presence of gelatin due to the –COOH residual groups. However, it could be also attributed to the cross-linking reaction between GPTMS and gelatin through the reaction of epoxy and carboxylic acid group respectively (Eq. 5.2).

5.3.3. Infrared spectroscopy (FT-IR)

The films obtained after the heat treatment were also studied by ATR technique. In Figure 5.8 the spectra for 35M:35G:30T and 35M:35G:30T-0.9% are shown.

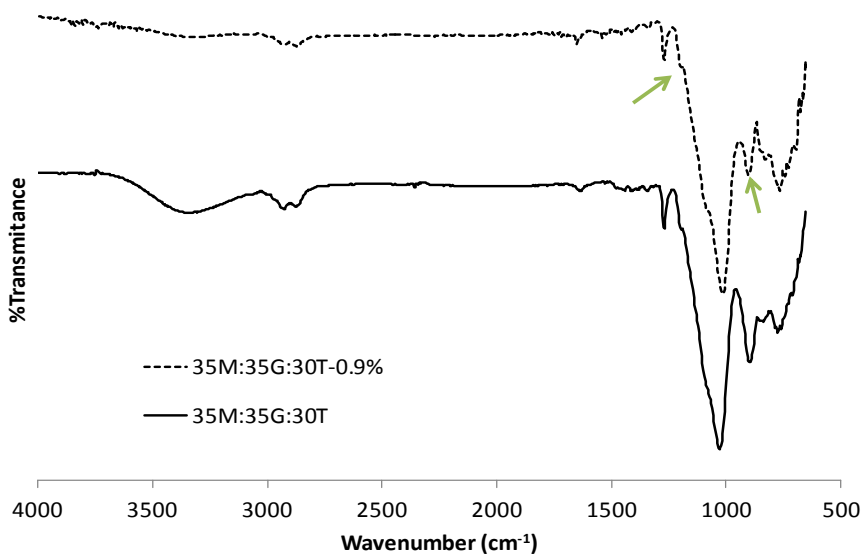

Figure 5.8. FT-IR spectra of 35M:35G:30T and 35M:35G:30T-0.9%. (green arrows: epoxide vibrations).

Both materials presented a similar spectrum with slight differences. In both cases the most intense band was found at 1020-1100 cm^{-1}, characteristic of siloxane bonds vibration. The organic chain of MTMOS is represented by the vibrations at 1270 and 2980 cm^{-1} of the methyl group. The characteristic IR adsorption bands of GPTMS appear at 2860 cm^{-1} due to the presence of $–CH_2$, at 1200 (a shoulder) corresponding to the epoxy ring breathing and at 900 and 750 cm^{-1} corresponding to antisymmetric epoxide ring deformation[14, 19, 20].

When comparing the intensity of the bands in both spectra, the decrease in the intensity of epoxy deformation band at 900 cm^{-1} can be seen. This behaviour has been attributed in literature to the ring opening and the possible subsequent reaction[19, 21]. So, these results combined with the NMR study confirmed the effective incorporation and chemical anchorage of gelatin to the siloxane network, unlike the 7M:3T-Gelatin hybrids where the main mechanism of interaction between different components was though hydrogen bonding and electrostatic interactions.

Furthermore, the fact of detecting epoxide vibration bands by ATR, confirms the presence of functional groups on the surface, what may play a crucial role in next steps of this work with proteins and cells studies.

5.3.4. X-ray Photoelectron Spectroscopy (XPS)

To complete the chemical surface characterization XPS measurements were performed on the coatings.

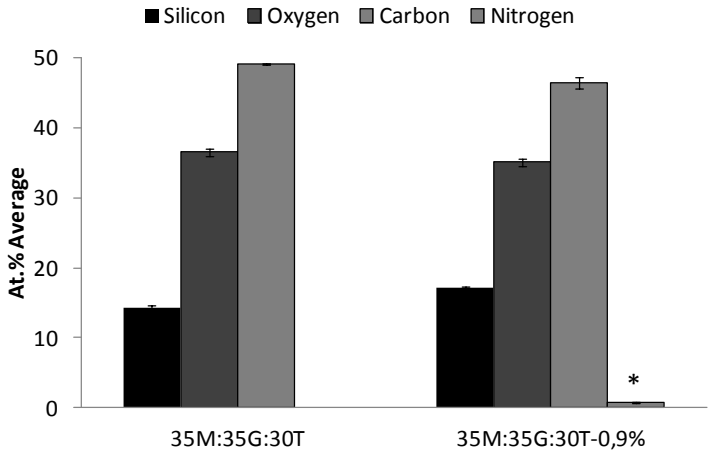

Figure 5.9. XPS elemental composition of 35M:35G:30T and 35M:35G:30T-0.9% coatings.

Figure 5.9 shows the atomic average obtained for the 35M:35G:30T and 35M:35G:30T-0.9% hybrids. There are just some slight differences between coatings with and without gelatin, as it is the case of the appearance of a new signal due to nitrogen in the hybrid 35M:35G:30T-0.9%, confirming the effective incorporation of gelatin and its presence in the surface of the coating.

Comparing with the results obtained for 7M:3T-Gelatin hybrids, the carbon percentage has almost been doubled due to the longer organic chain of GPTMS. This can indicate, in some way, the presence of the functionalization provided by this precursor on the surface, since the XPS technique penetrates just 10 nm in the top of the material.

In addition, these values are the result of the average of the obtained atomic percentages on three different points of each coating, and taking into account the small error bars, it gives us an idea about how homogeneous are the developed films.

5.4. Morphological characterization

As in previous cases, morphological properties and adhesion strength of the synthesized coatings were tested.

5.4.1. Cross-cut adhesion test

In Figure 5.10a, the finish properties of the surface such as uniformity, transparency, crack free and glossy appearance can be appreciated.

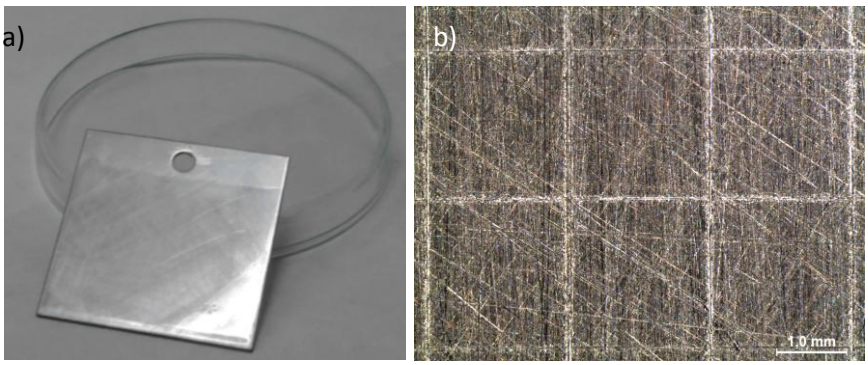

Figure 5.10. Appearance of 35M:35G:30T-0.9% coating (a) visually and (b) by optical microscope after cross-cut test.

The picture obtained for 35M:35G:30T-0.9% coating by optical microscopy after the cross-cut test is presented on the right (Figure 5.10b). For all the 35M:35G:30T-Gelatin hybrid series the highest value of adhesion strength was obtained.

5. 4. 2. Atomic Force Microscopy (AFM)

In the 3D height images (Figure 5.11) obtained by AFM, it is clearly appreciated the nanometer scale roughness provided by the 35M:35G:30T-Gelatin coatings, which values are summarized in Table 5.3. These results are in agreement with the findings obtained by other authors, where smooth surfaces with a nanostructure are obtained with silica based materials[22-24].

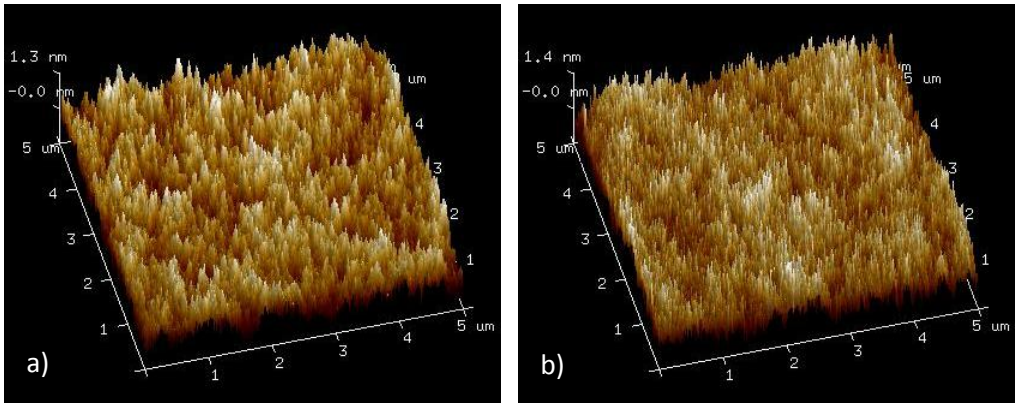

Figure 5.11. 3D height images for (a) 35M:35G:30T and (b) 35M:35G:30T-2.0%.

Owing to the average roughness (Ra) values, different conclusions can be taken. First of all, comparing with the values obtained for 7M:3T-Gelatin hybrids, lower values are obtained, indicating the formation of a smoother surface with the introduction of GPTMS. This behaviour is attributed to the obtaining of a thicker film in the case of the ternary system, able to hidden the imperfection or micrometer scale topography of the substrate. This hypothesis will be later discussed in chapter 7 where the effect of topography on cell adhesion will be tested.

Table 5.3. Roughness values for 35M:35G:30T-Gelatin hybrids.

	35M:35G:30T	35M:35G:30T -0.9%	35M:35G:30T-2.0%
R_a (nm)	0.33 ± 0.06	0.39 ± 0.01	0.35 ± 0.02

On the other hand, focusing on the effect of gelatin, an increase in the roughness with the incorporation of gelatin can be appreciated. However no significant differences were obtained.

Finally, in Figure 5.12, the phase images for 35M:35G:30T and 35M:35G:30T-0.9% coatings are presented. The most relevant conclusion taken from them is the homogeneity and uniformity of prepared coatings. The smooth and nanostructure surface can be also appreciated.

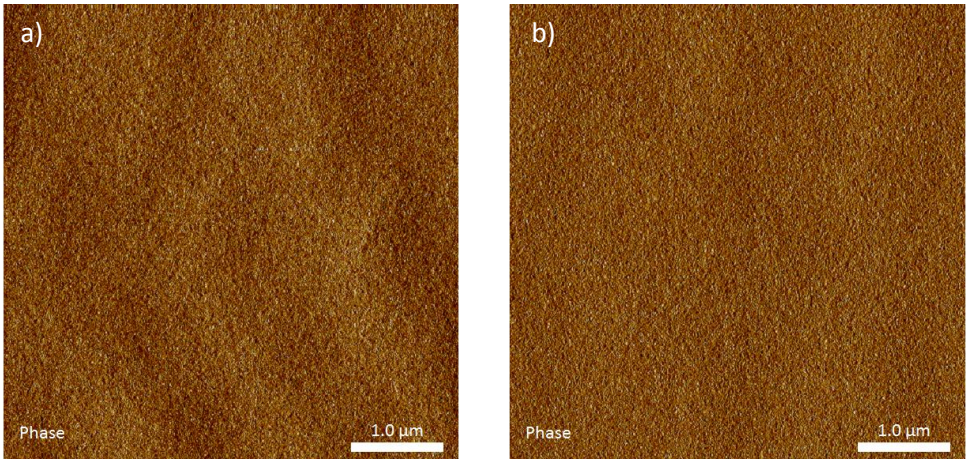

Figure 5.12. Phase images obtained by AFM for (a) 35M:35G:30T and (b) 35M:35G:30T-2.0%.

5.5. Determination of hydrophobicity/hydrophilicity

As done is previous chapter, water contact angle measurements were carried out for all the 35M:35G:30T-Gleatin hybrids in order to determine their hydrophobic/hydrophilic nature. Results are summarized in Table 5.4 and its value is an average of 9 measurements per sample and each coating in triplicates.

Table 5.4. Contact angle values for 35M:35G:30T -Gelatin series.

Coating	35M:35G:30T	35M:35G:30T-0.2%	35M:35G:30T-0.9%	35M:35G:30T-2.0%
Contact angle (°)	66.1 ± 2.3	64.4 ± 1.0	67.3 ± 0.5	67.8 ± 0.7

Comparing 35M:35G:30T (66.1° ± 2.3°) with 7M:3T (70.0° ± 0.8°), a lower value of contact angle was obtained. This is in good agreement with the behavior

observed in chapter 3, where an increase of GPTMS precursor in the formulation was translated in an increase of the wettability.

In this case there was not a clear trend when adding gelatin to the coating. It can be due to the synergy of different effects. On the one hand, in chapter 4 it was found the effect of gelatin increasing the wettability, which is a previously reported behavior[25, 26]. But on the other hand, the solid state ^{29}Si-NMR study showed the decrease of non-bridging oxygens (oxygen atoms which do not work as a bridge between two silicon atoms) when adding gelatin, what means that less silanol groups are in the surface compared to the hybrid without gelatin and this is translated in an increase in the contact angle value.

However, in all the cases, coatings showed a moderate hydrophilic nature with wettability around 70°, value described in bibliography as optimum for adequate interactions in the biological environment[4, 27, 28].

5.6. Hydrolytic degradation test

Glass substrates coated with different 35M:35G:30T-Gelatin hybrids were immersed in PBS for 8 weeks and their mass loss was determine at different periods of time. Study was performed in same conditions as for the other coatings described before. Results are plotted in Figure 5.13.

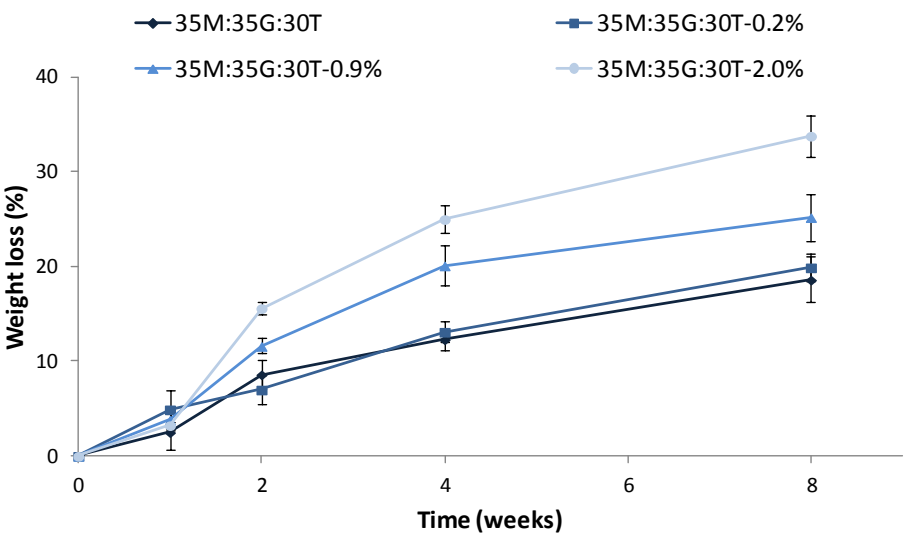

Figure 5.13. Mass loss due to hydrolytic degradation of 35M:35G:30T-Gelatin coatings.

When analyzing the obtained results, the same trend as in 7M:3T-Gelatin hybrids can be observed, where an increase of gelatin content means higher values of mass loss after 8 weeks of immersion. Such behaviour was attributed to water uptake ability of gelatin and its biodegradability properties[8-10].

5.7. Silicon release test

The characterization of these new developed coatings was complemented with Si release studies. The assay was performed keeping the same conditions as for the gravimetric degradation study and results are shown in Figure 5.14.

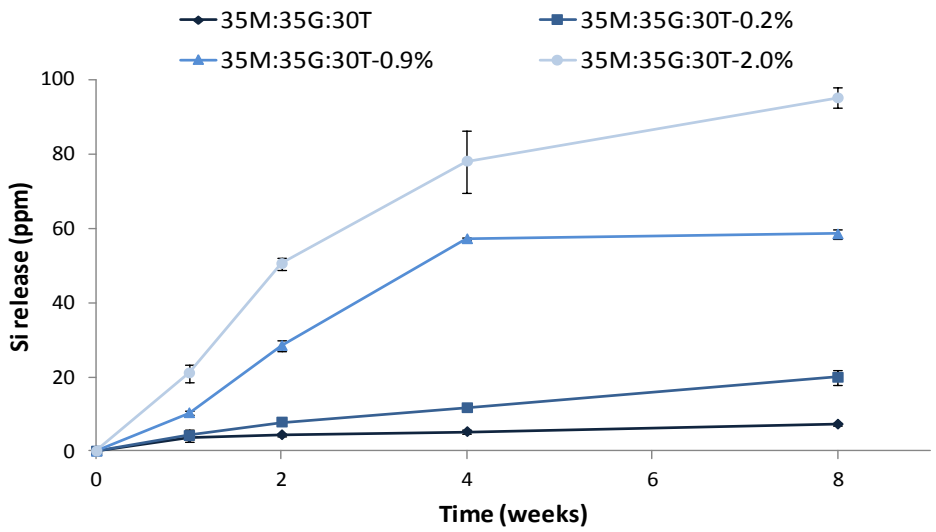

Figure 5.14. Si release profiles for 35M:35G:30T in PBS, measured by ICP.

The silicon release profiles show the same trend as in the degradation study, where the hybrids with higher content of gelatin are the ones that produce higher mass loss and also higher amounts of cumulative Si release. They are gradually dissolved overtime, obtaining 10 folds more of Si ppm in the case of coating with 2.0 %wt of gelatin compared to 35M:35G:30T.

It is also interesting to compare the behaviour for both types of hybrids, 7M:3T-Gelatin and 35M:35G:30T-Gelatin. In the case of coatings with GPTMS, higher Si values are obtained. However the gravimetric study showed lower mass losses compared to 7M:3T-Gelatin coatings. This may be explained taking into account the

results obtained in chapter 3 where the incorporation of both, TEOS and GPTMS, had the same effect making the matrix more soluble. So as expected, in 35M:35G:30T-Gelatin films there was a synergistic effect due to the combination of both precursors in the formulation and this was translated in a higher dissolution of the network.

However, this behaviour was not appreciated when studying the mass loss. In that case, 7M:3T-Gelatin hybrids gave higher values, fact that was attributed to the more rigid nature of the material, what lead to the obtaining of coatings with less integrity and adhesion strength to the substrate in comparison to the ones with GPTMS. As consequence, delamination and the detachment of fragments with a bigger size than the one that can be detected by ICP may occur.

Next, obtained results for EIS study will be shown in an attempt to go deeper in the degradation mechanism of these materials.

5.8. Electrochemical Impedance Spectroscopy (EIS)

The EIS test was performed to study the coatings' properties, such as the creation of pores and the water uptake, in order to find a correlation with previous degradation studies and the possible dissolution mechanism of developed materials.

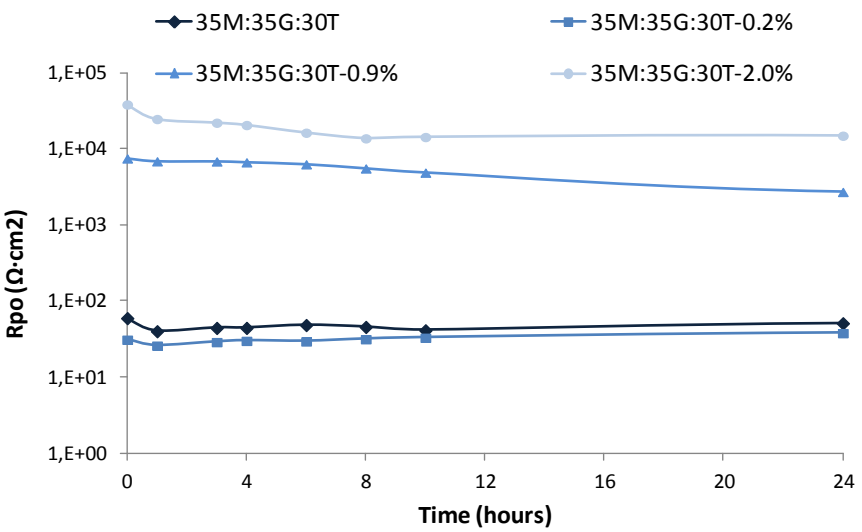

Figure 5.15. Evolution of the pore resistance versus time of contact with electrolyte of the 35M:35G:30T-Gelatin series hybrids.

Figure 5.15 shows the results obtained for the study of pore resistance. No significant differences are appreciated among 35M:35G:30T and 35M:35G:30T-0.2%, as well as happened for the gravimetric degradation test and silicon release quantification, due to the small amount of gelatin introduced into the hybrid. However, an increase in R_{po} is obtained when increasing the percentage of gelatin in the coating. Such behaviour is contrary to the one found in 7M:3T-Gelatin coatings, where the introduction of this biomolecule was translated in an increase of porosity. These differences can be explained through the fact of functionalization. The introduction of GPTMS is translated in a compatibility and homogeneity of the silica and gelatin components by the covalent bonding. Therefore, gelatin is retained in the network avoiding the formation of pores during its immersion in aqueous media.

It can also be related to the results obtained in solid state NMR spectroscopy, where a more condensed siloxane network was obtained with the introduction of gelatin (35M:35G:30T (76.3%) < 35M:35G:30T-0.2% (82.4%) < 35M:35G:30T-0.9% (84.2%) < 35M:35G:30T-2.0% (85.8%)).

The results for Cc parameter obtained by EIS, which is related to the water absorption capacity of the coating, are plotted in Figure 5.16.

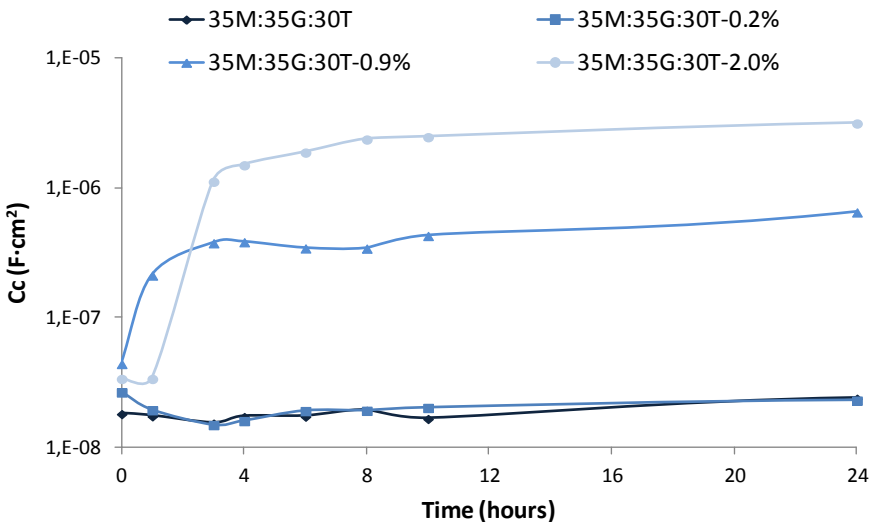

Figure 5.16. Evolution of the coating capacitance versus time of contact with electrolyte of 35M:35G:30T-Gelatin series hybrids

An increase in the Cc value is related to a higher permeability of the coating as a consequence of an increase of water content. Therefore, owing to the results plotted in Figure 5.16, the effect of gelatin augmenting the water uptake of the coating is clear, what was expected due to the well known adsorption properties of this protein.

To sum up, the combination of all the studies performed to test the dissolution properties suggest that the degradation properties of these coatings are favoured in the presence of gelatin. The increase of water uptake makes easier the hydrolysis of Si-O-Si bonds, releasing more Si to the environment as found by ICP. However, in the case of the 35M:35G:30T-Gelatin coatings, the degradation mechanism is not related to an increase on porosity with gelatin incorporation, as was seen for 7M:3T-Gelatin hybrids. The higher mass loss found on this last series of materials could be related to the obtaining of a non-compatible system where gelatin is not chemically immobilized and weaker adhesion is obtained between the substrate and the coating. On the other hand, one more time, the effect of GPTMS as compatibilizer agent remains clear.

5.9. Conclusions

Through sol-gel process homogeneous, transparent and crack-free coatings based on 35M:35G:30T-Gelatin hybrids have been obtained. Moreover, we could confirm the achievement of the chemical anchorage of gelatin to the siloxane network, as well as the presence of functional groups on the surface by the incorporation of GPTMS. This opens a range of possibilities for subsequent studies, as for example the ability to adsorb serum proteins, which will be studied in chapter 6.

It will also be tested if this increase in Si cumulative release, compared to previously synthesized hybrids, is translated into a better cell osteogenic differentiation.

References

1. Keselowsky BG, Collard DM, García AJ. Surface chemistry modulates fibronectin conformation and directs integrin binding and specificity to control cell adhesion. *Journal of Biomedical Materials Research Part A.* 2003; **66:** 247-59.

2. Roach P, Farrar D, Perry CC. Interpretation of protein adsorption: Surface-induced conformational changes. *J Am Chem Soc.* 2005; **127:** 8168-73.

3. Beganskiene A, Raudonis R, Jokhadar SZ et al. Modified sol-gel coatings for biotechnological applications. In: *Journal of Physics: Conference Series, 2007.* p. 012050. IOP Publishing, .

4. Rupp F, Gittens RA, Scheideler L et al. A review on the wettability of dental implant surfaces I: Theoretical and experimental aspects. *Acta Biomaterialia.* 2014; **10:** 2894-906.

5. Gittens RA, Scheideler L, Rupp F et al. A review on the wettability of dental implant surfaces II: Biological and clinical aspects. *Acta Biomaterialia.* 2014; **10:** 2907-18.

6. Thevenot P, Hu W, Tang L. Surface chemistry influences implant biocompatibility. *Curr Top Med Chem.* 2008; **8:** 270-80.

7. Scotchford CA, Gilmore CP, Cooper E et al. Protein adsorption and human osteoblast-like cell attachment and growth on alkylthiol on gold self-assembled monolayers. *J Biomed Mater Res.* 2002; **59:** 84-99.

8. Ren L, Tsuru K, Hayakawa S et al. Sol–gel preparation and in vitro deposition of apatite on porous gelatin–siloxane hybrids. *J Non Cryst Solids.* 2001; **285:** 116-22.

9. Tsuru K, Robertson Z, Annaz B et al. Sol-gel synthesis and in vitro cell compatibility analysis of silicate-containing biodegradable hybrid gels. *Key Eng Mat.* 2008; **361:** 447-50.

10. Mahony O, Tsigkou O, Ionescu C et al. Silica-Gelatin hybrids with tailorable degradation and mechanical properties for tissue regeneration. *Advanced Functional Materials.* 2010; **20:** 3835-45.

11. Ren L, Tsuru K, Hayakawa S et al. Synthesis and characterization of gelatin-siloxane hybrids derived through sol-gel procedure. *J Sol Gel Sci Technol.* 2001; **21:** 115-21.

12. Tsuru K, Shirosaki Y, Hayakawa S et al. Sol–gel-derived silicate nano-hybrids for biomedical applications. *Biological and Pharmaceutical Bulletin.* 2013; **36:** 1683-7.

13. Mahony O, Yue S, Turdean-Ionescu C et al. Silica–gelatin hybrids for tissue regeneration: Inter-relationships between the process variables. *J Sol Gel Sci Technol.* 2014; **69:** 288-98.

14. Yoon B, Kim H, Kim H. Bioactive microspheres produced from gelatin–siloxane hybrids for bone regeneration. *J Mater Sci Mater Med.* 2008; **19:** 2287-92.

15. Greenwood P, Gevert B. Aqueous silane modified silica sols: Theory and preparation. *Pigment & Resin Technology.* 2011; **40:** 275-84.

16. Gabrielli L, Russo L, Poveda A et al. Epoxide opening versus silica condensation during sol–gel hybrid biomaterial synthesis. *Chemistry-A European Journal.* 2013; **19:** 7856-64.

17. Davis SR, Brough AR, Atkinson A. Formation of silica/epoxy hybrid network polymers. *J Non Cryst Solids.* 2003; **315:** 197-205.

18. Gizdavic-Nikolaidis MR, Zujovic ZD, Edmonds NR et al. Spectroscopic characterization of GPTMS/DETA and GPTMS/EDA hybrid polymers. *J Non Cryst Solids.* 2007; **353:** 1598-605.

19. Zand RZ, Langroudi AE, Rahimi A. Synthesis and characterization of nanocomposite hybrid coatings based on 3-glycidoxypropyl-trimethoxysilane and bisphenol A. *Iranian Polymer Journal.* 2005; **14:** 371-7.

20. Dhawade P, Jagtap R. Comparative study of physical and thermal properties of chitosan-silica hybrid coatings prepared by sol-gel method. *Der Chemica Sinica.* 2012; **3:** 589-600.

21. Innocenzi P, Brusatin G, Guglielmi M et al. New synthetic route to (3-glycidoxypropyl) trimethoxysilane-based hybrid organic-inorganic materials. *Chemistry of Materials.* 1999; **11:** 1672-9.

22. Ääritalo V, Areva S, Jokinen M et al. Sol-gel-derived TiO2–SiO2 implant coatings for direct tissue attachment. part I: Design, preparation and characterization. *J Mater Sci Mater Med.* 2007; **18:** 1863-73.

23. Philipavičius J, Kazadojev I, Beganskienė A et al. Hydrophobic antireflective silica coatings via sol–gel process. *Mater Sci.* 2008; **14:** 283-7.

24. Chernev G, Borisova B, Kabaivanova L et al. Silica hybrid biomaterials containing gelatin synthesized by sol-gel method. *Open Chemistry.* 2010; **8:** 870-6.

25. Van Vlierberghe S, Vanderleyden E, Boterberg V et al. Gelatin functionalization of biomaterial surfaces: Strategies for immobilization and visualization. *Polymers.* 2011; **3:** 114-30.

26. Shi C, Yuan W, Khan M et al. Hydrophilic PCU scaffolds prepared by grafting PEGMA and immobilizing gelatin to enhance cell adhesion and proliferation. *Materials Science and Engineering: C.* 2015; **50:** 201-9.

27. Tamada Y, Ikada Y. Effect of preadsorbed proteins on cell adhesion to polymer surfaces. *J Colloid Interface Sci.* 1993; **155:** 334-9.

28. Zolkov C, Avnir D, Armon R. Tissue-derived cell growth on hybrid sol–gel films. *J.Mater.Chem.* 2004; **14:** 2200-5.

Chapter 6

Effect of siloxane-gelatin coatings and surface functionalization on protein adsorption

Chapter 6:

EFFECT OF SILOXANE-GELATIN COATINGS AND SURFACE FUNCTIONALIZATION ON PROTEIN ADSORPTION

6.1. Introduction

As soon as the implant is in the body, the first event taking place at biomaterial-tissue interface is the immediate formation of a layer with blood proteins and interstitial fluids. The resulting protein film acts to mediate all subsequent biological interactions between the material and surrounding environment. When cells reach the implant surface, they scan the protein layer looking for specific binding motifs to attach to them. Hence, it is this spontaneously formed protein layer, rather than the surface itself, to which cells initially respond[1-3].

The recruitment, retention and conformational structure of proteins on a biomaterial surface are important properties that can synergistically interact to promote either favourable or adverse cellular and tissue response. That is, the composition of the adsorbed layer is a key mediator of cell behaviour, and the required proteins, correctly presented, can stimulate a constructive cell response favoring repair and tissue integration. Nevertheless, proteins in an unrecognizable state may indicate a foreign material to be removed or isolated[1].

6.1.1. Proteins' structure and conformation

Proteins are biological macromolecules constructed for specific and unique functions which participate in many fundamental and essential processes within cells. They are high molecular weight molecules built up by the specific co-polymerization of 20 different amino acids.

The amino acid sequence, called primary structure, is unique for each particular protein. The secondary structure refers to the interaction between amino acids of the polypeptide chain which cause folding, bending and coiling of the same to give a specific three dimensional structure. The α-helix and β-helix are the most thermodynamically stable secondary structures. These helixes are further folded into a more compact tertiary structure, where the hydrophobic groups are generally placed towards the interior of the structure and polar amino acid side chains are exposed to the physiological environment. Finally, the quaternary structure is referred to the interaction between subunits or individual polypeptide chains in multichain proteins[4, 5].

A protein can take different conformations, but not all of them will be active. Binding of proteins to surface provides changes in the conformation of the

biomolecule, what has a determinant effect in mediating interactions between cells and biomaterials at the tissue-implant interface[4].

6.1.2. Protein-Surface interactions

The interfacial behaviour will be determined by both protein and surface properties.

a) Protein properties

The structure properties of proteins that influence surface activity are related to the primary structure, meaning that the sequence of amino acids affects protein-surface interactions. Big proteins are likely to interact with the substrate surface since they have more binding sites. However, it is not the sole determinant, there are many other parameters.

For multi-protein systems such as serum, the more concentrated and/or smaller molecules will have greater diffusion rate and will arrive quickly to the surface, being the first proteins adsorbed onto the surface. In the course of time, molecules having greater affinity for the surface, but slower rate because of lower concentration or larger size, will approach and replace them. This is known as the Vroman effect[4, 6].

Depending on their nature, proteins will have different residual groups (nonpolar, polar, positively charged or negatively charged), which will influence the interactions with the biomaterial surface, what is illustrated in Figure 6.1. Thus, protein adsorption is a dynamic process involving non-covalent interactions such as hydrophobic interactions, electrostatic forces, hydrogen bonding and Van der Waals-forces[2].

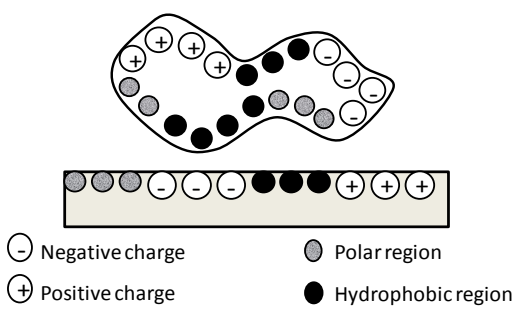

Figure 6.1. Scheme illustrating both molecular and substrate chemical properties.

In addition, as a consequence of the heterogeneity of both the protein molecule and the surface, proteins can exist on the surface in different orientations (Figure 6.2). The different conformation of adsorbed molecules not only affects the amount of protein bound to the surface, but they also have functional significance. For example, in the case of adhesive proteins, the ones with RGD domains, depending on their orientation, the active site needed for subsequent cell attachment may not be accessible, making not possible the interaction with cells[4].

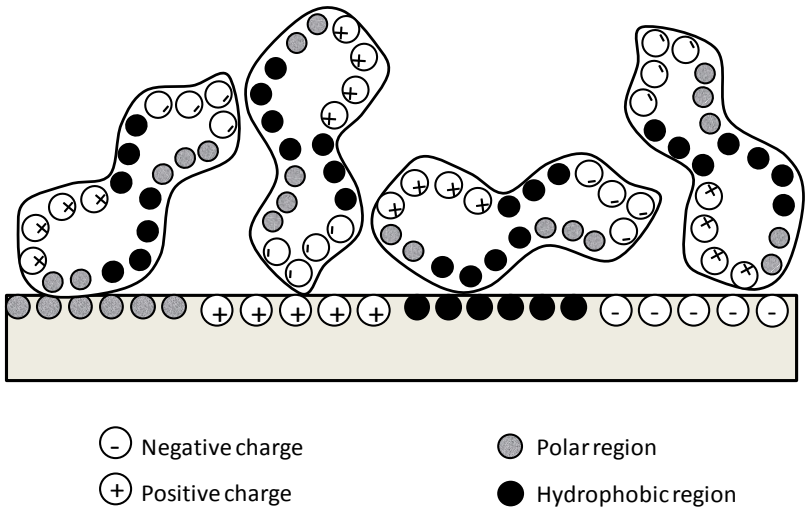

Figure 6.2. Different orientation of adsorbed protein molecules resulting from the heterogeneity of both protein and surface.

b) Surface properties

Surface properties affect the extent of protein adsorption, denaturation and epitope (active domains) exposure. This will be influenced by the chemistry, wettability, charge and surface morphology/topography.

The effect of surface functionality on different serum proteins has been vigorously investigated. Benesch *et al.*[7] studied the adsorption of fibrinogen onto self assembled monolayer with different terminal groups finding that proteins were more firmly bound to hydroxyl-terminated SAMs. Roach *et al.*[8] investigated the adsorption pattern of fibrinogen and albumin on OH and CH_3-terminated surfaces. They found the highest affinity of albumin to bind to hydrophobic surface (CH_3-terminated), while fibrinogen adsorbed in the same way to both surfaces.

Apart from the amount of adsorbed protein, this functionality on the surface has shown to have an effect on the conformation. Keselowsky *et al.*[9, 10] demonstrated that fibronectin undergoes significant structural changes upon adsorption depending on the underlying film's chemistry. These alterations modulate integrin binding and differentiation. Their results indicated that binding domains were more accessible when fibronectin was adsorbed on surfaces following next pattern: -OH > -COOH = $-NH_2$ > $-CH_3$. It was also proved their effect on cell differentiation[11]. In a recent study Felgueiras *et al.*[12] tested the ability of different biomaterial's surface to adsorb albumin, fibronectin and collagen type I, where they found the preference of protein adsorption on Ti6Al4V surfaces functionalized with sulfonate groups and their favourable conformation for subsequent MC3T3-cells attachment.

The hydrophilic/hydrophobic nature of a biomaterial surface is considered to be one of the most influential parameter affecting protein adsorption. Most literature suggests that protein adsorption tends to occur more favourably on hydrophobic surfaces or on surfaces with an intermediate wettability (60-90°)[13]. However, there is no consensus on that due to the many other parameters which influence protein adsorption, as for example roughness.

An investigation of albumin and fibronectin adsorption performed by Tamada *et al.*[14], on different polymeric substrates with variable water contact angle values, proved both maximal protein and cell adhesion on surfaces with values around 70°. Most works suggest the preferential adsorption of albumin on hydrophobic surfaces. Arima *et al.*[15, 16] found that when evaluating the competitive adsorption of these two proteins on four kinds of SAMs of alkanethiols carrying different functional groups ($-CH_3$, -OH, -COOH or $–NH_2$), albumin was barely displaced by cell adhesive proteins due to the strong adhesion on hydrophobic SAMs.

Some works have studied how surface topography and chemistry influence the structure of bound proteins. Roach *et al.*[17] focused their work on evaluating the effect of hydrophobicity and topography on albumin and fibrinogen structure after adsorption on different silica spheres. They found that proteins became denatured on hydrophobic surfaces and they concluded that surface chemistry and topography play key roles in determining the structure of the bound proteins. Stallard *et al.*[13]

evaluated fibrinogen and albumin adsorption on siloxane and fluorinate siloxane coatings varying their roughness and wettability, finding the highest adsorbed mass for the surface with a water contact angle value of 95° and a rough surface. A similar study performed by Molino *et al.*[3] proved the opposite tendency between fibronectin and albumin, where the first one demonstrated the least binding mass in hydrophilic biocomposites and the second one decreased when decreasing the wettability. In both cases surface roughness did not appear to clearly affect the total mass adsorbed. On the contrary, Sela *et al.*[18] proved the effect of roughness improving protein adsorption on titanium with different surface treatments.

Despite all these findings, the effect of a surface to favour protein adsorption and promote the bioactive conformation is still unclear due to the complex process where many different parameters are involved.

6.1.3. Studied blood proteins

There are many proteins in human blood plasma. Among them, the selected proteins for this study were albumin, fibrinogen, fibronectin and collagen. Albumin is the major protein component in the blood and is known to eliminate cell attachment and block nonspecific binding[19]. Fibrinogen is a mediator of platelet activation via its direct interaction with platelet receptors[2, 20]. In addition, some types of ECM proteins possess an RGD peptide sequence such as fibronectin and collagen, which has the ability to adhere to cells via integrin receptor. These were the main reasons that made us select them as model proteins for this study.

a) Bovine serum albumin

With a molecular weight of 66 kDa, albumin acts as a multifunctional transporter protein and it is presented in a concentration of approximately 3.5-5 g/100mL in plasma[8, 21]. This globular protein has an ellipsoid shape with dimensions of 14 nm length and 4 nm width[22]. When it is adsorbed, its conformation may become distorted due to interaction with the surface[8] (Figure 6.3).

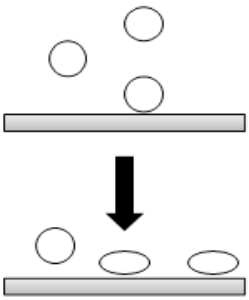

Figure 6.3. Schematic illustration of albumin's shape distortion after adsorption.

Bovine serum albumin is pretty much used for protein adsorption studies because it shares similar structure and properties with human serum albumin[23, 24].

b) Fibrinogen

Fibrinogen is a large plasma protein that plays a critical role in blood clotting as well as in other several physiological and pathological processes. It is found at a concentration of 2-4 mg/mL[25] in the circulatory system. It is a 340 kDa rod-shaped protein, with a long axis of 40-50 nm and 4-10 nm of width[4, 26]. This type of protein can undergo a multistage adsorption process where initially the protein adsorbs with its long axis parallel to the surface (side-on) and then rearrangement occurs to increase protein-protein interaction and surface concentration of protein (end-on)[8]. This phenomenon is illustrated in Figure 6.4, and the ability of fibrinogen to adsorb in one or another conformation will be influenced by substrate properties. Apart from its function as platelet mediator, fibrinogen has other adhesive sides, two of which are RGD sequence.

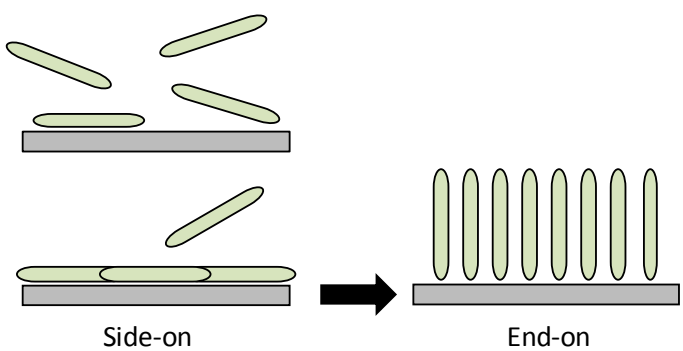

Figure 6.4. Fibrinogen molecules' arrangement on biomaterial's surface.

c) Fibronectin

Fibronectin is a non-collagenous adhesive protein which is presented in extracellular matrix (ECM) and plays important roles in organizing the ECM and in enabling cells to attach to it[4]. It is a dimer of a molecular weight of 440 kDa and a plasma concentration of 0.3 mg/ml[27]. Each subunit has a modular architecture constructed of three types of repetitive structures named type I, II and III, and its multifunctionality is provided by domains having affinity for various molecules such as cell surface receptor, collagen/gelatin and heparin[4] (Figure 6.5). The cell-binding tripeptide RGD is of particular importance, since it regulates cell adhesion.

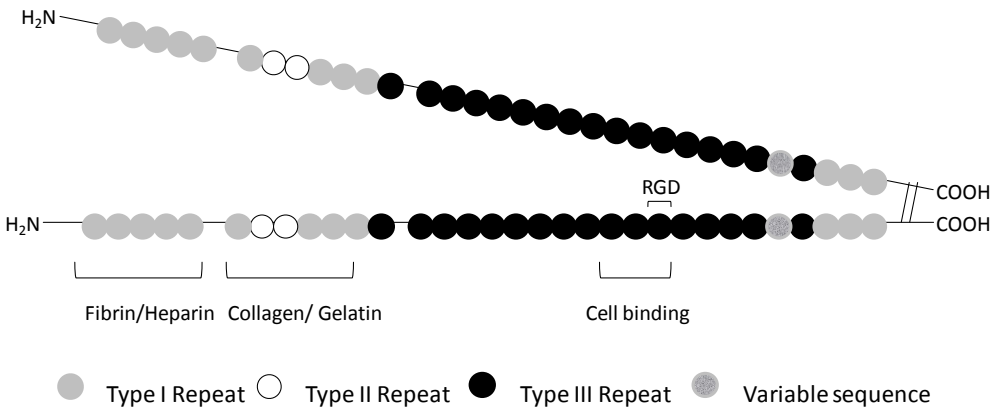

Figure 6.5. Schematic representation of fibronectin showing its modular architecture and functionality of various domains.

Fibronectin molecule in solution presents a compact conformation that may be disturbed when it is adsorbed on a biomaterial surface. A number of studies have investigated the nature of fibronectin adsorption to model surfaces finding that protein arms undergo greater extension on hydrophilic surfaces compare to hydrophobic, what was translated in an enhancement in cell adhesion[28]. Studies with quartz crystal microbalance revealed that an increase in the viscoelastic properties of the adsorbed layer enhanced the bioactivity of fibronectin facilitating the access to epitope on the protein surface[29]. This increase in the viscoleasticity correlates to the unfolding of the molecule once is adsorbed on the surface of the biomaterial, giving a more hydrated layer and presenting a more desirable conformation of the fibronectin[3] (Figure 6.6).

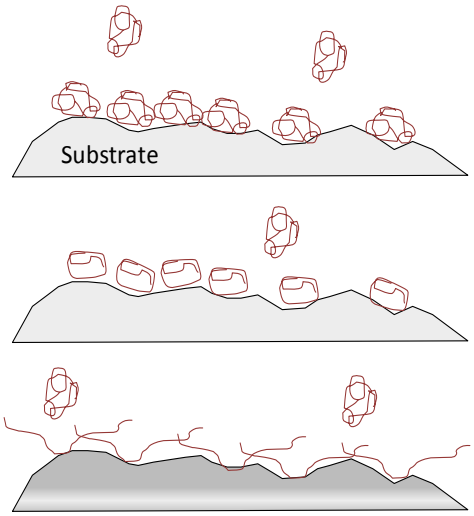

Figure 6.6. Fibronectin conformations adsorbed on biomaterial's surface.

d) Type I Collagen

Collagen is the major insoluble fibrous protein in the ECM. This family of proteins accounts for 25% of total body proteins and provides an important structural framework for most body structures. Type I collagen, found in bone, skin, tendon, ligaments and dentin, is the most abundant one[4, 30]. Apart from its structural role, it is also important because it posses RGD sequences[19].

The fundamental structure unit of type I collagen is 1.5 nm in diameter and 300 nm long, and these molecules undergo a self-assembly process to form collagen fibrils with a diameter of 50-200 nm in overlapping rows[30]. These structures are presented in Figure 6.7.

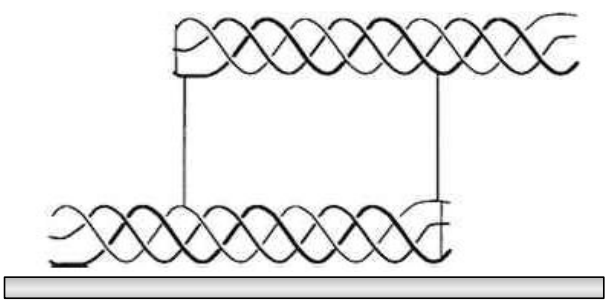

Figure 6.7. Collagen molecules and their interaction to form overlapping rows.

6.1.4. Fundamentals of Quartz Crystal Microbalance with Dissipation

Among different techniques of protein adsorption study, quartz crystal microbalance with dissipation (QCM-D) has emerged as one of the most convenient and highly sensitive instrument, which allows measuring the kinetics of both mass changes and structural properties of adsorbed layer in real time.

The principle of QCM-D is based on the resonance frequency of the quartz crystal, a sensor, induced by applying an alternating electric field across the crystal. The equipment simultaneously collects both the resonant frequency, which changes are related to mass changes, and the energy dissipation signals, connected with viscoelastic properties of the layer.

When a substance is adsorbed on the crystal surface, causes an increase in mass (Δm) bound to the quartz and the crystal oscillation frequency decreases, obtaining a negative shift of the resonance frequency (-Δf). If the adsorbed mass is rigid, evenly distributed, and small compared to the mass of the crystal, the Δf is proportional to Δm under **Sauerbrey model**[31] (Eq. 6.1):

$$\Delta m = -\frac{C \cdot \Delta f}{n} \qquad \text{(Eq. 6.1)}$$

where C is the mass sensitivity constant (C = 17.7 ng/cm^{2}Hz at f = 5 MHz) and n is the overtone number (n = 1, 3, 5…).

However, if the adsorbed layer is not rigid enough, the energy dissipation in the oscillation will be changed. Due to the fact that most protein layers adsorbed at the interface are hydrated and highly viscoelastic, they are not completely rigid and can cause dissipation factor (D) to change significantly. In such cases, for viscoelastic or soft films, the Sauerbrey relation based on the frequency alone will underestimate the mass since the film is not fully coupled to the motion of the sensor surface. In order to obtain more accurate mass change and structural properties of the adsorbed protein layer, energy dissipation should be considered. All these viscoelastic properties such as density, viscosity, elasticity and thickness can be correlated to the Δf and D from the **Voight model**[31]. This model provides a complete analysis by the use of the software of the QCM-D system.

Even though increasing number of studies have investigated about the field of proteins and the study of their adsorption on biomaterials surfaces, there is no much literature about the study of this behaviour for siloxane sol-gel coatings. In this context, our aim was to investigate the adsorption kinetics of the four proteins mentioned before on the developed hybrid materials, comparing them to pure titanium, by the use of the QCM-D and test both the effect of gelatin and the functionalization introduced in 35M:35G:30T formulations by the GPTM precursor.

6.2. Materials and methods

6.2.1. QCM-D sensors

Gold (QSX 301) and titanium (QSX 310) QCM-D sensors were purchased at Q-Sense (Sweden). The sensors consisted of gold and titanium coated quartz crystals of 14 mm in diameter and a fundamental resonance frequency of 5 MHz. Titanium sensors were used as received and as control of the protein adsorption study. Gold sensors were divided in three groups: the first was spin-coated with 7M:3T-Gelatin hybrids (7M:3T, 7M:3T-0.9% and 7M:3T-2.0%), the second one with 35M:35G:30T-0.9% and the last group was kept uncoated and used as control.

Spin-coater conditions were established in order to obtain continues, homogeneous and defect free coatings, with enough thickness to be detected by QCM-D. 60 µL of solution were placed on sensor surface and it was spin at 3000 rpm for 30 seconds. Then, corresponding heat treatment was applied to each material and their homogeneity was confirmed by XPS and SEM.

Prior to each experiment and after it, sensor surfaces were cleaned. There were two different protocols depending on the type of sensor.

- Gold sensor: (1) 15 min sonication with THF; (2) place the sensors in piranha solution (5:1:1 mixture of miliQ water, ammonia at 25 wt% and hydrogen peroxide at 30 wt%) heated at 75 °C for 5 minutes; (3) rinse gently with miliQ water; (4) dry with nitrogen gas; and (5) UV/ozone treat for 10 minutes.
- Titanium sensor: (1) 15 min sonication with THF; (2) immerse sensors in Sodium Dodecyl Sulfate (SDS) 2 wt% solution and sonicate for 30 min at

room T; (3) rinse with miliQ water; (4) dry with nitrogen gas; and (5) UV/ozone treat for 10 minutes.

6.2.2. Protein solutions

Bovine serum albumin (BSA), human fibrinogen (Fbg), human fibronectin (Fn) and type I collagen (Col I) were purchased at Sigma-Aldrich. They were used at different concentrations mimicking, approximately, their proportion in the human blood plasma (BSA/Fbg/Fn)[2, 12, 27]. BSA was 5 mg/ml in phosphate buffer saline solution (PBS, Sigma), Fbg at 500 µg/ml in PBS, Fn at 50 µg/ml in PBS and Col I at 10 µg/ml in acetate buffer (0.1 M, pH 5.6).

6.2.3. Protein adsorption test

For protein adsorption study, sensors were placed in the QCM-D (model E4, Q-Sense, Inc. MD) and tests were conducted at 37° and a constant flow rate of 25 µL/min. After establishing a stable base line in PBS, the surface was exposed to different serum proteins (one protein per experiment) monitoring frequency and dissipation changes. Then, when the frequency and dissipation shift reached a stable point (defined as less than 1 Hz shift in 10 min), PBS was introduced in the chamber to remove the reversibly adsorbed proteins on the surface and reach a new plateau.

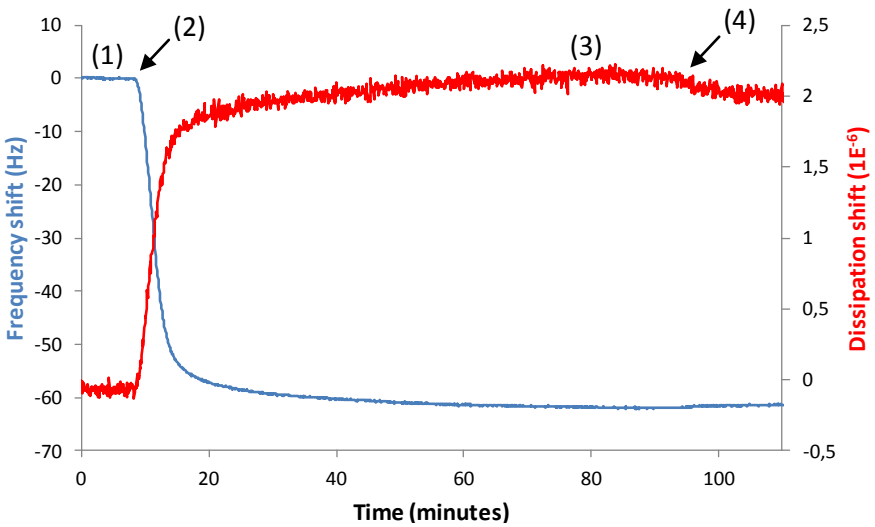

Figure 6.8. Representative plot of a single-protein adsorption experiment with the corresponding steps: (1) PBS base line; (2) protein solution introduction to the QCM-D chamber; (3) Δf and ΔD stable point; and (4) cleaning of the non-attached proteins.

Test was performed at least three times for each coating type and protein solution and data from the 3rd to the 13th overtones was monitored. The fundamental overtone is usually disregarded since it is too sensitive.

6.2.4. QCM-D results analysis

The results acquired from the QCM-D system were analyzed using the QTools software. First of all, in order to determine which approach should be used, Sauerbrey or Voigt model, f and D shifts for each overtone were analyzed. Data will require Voight viscoelastic modelling if D values are not close to zero or if D shifts (in 1E-6) are higher than 5% of f shifts (in Hz). Furthermore, if there are significant differences between overtones, this modelling is also recommendable.

For the adsorption study of BSA, a rigid layer was obtained and in consequence Sauerbrey model was applied to obtain the areal mass (ng/cm^2) and the thickness (nm). For this calculation frequency shift data from the 3rd to 9th overtones were used in all the cases.

On the other hand, when studying the adsorption behaviour for Fbg, Fn and Col I, a viscoelastic adlayer was obtained and therefore Voight modelling was used. For the viscoelastic modelling, QTools software needs the input of some fix initial parameters and a range of floating variables that might be changed to obtain the best fitting.

These initial parameters need to be as close as possible to the real experiment conditions. These fixed parameters were fluid density, fluid viscosity and layer density. For the parameters related to the fluid, the values for water were selected since it is the main component of the system, and results in a good estimation. The density of the protein layer might vary between 1000 kg/m^3 (water) and 1350 kg/m^3 (protein) depending on protein coverage[2]. An intermediate value is usually used for the fitting on the basis of non-completely saturated protein coverage. In our case 1150 kg/m^3 gave the best fitting[2, 3, 32]. Fixed parameters are presented in Table 6.1.

Table 6.1. Fixed parameters for Voigt model calculations

Fixed parameters	Input value
Fluid density (kg/m^3)	1000
Fluid viscosity (kg/m·s)	0.001
Layer density (kg/m^3)	1150

The parameters fitted were layer viscosity, layer shear modulus and layer thickness/mass. All fitted values are summarized in Table 6.2.

Table 6.2. Fitted parameters for Voigt model calculations

Fitted parameters	Values range
Layer viscosity (kg/m·s)	0.0001 - 0.01
Layer shear modulus (Pa)	100 - 10^{12}
Layer thickness (m)	10^{-10} - 10^{-6}

In normal conditions and when there were no interferences problems with any overtones, four of them were used for Voigt modelling (3rd, 5th, 7th and 9th).

6.3. Results

6.3.1. Surface characterization

First, substrates surface composition was study by XPS. Table 6.3 shows the average chemical composition of gold and titanium sensors for the most abundant elements (composition of coatings was shown before in chapters 4 and 5). Small amount of other trace elements as N, Sn or Si were obtained. Their presence and the considerably big C percentage are residual components from the fabrication process, what makes clear the importance of the cleaning process step before using them in the QCM-D.

Table 6.3. XPS elemental composition of Gold and Titanium sensors (%).

	Au	Ti	O	C
Gold sensor	74.3 ± 0.3	-	6.1 ± 0.3	14.0 ± 0.7
Titanium sensor	-	18.1 ± 0.3	48.1 ± 0.2	25.2 ± 0.3

The fact of being O the main component of Titanium sensors is due to the spontaneously formed TiO_2 layer in every surface based on this element.

Afterwards, obtained siloxane-gelatine coatings' thickness was measured using QCM-D and obtaining values around 100 nm with the selected spin-coating parameters. SEM was used to verify the uniformity of all surfaces where defect free surfaces were observed.

Contact angle measurements for gold and titanium controls are presented in Table 6.4. The results show that gold wettability is in the range of the previously obtained values for siloxane-gelatin coatings, while titanium sensor is the most hydrophilic surface from all the studied materials.

Table 6.4. Contact angle values of surfaces under study.

Surface type	Contact angle (°)
Gold	64.3 ± 2.0
Titanium	15.8 ± 4.7

6.3.2. Protein adsorption: Siloxane-gelatin coating effect

First of all, the adsorption properties of the 7M:3T, 7M:3T-0.9% and 7M:3T-2.0% coatings for the selected four serum proteins were tested using as controls gold and titanium sensors. The aim was to assess the effect on the adsorption behaviour of the siloxane network from one side, and the influence of gelatin from the other one.

a) BSA

In Table 6.5 the frequency and dissipation shift values obtained at the end point (plateau) of the experiment after removing the non-attached proteins with PBS are presented. D values are small enough to allow using Sauerbrey model to calculate BSA mass density on the surface.

Table 6.5. Frequency and dissipation shifts value obtained at the end of the experiment for BSA protein adsorption and calculated areal mass by Sauerbrey model.

Coating	Frequency shift (Hz)	Dissipation shift (1E-6)	Surface mass density (ng/cm^2)	Thickness (nm)
Gold	-33 ± 2	1.1 ± 0.3	621 ± 38	5.6 ± 0.3
Titanium	-30 ± 1	1.2 ± 0.1	608 ± 87	5.5 ± 0.3
7M:3T	-27 ± 1	1.0 ± 0.1	537 ± 39	4.9 ± 0.4
7M:3T-0.9%	-27 ± 1	0.8 ± 0.1	563 ± 19	5.1 ± 0.2
7M:3T-2.0%	-24 ± 1	1.3 ± 0.2	494 ± 24	4.5 ± 0.2

In spite of not being significant differences between all the areal mass values for different substrates, a slight trend to decrease the amount of adsorbed BSA mass comparing coatings to both controls (gold and titanium) can be appreciated, and also with the incorporation of gelatin. Such behaviour could be attributed to the decrease in roughness due to the addition of gelatin (shown in chapter 4), what may lead to smaller surface area and in consequence lower BSA levels.

Thickness values together with the BSA protein molecule size are indicative of a protein monolayer formation, with values not far from the 4.0 nm width.

b) Fbg

Results obtained for the fibrinogen adsorption (Table 6.6) show higher frequency shifts compared to the adsorption of BSA, showing a preference of Fbg to be adsorbed on studied surfaces. In this case, a new parameter has been added, ΔD/Δf, which is a measurement of the change in the dissipation of the protein layer per frequency unit. As mentioned before, when the dissipation shift is higher than a 5% of the frequency shift, a viscoelastic modelling is required[2]. Furthermore, the changes in the dissipation of a protein layer are believed to arise from two coupled mechanism: (1) the conformational changes in the structure of the protein layer and (2) the amount of water bound in the protein layer[33].

Table 6.6. Frequency and dissipation shift values obtained at the end of the experiment for Fbg protein adsorption and calculated ΔD/Δf factor and areal mass by Voigt model.

Coating	Frequency shift (Hz)	Dissipation shift (1E-6)	ΔD/Δf (%)	Surface mass density (ng/cm^2)
Gold	-69 ± 4	2.5 ± 0.2	3.7	1885 ± 104
Titanium	-98 ± 5	5.2 ± 0.4	5.3	2827 ± 99
7M:3T	-94 ± 11	6.2 ± 0.1	6.6	2806 ± 11
7M:3T-0.9%	-86 ± 9	5.8 ± 0.2	6.7	2684 ± 126
7M:3T-2.0%	-96 ± 4	6.6 ± 0.2	6.9	2826 ± 75

Taking into account the D values, it is clear that in the case of Fbg adsorption on gold, a more rigid layer was obtained. These differences can be attributed to the chemistry of the surface, since both titanium sensor surface and siloxane-gelatin coatings share their oxide chemical structure, what seems to favour the adsorption of this protein and the formation of a more viscous layer. Nevertheless, there could not be appreciated a difference among the different gelatin percentages.

c) Fn

Table 6.7 summarizes the frequency and dissipation values obtained at the stable point of Fn adsorption and the calculated ΔD/Δf factor related to the viscoelastic properties of the adlayer. Due to the high D values, it was necessary to use the viscoelastic model to calculate the real adsorbed mass. So, obtained surface mass values using the Voight model are also presented.

Table 6.7. Frequency and dissipation shift values obtained at the end of the experiment for Fn protein adsorption and calculated ΔD/Δf factor and areal mass by Voigt model.

Coating	Frequency shift (Hz)	Dissipation shift (1E-6)	ΔD/Δf (%)	Surface mass density (ng/cm^2)
Gold	-55 ± 3	3.0 ± 0.8	6.3	2181 ± 71
Titanium	-59 ± 3	4.0 ± 0.2	6.8	2438 ± 11
7M:3T	-53 ± 8	5.0 ± 0.4	9.4	2886 ± 92
7M:3T-0.9%	-60 ± 5	5.0 ± 0.4	8.3	2759 ± 117
7M:3T-2.0%	-52 ± 6	4.6 ± 0.4	8.8	2838 ± 44

From these results two conclusions can be taken. From one side, there is a noticeable effect of coatings increasing the surface mass density in comparison to

gold and titanium. This could imply a better *in vitro* and *in vivo* behaviour since, as said before, Fn is one of the most important proteins triggering cell adhesion, so a preference of this protein to be adsorbed on developed materials could be translated in an improvement of the cell response.

On the other hand, the increase of ΔD/Δf factor indicates the formation of a softer or more hydrated protein layer[33] (8.3-9.4) compared to gold (6.3) and titanium (6.8) controls; and this increase of the viscoelasticity has been shown to enhance the bioactivity of surface-bound proteins[3]. Therefore, it can be said that sol-gel coatings promote the unfolding or extension of Fn molecule on the surface what makes more accessible the binding points RGD for subsequent cell attachment. This behaviour is illustrated in Figure 6.6.

d) Col I

Obtained results for Col I adsorption assays are summarized in Table 6.8.

Table 6.8. Frequency and dissipation shift values obtained at the end of the experiment for Col I protein adsorption and calculated ΔD/Δf factor and areal mass by Voigt model.

Coating	Frequency shift (Hz)	Dissipation shift (1E-6)	ΔD/Δf (%)	Surface mass density (ng/cm^2)
Gold	-34 ± 3	4.3 ± 0.8	12.4	871 ± 21
Titanium	-41 ± 8	4.8 ± 1.2	11.9	2627 ± 300
7M:3T	-36 ± 4	6.1 ± 1.7	17.5	3182 ± 574
7M:3T-0.9%	-38 ± 4	6.8 ± 0.7	18.0	3152 ± 116
7M:3T-2.0%	-30 ± 4	5.6 ± 0.9	18.4	3057 ± 293

The great differences among overtones together with the high dissipation shift values makes necessary to use Voigt model. Such behaviour was also the responsible of the big standard deviations obtained for the calculated adsorbed surface mass density, since when there are such differences among overtones, the appropriate modelling is much more difficult.

As it was explained before, collagen molecule has a large fibrous structure which undergoes a self-assembly process to form a structure of overlapping collagen rows[19, 30]. This leads to the formation of a layer with high amount of solvent entrapped in the structure and high viscoelasticity. That is the reason of obtaining ΔD/Δf values higher than a 15%.

Once again, the increase of protein adsorbed mass in the cases of the siloxane-gelatin coatings compared to titanium can be seen. Col I is, as well as Fn, an adhesive protein which due to its RGD domains plays an important role in cell adhesion process. For that reason, it is important to stimulate its adsorption on biomaterials' surfaces.

Finally, in Figure 6.9 the adsorption kinetics for all the studied proteins on titanium surface are presented, as an example.

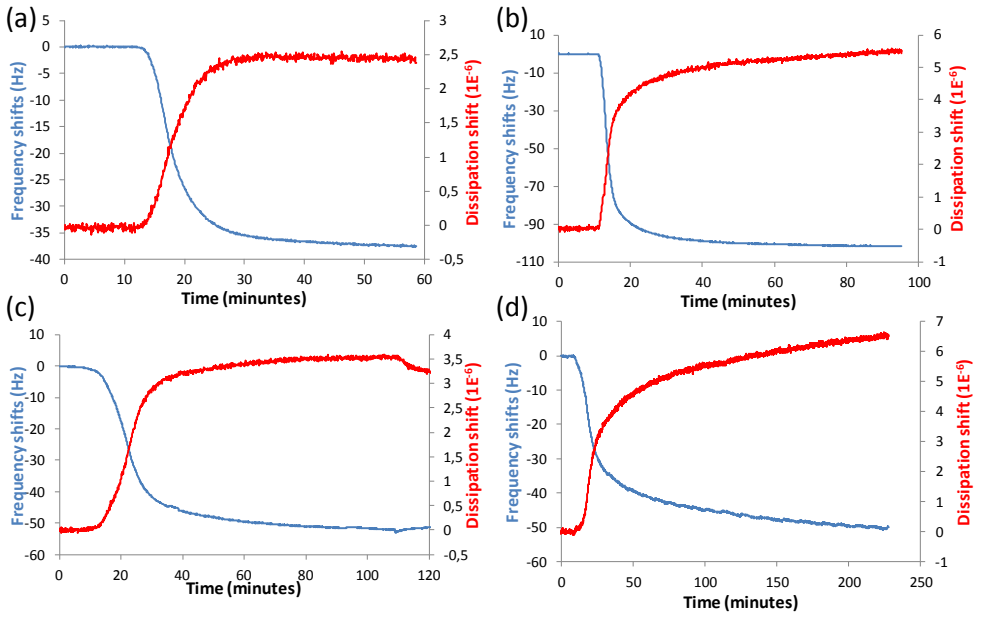

Figure 6.9. Frequency and dissipation plots for: (a) BSA, (b) Fbg, (c) Fn and (d) Col I on titanium.

The adsorption kinetic was similar for the four proteins regardless the substrate. There were differences in the amount of adsorbed protein mass but not in the kinetic of the obtained curves. Secondly, comparing the four proteins, Col I adsorption kinetic was the slowest one owing to the obtained frequency and dissipation shift plots, where reaching the plateau took more than three hours and, as it can be seen, it was not as flat and stable as for the other studied proteins. This can be explained by the constant self-assembly process among Col I fibres.

Figure 6.10 collects the results of adsorbed mass values for all the experiments. BSA shows lower areal mass values compared to the adsorption of the rest of proteins, even though its concentration (5 mg/mL) was higher than the one for Fbg (500 µg/mL), Fn (50 µg/mL) and Col I (10 µg/mL). Although BSA could be expected to be the most likely protein due to its high concentration and small size that facilitates diffusion rate, it seems that other factors such as the affinity and ability to assume different conformation/orientation of large proteins prevail.

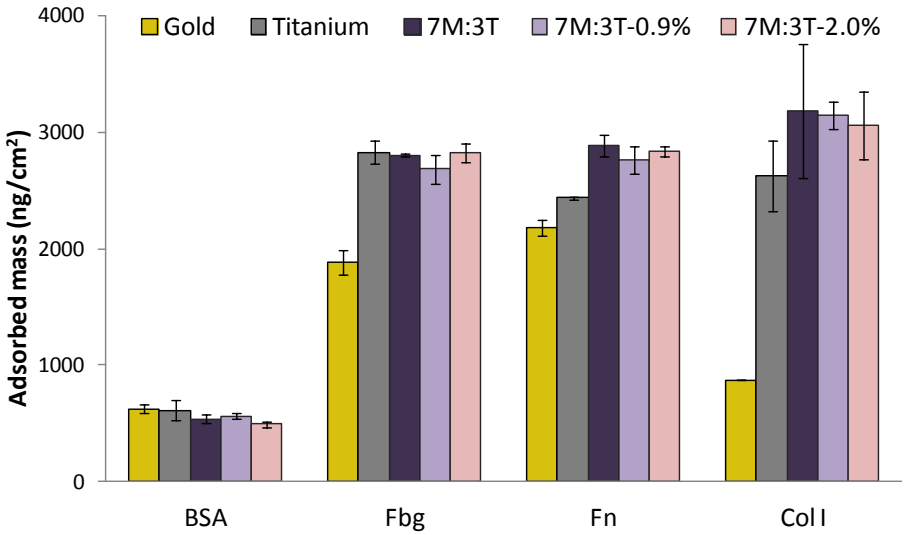

Figure 6.10. Single protein adsorbed mass of BSA, Fbg, Fn, and Col I on different surfaces after saturation (stable point) at 37°.

Comparing the adsorption rate for Fbg, no significant differences were obtained among different surfaces, except for gold where much lower levels were obtained. However, in the case of adhesive proteins such as Fn and Col I, the effect of coatings improving the amount of adsorbed protein on the surface can be appreciated in comparison to both gold and titanium, which is more important for the purpose of this work.

In addition, no noticeable effect of gelatin content of coatings in protein adsorption test could be observed. Nevertheless, its influence in cell adhesion will be later studied.

6.3.3. Protein adsorption: Functionalization effect

After obtaining a good behaviour of developed coatings for serum protein adsorption, in some cases better than the one obtained for titanium, we proceeded to assess the role of epoxy group on the new designed ternary system with the incorporation of GPTMS silicon precursor. As it was mentioned before, the effect of functional groups on the surface can influence cell growth via protein adsorption and subsequent protein:cell interaction steps. Therefore, this section will be focused on comparing the adsorption behaviour of 35M:35G:30T-0.9% hybrid, with its previously studied homologous 7M:3T-0.9% coating, taking into account the changes in mass density and the conformation of adsorbed protein layer.

a) Adsorbed mass

In Figure 6.11 the adsorbed mass results obtained for titanium, 7M:3T-0.9% and 35M:35G:30T-0.9% with the chosen four proteins are plotted.

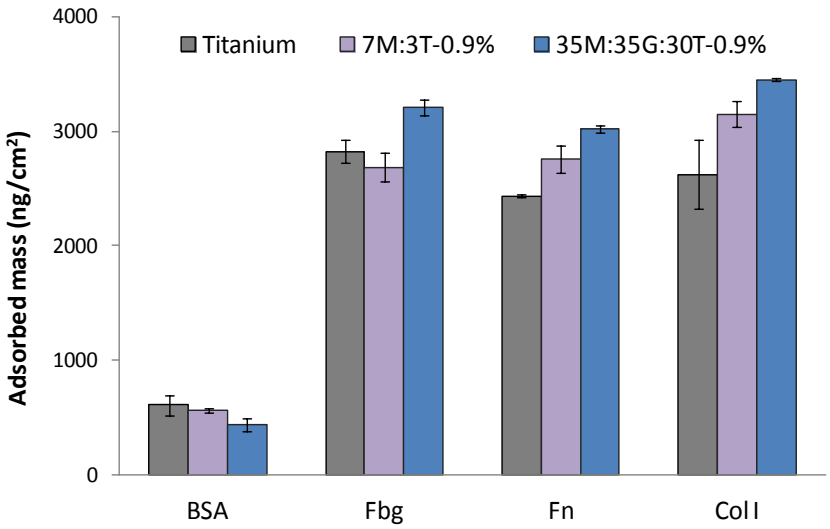

Figure 6.11. Single protein adsorbed mass of BSA, Fbg, Fn, and Col I on titanium, 7M:3T-0.9% and 35M:35G:30T-0.9% after saturation (stable point) at 37°.

For BSA adsorption and comparing sol-gel coatings to titanium, a small decrease on adsorbed mass was obtained, which, as said before, could be attributed to a decrease in surface area related to the roughness decrease. A significant fact is the great differences in adsorbed mass values for this protein compared to the

others, which are much lower. It was explained before that due to its concentration and size, BSA was expected to be more favourably adsorbed. However opposite effect was obtained. This preference of surfaces for the large and less concentrated adhesive proteins may result beneficial for the subsequent cell attachment since albumin is a non-adhesive protein known to eliminate cell attachment and block nonspecific binding[19, 34, 35]. Nevertheless, further studies where competitive adsorption of different proteins is tested will be needed to confirm this.

Now, focusing on the effect of the epoxy group of the 35M:35G:30T-0.9% coating, a significant increase on adsorbed protein mass is observed comparing both with titanium and 7M:3T-0.9% surfaces, for Fbg, Fn and Col I. Owing to these results, we can say that the incorporation of GPTMS to the formulation has successfully improved the affinity of adhesive proteins toward the siloxane coating.

b) Orientation approach of surface-adsorbed proteins

Taking some parameters and the results obtained using Voigt model into account, a conformation/orientation approach can be done.

In the case of BSA, it was said in the previous section that taking into account protein's shape and the thickness values obtained for the adsorbed layer, a monolayer was formed with no structural changes.

Fbg, however, has a rodlike structure of width approximately 10 nm, which may lie planar at the biomaterial interface (side-on) or may undergoes a rearrangement perpendicular to the surface (end-on). Since the tested surfaces showed thicknesses greater than 10 nm (Table 6.9), this might indicate an end-on adsorption of Fbg molecules to these surfaces (assuming a monolayer)[32]. The preference to adopt this conformation on studied surfaces is important, since it favours the adsorption of greater amounts of protein.

Moreover, the increase of the thickness, related to higher number of molecules adsorbed on the surface and also the different angle of inclination adopted in each material by proteins molecules, is translated in an increase on the $\Delta D/\Delta f$ factor, or what is the same, in the viscosity of the adsorbed layer.

Table 6.9. Surface adsorbed thickness calculated by Voigt model and ΔD/Δf factor for Fbg (500 µg/mL) adsorption.

Coating	Thickness (nm)	ΔD/Δf (%)
Gold	17.1 ± 0.9	3.7
Titanium	25.7 ± 0.9	5.3
7M:3T-0.9%	24.4 ± 1.3	6.7
35M:35G:30T-0.9%	29.2 ± 0.6	6.6

For Fn the different conformations adopted once it is adsorbed on biomaterials' surface, have been extensively studied in literature[3, 28, 36], concluding that an unfolded and elongated structure promotes the interaction between binding point of Fn and integrin domains of cells. In previous studies with QCM-D[3, 29], an increase in the ΔD/Δf value (increase in viscoelasticity) has been shown to enhance the bioactivity of surface-bound proteins, including Fn. Hence, we assume that the increase in the viscoelasticity on the formed Fn layer correlates to the unfolding of the Fn molecules on the surface (more hydrated) presenting a more open conformation allowing the interaction with cells (as shown in Figure 6.6). Obtained values for this study are shown in Table 6.10.

Table 6.10. D shift and ΔD/Δf factor for Fn adsorption.

Coating	Dissipation shift (1E-6)	ΔD/Δf (%)
Gold	3.0 ± 0.8	5.4
Titanium	4.0 ± 0.2	6.8
7M:3T-0.9%	5.0 ± 0.4	8.3
35M:35G:30T-0.9%	5.5 ± 0.2	8.3

Owing to the dissipation and ΔD/Δf values, it is clear the formation of a more viscoelastic layer in the cases where Fn is adsorbed on the developed sol-gel coatings. This may make these surface more suitable materials for cell adhesion and spreading, what will be test in next chapter.

Finally, Col I adsorbed forming a structure similar to a scaffold where Col I monomers are interconnected forming rows (illustrated in Figure 6.7)[19, 30]. This conformation facilitates the entrapment of solvent and gives a layer with a high viscoelasticity, what is translated in high ΔD values shown before.

6.4. Conclusions

To conclude, two effects can be highlighted. From one side the general preference of studied serum proteins, moreover adhesive ones, to developed materials in comparison to gold and titanium. From the other side the clear effect of the introduced functionalization on 35M:35G:30T-0.9% coating on the increase of the interaction at the interface between the biomaterial surface and Fbg, Fn and Col I.

It is also important to underline the favourable conformation/orientation of Fbg on hybrid coatings, allowing the adsorption of high amounts of molecules, and Fn acquiring a more bioactive conformation when is adsorbed on sol-gel coatings.

No overall correlation was found between water contact angle values and protein adsorption levels, but as it was found by other authors and mentioned before, protein adsorption is a complex process where the effect of many different variables converges.

In next chapter the correlation between these results and *in vitro* cell studies will be tried to be found.

References

1. Wilson CJ, Clegg RE, Leavesley DI et al. Mediation of biomaterial-cell interactions by adsorbed proteins: A review. *Tissue Eng.* 2005; **11:** 1-18.

2. Pegueroles M, Tonda-Turo C, Planell JA et al. Adsorption of fibronectin, fibrinogen, and albumin on TiO2: Time-resolved kinetics, structural changes, and competition study. *Biointerphases.* 2012; **7:** 48.

3. Molino PJ, Higgins MJ, Innis PC et al. Fibronectin and bovine serum albumin adsorption and conformational dynamics on inherently conducting polymers: A QCM-D study. *Langmuir.* 2012; **28:** 8433-45.

4. Dee KC, Puleo DA, Bizios R. *An Introduction to Tissue-Biomaterial Interactions.* John Wiley & Sons, 2003.

5. Shi D. *Biomaterials and Tissue Engineering.* Springer, 2004.

6. Wang K, Zhou C, Hong Y et al. A review of protein adsorption on bioceramics. *Interface Focus.* 2012; **2:** 259-77.

7. Benesch J, Svedhem S, Svensson SC et al. Protein adsorption to oligo (ethylene glycol) self-assembled monolayers: Experiments with fibrinogen, heparinized plasma, and serum. *Journal of Biomaterials Science, Polymer Edition.* 2001; **12:** 581-97.

8. Roach P, Farrar D, Perry CC. Interpretation of protein adsorption: Surface-induced conformational changes. *J Am Chem Soc.* 2005; **127:** 8168-73.

9. Keselowsky BG, Collard DM, García AJ. Surface chemistry modulates fibronectin conformation and directs integrin binding and specificity to control cell adhesion. *Journal of Biomedical Materials Research Part A.* 2003; **66:** 247-59.

10. Keselowsky BG, Collard DM, García AJ. Surface chemistry modulates focal adhesion composition and signaling through changes in integrin binding. *Biomaterials.* 2004; **25:** 5947-54.

11. Lan MA, Gersbach CA, Michael KE et al. Myoblast proliferation and differentiation on fibronectin-coated self assembled monolayers presenting different surface chemistries. *Biomaterials.* 2005; **26:** 4523-31.

12. Felgueiras HP, Sommerfeld SD, Murthy NS et al. Poly (NaSS) functionalization modulates the conformation of fibronectin and collagen type I to enhance osteoblastic cell attachment onto Ti6Al4V. *Langmuir.* 2014; **30:** 9477-83.

13. Stallard CP, McDonnell K, Onayemi O et al. Evaluation of protein adsorption on atmospheric plasma deposited coatings exhibiting superhydrophilic to superhydrophobic properties. *Biointerphases.* 2012; **7:** 31.

14. Tamada Y, Ikada Y. Effect of preadsorbed proteins on cell adhesion to polymer surfaces. *J Colloid Interface Sci.* 1993; **155:** 334-9.

15. Arima Y, Iwata H. Effect of wettability and surface functional groups on protein adsorption and cell adhesion using well-defined mixed self-assembled monolayers. *Biomaterials.* 2007; **28:** 3074-82.

16. Arima Y, Iwata H. Effects of surface functional groups on protein adsorption and subsequent cell adhesion using self-assembled monolayers. *Journal of Materials Chemistry.* 2007; **17:** 4079-87.

17. Roach P, Farrar D, Perry CC. Surface tailoring for controlled protein adsorption: Effect of topography at the nanometer scale and chemistry. *J Am Chem Soc.* 2006; **128:** 3939-45.

18. Sela MN, Badihi L, Rosen G et al. Adsorption of human plasma proteins to modified titanium surfaces. *Clin Oral Implants Res.* 2007; **18:** 630-8.

19. Tagaya M, Ikoma T, Takemura T et al. Effect of interfacial proteins on osteoblast-like cell adhesion to hydroxyapatite nanocrystals. *Langmuir.* 2011; **27:** 7645-53.

20. Rodrigues SN, Gonçalves IC, Martins MCL et al. Fibrinogen adsorption, platelet adhesion and activation on mixed hydroxyl-/methyl-terminated self-assembled monolayers. *Biomaterials.* 2006; **27:** 5357-67.

21. Oliva FY, Avalle LB, Cámara OR et al. Adsorption of human serum albumin (HSA) onto colloidal TiO2 particles, part I. *J Colloid Interface Sci.* 2003; **261:** 299-311.

22. Kim J, Yoon J. Protein adsorption on polymer particles. *Encyclopedia of Surface and Colloid Science.* 2002; **1:** 4373-81.

23. Gelamo E, Tabak M. Spectroscopic studies on the interaction of bovine (BSA) and human (HSA) serum albumins with ionic surfactants. *Spectrochimica Acta Part A: Molecular and Biomolecular Spectroscopy.* 2000; **56:** 2255-71.

24. Gelamo EL, Silva CHTP, Imasato H et al. Interaction of bovine (BSA) and human (HSA) serum albumins with ionic surfactants: Spectroscopy and modelling. *Biochimica Et Biophysica Acta (BBA) - Protein Structure and Molecular Enzymology.* 2002; **1594:** 84-99.

25. Bai Z, Filiaggi MJ, Dahn JR. Fibrinogen adsorption onto 316L stainless steel, nitinol and titanium. *Surf Sci.* 2009; **603:** 839-46.

26. Höök F, Vörös J, Rodahl M et al. A comparative study of protein adsorption on titanium oxide surfaces using in situ ellipsometry, optical waveguide lightmode spectroscopy, and quartz crystal microbalance/dissipation. *Colloids and Surfaces B: Biointerfaces.* 2002; **24:** 155-70.

27. Grunkemeier J, Tsai W, McFarland C et al. The effect of adsorbed fibrinogen, fibronectin, von willebrand factor and vitronectin on the procoagulant state of adherent platelets. *Biomaterials.* 2000; **21:** 2243-52.

28. Baugh L, Vogel V. Structural changes of fibronectin adsorbed to model surfaces probed by fluorescence resonance energy transfer. *Journal of Biomedical Materials Research Part A.* 2004; **69:** 525-34.

29. Dolatshahi-Pirouz A, Jensen T, Foss M et al. Enhanced surface activation of fibronectin upon adsorption on hydroxyapatite. *Langmuir.* 2009; **25:** 2971-8.

30. Lodish HF, Berk A, Zipursky SL *et al*. *Molecular Cell Biology.* Citeseer, 2000.

31. Q-Sense. QCM-D. http://Www.biolinscientific.com/q-sense/. 2014; **2013:** .

32. Weber N, Pesnell A, Bolikal D et al. Viscoelastic properties of fibrinogen adsorbed to the surface of biomaterials used in blood-contacting medical devices. *Langmuir.* 2007; **23:** 3298-304.

33. Hemmersam AG, Foss M, Chevallier J et al. Adsorption of fibrinogen on tantalum oxide, titanium oxide and gold studied by the QCM-D technique. *Colloids and Surfaces B: Biointerfaces.* 2005; **43:** 208-15.

34. Koenig AL, Gambillara V, Grainger DW. Correlating fibronectin adsorption with endothelial cell adhesion and signaling on polymer substrates. *Journal of Biomedical Materials Research Part A.* 2003; **64:** 20-37.

35. Jeyachandran Y, Mielczarski E, Rai B et al. Quantitative and qualitative evaluation of adsorption/desorption of bovine serum albumin on hydrophilic and hydrophobic surfaces. *Langmuir.* 2009; **25:** 11614-20.

36. Vanterpool FA, Cantini M, Seib FP et al. A material-based platform to modulate fibronectin activity and focal adhesion assembly. *BioResearch Open Access.* 2014; **3:** 286-96.

Chapter 7

In vitro biological evaluation

Chapter 7:

IN VITRO BIOLOGICAL EVALUATION

7.1. Introduction

After the complete physicochemical characterization performed for all the developed materials in previous chapters, the next step is the biological evaluation of these coatings and its comparison with commercially pure titanium.

Titanium is the most widely used material for metallic dental implants due to its good properties, osteoconductivity among others, what allows its complete osseointegration with a low rate of failure. However, when patients' conditions are not favourable[1, 2], as for example poor bone regeneration or some diseases, the therapy success rate decreases making, in some cases, impossible to use this treatment.

The search of an osteoinductive material which promotes bone formation and makes the use of these types of implants widespread brought us to the development of siloxane-gelatin coatings where the silica release will enhance the bone-forming cell activity[3-5]. This property is going to be tested in this chapter by *in vitro* assays together with the non-citotoxicity and proliferation ability of cells seeded onto developed coatings.

Previously studied properties such as coating chemistry, topography, silicon release kinetic or protein adsorption ability, will be correlated with the results obtained in cell studies, since, as it is known, there are many parameters that will influence *in vitro* response. Furthermore, different cell lineages were used in order to obtain a complete biological characterization.

7.2. Materials and methods

7.2.1. Materials

Grade 4 pure titanium discs measuring 12 and 10 mm in diameter and 1.2 mm in thickness provided by Ilerimplant S.L. (Lleida, Spain) were used. They presented a heterogeneous topography produced by blasting with corundum (Al_2O_3) particles and an acid-etching, and they were already supplied decontaminated and sterilized by gamma radiation.

The metallic surfaces were then coated with the different sol-gel formulations using a dip-coater under the conditions described in chapter 2. Before

the *in vitro* evaluation, samples were sterilized by UV light for 30 min from each side of the discs and before spreading cells, they were conditioned with the adequate media at 37° and 5% CO_2 overnight. The control used for all the biological evaluation was the uncoated titanium disc, since it is the material under study to be improved.

7.2.2. Surface Perfilometry

With the aim of evaluating the changes produced in titanium discs' topography as a consequence of the coating, perfilometry studies were performed. The studied materials in this case were 7M:3T, 35M:35G:30T, 7M:3T-0.9% and 35M:35G:30T-0.9%, just to see the differences among the two different siloxane matrixes and the effect of the incorporation of gelatin.

Samples were prepared as shown in Figure 7.1, where the half of the disc was kept uncoated.

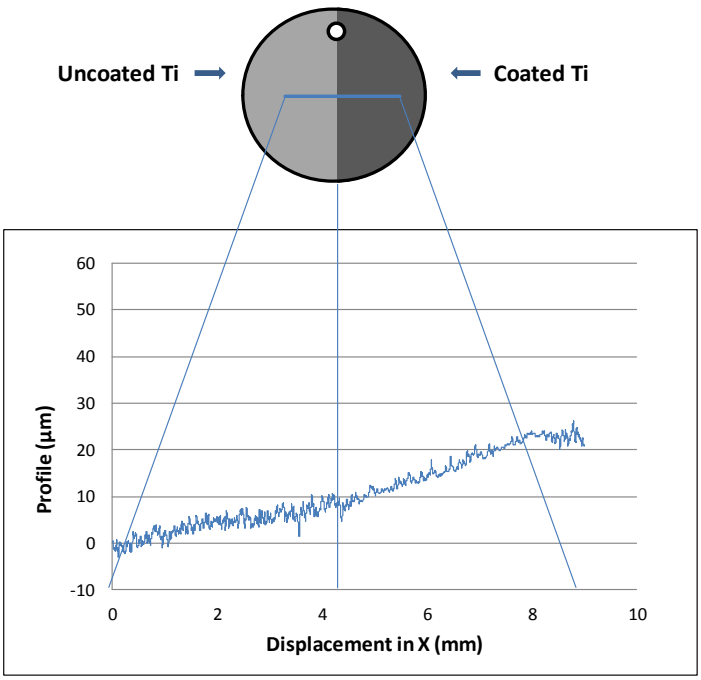

Figure 7.1. Schematic representation of samples' preparation and measurement conditions.

Three profile measurements were performed in each disc and triplicates per formulation. The equipment used for the study was a Dektak 6 (Veeco Instruments

Inc.). Roughness average (R_a) was calculated using the software of the equipment and, from these values, the change in titanium's macrotopography was calculated.

7.2.3. Biological evaluation with bovine fibroblasts (BF)

A preliminary study with bovine skin fibroblasts (BF) was performed to test the adhesion ability and proliferation rate of the 7M:3T and 7M:3T-2.0% sol-gel coatings compared to titanium discs with the surface treatment previously described. The aim was both to confirm the viability of developed materials and study the effect of roughness for cell adhesion.

Furthermore, it is well established that a stable soft tissue attachment is crucial for the long-term implant success rate. Fibroblast cell culture is a suitable choice to model soft tissue conditions based on *in vivo* studies, where it has been observed that proliferating fibroblast has a close relation to the materials ability to adhere to this tissue[6].

a) Adhesion and proliferation test by Alamar Blue

The Alamar Blue assay is designed to quantitatively measure the proliferation of different types of cells. This reagent incorporates a fluorometric/colorimetric growth indicator based on detection of metabolic activity of seeded cells, what allows a choice of detection method. Specifically, the system incorporates an oxidation-reduction (REDOX) indicator that both fluoresces and changes colour in response to chemical reduction of growth medium resulting from cell growth. As cells being tested grow, innate metabolic activity results in a chemical reduction of Alamar Blue reagent. It is a resazurin salt (7-Hydroxy-3H-phenoxazin-3-one 10-oxide) which, due to mitochondrial activity, is reduced to resorufin. Reduction related to growth causes the REDOX indicator to change from oxidized form (non-fluorescent, blue) to reduced form (fluorescent, red).

To perform this study BF cells, at a density of 20,000 cells/well, were cultured on 7M:3T and 7M:3T-2.0% coatings and titanium discs as control and incubated at 37° and 5% CO_2 for 1, 5, 7 and 14 days of culture in 0.50 mL of growth medium DMEM (Dulbecco's Modified Eagle Medium, Gibco, Invitrogen) containing 10% (v/v) fetal bovine serum (FBS). After these different periods of time, discs were moved to a new 48 well plate to avoid the interferences related to cell attached to the bottom of the well and not on the discs, before starting with the Alamar Blue

protocol. Then, 200 µL of 10% (v/v) Alamar Blue reagent (Invitrogen) was added to each well and samples were incubated (37° and 5% CO_2) for 2 h in dark. Afterwards, 100 µL from each well were put in a 96 well plate (each coating and control were tested in triplicate) and fluorescence was monitored using a TECAN fluorometer at 560 nm excitation wavelength and 590 nm emission wavelength.

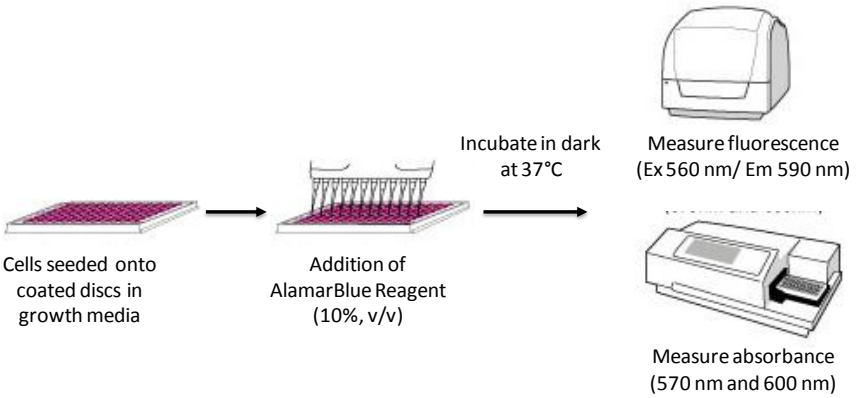

Figure 7.2. Schematic representation of AlamarBlue assay procedure.

Results were plot as O.D. measure for each material, which is directly proportional to viable cell number, and also the proliferation rate as the O.D. at different time points with respect to the O.D. at the first day (adhesion):

$$Proliferation\ rate: \frac{O.D.sample}{O.D.adhesion}\ x\ 100 \qquad \text{(Eq 7.1.)}$$

7.2.4. Biological evaluation with osteoblastic cell line MC3T3-E1

For this part of the study, MC3T3-E1 mouse calvarial pre-osteoblastic cells were chosen since they have been previously used by Ren *et al.*[7] to test the *in vitro* behaviour of sol-gel hybrid coatings and by Kim *et al.*[5] in order to investigate whether Si stimulates osteoblast activity and mineralized nodule formation. The performed studies were the study of the viability, proliferation and differentiation.

a) Citotoxicity assay (MTS)

The aim of this study is to determine the toxicity of developed materials. The quantification of cell viability by MTS (3-(4,5-dimethylthiazol-2-yl)-5-(3-

carboxymethoxyphenyl)-2-(4-sulfophenyl)-2H-tetrazolium) is a colorimetric method which quantifies the metabolic cell activity. Due to the mitochondrial activity, MTS is reduced in cells, in the presence of phenazine ethanosulfate (PES), to formazan. This product is soluble in culture media and presents a dark blue colour.

There are two different ways to perform this test, by measuring the direct citotoxicity on the biomaterial (cells are spread on it) or indirectly, measuring the citotoxicity of the extract of the material (adding the extract of the material to cells spread on the cell culture dish). In this case, the indirect extract citotoxicity quantitative determination was chosen, following the ISO 10993-5 for biomedical devices and using CellTiter 96® Aqueous One Solution Cell Proliferation Assay kit (Promega). As positive control (tested material which provides a reproducible cytotoxic response) latex was used. As negative control material (material that does not provide cytotoxic response) cells spread on polystyrene well without extract was used.

Latex (positive control) and 0.5 g of each sample (materials under study and titanium discs) were incubated in a volume of 1 mL of DMEM for 24 h at 37° and 5% CO_2 humidified atmosphere.

MC3T3 cells were seeded in a P24 multiwell plate at a cell density of 18,400 cells/cm^2 for 24 h in DMEM supplemented with 10% (v/v) of fetal bovine serum (FBS, ThermoFisherScientific) and 1% (v/v) of penicillin/streptomycin (P/S, Lonza). After the indicated time, the medium was removed and previously obtained extracts were added. After 24 h of incubation, the liquid was removed, adding MTS and DMEM in proportion 1:5 and incubating them at 37° and 5% CO_2 in dark for 3 h. Finally, the absorbance was held in a Victor^{TM}X3 multilabel plate reader at a 490 wavelength.

The formazan quantity registered by the absorbance reading is directly proportional to viable cell number. The way to calculate the viability of each material is using next equation.

$$Cell\ Viability\ (\%) = \frac{O.D.sample}{O.D.control} \times 100 \qquad \text{(Eq 7.2.)}$$

Where *O.D. sample* is the average value for the optical density measured at 490 nm for cells seeded with samples' extracts and *O.D. control* is the average

optical density value for the negative control. The lower the obtained viability value, the higher the cytotoxic behaviour of the material. If viability is reduced more than a 30% in comparison with the negative control, it is concluded that studied material has a cytotoxic effect.

b) Proliferation assay (Alamar Blue)

The protocol to determine the proliferation of MC3T3 cells by Alamar Blue was similar to the one described before for BF cells. In this case MC3T3 cells (35,000 cells/well) were incubated at 37° and 5% CO_2 on developed materials and titanium discs as control using 1 mL of growth medium DMEM, for 1, 3, 7 and 14 days of culture. Then, discs were moved to a new 24 well plate and 1 mL of 10% (v/v) Alamar Blue reagent (Invitrogen) was added to each well. Samples were incubated (37° and 5% CO_2) for 12 h in dark. Afterwards, 200 µL from each well were put in a 96 well plate (made in triplicates per sample) and absorbance was monitored at 570 nm and 600 nm using a Victor^{TM}X3 multilabel plate reader.

Results were plot as O.D. measured for each material over time, which is directly proportional to viable cell number.

c) Differentiation (Alkaline Phosphatase quantification, ALP)

Alkaline phosphatase (ALP) enzyme is usually found anchored to the extracellular surface of the cell membrane and its activity is an early marker of the osteoblastic differentiation and plays an important role in the mineralization process of the extracellular matrix. This enzyme catalyzes the hydrolysis of phosphate esters (organic phosphorous) and produces an organic radical and inorganic phosphate. The release of the inorganic form of phosphorous is involved in bone hydroxyapatite formation.

MC3T3 cells were seeded on developed materials at a density of 35,000 cells/well with 1 mL of DMEM medium (supplemented with 10% FBS and 1% P/S) and were incubated (37°C and 5% CO_2) for 24 h. Afterwards, the osteogenic differentiation was induced adding to the culture media 1% ascorbic acid (Sigma-Aldrich) and 0.21% β-glycerol phosphate (Fluka). When culture periods of 7 and 14 days were finished, the ALP activity was quantify.

This protocol is based on the measurement of p-nitrofenilphosphate (pNPP) substrate's conversion into p-nitrofenol (PNP) as consequence a of the ALP activity. Firstly 100 µL of cold lysis buffer (0.2% triton X-100, 10 mM Tris HCl ($C_4H_{11}NO_3$*ClH) pH 7.2) was added to each sample keeping the plate in ice for 7 min and then, sonicating it for 2 min. Afterwards, it was centrifuged at 13,000 rpm at 4 °C for 7 min to precipitate the cellular residues. 50 µL of pNPP (Sigma-Aldrich) solution at 1 mg/mL in assay buffer was added to supernatants and it was incubated for 2 h (37°C and 5% CO_2) in dark. Once this time was passed, the reaction was stopped by adding 50 µL of NaOH 1M. Finally, samples were transferred to a 96 well plate and absorbance was monitored at 405 nm using a Victor^{TM}X3 multilabel plate reader. Results were normalized using a standard curve.

ALP value is given relative to the total protein amount quantified by using the bicinchoninic acid (BCA) protein assay (kit O-42).

$$Diferentiation = \frac{ALP\ activity}{Total\ protein} = \frac{mM\ PNP/h}{\mu g\ BCA} \qquad \text{(Eq 7.3.)}$$

7.2.5. Biological evaluation with human Mesenchymal Stem Cells (hMSC)

For the final step of the *in vitro* evaluation hMSC cells were selected. They are pluripotent cells that can be differentiated into different cell lineages as for example adipocytes, chondrocytes and osteoblasts. The main goal of this study was to test the ability of these cells to differentiate to the osteoblastic lineage seeded on developed coatings and compare this behaviour to uncoated titanium.

a) Adhesion and proliferation by DNA quantification

Firstly, the ability of hMSC to adhere to different substrates and its proliferation after 1, 7 and 14 days of culture (37° and 5% CO_2) was tested. To perform this study, a commercial kit, Quant-iT Picogreen® dsDNA reagent and kit (Invitrogen) was used, were this reagent is an ultrasensitive fluorescent nucleic acid stain for quantitating double-stranded DNA (dsDNA) in solution.

hMSC cells were spread at a density of 10,000 cell/well in 0.50 mL of MEM (Minimum Essential Media, GIBCO, Invitrogen) supplemented with 10% (v/v) FBS and gentamicin (50 mg/ml, Gibco, Life Technologies) to a total concentration of 25

μg/mL. After desired periods of time, total DNA quantification for each sample was studied.

Discs were moved to a new 48 well plate to avoid interferences of cells not attached to the samples and they were cleaned with DPBS. Then cells were lysed adding 200 μL of 1X Lysis buffer (Cell Signaling Technology) and incubating them at room temperature on orbital shaker for 30 min. Afterwards, lysate was transferred to 1.5 mL centrifuge tubes and they were centrifuged at 10K rpm for 3 min to remove the insoluble material. 10 μL of lysate from each sample were placed into three individual wells of a 96 well plate and they were diluted by adding TE buffer (1:10) to reduce the concentration of Triton X100 and 100 μL of PicoGreen reagent (dilution 1:200 in TE buffer) were added to each well. They were incubated in dark for 5 min and fluorescence was read at 480 nm excitation and 520 nm emission using a Tecan fluorometer. Results were compared with a standard curve and proliferation results were expressed as total DNA μg.

b) Gene expression quantification by quantitative polymerase chain reaction (qPCR)

In order to test the ability of developed siloxane-gelatin coatings to promote hMSC's differentiation into osteoblasts, different genes' expression of the osteoblastic lineage were studied. This study is of great relevance since it will give quantitative information about in which state of the differentiation process are cells seeded on different materials and comparing them to titanium control. Moreover, this study was performed in two different ways, in the first one cells were spread in an inductive media (MEM doped with osteogenic differentiation induction cues) whereas in the alternative way, cells were spread in regular growth media without any external stimulation, so in this case the ability of material to induce by themselves the osteogenic differentiation will be tested as well as the effect of released Si.

To study the differentiation ability of cells placed on hybrid coatings, quantitative RT-PCR test was chosen. This method is based on the determination and quantification of different genes which correspond to the osteogenic lineage and are presented in the RNA of the cells. In this case four genes were studied. Initially RNA is extracted from cells after lysis, then RNA strand is reverse transcribed (RT) into its DNA complement and finally amplified with the polymerase chain

reaction technique (PCR), for that reason the overall process is called RT-PCR. Quantitative PCR is identical to RT-PCR except that the progress of the reaction is recorded in real time, what is possible due to the use of a fluorescent reporter molecule, SYBR green which is linked to amplified product.

The first studied gene, glyceraldehyde phosphate dehydrogenase (GAPDH), is a gene expressed in every type of cell, so it was used as house-keeping or internal control for each set of conditions. Next gene was RunX2 (runt DNA-binding domain transcription factor), which is a transcription factor associated to the preosteoblastic differentiation stage and its presence indicates the initiation of the differentiation cascade. The third gene was alkaline phosphatase (ALP), an early marker of the osteoblastic differentiation and, finally, bone gamma-carboxyglutamate protein (BGLAP), a gene which encodes osteocalcin (Ocn) protein synthesis. BGLAP or Ocn are produced by osteoblasts, so the presence of these gens is a marker of bone formation process. Figure 7.3 summarizes the osteogenic differentiation process of hMSCs and the different genes expressed in each stage.

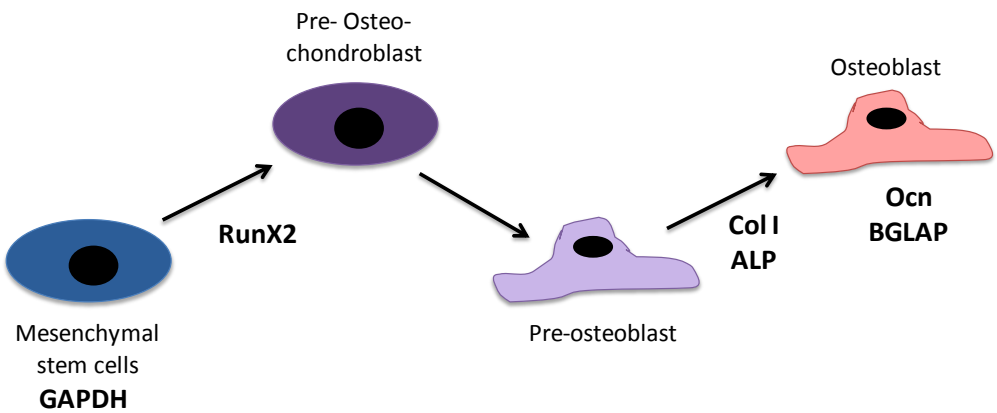

Figure 7.3. Osteogenic pathways in mesenchymal stem cells.

In the same conditions as in the proliferation study, cells were spread onto coated and uncoated discs at a density of 10,000 cells/well in 0.50 mL of α-MEM medium (supplemented with 10% (v/v) FBS and 250 µL of gentamicin) and they were incubated at 37° and 5% CO_2 for 24 h. After this adhesion period, osteogenic differentiation was induced to the half of the samples by adding to the α-MEM medium β-glycerol phosphate, ascorbic acid and dexamethason with a

concentration of 20 mM, 50µg/mL and 100 nM respectively (Sigma-Aldrich). The other half of the samples were kept with regular growth media. Studied time points were 7 and 14 days after induction. For this study the following protocol was performed: (a) mRNA extraction; (2) Spectrophotometric quantification of RNA; (3) Reverse transcription; and (4) Polymerase chain reaction.

At established incubation periods, total cellular RNA was isolated from the hMSC cells seeded on all the different materials and for both culture media conditions. RNA was extracted adding 200 µL of lysis buffer (Promega Total RNA Isolation kit) and purified according to the manufacturer's instructions. Then the total RNA concentration was measured by spectrophotometer (NanoDrop 2000c/2000 UV-Vis) to make sure of the efficient extraction process.

For each sample, 30 µL (in triplicate) of the purified total RNA were reverse transcribed to complementary DNA (cDNA). In the first step 10 µL of 4x primer mix were added to RNA, which was obtained by mixing Random Decamer solution (Ambion) with nuclease free water (RNase-free, molecular grade ddH_2O), 1:4, and samples were placed in Biometra T-Gradient Thermocycler heating them to 70 °C for 1 min and after cooling to 16 °C. Then, they were removed and 30 µL of 2.3x master reverse transcriptase master mix (9.8 µL of RNase-free water, 14 µL of 5x MMLV-RT buffer, 3.5 µL of 10 mM dNTP mix, 0.7 µL of RNasin Plus RNase Inhibitor and 2 µL of 2000u/µL MMLV-RT, all of them purchased from Promega) were added to each reaction tube and they were returned to thermocycler where they were subjected to different steps (16 °C for 5 min, 37 °C for 15 min, 42 °C for 15 min, 45 °C for 15 min, 92 °C for 2 min and finally hold at 4 °C). When thermocycler reached the second hold, tubes were removed and 10 µL of 8x RNase cocktail, previously prepared by mixing 9.8 µL RNase-free water and 0.2 µL of RNase-It ribonuclease cocktail (Stratagene), were added to each sample. Tubes were taken again to the thermocycler to proceed with the last step of the transcription (37 °C for 30 min and hold at 4 °C).

In the last step of PCR, the cDNA amplification and quantification was carried out using the SYBR Green detection method. This requires a double-stranded DNA dye in the PCR reaction which binds to a newly synthesized double-stranded DNA and gives fluorescence (Quantitec SYBR Green kit, QIAGEN). For that, firstly 1:10 dilutions of above obtained cDNA with nuclease-free water and 5 µL of each one

were pipetted into wells of a 384 well qPCR plate. After preparing a 1x Master Mix for each gene (3 µL nuclease-free water, 2 µL gene specific primer (QIAGEN) and 10 µL 2x SYBR Green Mater Mix (Roche)), 15 µL were added to each well and the plate was loaded in a SPECTRAmax Gemini II Fluorescecce plate reader to cDNA detection and quantification by fluorescence. Plate was run under following conditions:

1. Pre-incubation: 1 cycle, no analysis mode
2. 95 °C for 5 min, 4.4 °C/s ramp
3. Amplification: 45 cycles, quantification mode
4. 95 °C for 10 s, 4.4 °C/s ramp
5. 60 °C for 10 s, 2.2 °C/s ramp
6. 72 °C for 10 s, 4.4 °C/s ramp
7. Melting curve: 1 cycle, melting curve mode
8. 95 °C for 5 s, 4.4 °C/s ramp
9. 65 °C for 1 min, 2.2 °C/s ramp
10. 97 °C, continuous acquisition for 10 s, 0.11 °C/s ramp
11. Cooling: 1 cycle, no analysis mode
12. 40 °C for 30 s, 2.2 °C/s ramp

The obtained counts for each gene were normalized to GAPDH gene and to the value of titanium control in growth media.

7.2.6. Morphological Analysis

After different culture periods in the conditions described above, cell morphology and confluence was analyzed by scanning electron microscopy (SEM).

Cells were fixed in 4 % paraformaldehyde phosphate buffer solution (PFA, pH 7.4) overnight at room temperature. Then, they were cleaned twice with DPBS and dehydrated stepwise in a series of water and ethanol solutions (50 %, 65 %, 75 % and 85%) for 15 min each and finally placed in 100 % ethanol keeping them overnight at 4 °C.

For SEM examination, samples were critical point dried (CPD 020), sputter-coated with gold/palladium (SCD 004, 30 milliAmps for 120 s) and imaged by SEM (Amray 1830I, acceleration voltage of 20kV). From each sample images at 100X, 250X, 500X and 1000X were recorded.

7.3. Results and discussion

After preparing coated titanium discs as explained before, their surface topography and biological behaviour was tested by different methods.

7.3.1. Surface topography

From perfilometry study, profiles shown in Figure 7.4 were obtained, where values on the left of the arrow correspond to uncoated titanium, and the topography values on the right to the coated one. All the developed hybrid types were not analyzed due to the small differences among the different gelatin amounts in previous roughness studies. The materials under study were 7M:3T, 7M:3T-0.9%, 35M:35G:30T and 35M:35G:30T-0.9%, in order to test the differences between both types of siloxane matrixes and also the effect on topography due to the incorporation of gelatin.

A slope can be appreciated, which diverts from the baseline of the disc. This is due to the non flat nature of discs as consequence of the machining process. However this diversion was corrected by the software of the equipment to obtain the roughness value.

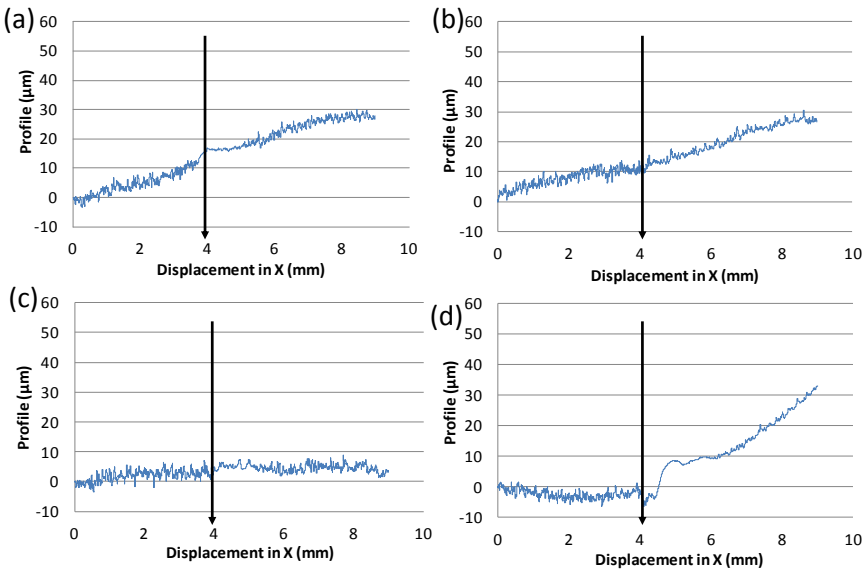

Figure 7.4. Coatings' surface profiles for : (a) 7M:3T, (b) 7M:3T-0.9%, (c) 35M:35G:30T and (d) 35M:35G:30T-0.9%.

In next table (Table 7.1) the obtained values from the perfilometry profile analysis are summarized, where a roughness decrease is obtained in all cases due to the presence of the coating on titanium disc.

Table 7.1. Roughness percentage variation between uncoated titanium disc and the siloxane coating, measured by perfilometry.

	Roughness variation between titanium disc and coating (%)
7M:3T	-16 ± 10
7M:3T-0.9%	-32 ± 7
35M:35G:30T	-11 ± 8
35M:35G:30T-0.9%	-49 ± 6

The greatest effect on disc topography was observed when gelatin was added, even more in the case of the ternary system where almost a 50% of the initial topography was hidden. When comparing the two types of siloxane matrixes, 7M:3T and 35M:35G:30T, there cannot be found significant differences due to the big statistical deviation of the mean values of roughness decrease, which can be attributed to the heterogeneous topography of the substrate. Nevertheless, if we compare 7M:3T-0.9% (-32%) and 35M:35G:30T-0.9% (-49%), it can be found a higher decrease of the initial roughness with the incorporation of GPTMS precursor into coating's formulation.

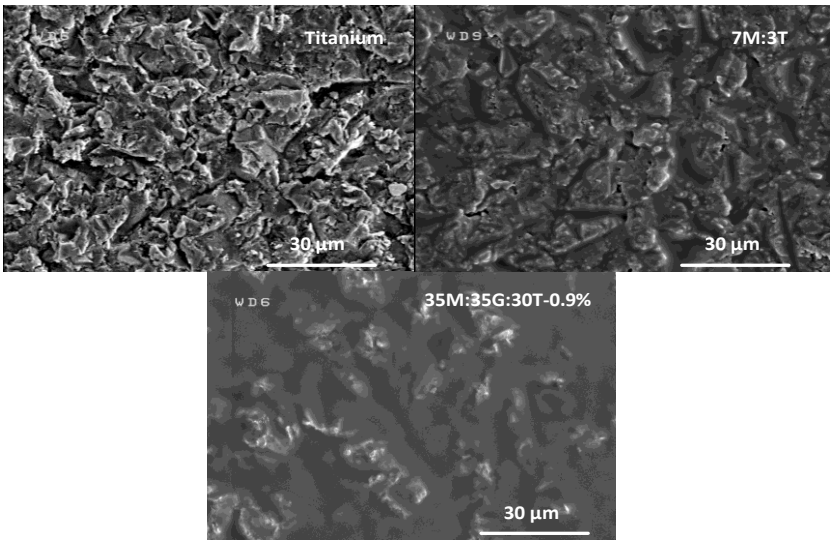

Figure 7.5. SEM images of disc surfaces: titanium, 7M:3T and 35M:35G:30T-0.9.

SEM images above are shown as example of the changes produced on rough titanium surface as consequence of the different sol-gel coatings. Next will be studied the answer of cells to these different topographies.

7.3.2. Adhesion and proliferation of BF cells

In order to perform a preliminary study to test the adhesion of cells to some of the developed coatings in comparison to uncoated titanium (used as control), BF were seeded on 7M:3T, 7M:3T-2.0% and titanium discs. After 24 h of incubation Alamar Blue assay was done and the obtained optical density values with respect to titanium (%) are plotted in Figure 7.6.

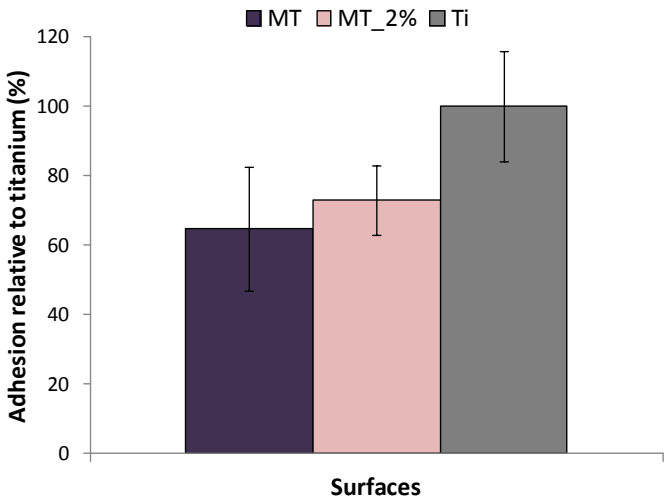

Figure 7. 6. BF adhesion after 24 h of incubation on 7M:3T, 7M:3T-2.0% and titanium (values presented as cell adhesion on each coating relative to titanium's adhesion).

This assay showed higher cellular adhesion for titanium compared to sol-gel coatings. This fact can be attributed to the decrease on discs roughness once they are coated, as it has been shown in the section above. The effect of biomaterials' roughness promoting cell adhesion has been previously reported by other authors[8, 9].

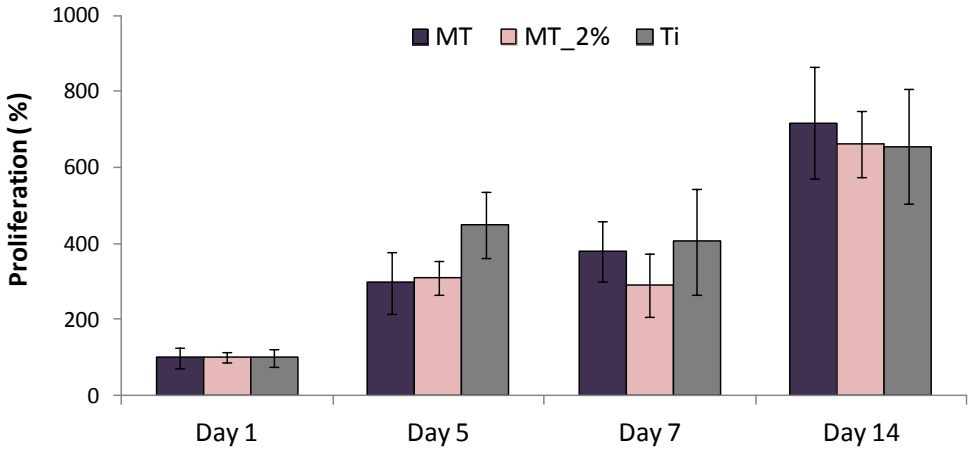

Figure 7.7. BF proliferation on 7M:3T, 7M:3T-2.0% and titanium after 1, 5, 7 and 14 days of culture (values relative to adhesion value).

However, in spite of the initial lower number of cells attached to the coated surfaces, we considered of greater importance the ability of attached cells to growth and proliferate healthily on developed materials over culture time. For this, it was studied the proliferation rate for 1, 5, 7 and 14 days after spreading cells, and values are presented relative to the adhesion on each material. The obtained results, presented in Figure 7.7, showed how the presence of coating did not interfere in cells' proliferation speed and after 14 days of culture, the cell number has increased in 800% compared to the first day of adhesion. Owing to these results, the influence of coatings decreasing the initial adhesion is clear, but they do not present any negative effect on proliferation rate, showing a similar behaviour to titanium. Linez-Bataillon *et al.*[10] studied Ti-alloys with variable surface roughness revealing, on the one hand, that roughened surfaces exhibited better early MC3T3-E1 cell attachment, and, on the other hand, an increase of cell growth on smoother surfaces. Same behaviour was obtained by Nishimoto *et al.*[9] in a similar study performed with osteoblast-like MG-63 cells.

Finally, in Figure 7.8, the morphology of cells adhered to different substrates was studied by SEM.

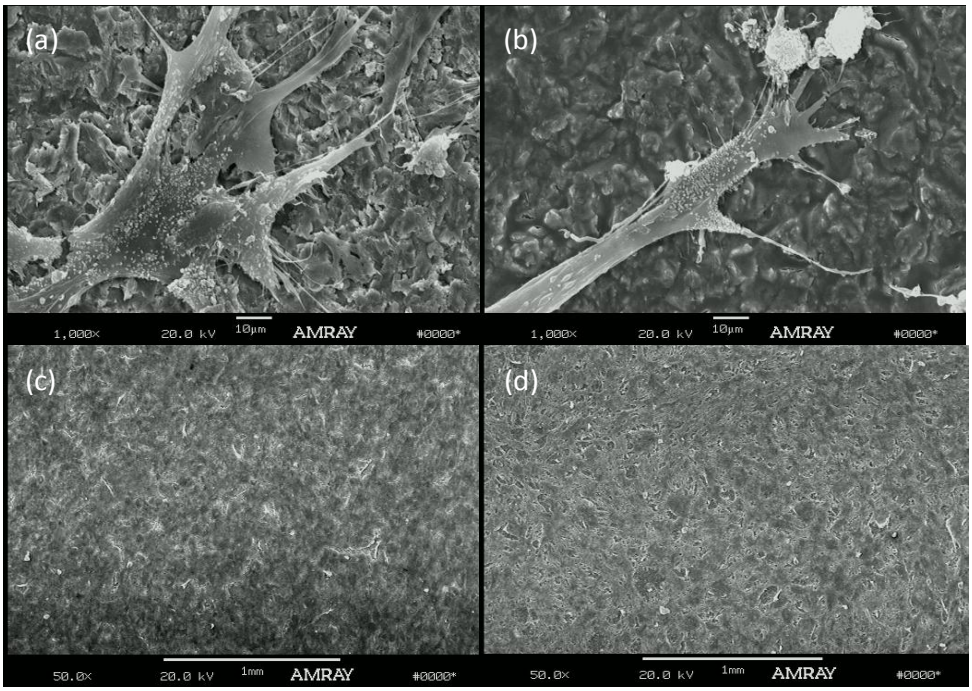

Figure 7.8. SEM images of BF adhered to (a) titanium control and (b) 7M:3T after 24 h of incubation and proliferation on (c) titanium and (d) 7M:3T after 14 days of culture.

It can be appreciated how for the case of titanium after 24 h of adhesion (Figure 7.8.a) the morphology of BF cells' cytoskeleton has a high stellate shape, what allows more anchor points to the substrate. For 7M:3T (Figure .7.b), a less extended structure was obtained; even so, enough cell filopodia were bound to the surface. After 14 days of culture, a continuous cell layer was formed in both materials, proving that despite fewer cells were adhered at the first day on the sol-gel coating, they were able to grow and proliferate in same way as they do in titanium.

7.3.3. Cytotoxicity, proliferation and differentiation of MC3T3-E1

With the aim of evaluating the possible toxic effect of developed coatings on these preosteoblastic cells, cell viability was quantified, by extract, with respect to the negative control (Thermanox®) after 24 h of incubation. In Figure 7.9 are shown the results measured as optical density with the MTS assay.

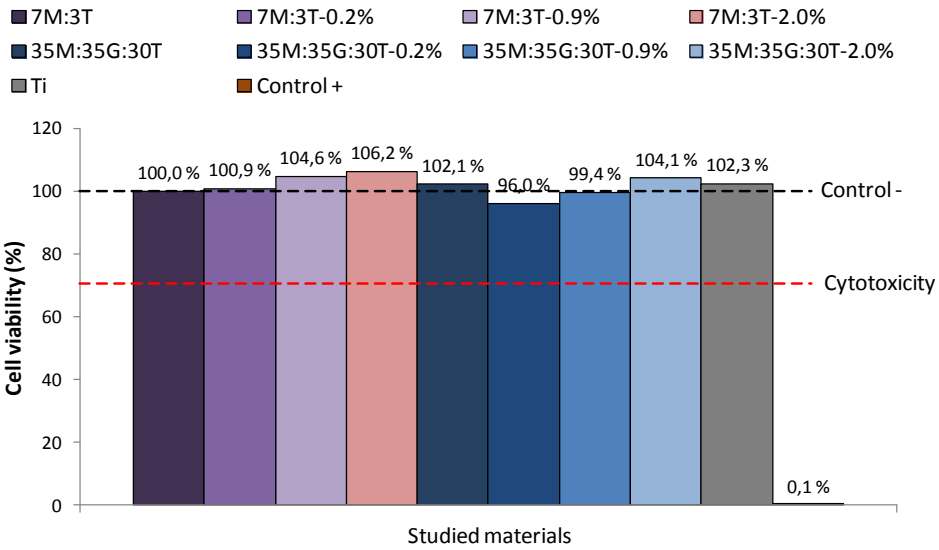

Figure 7.9. Cell viability for all the materials under study expressed as percentage with respect to Control – (Thermanox®).

No one of the developed materials presented a cytotoxic behaviour, since all of them induced cell viability higher than a 70% as compared to Control – (requirement established by ISO 10993-5). After testing this property, next step was to study the ability of MC3T-E1 to adhere and proliferate on siloxane-gelatin coatings.

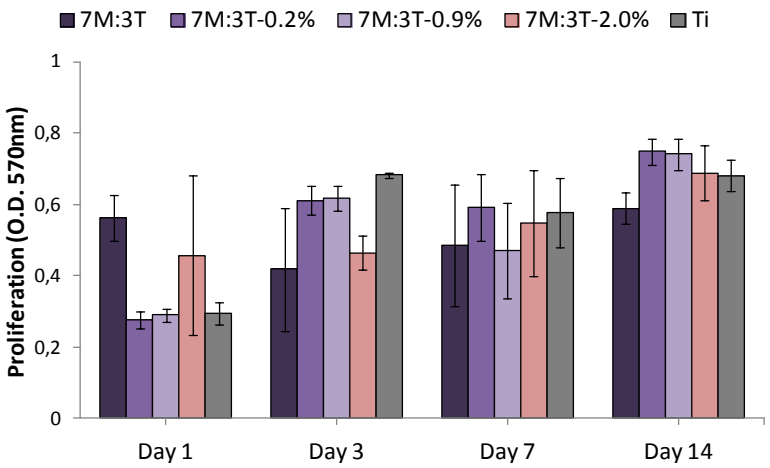

Figure 7.10. MC3T3-E1 proliferation on 7M:3T-Gelatin coatings and titanium after 1, 3, 7 and 14 days of culture.

Figure 7.10 collects the optical density values measured over time for cells cultured on 7M:3T-Gelatin coatings compare to titanium control and determined by Alamar Blue assay. Results show how after 24 h of incubation more cells were adhered to 7M:3T and 7M:3T-2.0% coatings compare to other materials. However, after 3 days of culture time, their increase was slowed down, obtaining a higher proliferation for 7M:3T-0.2%, 7M:3T-0.9% and titanium control. At the final point of this experiment, 14 days, these three materials duplicated their initial optical density value proving cell ability to proliferate on them. Despite that, all the materials reached similar values.

Same study was performed for 35M:35G:30T-Gelatin series comparing their ability to promote cell adhesion and proliferation to titanium. Results are plotted in Figure 7.11.

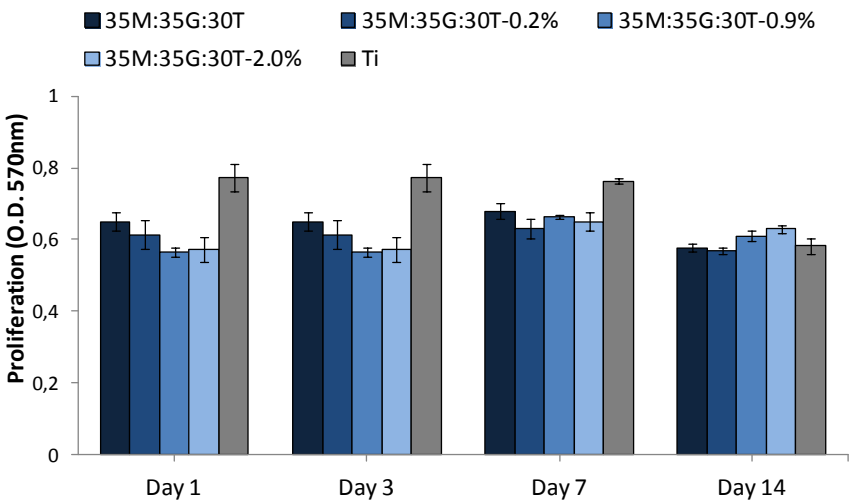

Figure 7.11. MC3T3-E1 proliferation on 35M:35G:30T-Gelatin coatings and titanium after 1, 3, 7 and 14 days of culture.

In this case, the higher adhesion values after 24 h of incubation were for titanium control, behaviour that may be attributed to disc's roughness. When comparing the optical density measurements for the different studied periods of time, it cannot be appreciated an evolution over time, all the materials kept almost the same values over time. Nevertheless, since titanium's biocompatibility is widely

accepted and after 14 days of culture, coatings presented similar behaviour to titanium, these results were considered as acceptable for next steps of this study.

All of this aside, it needs to be taken into account that the main aim of the present work is to promote the regeneration ability to ensure a proper osseointegration, what is related to the ability of a biomaterial to promote and earlier osteogenic differentiation. Therefore, the study of differentiation of cells cultured on different surfaces will give more information about this phenomenon than the previous proliferation test.

The ability of coatings to promote the osteogenic differentiation was determined by the quantification of the ALP activity, a marker of the osteoblastic differentiation and which's activity is essential for the extracellular matrix mineralization. In Figure 7.12, obtained differentiation values for 7M:3T-Gelatin coatings and titanium control are presented, expressed as mM PNP/(µg BCA*h).

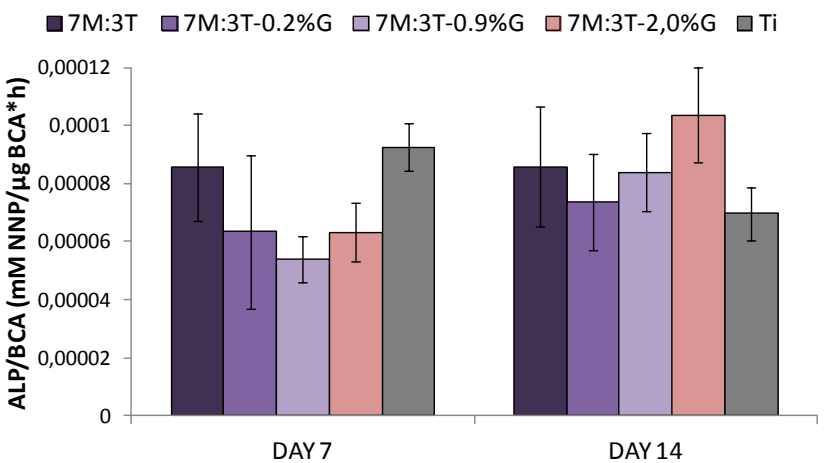

Figure 7.12. Differentiation assay of MC3T3-E1 cells cultured in osteogenic inductive media for 7 and 14 days, by ALP activity quantification for 7M:3T-Gelatin coatings and titanium (relative to total protein value, BCA).

For the first studied period, 7 days, only 7M:3T coating gave similar values of differentiation compared to titanium. However, after 14 days of induction, all the coatings promote more the osteogenic differentiation than titanium, according to the higher ALP enzyme activity. As was seen in chapter 4, Si release increased over time, what could explain that at first period, where Si levels are low, differentiation

was not enough promoted, but after two weeks more Si is on the media increasing the ALP activity. Shirosaki *et al.*[11] studied the effect of Si released from different GPTMS-Chitosan-TEOS scaffolds on MG63 cells' differentiation, where they obtained that an increase of ALP activity was directly related to an increase in Si content. Therefore, the release of Si might directly affect cell differentiation, and one of the ways can be through the mechanism explained in the first chapter of this work where Si interacts with propyl hydroxylase enzyme which catalyzes collagen formation[12].

ALP activity in the presence of an osteogenic inductive media was also evaluated and quantified for MC3T3-E1 cells cultured on 35M:35G:30T-Gelatin coatings. Results are also expressed as mM PNP/(µg BCA*h) and they are plotted in Figure 7.13.

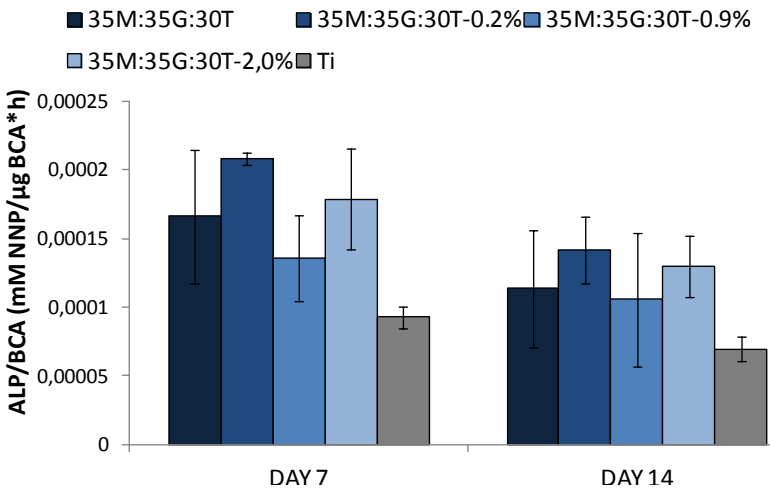

Figure 7.13. Differentiation assay of MC3T3-E1 cells cultured in osteogenic inductive media for 7 and 14 days, by ALP activity quantification for 35M:35G:30T-Gelatin coatings and titanium (relative to total protein value, BCA).

35M:35G:30T-Gelatin hybrids gave higher values than titanium control for the ALP activity at the first period of 7 days, reaching in some cases the double of it. This suggests that the ternary system promotes a faster osteoblastic differentiation in comparison with the hybrid type studied before, 7M:3T-Gelatin, and what is more important in comparison with the control. A decrease of this enzyme's activity was observed after 14 days of culture for all the coatings. Even so, they were still higher

that the ones for titanium. Tsuru *et al.*[13] obtained a similar behaviour when they synthesised gelatin-GPTMS-TEOS scaffolds and examined their ability to induce differentiation using MG63 osteoblast-like cells. They observed how ALP activity reached a maximum at days 4-7 of culture followed by a gradual lowering of the values. This decrease was consistent with a complementary study of osteocalcin protein quantification where a peak occurred at 13 days for all samples. In this way, the decrease of ALP activity might indicate an evolution of cells to next steps of the osteogenic differentiation pathway (Figure 7.3).

Finally, comparing the results obtained for both type of hybrids, higher differentiation ability was observed in the ternary system compared to 7M:3T-Gelatin coatings. After 7 days of induction, in the case of 35M:35G:30T-Gelatin hybrids, unlike 7M:3T-Gelatin coatings, higher ALP activity values were obtained compared to titanium. This results are supported by cumulative Si quantification study, where more Si was released in these type of materials.

7.3.4. Osteogenic differentiation of hMSC quantified by qPCR

Before studying hMSCs' differentiation, their adhesion and proliferation was tested by total DNA quantification. Obtained values are plotted in Figure 7.14 and presented as total DNA concentration per disc (sample).

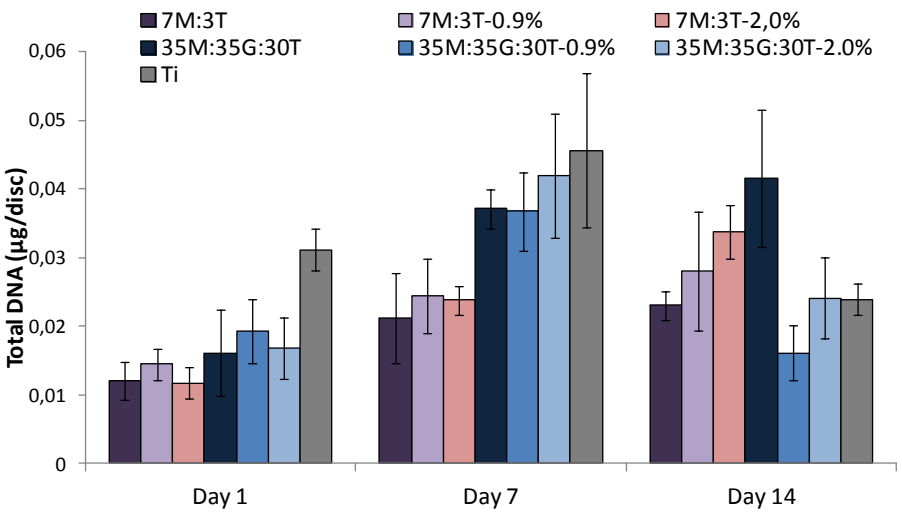

Figure 7.14. hMSC's total DNA quantification on siloxane-gelatin coatings compared to titanium after 1, 7 and 14 days cultured in growth media.

At first day of assay, 24 h of adhesion, DNA quantification showed a higher number of cells adhered to titanium substrate compared to developed coatings. However, protein adsorption study showed a higher amount of adhesive proteins adsorbed onto coatings' surface and also a more bioactive conformation. The reason to do not find a direct correlation between both assays can be explained by the fact that significantly smooth surfaces have to be tested when using real time protein adsorption technique, QCMDQ, what is a known limitation of this technique and does not allow to reproduce the real roughness of surfaces under study. So just focussing on the chemistry of materials' surfaces, where all the substrates present a similar topography, coatings seemed to promote the adsorption of serum proteins, but when roughness is a variable, cells adhered better to titanium due to the effect of coatings decreasing this property as was shown by perfilometry and SEM. Comparing the adhesion among different coatings, in the case of hybrids with GPTMS more DNA was quantified, what is in good agreement with protein study's results, where an improvement of Fn and Col I adsorption was found due to the functionalization by the epoxy group.

After 7 days of incubation, a noticeable increase was observed in all the materials as prove of the proper proliferation of cells. This improvement was considerably higher in the case of ternary hybrids, where values are more than the double compared to the first day. Comparing the behaviour among 7M:3T-Gelatin series, a slight increase of DNA amount can be appreciated when adding gelatin; as well as happened when incorporating a 2% of gelatin to 35M:35G:30T coating. This could be due to the good cell adhesive properties of gelatin[14, 15]. Even so, these small differences are not enough to confirm it.

After 14 days, cells cultured on 7M:3T-Gelatin materials continued growing, moreover for 7M:3T-2% coating which triplicates the initial number. Same tendency was observed for hMSCs on the 35M:35G:30T coating. However, a decrease in the proliferation was obtained for 35M:35G:30T-0.9%, 35M:35G:30T-2.0% and Ti.

Next step, after proving their biocompatibility *in vitro*, was to study cells' ability to differentiate seeded on different materials. As it was explained before, this study was performed in two different conditions of culture media. In the first one, after 24 h of adhesion, osteogenic differentiation was induced by the addition to the media of different induction cues, while in the second way, the study was performed

in the regular growth media without any external factor. So in the last case, the ability of materials by themselves to induce differentiation was tested.

a) mRNA expression of RunX2, ALP and BGLAP with inductive media

In Figure 7.15 the values for RunX2 gene expression are presented (normalized to GAPDH and relative to titanium values).

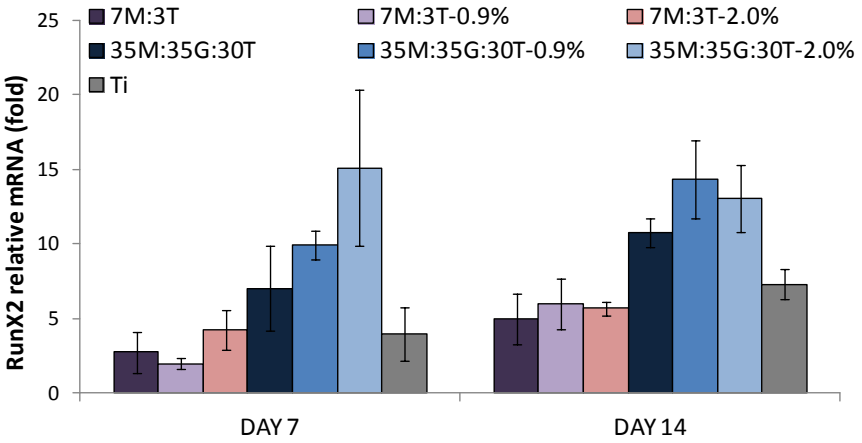

Figure 7.15. Relative mRNA expression for RunX2 gene on hMSC up to 7 and 14 days of culture with inductive medium.

Results show a faster RunX2 gene expression in the case of cells cultured on 35M:35G:30T-Gelatin coatings compared both to 7M:3T-Gelatin series and titanium after 7 days of assay. This early expression indicates that these coatings promote an earlier pre-osteoblastic differentiation. There also can be seen a tendency of increase gene expression at the same time as the gelatin concentration increases in the formulation of the material, what might be due to a beneficial effect of gelatin promoting cell differentiation or to the fact that as was studied in previous chapters, the introduction of gelatin was translated in a higher solubility of the film releasing more Si to the medium. So, as the same time as cumulative Si release increases, RunX2 expression increases as follow: 35M:35G:30T (3.7 ppm Si) < 35M:35G:30T-0.9% (10.3 ppm Si) < 35M:35G:30T-2.0% (21.0 ppm Si). Furthermore, ternary hybrids release more Si than their homologous in 7M:3T materials: 7M:3T (1.8 ppm Si) < 7M:3T-0.9% (7.3 ppm Si) < 7M:3T-2.0% (17.7 ppm Si). However, these differences

might be also related to the surface chemistry of the different materials, not only to the Si release rate.

After 14 days of incubation, there is a slight progress on this gene's expression obtaining again similar values for 7M:3T-Gelatin coating and titanium, and almost a double of them for 35M:35G:30T-Gelatin. The fact of not finding a big difference may indicate that after 14 days cell have moved to different stage of the osteogenic differentiation. To confirm this, expression of ALP gene was quantified (Figure 7.16).

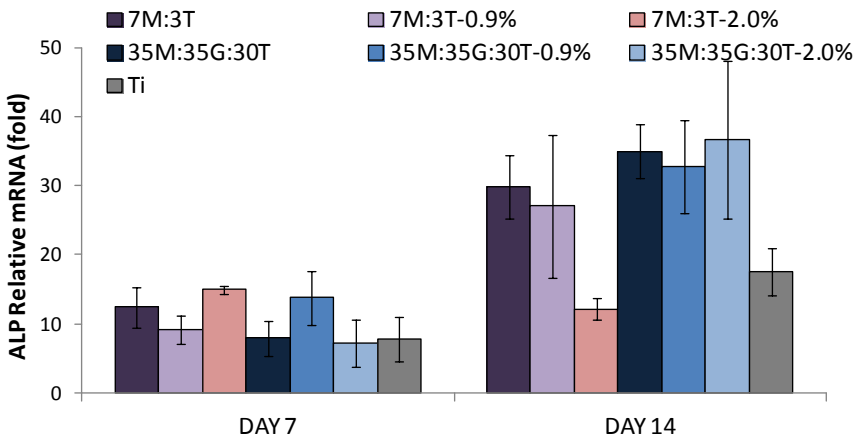

Figure 7.16. Relative mRNA expression for ALP gene on hMSC up to 7 and 14 days of culture with inductive medium.

The increase observed for ALP relative mRNA from day 7 up to 14 days of culture, is indicative of the proper progression on the osteogenic differentiation process. All the developed siloxane-gelatin coatings (in spite of 7M:3T-2.0%) presented higher levels of ALP gene's expression in comparison with the value obtained for titanium control. The earlier expression agrees with the results obtained for MC3T3-E1 cells where higher values of ALP enzyme's activity were obtained in the cases of cells seeded on coatings.

The studied last gene was BGLAP and results are presented in Figure 7.17. Obtained BGLAP expression levels where lower compared to ones obtained for ALP after 14 days of incubation with inductive media, what may indicate that a low number of cells have reached the last stage of the differentiation. Nevertheless,

comparing the relative mRNA values at the end point of this study, cells seeded on the 35M:35G:30T, 35M:35G:30T-0.9% and 35M:35G:30T-2.0% coatings presented higher levels. These were also the first coatings promoting cell differentiation according to their earlier RunX2 gene expression.

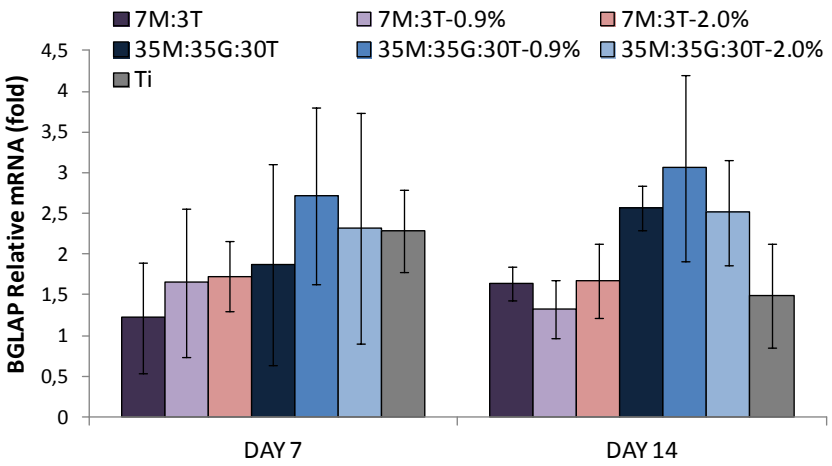

Figure 7.17. Relative mRNA expression for BGLAP gene on hMSC up to 7 and 14 days of culture with inductive medium.

b) mRNA expression of RunX2, ALP and BGLAP in growth media

Finally, same assay was performed on hMSC but this time cultured in regular growth media without any external inductive cue. The aim of this experiment was to test the ability of hMSC to differentiate into the osteogenic lineage seeded on different surfaces by the quantification of the same genes studied in section before as well as the role of released Si to the medium inducing this differentiation.

Figure 7.18 summarizes the relative quantitative amounts obtained for each gene's expression on all the surfaces under study and up to 7 and 14 days of incubation.

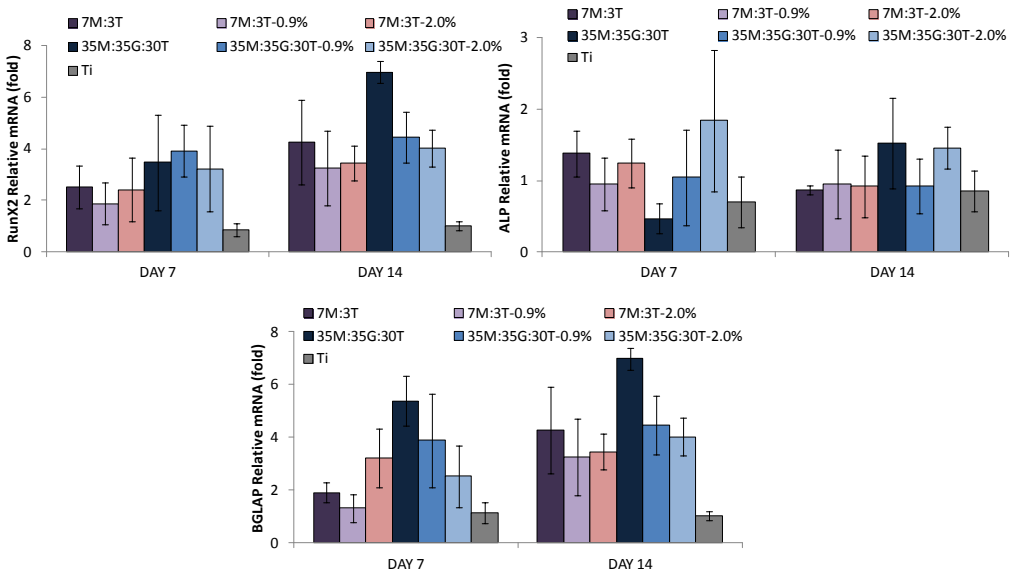

Figure 7.18. Relative mRNA expression of genes related to osteogenic differentiation in hMSC cultured in growth medium up to 7 and 14 days: (a) RunX2, (b) ALP and (c) BGLAP.

Overall, all the materials induce the differentiation of hMSCs compared to titanium control owing to their earlier gene expression. This finding is of great interest, since they suggest that with no external stimulation developed coatings are able to promote the osteogenic differentiation by themselves what also proves that Si effectively enhanced the bone formation.

In spite of lower absolute values are obtained in this assay compared to the one where external inductive cues were used, differences among coatings and titanium are much higher, proving that titanium is a good osteoconductive material where cells are able to attach and spread, but it does not induce the osteogenesis in the absence of external inductive cues, ability that has been confirmed for siloxane-gelatin coatings.

However, the exact role by which Si enhances cells' differentiation is unclear, as well as the specific doses that gives the best results. Many authors have studied the effect of treating cells with different Si concentrations in order to obtain a correlation between the Si amount and the cell response, finding in some cases conflicting literature. On the one hand, Areva *et al.*[6] studied sol-gel TiO_2-SiO_2 coatings testing the effect of increasing SiO_2 on cells performance and they found an

improvement of osteoblasts proliferation with its increase. On the other hand, Gough *et al.*[16] reported that more than 8.2 mM Si released from Bioglass in medium caused cell apoptosis. Shirosaki *et al.*[17] found that Si released from membrane hybrids with TEOS inhibited MG63 cells proliferation due to the high amounts of Si in the environment. However, after studying differentiation by ALP activity they concluded that Si ions might directly affect cell differentiation improving ALP activity[11]. Similar behaviour was obtained by Kim *et al*[5], where at high levels of Si treated medium, 10 mM, MC3T3-E1 cells' viability was decreased, at the same time that Col I gene's expression and bone nodule formation activity was increased. Owing to results obtained for BF, MC3T3-E1 and hMSC proliferation, no one of the developed materials released cytotoxic amounts of Si to the medium, since it was not obtained any estrange behaviour which suggested cell apoptosis.

7.5. Conclusions

Cell adhesion and proliferation assays studied with the three different cell lineages make evident the biocompatible behaviour of these materials. Furthermore, it was found a correlation between the results obtained here and the ones for protein adsorption study where coatings with GPTMS promote both serum protein adsorption (and bioactive conformation) and a better cell response.

At the beginning of these work it was hypothesized the osteoinductive behaviour of these coatings, property that have been proved with the qPCR study where an earlier gene expression was obtained on siloxane-gelatin coatings compared to titanium.

Overall, the biological evaluation of developed sol-gel coatings proves that they are good candidates for orthopaedic applications where stimulation for bone formation is needed. Moreover, this strategy may reduce the need for growth factors, usually added in regenerative approaches, decreasing the associated costs and overcoming stability issues.

7M:3T, 7M:3T-0.9%, 35M:35G:30T and 35M:35G:30T-0.9% coatings were chosen for the final step of this work, where *in vivo* biocompatibility and osseointegration will be tested. Some reasons to select these materials among others were their degradation properties and good behaviour in contact with cells. Hybrids with higher amounts of gelatin were discarded due to their excessively fast

degradation and because protein adsorption and *in vitro* results proved similar response regardless the gelatin content.

References

1. Klokkevold PR, Han TJ. How do smoking, diabetes, and periodontitis affect outcomes of implant treatment? *Int J Oral Maxillofac Implants.* 2007; **22 Suppl:** 173-202.

2. Koldsland OC, Scheie AA, Aass AM. Prevalence of implant loss and the influence of associated factors. *J Periodontol.* 2009; **80:** 1069-75.

3. Reffitt D, Ogston N, Jugdaohsingh R et al. Orthosilicic acid stimulates collagen type 1 synthesis and osteoblastic differentiation in human osteoblast-like cells in vitro. *Bone.* 2003; **32:** 127-35.

4. Zolkov C, Avnir D, Armon R. Tissue-derived cell growth on hybrid sol–gel films. *J.Mater.Chem.* 2004; **14:** 2200-5.

5. Kim E, Bu S, Sung M et al. Effects of silicon on osteoblast activity and bone mineralization of MC3T3-E1 cells. *Biol Trace Elem Res.* 2013; **152:** 105-12.

6. Areva S, Ääritalo V, Tuusa S et al. Sol-gel-derived TiO2–SiO2 implant coatings for direct tissue attachment. part II: Evaluation of cell response. *J Mater Sci Mater Med.* 2007; **18:** 1633-42.

7. Ren L, Tsuru K, Hayakawa S et al. In vitro evaluation of osteoblast response to sol-gel derived gelatin-siloxane hybrids. *J Sol Gel Sci Technol.* 2003; **26:** 1137-40.

8. Marinucci L, Balloni S, Becchetti E et al. Effect of titanium surface roughness on human osteoblast proliferation and gene expression in vitro. *Int J Oral Maxillofac Implants.* 2006; **21:** 719-25.

9. Nishimoto SK, Nishimoto M, Park SW et al. The effect of titanium surface roughening on protein absorption, cell attachment, and cell spreading. *Int J Oral Maxillofac Implants.* 2008; **23:** 675-80.

10. Linez-Bataillon P, Monchau F, Bigerelle M et al. In vitro MC3T3 osteoblast adhesion with respect to surface roughness of Ti6Al4V substrates. *Biomol Eng.* 2002; **19:** 133-41.

11. Shirosaki Y, Tsuru K, Hayakawa S et al. Effects of si (IV) released from chitosan-silicate hybrids on proliferation and differentiation of MG63 osteoblast cells. *Bioceram Dev Appl.* 2011; **1:** 1-4.

12. Qiu Z, Noh I, Zhang S. Silicate-doped hydroxyapatite and its promotive effect on bone mineralization. *Frontiers of Materials Science.* 2013; **7:** 40-50.

13. Tsuru K, Robertson Z, Annaz B et al. Sol-gel synthesis and in vitro cell compatibility analysis of silicate-containing biodegradable hybrid gels. *Key Eng Mat.* 2008; **361:** 447-50.

14. Huang Y, Onyeri S, Siewe M et al. In vitro characterization of chitosan–gelatin scaffolds for tissue engineering. *Biomaterials.* 2005; **26:** 7616-27.

15. Shi C, Yuan W, Khan M et al. Hydrophilic PCU scaffolds prepared by grafting PEGMA and immobilizing gelatin to enhance cell adhesion and proliferation. *Materials Science and Engineering: C.* 2015; **50:** 201-9.

16. Gough JE, Jones JR, Hench LL. Nodule formation and mineralisation of human primary osteoblasts cultured on a porous bioactive glass scaffold. *Biomaterials.* 2004; **25:** 2039-46.

17. Shirosaki Y, Tsuru K, Hayakawa S et al. Physical, chemical and in vitro biological profile of chitosan hybrid membrane as a function of organosiloxane concentration. *Acta Biomaterialia.* 2009; **5:** 346-55.

Chapter 8

In vivo biological evaluation

Chapter 8:

IN VIVO BIOLOGICAL EVALUATION

8.1. Introduction

The last step of this thesis work was the *in vivo* evaluation of developed sol-gel coatings. In spite of *in vitro* biological evaluation gives fundamental information about cell-biomaterial interaction, the *in vivo* study is essential to test the new materials, since they have been designed to be used in humans.

In this way, dental implants were surgically placed in white New Zealand rabbits' tibia, in order to assess the *in vivo* biocompatibility and osseointegration capacity of chosen coatings. The study complied with the ethical and legal working conditions laid in RD 1201/2005 of the Spanish Government Law, of October 10th, about the protection of animals used for experimentation and other scientific purposes. This work was carried out in the Animal Facility at Biomechanics Institute of Valencia.

This study was divided in two parts: biocompatibility evaluation and osseointegration study. Furthermore, before carrying out both studies, an adhesion test was performed to ensure the suitable adhesion strength between coatings and titanium screw.

8.2. Materials and methods

8.2.1. Coatings under study and samples' preparation procedure

As well as for the *in vivo* study described in chapter 3 (for the selection of the appropriate siloxane matrix), implants were provided by Ilerimplant S.L. GMI Frontier internal connection hexagonal implants were used, which are machined in CP grade IV titanium with a 3.75 mm of diameter and a length of 8 mm; the outer surface of the implant has ADS® treatment (Advanced Double-Grip Surface) which combines a white corundum micro-bubble treatment and acid etching.

Owing to their good results in the *in vitro* biological evaluation and the values obtained in the hydrolytic degradation study and silicon release quantification where a more gradual degradation and release kinetic was observed, 7M:3T, 7M:3T-0.9%, 35M:35G:30T and 35M:35G:30T-0.9% were the chosen coatings for this study. Implants were coated with each of the formulations by dip-coating method and they were subjected to the heat treatment. Finally they were sterilized before their use.

8.2.2. Adhesion strength

An *ex vivo* assay was performed to test the screw and unscrew resistance of developed coatings in pig knee bone. By images obtained with the Scanning Electron Microsopy (SEM) and the microanalysis performed with Energy Dispersive X-ray spectroscopy (EDX), the resistance of coatings was analyzed.

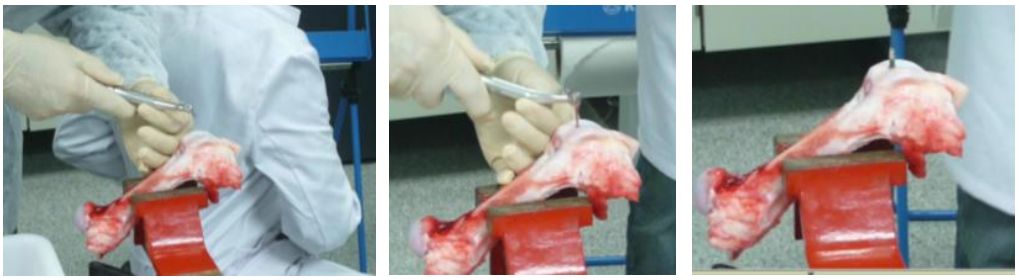

Figure 8.1. Resistance test to the surgically implantation process in pig knee bone.

8.2.3. Animal model and implantation site selection

For this study, dental implants' osseointegration model in rabbit tibia was selected since it has been extensively described in literature[1-4]. Furthermore, it is a low cost animal model with docility and easy provision and maintenance, which serves as an initial approximation, prior to a possible next experimental stage with bigger animals. A total amount of twenty-six adult rabbits with an age of 18 weeks were used. All of them were females with a weight average of 3,000 and 3,500 g.

The chosen site was tibia due to its suitability for the reception of the implant on account of its size, high resistance to infections and accelerated bone metabolism for obtaining differences among samples in short periods of time. The exact site was proximal tibia because in this point both cortical and trabecular bone can be found, what is of great interest in order to have comparable approach to the mandible alveolar bone.

8.2.4. Studied implantation periods and samples' number

Periods of time among 4 and 6 weeks can be found in literature for the complete osseointegration of titanium implants in experimental animals[5]. For that reason the studied periods of time in the first *in vivo* study showed in chapter 3 were

1, 2, 4 and 8 weeks. With this planning we covered all the osseointegration process guaranteeing a complete fixation of the implant at the end of the study.

However, due to the high cost of these type of studies and the previously obtained results, for this second implantation it was decided that the new experimental design will have only two shorter periods of evaluation, 1 and 2 weeks, since the biggest differences among Control and coatings were observed at these periods.

Another difference between both implantations was the number of screws per tibia. As was concluded, in the first *in vivo* evaluation test, there was a lack of primary stability what lead to the formation of a fibrous capsule in all the studied materials in contact with the cortical bone. Such behaviour was attributed to the design of the experiment were two screws were implanted per tibia. In this case only one implant was placed per tibia and a total of 42 screws were used. Table 8.1 summarizes the number of implants used per material and studied period of implantation. The used Control was the uncoated commercial implant. Furthermore, it was tried to place the implant in a way where the end part of the screw relied on the opposite cortical bone to favour the primary stability.

Table 8.1. *In vivo* experimental design.

Weeks	7M:3T	7M:3T-0.9%	35M:35G:30T	35M:35G:30T-0.9%	Control
1	4 implants	4 implants	4 implants	4 implants	4 implants
2	4 implants	4 implants	5 implants	4 implants	5 implants

8.2.5. Surgery and implantation process

After two weeks of quarantine period, operation period began. Firstly, animals were sedated; they were given antibiotic to prevent possible infections and were prepared for the surgery. Once in the operating room, general anaesthesia was administered to all the specimens.

For the surgery, an incision of 20 mm was made in the skin, in the place of the implantation, then the drilling area was exposed and the periosteum was removed. The drilling protocol was followed as described by Ilerimplant S.L. for GMI Frontier prosthesis, as would be done in a common operation procedure in a dental

clinic. For that, a bone defect was made by successive milling (growing diameter drills: 2.8, 3.0 and 3.5 mm) with a low speed micrometer and constant irrigation of the area with physiologic serum, to minimize the damage to surrounding tissues. After placing the implants by press-fit procedure, wound was sutured.

At the first signals of awakening, animals were transferred to their corresponding cages. After surgery, they were monitored every eight hours for the next three days to check the evolution of the hematoma and make sure there was no infection.

At the end of the different studied periods of 1 and 2 weeks, animals were euthanized by intravenous injection. After verifying the absence of vital signs, proximal tibia region was cleaned of soft tissues and a dissection osteotomy was performed, with an oscillating saw, at a 5 mm of distance on both sides of the implant, as shown in Figure 8.2.

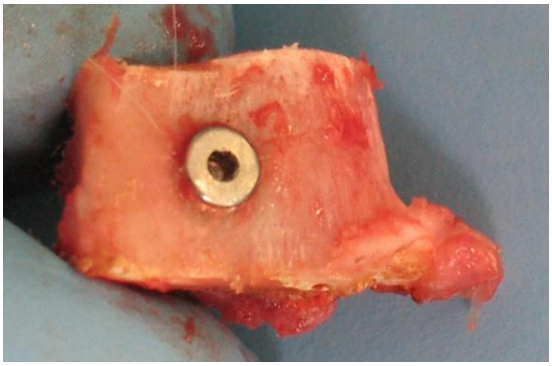

Figure 8.2. Tibial section with the implant, obtained by osteotomy after sacrifice.

8.2.6. Sample processing

To evaluate the biocompatibility and osseointegration of titanium implants, optical microscopy technique was used. For that purpose, sample obtained in the previous step need to be subjected to a special treatment which consists of four steps: fixation, polymethyl methacrylate (PMMA) embedding, cut and samples' dyeing.

Thus, as soon as samples are obtained, they need to be fixed by immersing them in 40% (v/v) ethanol. Afterwards, the histological inclusion processing in

PMMA was performed according to the protocol described by Peris *et al.*[6] in 1993. Obtained PMMA blocks were cut obtaining samples with a thickness of 30 µm. Since we are using titanium implants, they can only be cut by the dual-band cutting system and EXAKT micropolishing. These thin cuts were placed on microscope slides and stained by Gomori trichrome technique. By this method, tissues are stained in different colors; bone takes different color-scheme depending on the maturity and calcification degree: not calcified bone acquires a reddish hue, and as it matures it will take a more bluish hue. Moreover, fibrous tissue turns red.

The histological study of all samples was performed by a vertical Eclipse 80i (Nikon) optical microscope.

8.2.7. *In vivo* biocompatibility evaluation

After examining the samples by microscope, different images were recorded to evaluate the different parameters related to the biocompatibility. Two different studies were performed, in the first one a qualitative analysis of obtained images was done, as was performed in the first implantation described in chapter 3; and in this case, a semi-quantitative evaluation was also designed.

a) Qualitatively evaluated parameters

A material is biocompatible when it is accepted by the organism. In this work the body response towards the implant was qualitatively evaluated as a sign of the biocompatibility of the materials under study.

To assess the tissue response to coated and uncoated implants, different parameters were taken into account: bone marrow state, foreign body reaction giant cells' presence and the fibrous capsule evolution.

b) Semi-quantitative study of the foreign body reaction response

A semi-quantitative method was developed, according to the ISO 10993-6 rule and literature[4, 7], to assess the local effect of the different sol-gel coatings after the implantation. The evaluated parameters were:

1. Bone marrow condition, aplasia.
2. Bone marrow's architecture loss.
3. Bone marrow conditions in areas where there is no contact with the implant.

4. Fat rate.
5. Cortical bone trauma.
6. Trabecular bone trauma.
7. Foreign body reaction giant cells' presence.
8. Fibrous capsule formation in contact with bone marrow.
9. Fibrous capsule formation in contact with cortical bone.
10. Fibrous capsule formation in contact with trabecular bone.
11. Thickness of the fibrous capsule.
12. Neovascularization.

The intensity of studied items was graded as follows: - = no (0); + = not much (1); ++ = moderately frequent (2); +++ = very frequent (3). After obtaining the total score for the 12 items, materials were classified as no irritant (score from 0 to 6), slightly irritant (score from 6 to 18), moderately irritant (score from 18 to 30) and severely irritant (score up to 36).

8.2.8. Osseointegration evaluation

As previously defined, osseointegration is the ability of a material to achieve a direct structural and functional connection between the implant and bone without any intervening tissue layer[8, 9]. In this work a histological evaluation was performed, in which coated and uncoated implants´ osseointegration was qualitatively evaluated in areas in contact with cortical and spongy bone.

For this purpose, all the slides obtained from cutting the different samples were analyzed by optical microscope, paying special attention to the signals indicative of the osseointegration as: bone necrosis, intervening fibrous capsule formation between bone and implant, osteoblastic activity, new bone spicules formation, close contact between bone and implant at the end of the study, etc.

8.2.9. Comparison of 1st ad 2nd implantation (Histomorphometric analysis)

Due to the differences in the implantation model design for both implantations, where in the first one (chapter 3) there was no primary stability and in the last one a new experimental design was develop to overcome this limitation; it was considered of great interest to assess the response of coatings in comparison with titanium in both situations. With this aim, a histomorphometric study was performed obtaining a statistical analysis of achieved osseointegration. Since the

7M:3T coating and titanium Control are the only materials studied in both procedures, their behaviour in both situations will be compared.

To perform this study, different images of the perimeter from each of the implanted prosthesis recorded by the optical microscope at 10X were used. After the montage of the partial images, a unique image was obtained for each implant (Microsoft Image Composite Editor Software).

An outline around the prosthesis (at 100 µm from it) was traced, setting the region of interest in which all the peri-implant histomorphometric measurements would be taken, as shown in Figure 8.3.

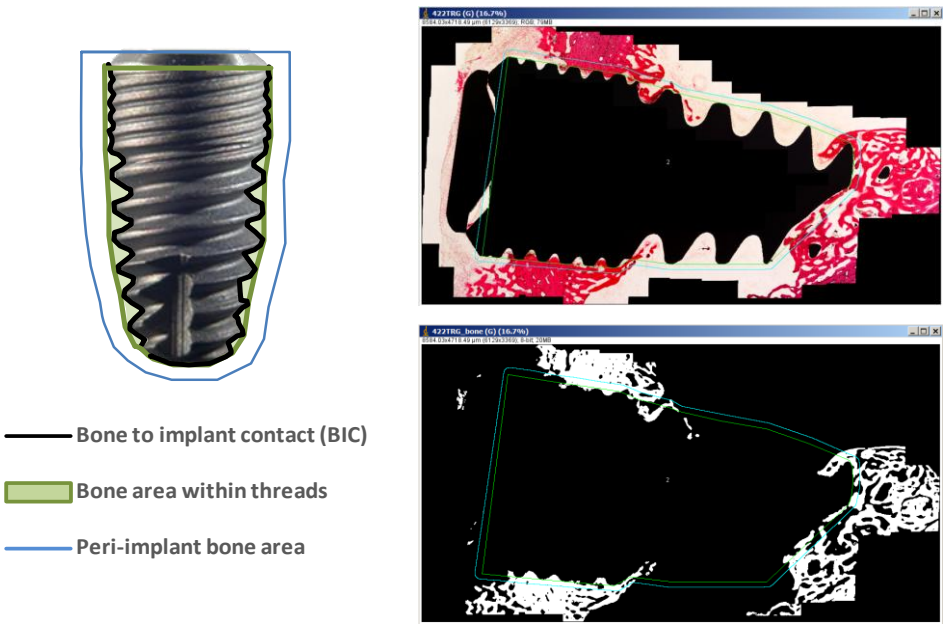

Figure 8.3. Position of studied areas on the image, for the histomorphometric analysis: surface to measure the bone to implant contact (black line), bone area within threads (green line) and region to measure the peri-implant bone area (100 µm width, from the surface of the implant to the blue line).

Studied parameters were:

- Bone to implant contact (BIC): determined as the amount of cortical and trabecular bone mineralized in close contact with the surface of the implant, expressed in mm.

- Bone area within threads: determined as mineralized tissue area in the space within the threads, existing between the line connecting peaks of the threads (green line in Figure 8.3) and at the bottom of the valleys.
- Peri-implant bone: determined as the existing mineralized bone inside the established region of interest (100 µm, blue line in Figure 8.3).

8.3. Results and discussion

8.3.1. Adhesion strength

As said before, first step before the *in vivo* evaluation was to test the adhesion between sol-gel coatings and titanium screw. A good adhesion is required since they are going to be used as bone implants and coatings have to show enough integrity to resist the screw stress produced during implantation process.

In order to test these properties, coated implants with the different formulations were placed in a pig knee bone, under normal surgery conditions. Afterwards, they were unscrewed and studied by SEM. In Figure 8.4 the obtained results are presented.

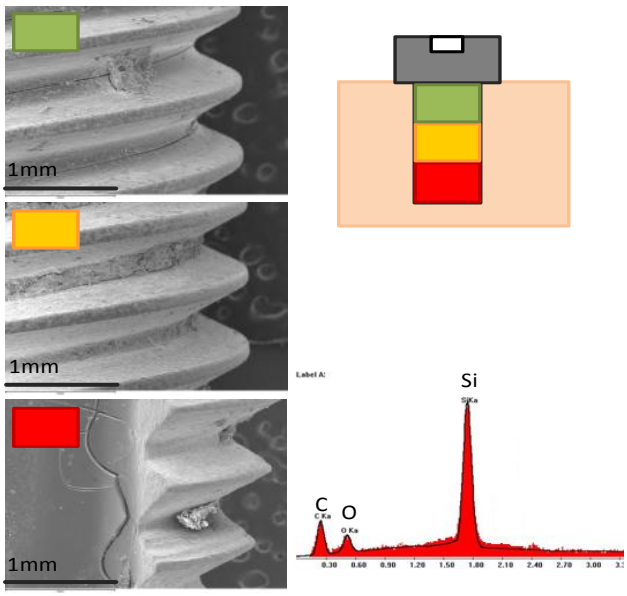

Figure 8.4. SEM images showing the resistance of sol-gel coatings in the different areas of the implant: proximal (green), media (yellow) and distal (red), and EDX spectrum (right down).

SEM images show (Figure 8.4) that the coatings resisted the implantation procedure. The use of EDX confirmed the coating presence even in the bottom of the screw (silicon detection on the surface). In spite of some cracks appeared, there was no delamination. It also needs to be taken into account, that in this *ex vivo* assay, coatings not only resisted the implantation process, but also the unscrewing. Thus, after confirming the high adhesion and resistance, we moved to next step.

8.3.2. Qualitative study of biocompatibility

The main histological events studied in this biocompatibility assessment were: foreign body giant cells presence, bone marrow state and fibrous capsule development.

- **Giant cells' presence**

In 7M:3T and Control, foreign body giant cells were observed at 1 and 2 weeks after implantation (Figure 8.5), in the same way that was found in the first implantation (chapter 3). These cells were also occasionally observed in the other studied materials.

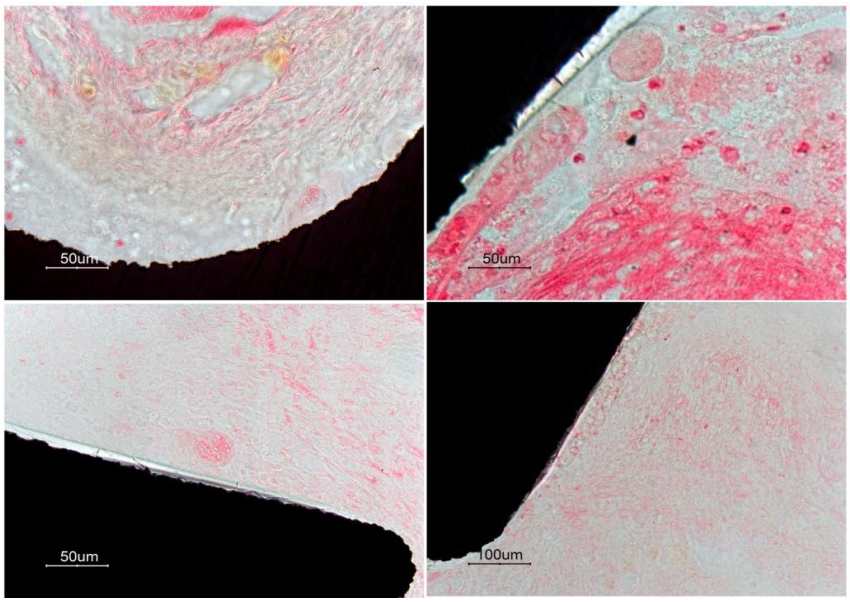

Figure 8.5. Foreign body giant cells found in Control (up) and 7M:3T (down) after 2 weeks of implantation.

However, in any of the cases, the presence of these cells exceeded the physiological pattern of the foreign body response of any organism against an implantation.

- **Bone marrow state**

Bone marrow state is a good indication of biomaterial's biocompatibility. In this study, to test the extension of the effect of implantation on it, different parameters were taken into account, such as the loss of bone marrow tissue's architecture, fat rate, cell load and the distance from the implant.

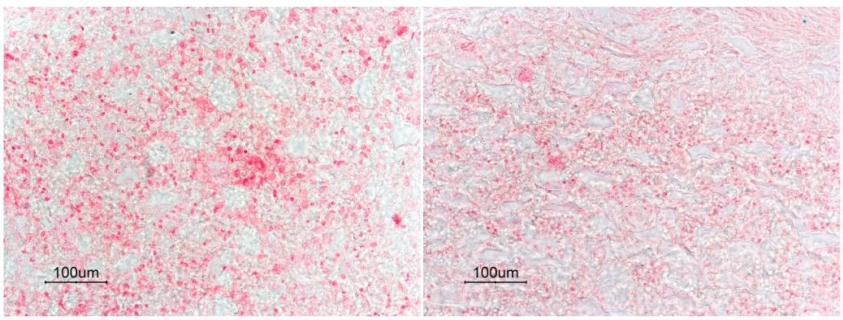

Figure 8.6. Bone marrow state for the 7M:3T coating after 1 week (left) and 2 weeks (right) after implantation.

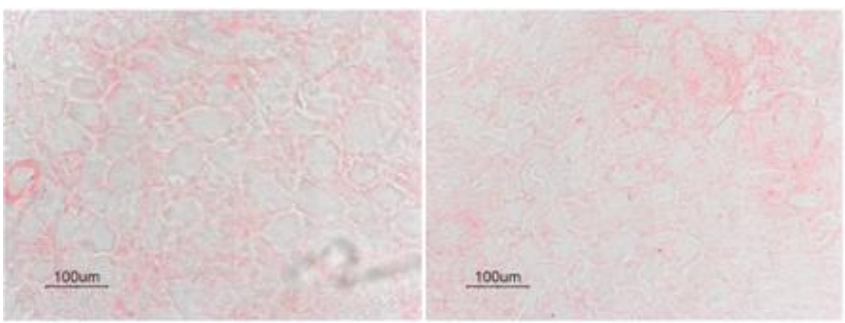

8.7. Bone marrow state for the 7M:3T-0.9% coating after 1 week (left) and 2 weeks (right) after implantation.

For the 7M:3T coating, bone marrow was not too much traumatized, especially in remote areas of the implant where there was a little repercussion. Nevertheless, the general state of the marrow worsened during the second week, as shown in Figure 8.6. These observations are consistent with those for the first

implantation procedure. However, 7M:3T-0.9% material (Figure 8.7) showed a very traumatized bone marrow in both 1 and 2 weeks of implantation, with a high proportion of adipocytes and an absence of cells in marrow tissue.

The same level of traumatism as for 7M:3T-0.9% was found in the case of 35M:35G:30T in both studied time periods. However, in this case, less fat was found and an excessive content of cells without keeping the architecture of the tissue (Figure 8.8).

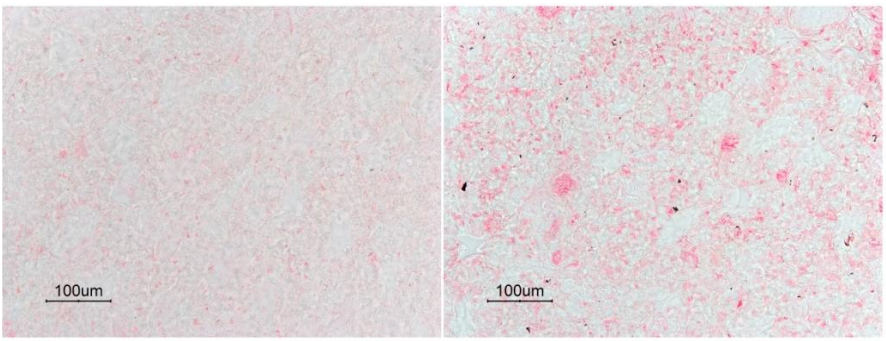

8.8. Bone marrow state for the 35M:35G:30T coating after 1 week (left) and 2 weeks (right) after implantation.

When gelatin was added to 35M:35G:30T formulation, it was found that bone marrow was less traumatized at first week, loosing cellular load and the architecture after 2 weeks of implantation (Figure 8.9).

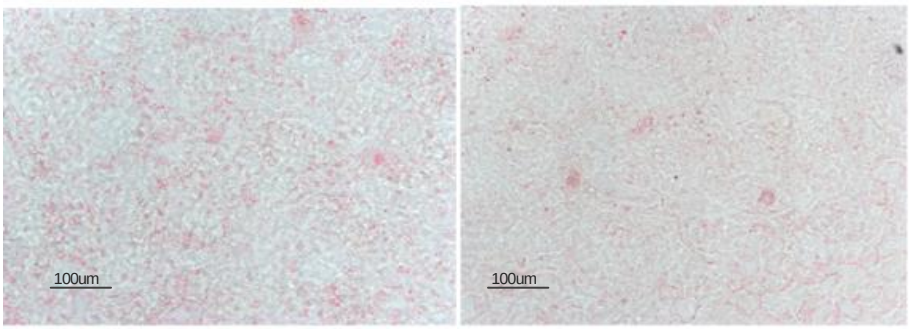

8.9. Bone marrow state for the 35M:35G:30T-0.9% coating after 1 week (left) and 2 weeks (right) after implantation.

Finally, Control material showed a significant aplastic bone marrow at the first studied period close to the areas in contact with the implant. However, it was slightly recovered after two weeks of implantation, restoring its architecture and cell loading (Figure 8.10). In the performed first *in vivo* study also happened that the Control presented a more traumatized bone marrow compared to 7M:3T coating, recovering both of them the normality after 4 weeks.

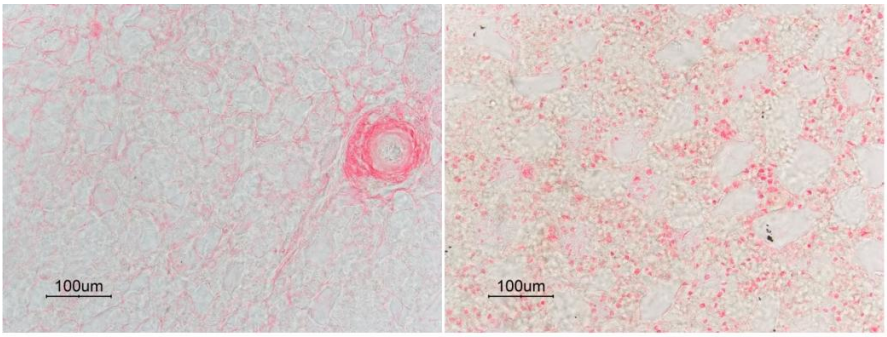

8.10. Bone marrow state for the Control after 1 week (left) and 2 weeks (right) after implantation.

- **Fibrous capsule development**

In Figure 8.11, obtained images for the formed fibrous capsule as response to the implantation for the first and the second week after surgery are shown. It could be seen the same general tendency for all the materials in the formation and development of this fibrous layer. At the studied first period of time, layers were thick and limp, getting denser and harder over time and showing thinner lines up to 2 weeks.

Fibrous capsule only appeared in places where there was no contact between the implant and the bone, as it is the case of bone marrow. This behaviour corresponds to images shown in Figure 8.11, where the profiles of all the materials are surrounded by this soft layer. The presence of the coating can be also observed in all images, proving that the material remains during short periods after the implantation.

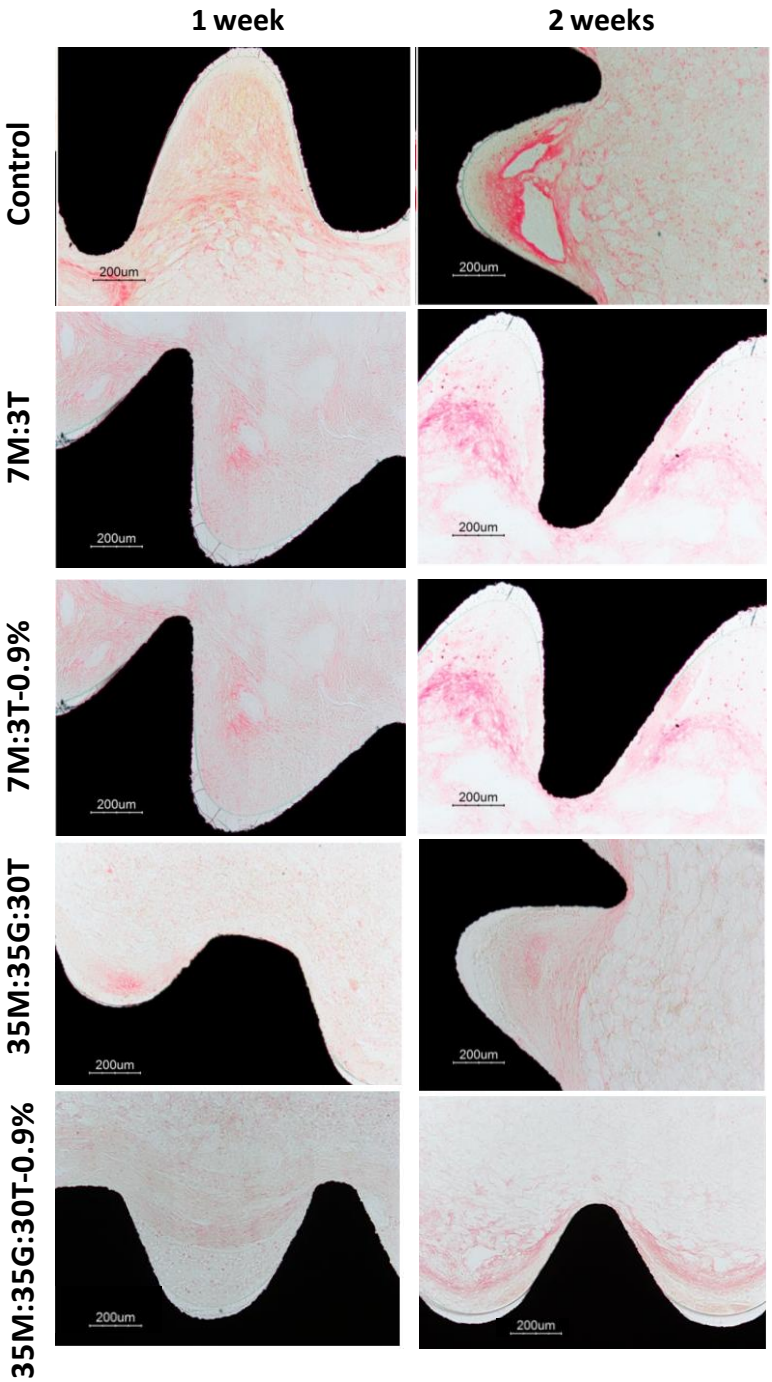

Figure 8.11. Fibrous capsule evolution for all the materials under study in bone marrow area.

At this time, significant differences among the different materials could not be obtained. No one of the developed coatings neither the titanium Control developed a fibrous capsule which surrounded all the implant in the way as happened in the performed first implantation for 5M:5G coating (chapter 3). This may be explained in part, with the degradation kinetics. It was found that the 5M:5G hybrids degraded too slow and we attributed the fibrous capsule formation to this phenomenon. With the design of a ternary system adding TEOS, and also the incorporation of a high hydrophilic and soluble molecule as gelatin, we have accelerated their resorption ability.

When studying the region of cortical bone and implant contact, it was not usual to find an interposed fibrous layer, as happened in performed first *in vivo* study. The reason for this observation lies on the fact that, in this case, implantation model was changed to ensure an appropriate primary stability. Implant was placed in rabbit's tibia trying to support them in opposite cortical, what was achieved in many cases and reduced the micromovements and, in consequence, the formation of the fibrous capsule

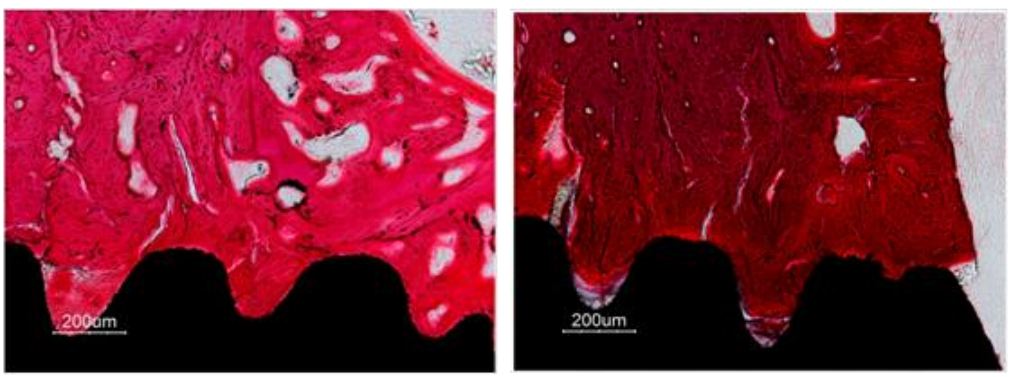

Figure 8.12. Area in contact between the cortical bone and the implant for Control (left) and 7M:3T coating (right) after 1 week of implantation.

In Figure 8.12 are shown as an example two images on the region of contact between implant and cortical bone, proving the absence of the fibrous tissue layer. These images also prove the presence of the coating and its resistance after the screw.

8.3.3. Semi-quantitative study of foreign body reaction response

For the semi-quantitative analysis of foreign body reaction, the scores for the previously listed 12 different items related to the biocompatible character of the host-implant system were obtained and the total scored is plotted in Figure 8.13 for two evaluated implantation periods.

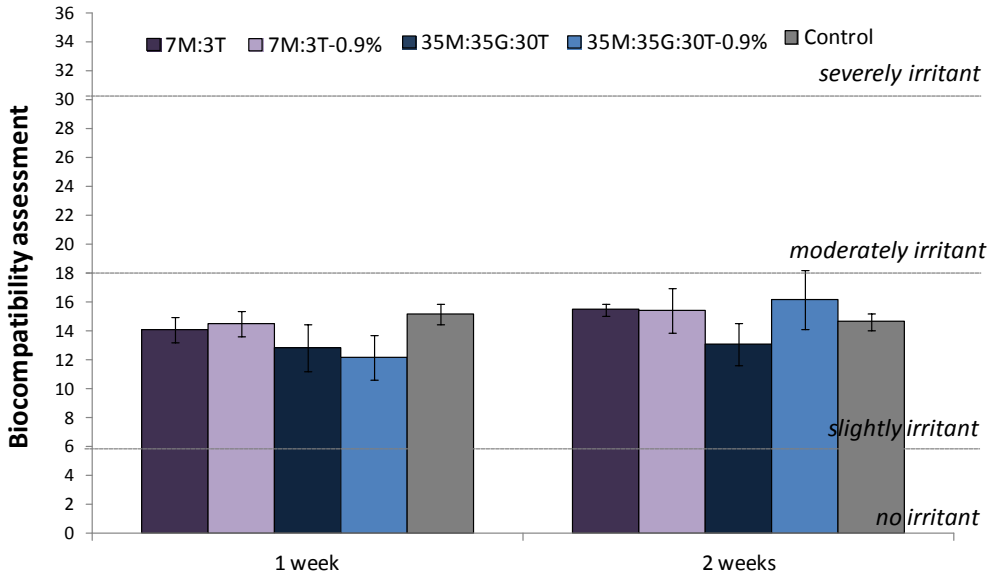

Figure 8.13. Graphical representation for the obtained values in biocompatibility's semi-quantitative analysis for 7M:3T, 7M:3T-0.9%, 35M:35G:30T, 35M:35G:30T-0.9% and Control.

This analysis showed similar values for siloxane-gelatin coatings and titanium Control at both 1 and 2 weeks after implantation, being all of them classified as slightly irritant materials. The statistical analysis proved that there were not differences among all the tested materials.

8.3.4. Qualitative evaluation of osseointegration

Osseointegration ability was evaluated in two areas: implant in contact with cortical bone and implant in contact with trabecular bone. Thus, different parameters were studied: compact bone regeneration (cortical) through the incorporation of screw's head into it, presence of active bone spicules in spongy bone region and osteoblastic activation.

- **Cortical bone's osseointegration**

Implant's osseointegration ability with compact bone establishes the premise to allow the formation of new trabecular bone around the prosthesis, giving the required long-term biological stability (secondary stability). Next, the recorded images for each type of studied material in contact with the cortical bone are shown.

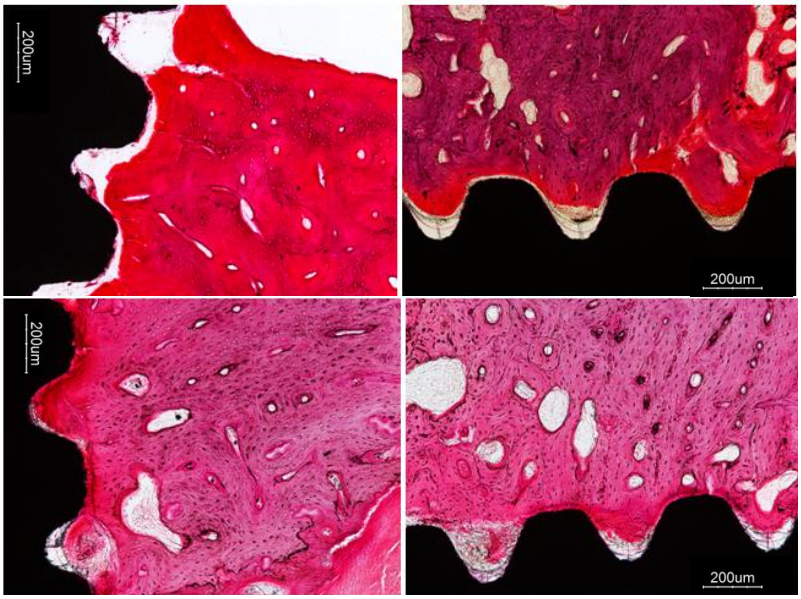

Figure 8.14. Cortical bone's osseointegration for the 7M:3T coating after 1 week (up) and 2 weeks (down) of implantation.

For the 7M:3T coating, the presence of cortical bone between threads was clear, allowing the direct contact between coating's surface and bone. Figure 8.14 also shows the absence of fibrous capsule, as well as that coating was kept intact up to 2 weeks. Comparing these results with the ones obtained in the performed first implantation for the same material, higher and better osseointegration was obtained in this case.

Similar behaviour was observed in the case of 7M:3T-0.9% (Figure 7.15), where cortical bone took up the valleys of the screw and the presence of the coating was clear after two weeks of implantation. However, the osseointegration degree achieved by this material seems to be slightly higher than the one for 7M:3T after 2 weeks.

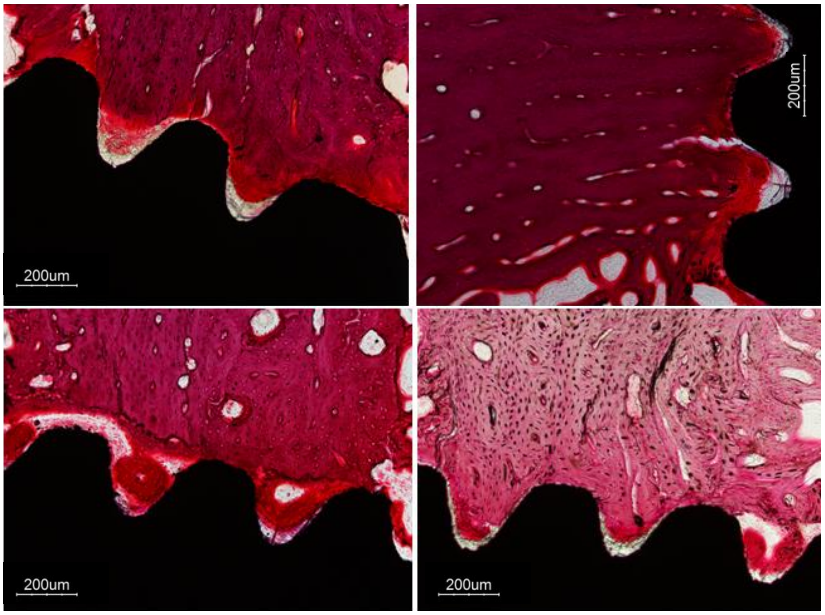

Figure 8.15. Cortical bone's osseointegration for the 7M:3T-0.9% coating after 1 week (up) and 2 weeks (down) of implantation.

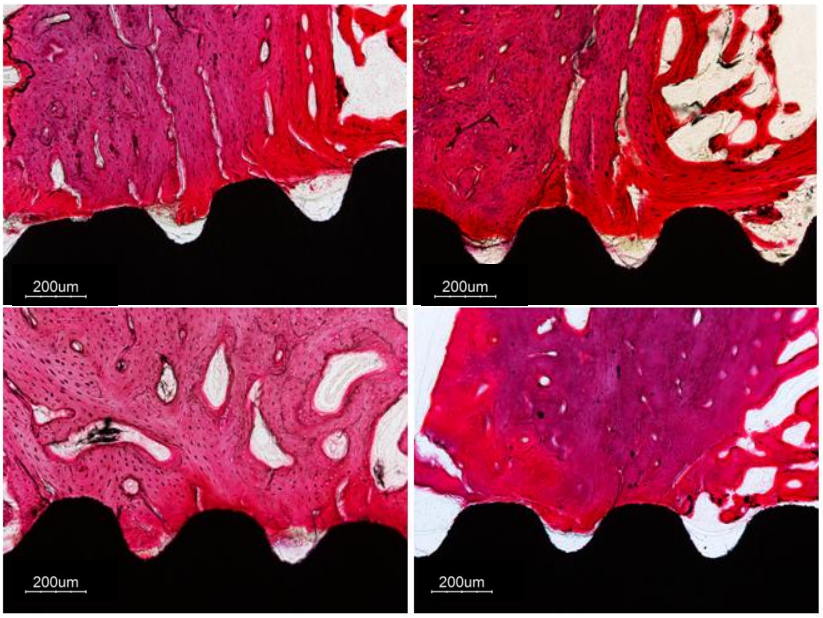

Figure 8.16. Cortical bone's osseointegration for the 35M:35G:30T coating after 1 week (up) and 2 weeks (down) of implantation.

For 35M:35G:35T (Figure 8.16) and 35:35G:30T-0.9% (Figure 8.17) formulations, thicker coatings were obtained; thus, the available area in the valleys of the implants to be in contact with cortical bone was reduced. In both cases, in the same way as happened for 7M:3T coatings, there was not fibrous capsule surrounding the implant. The osseointegration achieved for 35M:35G:30T material was inferior to the one obtained with previous studied coatings. However, an improvement was observed when adding gelatin (35M:35G:30T-0.9%).

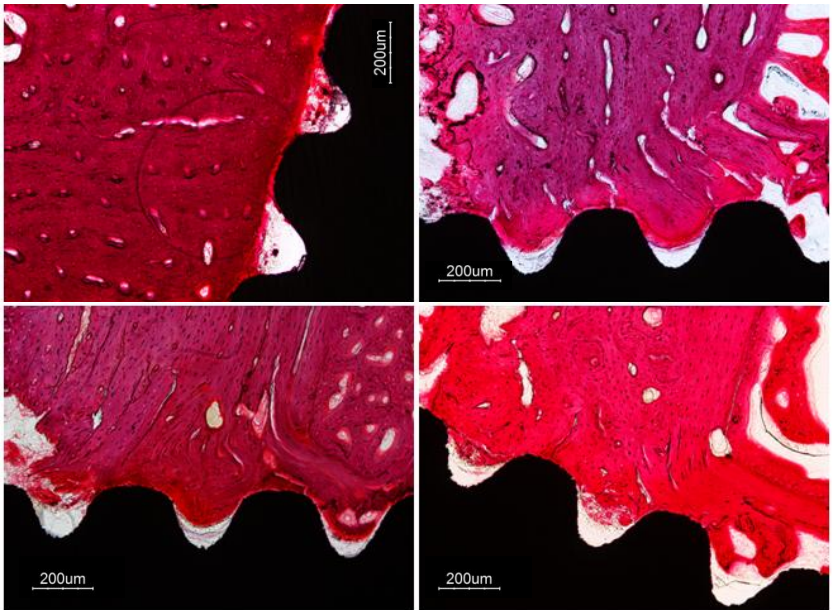

Figure 8.17. Cortical bone's osseointegration for the 35M:35G:30T-0.9% coating after 1 week (up) and 2 weeks (down) of implantation.

In titanium Control (Figure 8.18), since there was no coating in the areas between threads, all the available space could be filled by cortical bone. In this case fibrous capsule was neither observed.

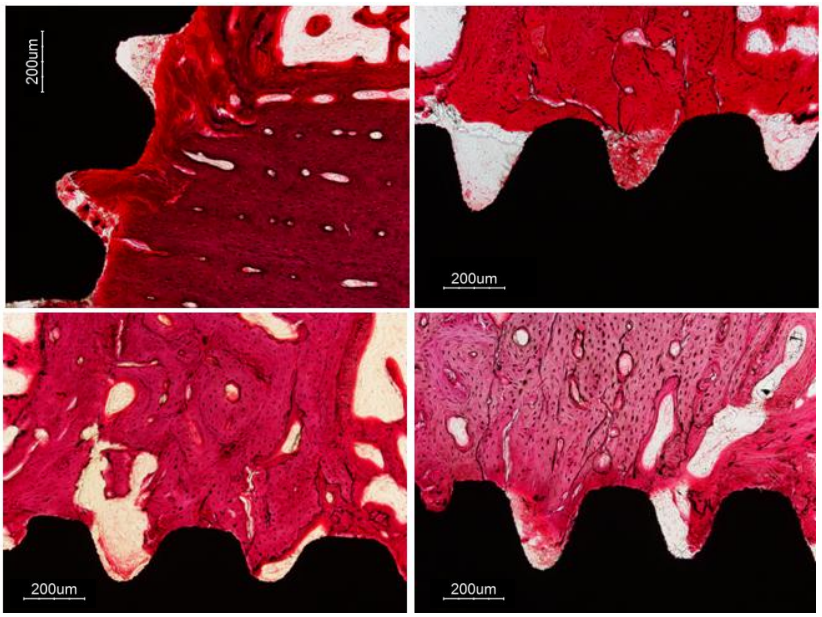

Figure 8.18. Cortical bone's osseointegration for Control material after 1 week (up) and 2 weeks (down) of implantation.

Due to the improvement of the primary stability achieved in this second implantation, all the cortical bone showed a better appearance without any intervening soft tissue layer. However, due to the implantation procedure, microfactures could be observed in many cases.

In spite of small differences were obtained among studied materials, 7M:3T-Gelatin hybrids and Control showed a higher degree of osseointegration compared to 35M:35G:30T. Furthermore, in both types of materials, 7M:3T and 35M:35G:30T, the response was improved by the addition of gelatin.

- **Trabecular bone's osseointegration**

As shown above, an appropriate primary stability was achieved in all the cases by the use of the new animal model implantation, what allowed a better osseointegration with the cortical bone. Next step was to test the regeneration of trabecular bone, since it will determine the long term success on the dental implant treatment. The formation of new bone spicules and trabecular bone will favour a higher biological stability.

Next, obtained optical microscope images are shown for all the materials, where the formation of new trabeculae is observed.

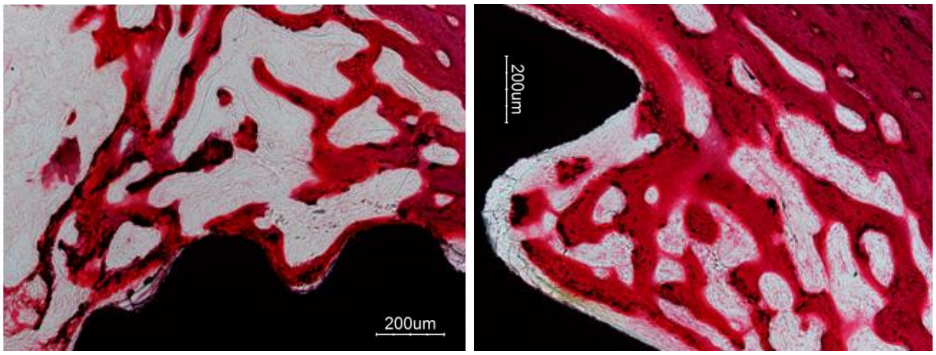

Figure 8.19. Trabecular bone's osseointegration for the 7M:3T coating after 1 week (left) and 2 weeks (right) of implantation.

For implants coated with 7M:3T formulation, an activation of the endostium (in the insertion cortical bone) was observed, what favoured the formation of active spicules. These spicules grew from the endostium to the surface of the implant, becoming mature and branched trabeculae after 2 weeks of implantation (Figure 8.19). The addition of gelatin, 7M:3T-0.9% coating, seemed to favour the formation of more trabeculae around the implant after 2 weeks (Figure 8.20).

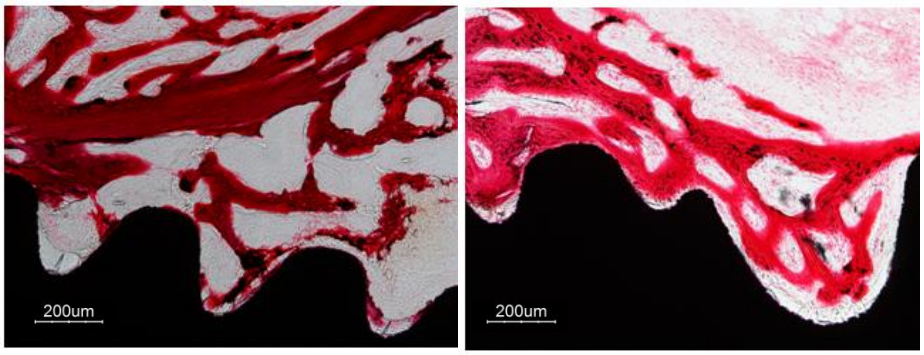

Figure 8.20. Trabecular bone's osseointegration for the 7M:3T-0.9% coating after 1 week (left) and 2 weeks (right) of implantation.

35M:35G:30T promotes the formation of straight and no branched spicules at first week of implantation. However, after 2 weeks of implantation, these spicules

are able to form a branched trabecular bone in the same way as other materials did on the first week (Figure 8.21). In the case of the ternary system with gelatin, 35M:35G:30T-0.9%, this trabecular bone is more extended at the second week (Figure 8.22).

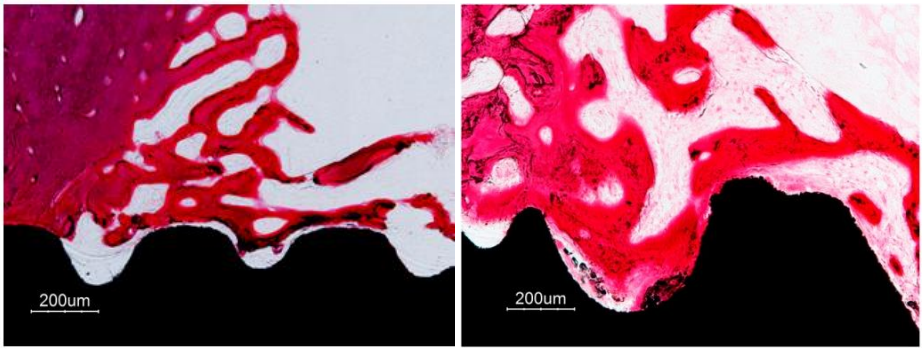

Figure 8.21. Trabecular bone's osseointegration for the 35M:35G:30T coating after 1 week (left) and 2 weeks (right) of implantation.

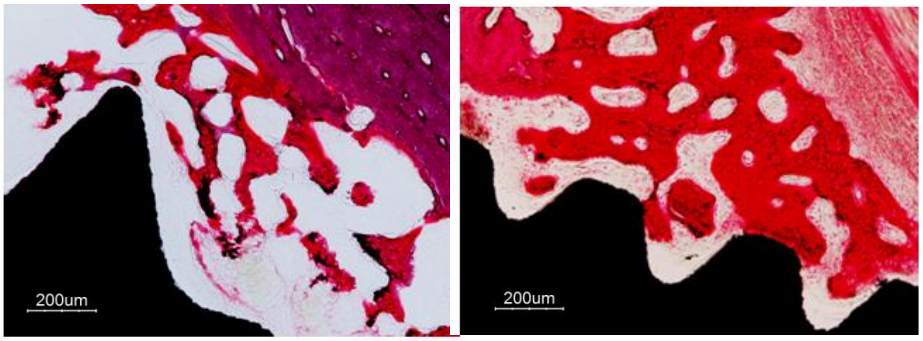

Figure 8.22. Trabecular bone's osseointegration for the 35M:35G:30T-0.9% coating after 1 week (left) and 2 weeks (right) of implantation.

When studying Control samples, a similar behaviour as for 7M:3T was observed, where at first week active spicules are formed, becoming in mature trabeculae after 2 weeks.

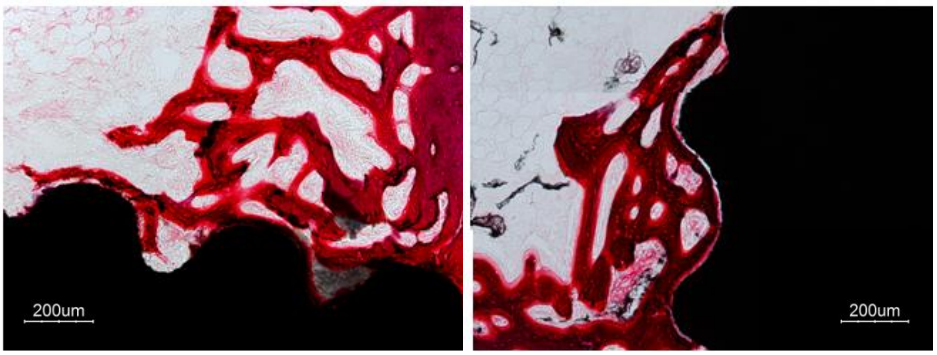

Figure 8.23. Trabecular bone's osseointegration for Control material after 1 week (left) and 2 weeks (right) of implantation.

Along this qualitative study the osteoconductive nature of titanium was clear, promoting the formation of new trabecular bone in close contact with the implant. Phenomenon that was not often observed in the case of coated screws.

To sum up, the results obtained in this second implantation stage proved that all the studied material are biocompatible, inducing a normal foreign body response with a slightly irritant character. The 7M:3T and 7M:3T-0.9% coatings showed a better osseointegration, both in cortical and trabecular bone, compared to the hybrid with GPTMS. However, all these results are referred just to a trend, since there are many variables and parameters that affect the *in vivo* response, such as the implantation position, cortical bone's thickness, coating's thickness, the contact with the opposite cortical bone among others, as well as differences resulting from each individual.

8.3.5. Comparison of 1st and 2nd implantations

The search of an appropriate animal model to ensure the primary stability, led us to obtain results with no significant differences among the different developed coating and titanium in this second *in vivo* study. In Figure 8.24 the comparison between the obtained histomorphometric parameters at first and second animal study are presented.

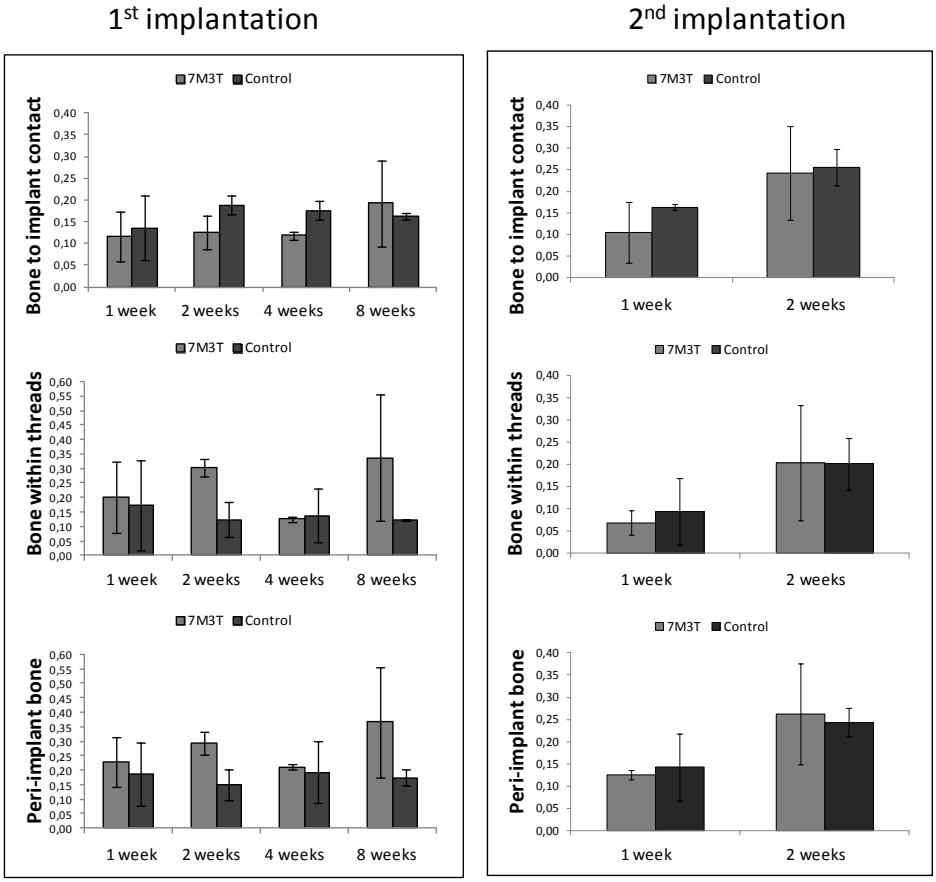

Figure 8.24. Obtained histomorphometric parameters in both implantation stages for 7M:3T and titanium Control.

Comparing both implantation procedures for titanium, it is clear that in the first case there was no evolution of its osseointegration ability up to two weeks, while in the second implantation (when primary stability is achieved), a progress over time can be appreciated.

Therefore, comparing the behaviour of 7M:3T coating and Control, we can say that both materials presented a similar trend inducing osseointegration during the second implantation characterization, and when the primary stability was not achieved (first implantation) more bone formation and earlier osseointegration are achieved in the case of the sol-gel coating. Thus, this suggests that in adverse

conditions (absence of this primary stability), the osteoinduction ability of 7M:3T coating prevails over titanium osteoconduction ability (Figure 8.25).

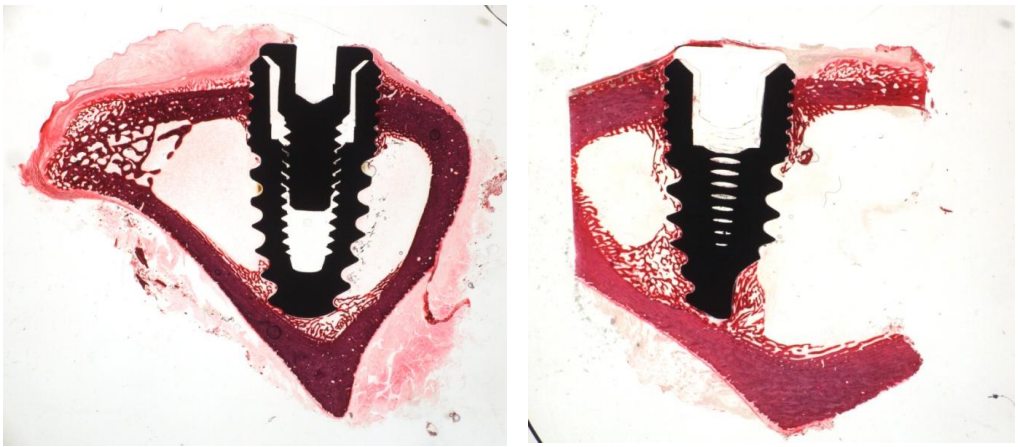

Figure 8.25. Osseointegration ability of titanium Control (left) and 7M:3T coating (right) after 2 weeks of implantation.

8.4. Conclusions

The developed materials and the coating method, allowed obtaining a good quality final implant. Transparent and high adhesion resistant coatings were obtained, according to the performed adhesion and screw-unscrew resistance test.

No one of the tested materials produced an adverse effect in adjacent tissues to implant area, obtaining in all the cases a slight irritant response indicative of their *in vivo* biocompatibility. Due to the design of a new experimental model, no statistical differences were obtained in this case between all the studied materials, since the obtained primary stability allowed them to reach a similar osseointegration degree. A qualitative improvement could be observed, both for biocompatibility and osseointegration assessment in the case of 7M:3T compared to 35M:35G:30T, an also when adding gelatin.

All these results combined with the ones obtained for the first *in vivo* assay (chapter 3), make 7M:3T material an advantage for unfavourable conditions as it is the case of the lack of a suitable primary stability. It would be interesting to design a new experimental model to test the osteoinduction ability of 35M:35G:30T-Gelatin hybrids in adverse conditions, due to the improvement achieved over all studied *in*

vitro properties, compared to 7M:3T. According to this, the next step of this work could be to test the osseointegration ability of developed materials in an osteoporotic animal model.

References

1. Mapara M, Thomas BS, Bhat K. Rabbit as an animal model for experimental research. *Dental Research Journal.* 2012; **9:** 111.

2. Stübinger S, Dard M. The rabbit as experimental model for research in implant dentistry and related tissue regeneration. *Journal of Investigative Surgery.* 2013; **26:** 266-82.

3. Naito Y, Jimbo R, Bryington MS et al. The influence of 1α. 25-dihydroxyvitamin D3 coating on implant osseointegration in the rabbit tibia. *Journal of Oral & Maxillofacial Research.* 2014; **5:** .

4. AENOR. Biological evaluation of medical devices - part 6: Tests for local effects after implantation (UNE-EN ISO 10993-6:2009).

5. Clark PA, Rodriguez A, Sumner DR et al. Modulation of bone ingrowth of rabbit femur titanium implants by in vivo axial micromechanical loading. *J Appl Physiol.* 2005; **98:** 1922-9.

6. Peris JL, Prat J, Comin M et al. Técnica histológica para la inclusión en metil-metacrilato de muestras óseas no descalcificadas. *Rev Esp Cir Osteoart.* 1993; **28:** 231-8.

7. Ikarashi Y, Tsuchiya T, Toyoda K et al. Tissue reactions and sensitivity to iron-chromium alloys. *Materials Transactions.* 2002; **43:** 3065-71.

8. Branemark P. Osseointegration and its experimental background. *J Prosthet Dent.* 1983; **50:** 399-410.

9. Brånemark P, Zarb G, Albrektsson T. *Prótesis Tejido-Integradas: La Oseointegración En La Odontología Clínica.* Barcelona: Quintessence, 1999.

Conclusions

From the research work done along the development of this thesis, different conclusions can be taken:

1. The sol-gel synthesis allowed us to obtain organic-inorganic hybrid coatings on metallic surfaces with high homogeneity, transparency and adhesion strength to the surface. Crack free coatings were achieved, able to resist the screw and unscrew process.

2. It was possible to tailor the physicochemical properties of developed coatings by controlling the chemical composition. The addition of increasing amounts of TEOS to MTMOS, led to the obtaining of more hydrophilic coatings able to release more silicon to the environment and with a faster degradation kinetic. Furthermore, the incorporation of TEOS was also translated in an improvement of hMSCs proliferation and matrix mineralization according to the results of the *in vitro* studies. The addition of GPTMS to MTMOS provided functionalized coatings and improved cell response.

3. *In vivo* study of 7M:3T and 5M:5G proved on the one hand, the ability of 7M:3T to induce bone formation and to improve titanium's behavior on first periods after implantation, and on the other hand, the no degradation of the 5M:5G coating, what led to the formation of a fibrous capsule surrounding all the implant. Therefore, 7M:3T was selected as the base coating for the next step of this study.

4. The incorporation of different percentages of gelatin physically entrapped in the 7M:3T coating, increased the porosity of the network and led to a higher mass loss and a faster silicon release.

5. The design of a ternary hybrid, 35M:35G:30T, allowed the effective chemical anchorage of gelatin under the chosen synthesis conditions. The combination of gelatin addition and GPTMS incorporation had a synergetic effect increasing the silicon release ability compared to the base coating 7M:3T.

6. The study of protein adsorption by using the QCM-D showed an increase on the affinity of adhesive proteins toward the functionalized coatings compared to titanium and 7M:3T-Gelatin hybrids. However, this behaviour did not directly agree with the *in vitro* cell adhesion results due to the roughness effect of uncoated titanium discs.

7. ALP activity and gene expression assays proved the ability of siloxane-gelatin hybrids to promote earlier the osteogenic differentiate of different cell lineages in the presence of an inductive media compared with titanium. Moreover, the ability of coatings to induce the osteogenic differentiation by themselves was also demonstrated, fact related to the silicon release ability.

8. According to both performed *in vivo* studies, titanium's osseointegration ability seems to be affected by the achievement of an appropriate primary stability. However, this factor did not affect when the implant was coated with 7M:3T material, probably because titanium osseointegration is by contact osteogenesis while in the case of coating is by distance osteogenesis. Thus, the use of coated implants could overcome the problems of osseointegration in unfavourable conditions and accelerates new bone formation process in early stages compared to titanium.

9. These findings suggest the promising use of developed materials to treat people with poor bone regeneration ability, making the use of dental implants widespread and accessible for a wide cohort of patients, which was the main aim of this thesis. Further *in vivo* studies using an osteoporotic animal model could clearly confirm the beneficial effects found by *in vitro* studies for the 35M:35G:30T-Gelatin hybrids.